A CONSTITUTIVE MODEL FOR FIBER-REINFORCED SOILS

A Dissertation
Presented to
the Faculty of the Graduate School
University of Missouri-Columbia

In Partial Fulfillment
of the Requirements for the Degree

Doctor of Philosophy

By
CHENG-WEI CHEN

Dr. J. Erik Loehr, Dissertation Supervisor

DECEMBER, 2007

The undersigned, appointed by the Dean of Graduate School, have examined the dissertation entitled

A CONSTITUTIVE MODEL FOR FIBER-REINFORCED SOILS

Presented by Cheng-Wei Chen

A candidate for the degree of Doctor of Philosophy in Civil Engineering

And hereby certify that in their opinion it is worthy of acceptance.

J. Erik Loehr
Department of Civil and Environmental Engineering

John J. Bowders
Department of Civil and Environmental Engineering

Brent L. Rosenblad
Department of Civil and Environmental Engineering

Hani A. Salim
Department of Civil and Environmental Engineering

P Frank. Pai
Department of Mechanical and Aerospace Engineering

This body of work is dedicated to

my loving wife Pei-Ling Lee and my son Kai-Shin Chen, and

my parents Chin-Tsz Chen and Fang-Mei Cheng

ACKNOWLEDGEMENT

I would take this opportunity to express sincerely appreciation to my supervising professor, Dr. J. Erik Loehr for his valuable experience and encouragement during this research work. His willingness to share his comments and thoughts on the project and research make my study more meaningful. I thank Dr. John J. Bowders and Dr. J. Erik Loehr for their invaluable knowledge and teaching for the past four years, and gave me lots of opportunities to explore myself in the study and life. I also thank Dr. Hani Salim and Dr. Brent L. Rosenblad for the helpful suggestions and questions to complete this work and Dr. P. Frank Pai for kindly consenting to be on my dissertation committee.

It was a great experience for me to pursue my graduate study in the Geotechnical program at the University of Missouri-Columbia for past six years. I would like to thank my fellow students: Eng-Chew Ang, Awilda Blanco, Jorge Parra, and Ricardo Romero for their valuable comments and help, and other fellow students in the geotechnical program for their precious friendship and support. A special thanks to Maria Bios, for her extensive review and comments on this dissertation. I would like to thank the staff at the civil engineering office for kindly helping and supports whenever I need.

Finally, I would like to thank my parents back in Taiwan for their strong support and patience. To my dear wife, Pei-Ling, and son, Johnnie, thanks for providing me wonderful caring and giving me great support with patience during my studies.

TABLE OF CONTENTS

LIST OF TABLES

LIST OF ILLUSTRATIONS

Figure Page

A CONSTITUTIVE MODEL FOR FIBER-REINFORCED SOILS

Cheng-Wei Chen

Dr. J. Erik Loehr, Dissertation Supervisor

ABSTRACT

Fiber inclusion to improve the properties of compacted soil is becoming increasingly common in geotechnical engineering projects. However, the technique requires extensive testing on soil and fiber samples before it can be implemented. Although research performed over the last few decades has evaluated certain fiber-reinforced soil properties and formations, the development of constitutive models for fiber-reinforced soil has lagged. This dissertation aims to minimize testing requirements for fiber-reinforced specimens and thereby to encourage the implementation of fiber-reinforced soils in engineering.

Extensive testing on unreinforced and reinforced silty and Ottawa sand specimens was performed to develop and to validate a constitutive model for predicting the stress-strain-volume-pore pressure response of fiber-reinforced soils. Results showed that the effective friction angle and cohesion intercept increased significantly in consolidated-undrained ($\overline{CU}$) and consolidated-drained (CD) triaxial compression tests for both fiber-reinforced silty sand and Ottawa sand. The shear strength parameters of fiber-reinforced silty sand and Ottawa sand are strain dependent so more shear strain was needed to mobilize fiber resistance for specimens consolidated at higher effective stresses. Moreover, the laboratory results suggested that fiber-reinforcement provides both a deviatoric (q_f) and a hydrostatic (p_f) contribution to the stresses in the specimens.

However, the hydrostatic contribution of fibers varied according to different soil types and loading conditions.

The proposed constitutive model to predict the mechanical properties of fiber-reinforced soils is based on superposition of the response of unreinforced soil and the response due to fibers. Key assumptions in the model include: (1) fibers are uniformly distributed in the specimens. (2) f_{mob} accounts for the reductions in fiber strain due to relative slip between the fibers and the soil, and varies with effective consolidation stress, soil types, and loading conditions, (3) yielding is considered, (4) shear distortion (θ) is equal to triaxial shear strain (ε_q), (5) the total axial strain in the fibers (ε_t) is equal to 0.25 times axial strain plus 1.68 times volumetric strain from tests on unreinforced specimens, and (6) the initial p_{f0} and q_{f0} are used to account for the compaction, extrusion, and consolidation process.

The model was found to be capable of reproducing the deviatoric stress well for all reinforced silty sand and Ottawa sand. The predicted pore pressure and volumetric strain were all in a close agreement with the observed behavior up to large strains for both soils. However, the predicted volumetric strain behavior shows some tendency to over-predict the dilatancy of the reinforced silty sand specimens consolidated less than 20-psi (140-kPa). The predictions in fiber deviatoric and hydrostatic stresses in $\overline{CU}$ tests matched reasonably well and followed the same trends as the measured behavior, except for specimens consolidated at higher effective stresses. In CD tests, the deviatoric and hydrostatic stresses matched reasonably well and mimicked the measured behavior, but tended to deviate slightly from the observed response at large strains.

CHAPTER 1: INTRODUCTION

Inclusion of fibers to improve the engineering properties of compacted soil is becoming an increasingly common practice in geotechnical engineering projects. For example, reinforced soil is currently utilized for stabilization of shallow slope failures (Gregory and Chill, 1998), construction of new embankments with marginal soils, and reduction of shrinkage cracking in compacted clay liners (Rifai, 2000). It is also used to enhance the stability of earth retaining walls (Park and Tan, 2005), to reinforce roadway subgrades (Santoni et al, 2001), and to improve resistance to erosion by wind and water.

Fiber-reinforced soil is a mixture of soil and synthetic fibers. Synthetic fibers can be made of different materials, shapes and lengths. Polypropylene and polyester are the most common materials used to manufacture fibers. Fibers can be flat or round, and continuous or discrete. Discrete fibers are manufactured in several lengths, ranging from 0.5-in to 3-in, and are available in different types such as monofilament, fibrillated, tape, and mesh (Maher and Gray. 1990; Al-Refeai, 1991; Moher and Ho, 1994; Nataraj and McManis, 1997; Consoli et al., 2002).

Research has been performed over the last few decades to evaluate the basic shear strength properties and the formation of fiber-reinforced soils. The majority of this work has focused on the use of fibers for reinforcing granular materials (Consoli et al., 1998; Gray and Ohashi, 1983; Maher and Gray, 1990; Santoni et al, 2001; Shewbridge and Sitar, 1989). The behavior of fiber-reinforced clays has also been examined by Gregory and Chill (1998), Maher and Ho (1994), and Ding and Hargrove (2006). Their research

has shown that inclusion of fibers even in small quantities can increase both the shear strength and ductility of soils.

Despite the advances in soil reinforcement research, there remains a lag in the development of constitutive models for fiber-reinforced soil. Several efforts have been made to develop models for use in predicting the strength of fiber-reinforced soils (Gray and Ohashi, 1983; Maher and Gray, 1990; Prisco and Nova, 1993; Michalowski and Zhao, 1996; Ranjan et al., 1996; Zornberg, 2002; Ding and Hargrove, 2006). Of these efforts, the following two models are of particular interest – one models soil reinforced with continuum threads (Prisco and Nova, 1993), and the other models municipal solid waste (MSW) (Machado et al, 2002). The first model, however, is neither able to predict the stress-strain behavior well nor able to correctly reproduce the volumetric response of the reinforced soil. The second model is capable of reproducing the stress-strain-volume change response in drained triaxial compression tests on waste, but it is limited to predicting the overall MSW response (which is assigned to be composed of "paste" and fibers) and not the soil's (paste) individual behavior or the fiber's contribution. Therefore, the motivation for this work is to develop a constitutive model to predict the stress, pore pressure change, and volume change in fiber-reinforced soils as a function of the shear strain. In doing so, this work seeks to minimize the need for laboratory tests of fiber-reinforced specimens and thereby to encourage the implementation of fiber-reinforced soils in engineering practice.

The hypothesis for the proposed program is that the effective stress-strain-pore pressure change and effective stress-strain-volume change behavior of fiber-reinforced soils can be predicted from superposition of the response of unreinforced soil and the

response due to the fibers. The scope of this work herein includes developing a model to predict the fiber response in reinforced soils and to identify the soil's mechanical properties so that the fiber-reinforced soil's behavior can be categorized. Its ultimate goal is to contribute to the scholarship on fiber-reinforced soils by proposing a constitutive model that will increase testing efficiency for engineering projects that include reinforced soils.

The primary objective of the proposed work is to evaluate the hypothesis through an extensive series of laboratory tests on both unreinforced and reinforced soil specimens, and then to develop and evaluate a constitutive model for predicting the stress-strain-volume-pore pressure response of the fiber-reinforced soil based on the mechanical properties of the unreinforced soil and fibers. These tests on replicated unreinforced and reinforced soil specimens are used to establish a response due to fibers alone in different stress paths. Specifically, the proposed program seeks to accomplish the following tasks:

1. Measure the strength and stress deformation behavior of the unreinforced and fiber-reinforced silty sand and Otttawa sand when loaded along different stress paths,
2. Analyze the strength parameters based on strain dependence of the fiber-reinforced and unreinforced sand and silty sand,
3. Develop and evaluate a constitutive model to predict the stress-strain-volume-pore pressure response of fiber-reinforced silty sand and Ottawa sand, and

4. Validate and calibrate the proposed model for predicting the mechanical behavior of fiber-reinforced silty sand and Ottawa sand along with general stress paths.

In Chapter 2, a summary of previous research on fiber-reinforced soils that emphasizes the stress-strain response, load transfer mechanics, and constitutive models for predicting the behavior is presented. Chapter 3 provides the methodology for this research as it details the test materials, specimen preparation methods, and testing program undertaken for the analysis of fiber-reinforced soils. This chapter also presents the conventional consolidated-undrained ($\overline{CU}$ test) triaxial compression tests used to determine the stress-strain-pore pressure change behavior of fiber reinforced soils under undrained conditions and a discussion of the tests results. The stress-strain-volume change behavior of fiber-reinforced soils under drained conditions is evaluated in terms of the conventional consolidated-drained (CD test) triaxial compression test in Chapter 4. Furthermore, the results of isotropic consolidation tests for both reinforced and fiber-reinforced specimens of silty sand and Ottawa sand are presented and discussed. In Chapter 5, an interpretation and analysis of all the experimental results is presented. The proposed constitutive model to predict the engineering behavior of fiber-reinforced soils under undrained and drained loading conditions is presented in Chapter 6. Comparisons of measured and predicted behavior of fiber-reinforced soils under undrained and drained triaxial loading are presented in Chapters 7 and 8, respectively. Chapter 9 concludes this work by providing a summary of the work performed for this dissertation along with recommendations for future research to further the understanding of fiber-reinforced soils and to improve the development of constitutive models for fiber-reinforced soils.

CHAPTER 2: LITERATURE REWIEW

2.1 Introduction

In this chapter, the stress-strain behaviors of fiber-reinforced soil along with its effective stress shear strength properties are discussed. In addition, several constitutive models used to predict the stress-strain behavior of fiber-reinforced soil and similar materials are reviewed followed by a theoretical overview of load transfer mechanics for fiber-reinforced soils as it appears in the literature. Particular interest is paid to randomly distributed fibers that can increase the soil's strength and can avoid potential planes of weakness developed between the soil and the fiber reinforcement interface.

2.2 Mechanical Behavior of Fiber-Reinforced Soils

The stress-strain behavior of fiber-reinforced soils has been evaluated in unconfined compression tests, direct shear tests, and in consolidated-undrained and consolidated-drained type triaxial compression tests. Previous investigations have shown that inclusion of fiber reinforcement to soil increases the peak shear strength, reduces its post-peak strength loss, and increases the strain at failure (i.e. ductility).

Maher and Gray (1990) conducted drained triaxial compression tests to evaluate the static stress-strain response of sands reinforced with discrete fibers as well as with fibers randomly distributed within the specimens. These tests were carried out to observe the influence of various fiber properties (i.e. fiber content, aspect ratio, and modulus), soil granulometry (i.e. particle size, shape, and graduation), and to other test parameters on the soil behavior. The results showed that randomly distributed fiber inclusions

significantly increased the ultimate strength and stiffness of sands. The increase in shear strength and stiffness was a function of sand granulometry and of each fiber's properties.

Al-Refeai (1991) conducted laboratory drained triaxial compression tests to investigate the load-deformation behavior of sand reinforced with discrete, randomly oriented fibers. Tests were performed on fine and medium sand specimens with reinforcement in varying length and shape. The author found that all reinforced sands showed a significant improvement in load capacity. Also discovered was the fact that shorter fibers required a great amount of confining stress to prevent bond failure (e.g. soil-fiber friction interaction) and that shorter fibers decreased sand stiffness. Similar experiments were performed by Ranjan et al. (1994), who conducted consolidated-undrained triaxial compression tests on fine sand reinforced with randomly distributed plastic fibers in order to determine the soil's stress-strain behavior, to examine the influence of fiber properties, and to determine the effect of confining stress on the shear strength of reinforced sand. It was found that the shear strength of fiber-reinforced sand was a function of fiber content, fiber aspect ratio (l/d, where l is fiber length, and d is fiber diameter) and confining stress. As increased in fiber content and aspect ratio, the shear strength of the fiber-reinforced sand increased. The authors noticed that the shear strength envelopes for fiber-reinforced sand had a curved or bilinear shape with a change (break) of slope at a certain confining stress, called the "critical confining stress" (Figure 2.1). Further noticed was the fact that the critical confining stress increases with decreases in aspect ratio.

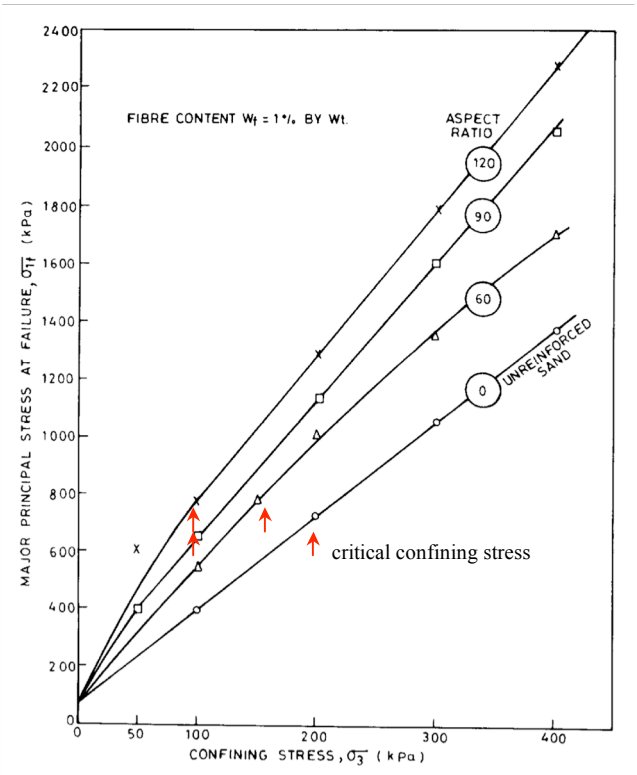

Figure 2.1 Effect of aspect ratio on critical confining stress (after Ranjan et al. 1994).

Maher and Ho (1994) investigated the mechanical properties of a kaolinite/fiber composite in unconfined compression tests. The randomly distributed fibers significantly increased the peak compressive strength and reduced the post-peak drop in the compression resistance of the kaolinite clay. The increase in compressive strength was most pronounced when the water content was decreased (Figure 2.2). The increase in shear strength was discovered to be a function of fiber length, fiber content, and the water content of the composite. However, the effect of fiber length was not as significant for kaolinite clay as it was for cohesionless soils. The authors found that increasing the fiber length decreased the contribution of fibers to the strength of the clay. This contrasts to the effect of increased fiber length on the strength of fiber-reinforced granular soils, in which case the fiber length contributed to the strength of the reinforced soil (Al-Refeai, 1991).

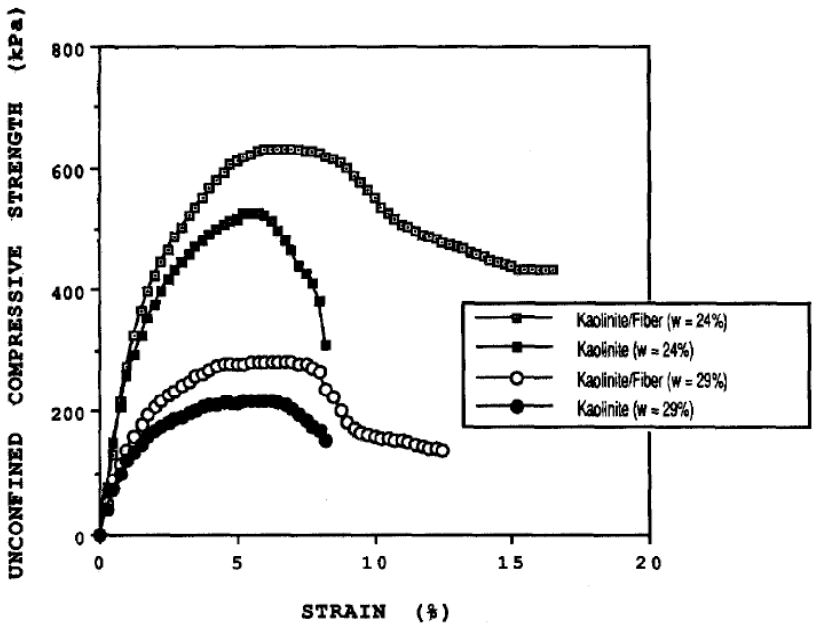

Figure 2.2 Effect of water content on contribution of fibers to unconfined compressive strength (from Maher and Ho, 1994).

Nataraj and McManis (1997) performed laboratory direct shear and unconfined compression tests on clay (CL) and sand (SP) reinforced with randomly distributed fibrillated fibers. The influence of fiber content, normal stress, and moisture content were addressed in the findings. The authors found that increases in fiber content resulted in substantial increases in the peak compressive strength of clay and sand. Moreover, the strength for fiber-reinforced soil increased with increasing moisture content before reaching an optimum moisture content (Figure 2.3). The different normal loads for reinforced specimens were observed to contribute to the dilation of the sand. It was found that dilation of sand occurred at a lower normal stress, whereas very little or no dilation occurred at a higher normal stress.

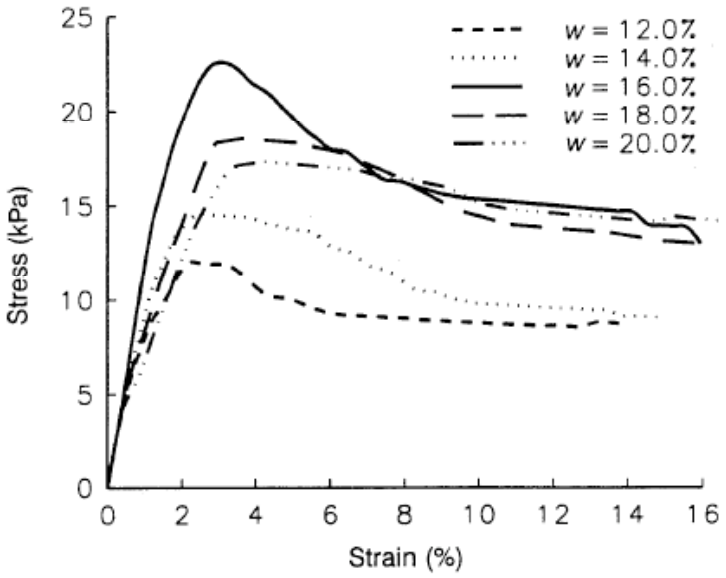

Figure 2.3 Stress-strain relationships at various moisture content for reinforced sand specimens with a 0.3% fiber content (from Nataraj and McManis, 1997).

Santoni et al. (2001) conducted unconfined compression tests on different sands reinforced with randomly oriented discrete fibers to isolate the effect of numerous variables on the performance of soil and fiber mixtures. The results of the research identified optimum values for each test parameter evaluated. The inclusion of fibers was found to significantly improve the unconfined compressive strength of sands. In addition, fibrillated fibers performed the best of the various fiber types, and the optimum fiber length was determined to be 2-in (51-mm).

Ang (2001) and Romero (2003) performed a series of laboratory triaxial compression tests on randomly distributed polypropylene fibers reinforced with silty clay under drained and undrained conditions. The results demonstrated that inclusion of fibers significantly improves the shear strength of soils. The authors found that more strains was needed to mobilize the fiber resistance for fiber-reinforced specimens consolidated at

higher effective stresses and greater strain was needed to mobilize fiber resistance in undrained tests than drained tests.

Kumar et al. (2006) carried out unconfined compression tests to investigate the strength of soft clay soil reinforced with polyester fibers and mixed with various proportions of sand. The results indicated that the unconfined compressive strength of fiber-reinforced clay was a function of the degree of compaction, fiber content, fiber length, fiber shape (i.e. plain or crimp), and the proportion of sand to clay.

Consoli et al. (2002) performed drained triaxial compression tests to evaluate the benefit of randomly distributed polyethylene terephthalate fibers obtained from recycled plastic bottles mixed with a uniform fine sand. It was found that the inclusions improved the ultimate strength of the mixture, while not significantly changing the mixture's initial stiffness or ductility. The volumetric strain for the fiber-reinforced sand was initially compressed and followed by the expansion (dilation) greater than in unreinforced sand. They found that the cohesive intercept did not appreciably change with addition of fibers; however, the friction angle increased with the added fibers and fiber length. Furthermore, Consoli et al. (2003) found that the compacted sandy soil reinforced with randomly distributed polypropylene fibers showed a marked hardening behavior at strains up to 20 percent. Figure 2.4 reveals that the volumetric behavior was affected by the inclusion of fibers, as reinforced specimens are slightly expansive at low confining stresses but compressive at higher confining stresses.

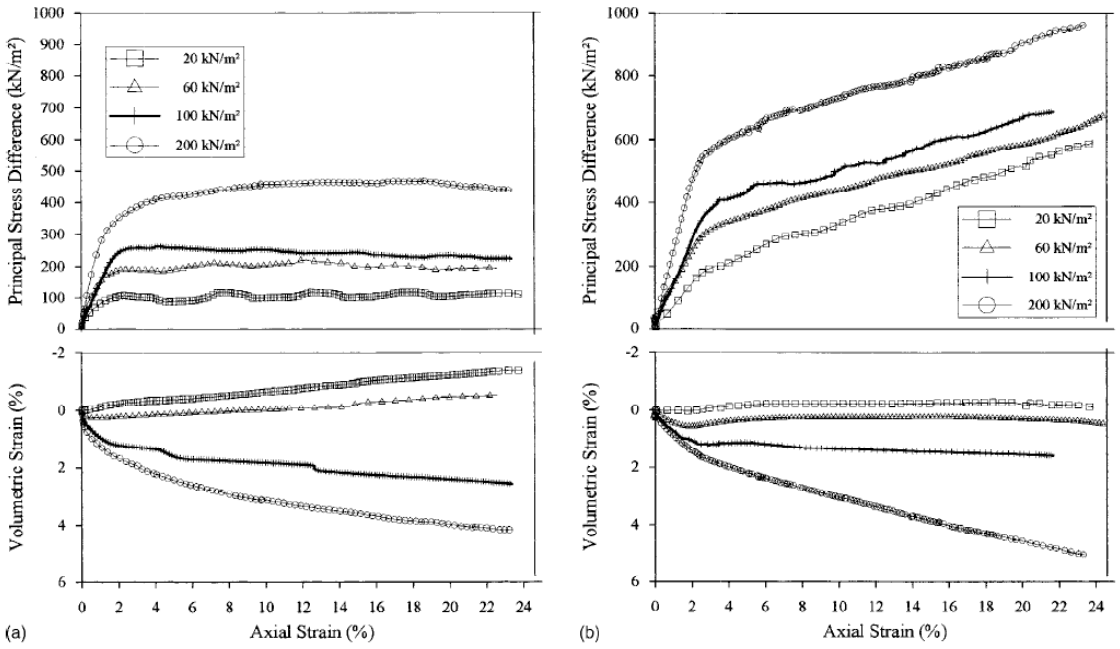

Figure 2.4 Deviator stress and volumetric strain versus axial strain for (a) compacted sandy soil, and (b) compacted fiber-reinforced sandy soil (from Consoli et al. 2003).

Michalowski and Čermák (2003) reported results from drained triaxial compression tests on specimens of fiber-reinforced granular soil. It was found that the addition of a small amount of synthetic fibers increases the failure stress of the composite (Figure 2.5a). They also found that addition of fibers to the sand inhibits its dilatancy (Figure 2.5b). The initial stiffness was not significantly affected at low fiber contents (0.5 percent). However, a substantial drop in the initial stiffness was observed as an increase in the strain at failure at higher fiber contents (2.0 percent). They found that benefit results from the increased inclusion of fibers and subsequent increases in fiber content and aspect ratio, but the benefit depends on the relative size of the soil grains and fiber length.

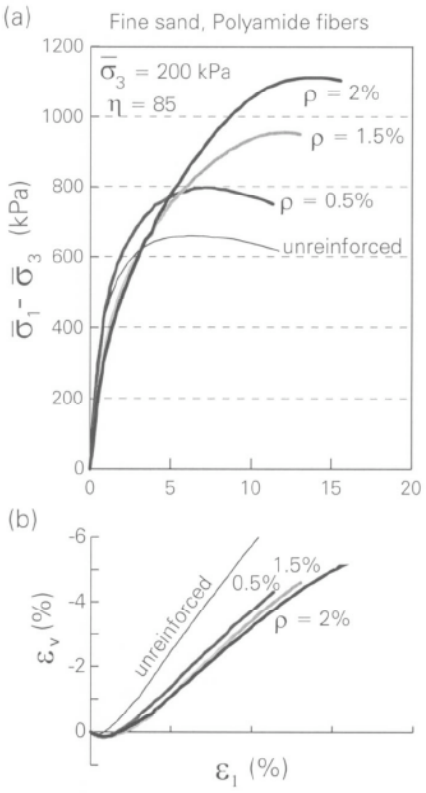

Figure 2.5 Triaxial compression tests on fine sand reinforced with polyamide fibers: a) stress-strain responses, and b) volumetric behaviors (from Michalowski and Čermák, 2003).

In order to investigate the effect of fiber-reinforced soils over a wide range of strains and displacements, Heineck et al. (2005) carried out bender element tests (very small strains), consolidated-drained triaxial compression test (small to intermediate shear strains) and ring shear tests (very large displacements) on silty sand, uniform sand, and bottom ash reinforced with randomly distributed polypropylene fibers. The results showed a marked influence of fiber reinforcement on the ultimate strength, with no loss on shear strength up to very large displacements. However, the inclusion of fibers was not observed to influence the initial stiffness of the materials studied at very small strains. The stress-strain-volumetric behavior evident in the *CD* tests is shown in Figure 2.6. The

authors observed that when comparing unreinforced to reinforced specimens at the same effective confining stress, the volumetric strains during the shearing of the Botucatu residual soil (BRS) were not affected by fiber reinforcement. On the other hand, the volumetric strains during the shearing of the Osorio sand appeared to be slightly affected by fiber reinforcement, particularly at large shear strains.

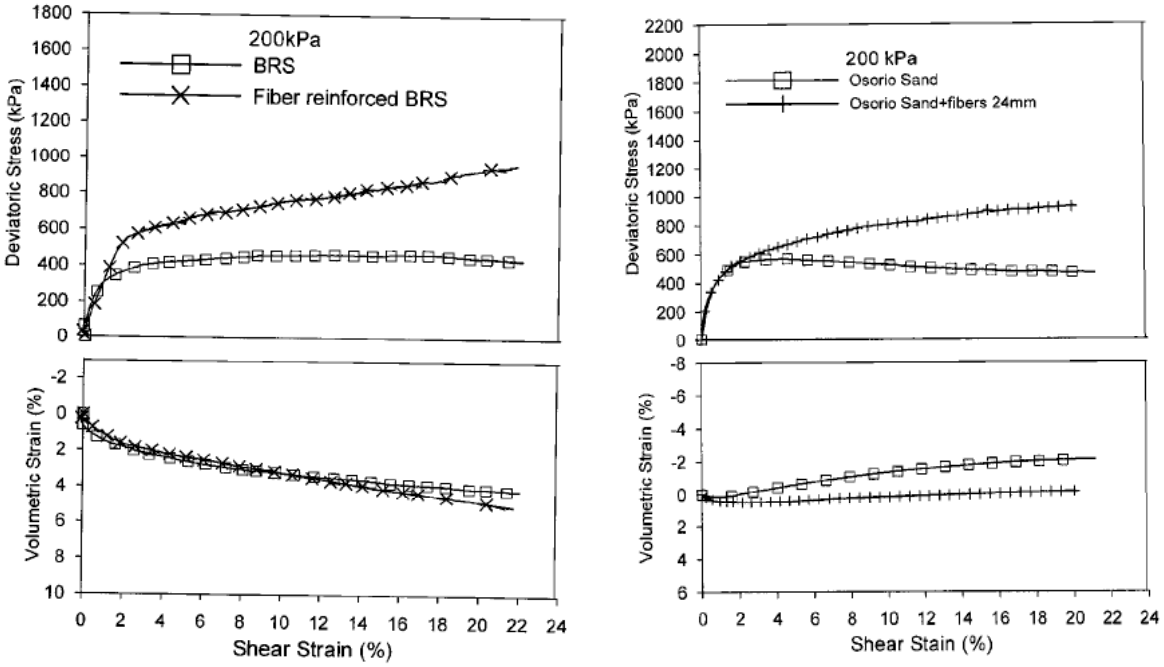

a) Botucatu residual soil (BRS) b) Osorio sand

Figure 2.6 Stress-strain-volumetric responses from the triaxial compression tests on silty sand and uniform sand reinforced with polypropylene fibers: a) Botucatu residual soil (BRS), and b) Osorio sand (from Heineck et al. 2005).

Much of the existing research has concentrated on the behavior of fiber-reinforced granular (i.e. sand) or clay in terms of total stresses (i.e. direct shear tests and unconfined compression tests) or effective stresses under drained loading conditions. The data gathered by these investigators has not been evaluated in terms of what contributions to fiber-reinforced soil behavior are possible when considering pore pressure under

undrained conditions. Given the many engineering applications involving both drained and undrained conditions and the scarcity of published investigations that address fiber-reinforced soils under such conditions, further study on the behavior of fiber-reinforced silty soil in terms of effective stresses under drained and undrained conditions is imperative.

2.3 Shear Strength Parameters for Fiber-Reinforced Soils

Gregory and Chill (1998) performed direct shear and drained triaxial compression tests on both fat clay (CH) and lean clay (CL) reinforced with randomly distributed, fibrillated polypropylene fibers to study shear strength parameters in comparison to unreinforced specimens. Both effective cohesion intercept and effective friction angle increased due to inclusion of fibers. It also found that the effective shear strength increased in a range of 20 to 50 percent for the fiber-reinforced specimens. Similar increases in shear strength parameters using fiber-reinforced soils have been reported by the other investigators (Gray and Maher 1989, Maher and Ho 1994, Nataraj and McManis 1997, Kumar et al. 2006). Consoli et al. (1998) observed an increase in the angle of internal friction as a result of fiber inclusion, but the cohesion intercept was only slightly affected by fiber reinforcement. In addition, Consoli et al. (2002) found that the cohesion intercept did not change as the friction angle increased with fiber content and fiber length. However, Nataraj and McManis (1997), and Romero (2003) found that the addition of fiber reinforcement with soil resulted in a significant increase in the angle of internal friction and the cohesion intercept. Prisco and Nova (1993), Bauer and Oancea

(1999), and Consoli et al. (2003) discovered the friction angle to be barely affected by fiber inclusion, whereas the cohesion intercept increased with increasing fiber content.

As it can be seen, there is a contradictory situation along with the available research data. Some literature found that inclusion of fibers contributed to increase in the friction angle of unreinforced soil. Several research results showed that the cohesion intercept increased with additional fiber content for reinforced specimens. It is not clear that which statement is correct or both are correct. Therefore, additional tests of fiber-reinforced soils are needed to confirm the response with different loading conditions.

2.4 Load Transfer Mechanics for Fiber-Reinforced Soils

Numerous investigators have conducted experiments on many aspects of fiber-reinforced soils. However, the consideration of the load-transfer mechanism for fiber-reinforced soil has been rarely addressed. The remainder of this chapter highlights the fundamental concepts from the literature that were integral for developing the constitutive model are presented in this research.

The simplest model was proposed by Waldron (1977) to describe the Mohr-Coulomb equation for the soils reinforced with plant roots. In this model, the shear strength of a fiber-reinforced soil (s_f) was defined as

$$s_f = c + \sigma \tan\phi + \Delta S \qquad (2.1)$$

in which c and ϕ are respectively the cohesion intercept and angle of internal friction for the Mohr-Coulomb failure envelope of the unreinforced soil, σ is the normal stress on the failure plane, and ΔS is the increase in strength attributed to the fiber reinforcement.

The basic load-transfer model used in predicting shear strength was created by Gray and Ohashi (1983) and is shown in Figure 2.7. The model is based on the simple direct shear test, which assumes the shear occurs along a discrete zone of soil. As the soil is sheared, tensile forces (T_R) are developed in fibers crossing the shear zone as a result of the pullout resistance provided by the interface friction. The interface friction occurs between the soil matrix and the length of fiber anchored outside of the shear zone. The magnitude of the tensile force (T_R) is a function of the shearing resistance at the fiber-soil interface.

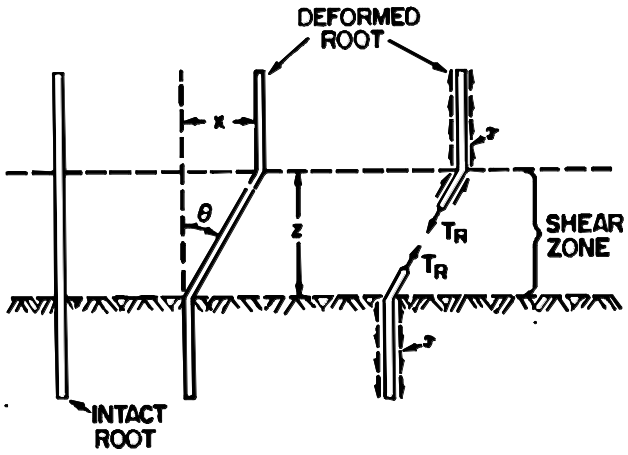

Figure 2.7 Basic model of load transfer for fiber-reinforced soils (from Gray and Ohashi, 1983).

Romero (2003) described that fibers intersecting the shear zone may provide additional resistance to shearing in two ways. Firstly, increased shear resistance arises from an increase in the normal stress acting on the shear zone induced by the component of T_R (Figure 2.7) which acts perpendicular to the shear zone. Secondly, increased shear resistance arises from the direct resistance to the shearing stresses provided by the

component of T_R that acts parallel to the shear zone. Both the normal (perpendicular direction) and shear (parallel direction) components of the reinforcement force act to increase the overall shear resistance of the soil reinforced with fibers over the resistance provided by the same soil without reinforcing fibers.

2.5 Model for Predicting Strength of Fiber-Reinforced Soils

Maher and Gray (1990) proposed a force-equilibrium model combined with statistical analysis for randomly distributed fiber-reinforced sand. The authors adopted Naaman (1972) statistical theory for composite materials to account for the fiber orientation and quantity at an arbitrarily chosen plane. In addition, previous work by the Waldron (1977) and Gray and Ohashi (1983) considered the contribution of randomly distributed fibers and increased shear strength of the reinforced sand. The shear strength increase from the fiber reinforcement, ΔS, was estimated to be:

$$\Delta S = N_f \left(\frac{\pi d^2}{4}\right)\left[2\left(\sigma_{conf} \tan\delta\right)\frac{l}{d}\right]\left(\sin\theta + \cos\theta\tan\phi\right)\left(\xi\right) \qquad (2.2)$$

for $0 < \sigma_{conf} < \sigma_{crit}$, and

$$\Delta S = N_f \left(\frac{\pi d^2}{4}\right)\left[2\left(\sigma_{crit} \tan\delta\right)\frac{l}{d}\right]\left(\sin\theta + \cos\theta\tan\theta\right)\left(\xi\right) \qquad (2.3)$$

for $\sigma_{conf} > \sigma_{crit}$

in which N_f is the average number of fibers per unit area crossing the shear plane, d is the fiber diameter, l is the length of fibers, σ_{conf} is confining stress, is δ fiber skin friction (degrees), θ is the angle of shear distortion (Figure 2.7), ϕ is the angle of internal friction of sand, and ξ is an empirical coefficient depending on sand granulometry and

fiber parameters. The investigators found that this model was a reasonable agreement between predicted and experimental values at a range of confining stresses.

Ranjan et al. (1996) performed a study of the reinforcement mechanism and the influence of fiber properties to propose an empirical model for the analysis of fiber-reinforced cohesionless soils. Since discrete fibers were randomly distributed in the soil samples, the position, direction, and number of fibers crossing a shear plane was difficult to estimate. Therefore, the authors conducted a regression analysis of the triaxial compression tests results to bring out the effect of the soil/fiber parameters and the confining stress of reinforced soil. The resulting illustrates shear strength of fiber-reinforced sand, σ_f, is:

$$\sigma_f = f(\omega_f,\ l/d,\ f^*,\ f,\ \sigma_{conf}) \qquad (2.4)$$

in which ω_f is weight fraction of fibers, f^* is the modified coefficient of soil/fiber surface friction, f is a modified coefficient of friction (effect of both c and ϕ), and σ_{conf} is the confining stress. The authors found that the model predictions in shear strength agreed reasonably well with the experiment results of the shear strength of uniformly graded cohesionless soils (Figure 2.8).

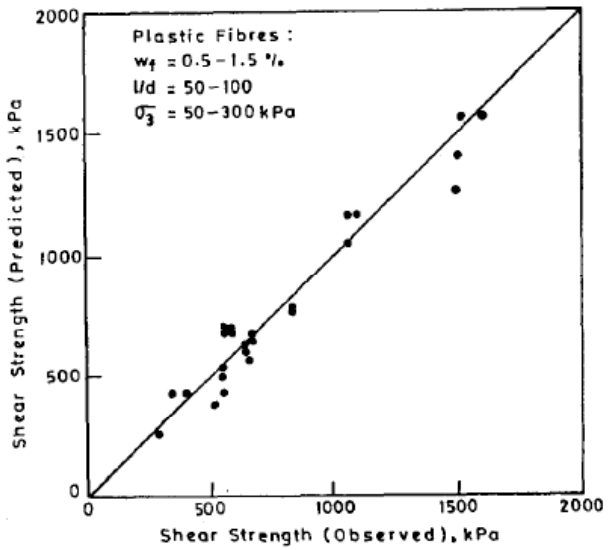

Figure 2.8 Predicted versus observed shear strength of plastic fiber-reinforced soils (from Ranjan et al. 1996).

Michalowski and his colleagues used energy-based homogenization technique to describe the yielding of fiber-reinforced sand in a plane strain condition (Michalowski and Zhao, 1996; Michalowski and Čermák, 2003). The authors developed a model for the prediction of failure stress in triaxial compression based on the frictional interaction of fiber and sand. The model was limited to cylindrical monofilament fibers with an isotropic distribution of fiber orientation, and the failure criterion developed was not applicable to fibrillated polypropylene fibers. There were five parameters needed to predict the failure stress: volumetric fiber content (ρ), fiber aspect ratio (η), fiber yield stress, soil/fiber interface friction angle, and internal friction angle of the granular matrix. The model's predictions of the failure stress for fiber-reinforced sand were in fairly good agreement with the laboratory results (Figure 2.9).

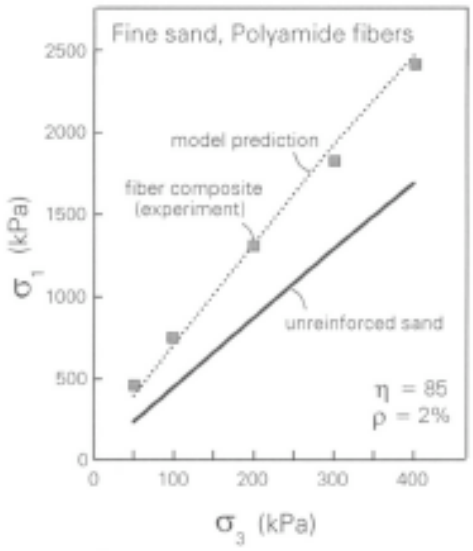

Figure 2.9 Comparison of prediction and experimental results for fine sand reinforced with polyamide fibers (from Michalowski and Čermák, 2003).

Zornberg (2002) and Li and Zornberg (2005) proposed a method for designing the fiber-reinforced soil slopes using a discrete framework to characterize the contribution of randomly distributed fiber inclusion to stability. This approach predicted an "equivalent" shear strength of the fiber-reinforced soil based on the independent properties of the soil specimens and fibers. The included fibers' behavior was assumed to be similar to that of discrete reinforcing elements that contribute to stability by mobilizing tensile stresses along the shear plane. Therefore, this method requires the testing of individual soil and fiber samples, but not of fiber-reinforced soil specimens to characterize the performance. The authors found that the fiber-induced tension was a function of volumetric fiber content, soil/fiber interface shear strength, and fiber aspect ratio. The authors conducted triaxial tests on unreinforced and fiber-reinforced specimens to validate the discrete methodology. The predicted results were found to agree well with the laboratory results

and the contribution of randomly distributed fibers in terms of fiber content and fiber aspect ratio (Figure 2.10).

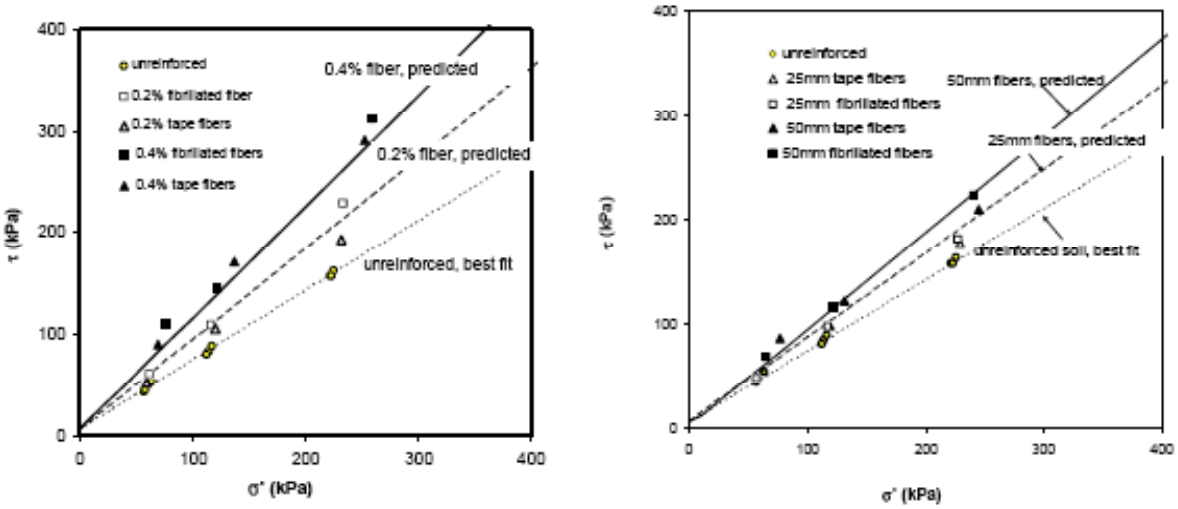

a) Effect of fiber content

b) Effect of fiber aspect ratio

Fiqure 2.10 Comparison of the predicted and experimental results for a) effect of fiber content, and b) effect of aspect ratio on the shear strength (from Li and Zornberg, 2005).

Most of the existing models used to predict the shear strength of soils reinforced with randomly discrete fibers are based on limit equilibrium, statistical analysis, and failure criteria methods. Such approaches can be partially insufficient. Based on published results (Ang 2001, Romero 2003, and Consoli et al. 2003), the failure of fiber-reinforced soils normally occurs at very large strains when compared to unreinforced soil specimens and exhibit a strain-hardening type behavior with no noticeable failure. The increase in strength of fiber-reinforced soils with respect to unreinforced soil is partially due to the resistance to strain provided by the inclusion of fibers within the soils. Since fibers can be considered essentially plastic material, the strength increase associated with the strain increase may be large. Therefore, significant strains may be required to achieve

the full strength of the fiber-reinforced soil. For some cases, displacements are controlling design parameters, so failure based models that do not consider strain levels may be of little help.

To analyze displacements, it is necessary to formulate a constitutive model to predict the stress-strain behavior of the fiber-reinforced soils at appropriate strain levels. Such models should include the constitutive law of the material composite, the soil, synthetic fibers and the soil/fiber interaction.

2.6 Constitutive Models for Fiber-Reinforced Soils

Some efforts have been made to develop constitutive models for predicting the stress-strain behavior of fiber-reinforced soils. Most common are models describing the response of granular soils and municipal solid waste (MSW) that is reinforced with randomly distributed fibers (threads). These models will be described in more detail below.

Prisco and Nova (1993) proposed a constitutive model for uniform granular sand reinforced by continuous threads of synthetic fibers. The model assumed the thread-reinforced soil could be seen as a continuum obtained by the superposition of two continua. One continua was unreinforced soil, and the other was a fictitious medium that was able only to sustain tensile stresses up to a certain failure level. Moreover, it was assumed that the two continua would act in a parallel manner so that strains would be the same. The authors found that this model made it possible to reproduce an acceptable agreement for the deviatoric stress-strain behavior of the fiber-reinforced soil in drained triaxial compression tests. However, the model was neither able to predict the peak

stresses under different confining stresses (Figure 2.11a), nor was it able to reasonably reproduce the volumetric behavior of the reinforced soil (Figure 2.11b). The predicted dilatancy at failure was greatly over-predicted.

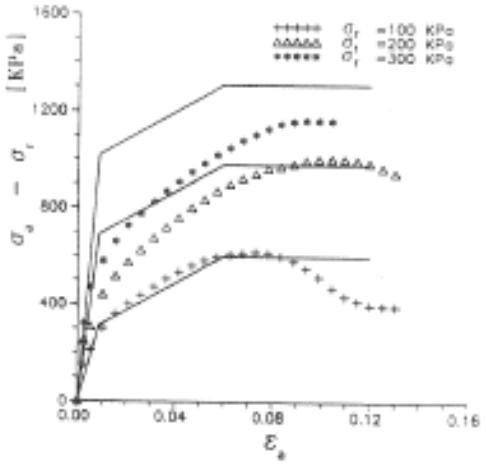

(a) Deviatoric stress versus axial strain

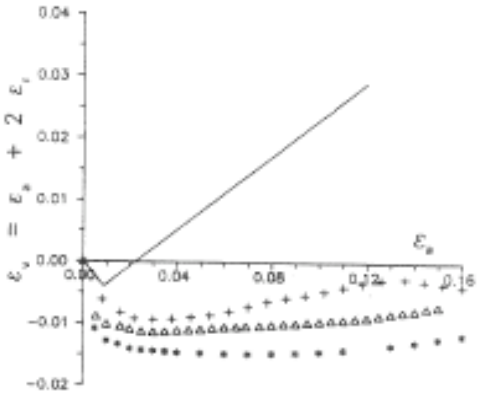

(b) Volumetric strain versus axial strain

Figure 2.11 Comparison of predicted and measured response of reinforced sample for Di Prisco and Nova model: (a) deviatoric stress versus axial strain, and (b) volumetric strain versus axial strain (from Prisco and Nova, 1993).

Jouve et al. (1995) introduced a formulation of elastoplastic constitutive relations to predict the behavior of fiber-reinforced sand by using five model parameters. It was assumed that the reinforced threads acted isotropically and only sustained tensile forces, which was considered as an elastic and non-linear response. The comparison between the

simulation and experimental results (Prisco and Nova, 1993) is shown in Figure 2.12. The numerical solutions revealed a reasonable agreement with the experimental data. The difference between the two predictions was due to the elastic perfectly plastic behavior of reinforced specimens as previously assumed by Prisco and Nova's model. In addition, the authors found the same divergent results when considering the model versus the test data for predicting the volumetric strain of reinforced sand. Jouve et al. (1995) concluded that the divergence might be due to the model's simplicity as well as the level of possible unreliability when measuring volumetric strain, suggesting more triaxial tests are needed to explain this difference.

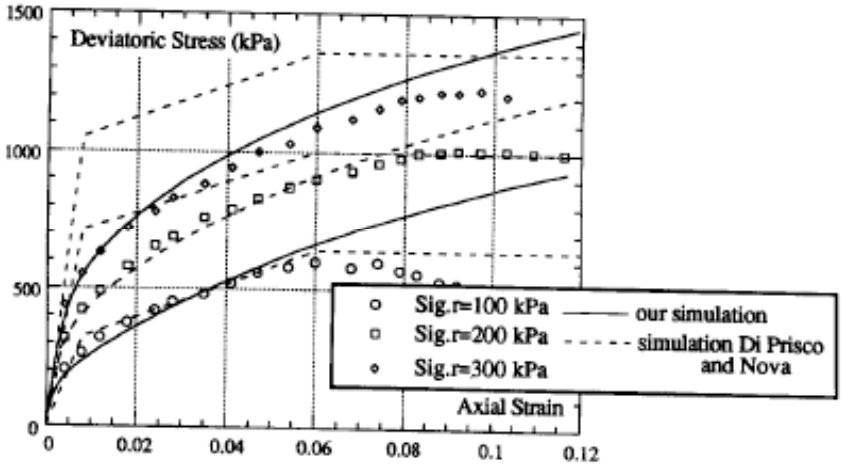

Figure 2.12 Comparison of numerical prediction and experimental response of reinforced sample of deviatoric stress versus axial strain (from Jouve et al., 1995).

Machado et al. (2002) proposed a framework to model the mechanical behavior of MSW based on triaxial compression tests on large samples. The overall behavior of the MSW was assumed to be the result of considering two distinct parts, the mechanical behavior of the paste (soil) and the synthetic fibers (presented to be composed by many types of polymers). A critical state framework for MSW paste and an elasto-plasticity framework for waste fibers were used to represent the main MSW characteristics. Of particular interest is the consideration of pullout stress for the fibers inside the MSW as a function of both the normal stress and the bonded length. To account for this, the authors considered the Young's modulus of the fibers (E_f) to be dependent on the radial stress (σ_r)

$$E_f = E_u + a_f \sigma_r \tag{2.5}$$

in which E_u is Young's modulus of fibers measured in tension test and a_f is a MSW fiber parameter. The range of a_f was chosen from 1,200 to 2,000, which was determined by adjusting the model to certain known MSW stress-strain responses. The increments of the elastic shear strain of the fibers ($d\varepsilon_{qf}$) are calculated as a function of the increments in the elastic shear strain of the paste ($d\varepsilon_{qp}$) through a mobilization function of the fibers (f_m)

$$d\varepsilon_{qf} = f_m d\varepsilon_{qp} \tag{2.6}$$

The authors assumed the fiber mobilization function to be described as,

$$f_m = \frac{2}{\pi} \tan^{-1}\left[\left(\frac{q}{p'}\right)^2\right] \tag{2.7}$$

with its value tending toward 1 for high values of q/p' ,where q is deviatoric stress, and p' is mean effective stress.

Machado et al. (2002) conducted a series of consolidated-drained triaxial compression tests on large MSW samples in order to compare the stress-strain behavior with the predicted stress-strain response. They concluded that the proposed model was capable of reproducing the stress-strain behavior of the MSW quite well up to large strains (Figure 2.13). In addition, the model was able to predict a decrease in volumetric strain as the confining stress increased. However, there was a tendency to overestimate the volumetric stain at a given shear strain under higher confining stresses.

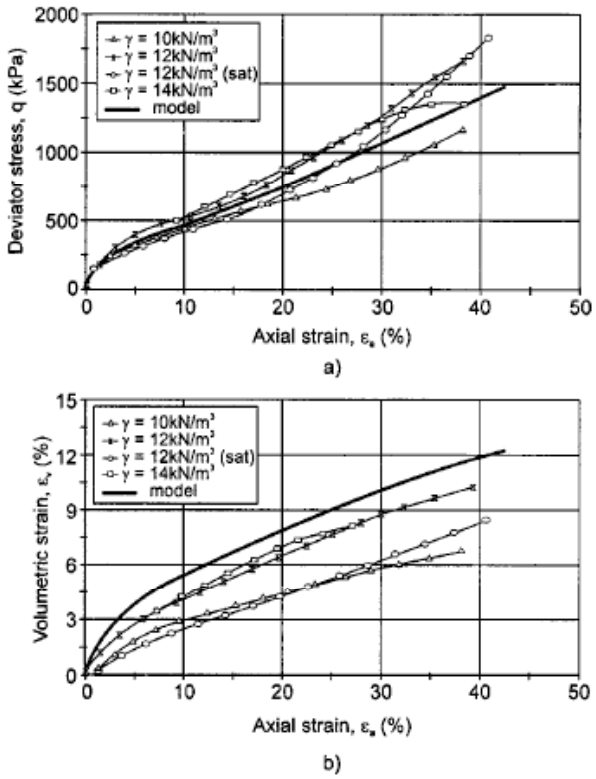

Figure 2.13 Comparison of experimental and predicted response of triaxial compression tests at confining stress of 400 kPa: a) deviatoric stress versus axial strain, b) volumetric strain versus axial strain (from Machado et al., 2002).

Ding and Hargrove (2006) carried out theoretical and experimental analyses to understand the effects and mechanisms of randomly oriented flexible fiber reinforcements for soil-fiber mixtures. The soil reinforced with fiber was viewed as a composite material. It was assumed that the nonlinear stress-strain behavior of the reinforced soil could be derived based on the nonlinear elastic response of the soil and the linear elastic response of the geofibers. The authors proposed a nonlinear stress-strain relationship for fiber-reinforced soil based on a homogenization technique to explain the effects of the fiber content, distribution, geometrical features, and the shear modulus of reinforced soils. It was assumed that there would be no slip at the soil/fiber interface and no breakage of fibers. The model describes shear modulus as the number of fibers and the axial strain affect (Figure 2.14a). When compared, the model calculations and the testing results demonstrated good agreement with each other in a stress-strain relationship (Figure 2.14b) of up to 10 percent strain. However, the model did not reproduce the stress-strain response of fiber-reinforced soil after slippage occurred at the soil/fibers interface, resulting in fiber breakage.

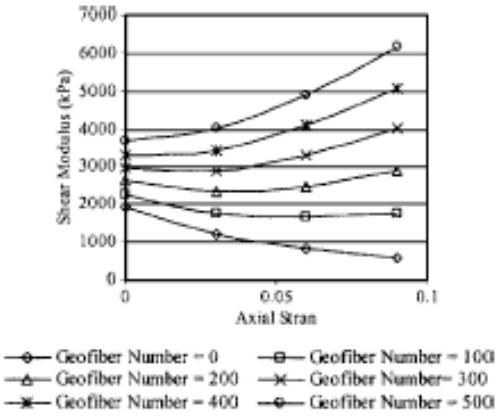

(a) Shear modulus versus axial strain based on model calculations

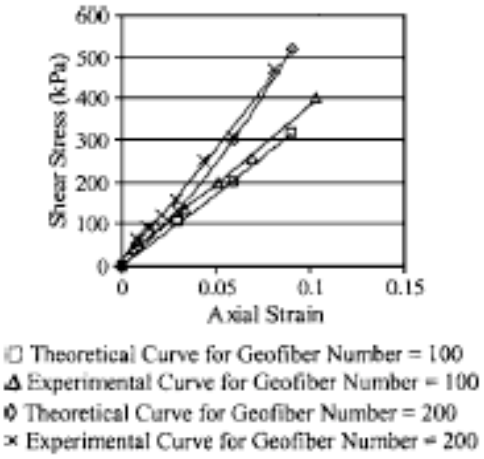

(b) Shear stress-strain behavior of experimental data and model simulations

Figure 2.14 Predicted results for geofibers reinforcing with soils: a) Shear modulus versus axial strain based on model calculations, b) Shear stress-strain behavior of experimental data and model simulations (from Ding and Hargrove, 2006).

A constitutive model is needed to predict the effective stress-strain-pore pressure change and effective stress-strain-volume change behavior of fiber reinforced soils based on the mechanical behavior of unreinforced soil and the response of the fibers' properties. The review of literature provided here reveals that the stress-strain behavior of fiber-reinforced soils can be reproduced by the superposition of deviatoric stress from the soil and response of fibers.

2.7 Summary

Research has been conducted over the last few decades to evaluate the basic shear strength properties and the deformation characteristics of fiber-reinforced soil. These studies have led to the development of soil improvement technique for many applications in geotechnical engineering practice. However, the review of literature shows significant gaps in the study of fiber-reinforced silts and clays, despite the growing prevalence of applications that include the use of reinforced soils. Furthermore, the literature review demonstrates the existence of few published results on the behavior of fiber-reinforced silty soil in terms of effective stresses under both drained and undrained conditions. In addition, there are inconsistencies in the fiber-reinforced behavior in terms of shear strength parameters. These inconsistencies can be attributed to previous investigators' excessively broad focus of experimentation relevant to material properties (soils and fibers) and testing conditions. As a result, the stress-strain pore pressure change and the volume change characteristics of reinforced soil under undrained and drained loading conditions have been ignored. This examination is required to develop a constitutive model for predicting the fiber-reinforced soil behavior that will encourage the use of fiber-reinforced soil in engineering projects.

CHAPTER 3: UNDRAINED BEHAVIOR OF FIBER-REINFORCED SOILS

3.1 Introduction

This chapter describes test materials, specimen preparation methods, and research programs undertaken in this research. A series of triaxial compression tests was performed to evaluate the stress-strain-pore pressure change behavior of fiber-reinforced soils under undrained loading conditions. Results of the consolidated-undrained triaxial compression tests are presented and discussed.

3.2 Test Materials

The first soil used in this research is silty sand from Mound City, Missouri. The soil has a liquid limit of 27 and a plastic limit of 25 (plasticity index of 2). The clay size fraction (percent finer than 2 mm) is approximately 16 percent. The specific gravity of the soil solids is 2.66 (ASTM D854). The soil is classified as silty sand (SM) according to the Unified Soil Classification System (ASTM D2487). The maximum dry unit weight and optimum moisture content of the soil are 110 lb/ft^3 (17.3 kN/m^3) and 16 percent, respectively, according to the Standard Proctor Test (ASTM D698).

The other soil tested is commercial Ottawa sand (Grade F-75), a well-known, laboratory-tested sand. The particles have a mean diameter (D_{50}) of 0.18 mm, a uniformity coefficient (C_u) of 1.7, a minimum void ratio ($e_{\min}$) of 0.46, a maximum void ratio ($e_{\max}$) of 0.77, and a specific gravity of 2.65. According to the Unified Soil Classification System, Ottawa sand is classified as poorly graded sand (SP).

The fibers used consist of commercially available 2-inch (51-mm), long fibrillated polypropylene fibers of 3600-denier. The specific gravity of the fibers is 0.91 gr/cm^3 (ASTM D792). The ultimate tensile strength (ASTM D2256) and modulus of elasticity (ASTM D2101) of the fibers are 45 ksi (310 MPa), and 700 ksi (4830 MPa), respectively.

3.3 Sample Preparation

Soil samples for all tests were prepared in the same manner to ensure consistency in the unreinforced and fiber-reinforced specimens. Large batches of soil were air dried at room temperature and then pulverized using a mechanical grinder. The soil used to prepare the unreinforced specimens was mixed in large quantities to achieve the desired moisture content by adding tap water to the soil in a mechanical mixer. After mixing, the soil was allowed to hydrate overnight prior to mixing with fibers.

All reinforced silty sand samples were prepared by adding fibers equivalent to either 0.2 percent or 0.4 percent of the soil's dry weight. Specimens were mixed to the desired moisture content that following the two-stage procedure suggested by Gregory (1996). The soil was first mixed with 70 percent of the total amount of water needed to bring the sample to the desired water content and allowed to hydrate overnight. Then, the fibers were uniformly distributed among the soil in five layers, and mixed in a mechanical mixer while the remaining 30 percent of the water was added to bring the soil to the desired water content. After the soil and fibers were mixed to the desired water content, the loose mixture was inspected and, if needed, mixed by hand to ensure that the fibers were uniformly distributed. The soil-fiber mixture was then again allowed to hydrate overnight prior to compaction.

After mixing, all silty sand specimens were compacted in a 2.92-in (74-mm) diameter by 5.7-in (145-mm) mold using a compactive effort equal to that used in the Standard Proctor (12,400 ft-lb/ft^3 or 600 kN-m/m^3). The compactive effort was held constant for all molding water contents. Prepared samples contained water content of 2 percent wet (18 percent water content) and 6 percent wet (22 percent water content) of the Standard Proctor optimum moisture content. Afterwards, specimens were extruded from the mold using a hydraulic jack extruder and immediately placed in the triaxial chamber. Slotted filter paper was placed around the specimens to reduce the drainage path in order to speed up saturation and consolidation. A thin, 0.012-in (0.3-mm) latex membrane was used to separate the specimens from the cell water.

An undercompaction process (Ladd, 1978) was selected to produce homogeneous samples using the Ottawa sand in the laboratory-testing program. Unreinforced and fiber-reinforced Ottawa sand samples were prepared and mixed to nominal 10 percent water content for "loose" sand specimens and 3 percent water content for "medium-dense" sand specimens, which had nominal relative densities equal to 10 percent ($e_0 = 0.74$) and 55 percent ($e_0 = 0.60$), respectively. These mixtures were also allowed to hydrate overnight prior to compaction.

The sand specimens studied were prepared according to the five-step procedure for sand specimen preparation suggested by Bardet (1997). First, four equal amounts of Ottawa sand were measured (based on the undercompaction calculation) and placed in a bowl to be compacted. Second, a thin, 0.012-in (0.3-mm) thick latex membrane along with two O-rings was placed at the bottom of a split mold. The membrane was then folded back from the top rim of the mold as shown in Figure 3.1. Third, the air between

the membrane and spilt mold was expelled using a vacuum pump. Subsequently, the sand or sand-fiber mixture was poured into the spilt mold, and the sand was compacted with a drop weight until the sand's desired thickness according to the calculations of the undercompaction process for each layer was reached. Fourth, the top cap was placed on the soil sample after the last layer's compaction was completed. An O-ring was then placed on the top cap and a vacuum was attached to the inside of the sample by means of valves which also connected the two drainage lines in the base of the triaxial cell. The mold was then opened and the internal vacuum that held the sample together removed. The O-rings originally placed at the bottom of the mold were roll back and were placed at the bottom of the cap to seal the membrane. Finally, the triaxial chamber was assembled filled with water.

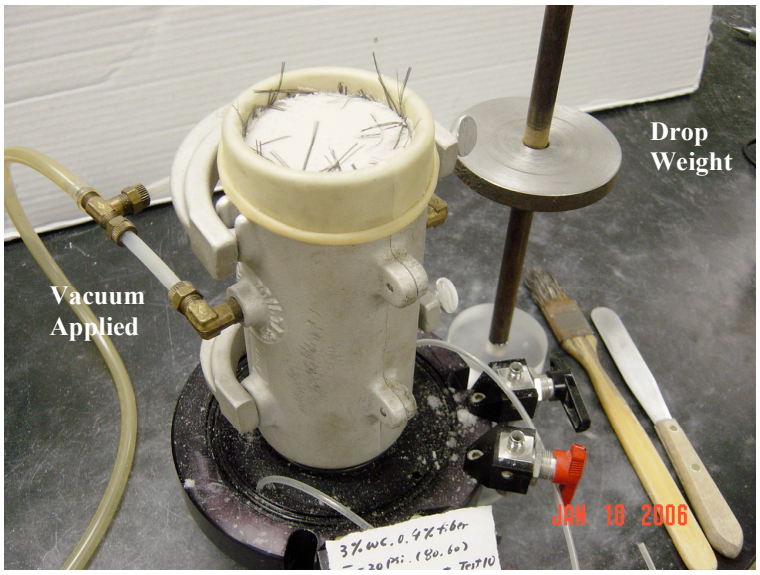

Figure 3.1 Split mold used for preparation of specimens of Ottawa sand.

All specimens were backpressure saturated at an effective consolidation stress of 2.5-psi (17.2-kPa), using the dry mounting method as specified in ASTM D4767. Skempton's (1954) pore pressure coefficient, B, was measured during saturation. Specimens were allowed to saturate until measured B-values reached at least 0.96 before consolidation and shear. Approximately 12 days were required to saturate the silty sand specimens to 0.96; 5 days were required for the Ottawa sand specimens.

Following saturation, specimens were isotropically consolidated to the target effective stress. The time corresponding to 100 percent primary consolidation (t_{100}) was less than 60 minutes for both unreinforced and fiber-reinforced silty sand specimens, and less than 1 minute for both unreinforced and reinforced Ottawa sand specimens.

The strain rate used to shear all silty sand specimens tested in triaxial tests was 1.25 percent per hour (deformation rate of 0.07-inch per hour or 1.78-mm per hour) to eliminate concern over the strain rate when comparing results from drained and undrained tests. For Ottawa sand specimens, the strain rate was 10 percent per hour (deformation rate of 0.5-inch per hour or 13-mm per hour) for all triaxial tests. Most specimens were sheared up to a maximum axial strain of 30 percent to permit evaluation of the post-peak stress-strain behavior.

3.4 Testing Program

The basic methodology for evaluating the stress-strain-pore pressure change and stress-strain-volume change behavior of the fiber-reinforced soils was to perform an extensive series of laboratory triaxial compression tests under undrained and drained loading. The response attributed to fiber0reinforced was drawn from unreinforced and fiber-reinforced specimens. The testing program consisted of approximately 86 triaxial compression tests.

Tables 3.1 and 3.2 summarized the testing program for the silty sand and Ottawa sand used to evaluate the stress-strain behavior of unreinforced and reinforced specimens in terms of effective stresses. A total of forty-six consolidated-undrained ($\overline{CU}$) triaxial compression tests (ASTM D4767) with pore pressure measurements were conducted to evaluate the stress-strain-pore pressure change behavior of reinforced and fiber-reinforced specimens under undrained loading conditions. There fifteen tests were performed on silty sand specimens compacted at 18 nominal percent water content, and another fifteen tests were performed on silty sand specimens compacted at 22 percent water content. Eight tests were conducted on "loose" Ottawa sand specimens while another eight tests were conducted on "medium-dense" Ottawa sand specimens.

Table 3.1 Triaxial Compression Tests Used to Evaluate the Stress-Strain Behavior of Unreinforced and Reinforced Specimens for Silty Sand

Type of Triaxial Testing	Fiber Content (%)	Effective Confining Stress									
		18 % Molding Moisture					22 % Molding Moisture				
		5 psi	10 psi	20 psi	40 psi	80 psi	5 psi	10 psi	20 psi	40 psi	80 psi
$\overline{CU}$	0.0	1	1	1	1	1	1	1	1	1	1
	0.2	1	1	1	1	1	1	1	1	1	1
	0.4	1	1	1	1	1	1	1	1	1	1
CD	0.0	1	1	1	1	1	1	1	1	1	1
	0.4	1	1	1	1	1	1	1	1	1	1

A total of thirty-six consolidated-drained (CD) triaxial compression tests were performed to evaluate the stress-strain-volume change behavior of unreinforced and fiber-reinforced specimens under drained loading conditions. Ten tests were performed on silty sand specimens compacted at 18 percent water content, and ten tests on specimens compacted at 22 percent water content. Eight tests were carried out on loose Ottawa sand specimens while another eight tests were run on medium-dense Ottawa sand specimens (Table 3.2). All silty sand specimens were nominally 2.92-in diameter by 5.7-in tall (74-mm x 145-mm) while all Ottawa sand specimens were nominally 2.5-in diameter by 5-in in length (64-mm x 127-mm). Tests on silty sand samples were consolidated to nominal effective confining stresses of 5, 10, 20, 40, and 80-psi (35, 70, 140, 280, and 550-kPa). Tests on Ottawa sand specimens were consolidated to effective confining stresses of 5, 20, 40, and 60-psi (35, 140, 280, and 415-kPa). Replicate tests were performed for both unreinforced and fiber-reinforced specimens to allow for directly computing the contribution of the fibers as discussed in Chapter 5.

Table 3.2 Triaxial Compression Tests Used to Evaluate the Stress-Strain Behavior of Unreinforced and Reinforced Specimens for Ottawa Sand (Chen, 2006)

Type of Triaxial Testing	Fiber Content (%)	Effective Confining Stress							
		Loose Specimens (D_r=10%)				Medium-Dense Specimens (D_r=55%))			
		5 psi	20 psi	40 psi	60 psi	5 psi	20 psi	40 psi	60 psi
$\overline{CU}$	0.0	1	1	1	1	1	1	1	1
	0.4	1	1	1	1	1	1	1	1
CD	0.0	1	1	1	1	1	1	1	1
	0.4	1	1	1	1	1	1	1	1

A series of isotropic consolidation tests was also performed to evaluate the consolidation behavior of unreinforced and reinforced specimens for the silty sand and the Ottawa sand, as summarized in Table 3.3. A total of eight isotropic consolidation tests were carried out: four on specimens of the silty sand and another four on specimens of the Ottawa sand. The specimens were consolidated to effective stresses of up to 140-psi (965-kPa). Two silty sand specimens were compacted at 18 percent water content, and two specimens were compacted at 22 percent water content. Two specimens of Ottawa sand were prepared in the "loose" condition ($D_r \approx 10\%$) and two specimens were prepared in the "medium-dense" condition ($D_r \approx 55\%$). The size of the silty sand and Ottawa sand specimens was the same as prepared for the triaxial compression tests. The results of all the isotropic consolidation tests were analyzed by comparing the stress-deformation relationship between the unreinforced and reinforced specimens. Furthermore, the compression parameters were used to predict the volumetric strain of fiber-reinforced soils and were used to model the behavior of both soils using critical state soil mechanics concepts (Wood, 1990).

Table 3.3 Isotropic consolidated behavior of unreinforced and reinforced specimens for the silty sand and the Ottawa sand

Fiber Content (%)	Silty Sand (SM)		Ottawa Sand (SP)	
	18 % Molding Moisture	22 % Molding Moisture	Loose Specimens (D_r=10%)	Medium-Dense Specimens (D_r=55%))
0.0	1	1	1	1
0.4	1	1	1	1

3.5 Results from Consolidated-Undrained ($\overline{CU}$) Triaxial Compression Tests for Silty Sand

A total of thirty consolidated-undrained triaxial compression tests were performed (Table 3.1) on unreinforced and fiber-reinforced silty sand specimens compacted at 18 percent and 22 percent nominal water content and consolidated to 5, 10, 20, 40, and 80-psi (35, 70, 140, 280, and 550-kPa) to evaluate the stress-strain-pore pressure change behavior under undrained loading conditions.

3.5.1 Stress-Strain Response

The stress-strain behavior observed in the $\overline{CU}$ tests for the unreinforced and fiber-reinforced silty sand specimens is shown in Figures 3.2 and 3.3 for samples compacted at 18 percent and 22 percent water content, respectively. The test results are plotted as deviatoric stress (q) versus triaxial shear strain (ε_q), where

$$q = \sigma_1 - \sigma_3 \tag{3.1}$$

in which σ_1 is the maximum principal stress and σ_3 is the minimum principal stress, and

$$\varepsilon_q = \varepsilon_a - 1/3\,\varepsilon_v \tag{3.2}$$

in which ε_a is the axial strain and ε_v is the volumetric strain.

The stress-strain behavior observed for the unreinforced specimens is typical of compacted soils. The peak deviatoric stress for the unreinforced specimens compacted at 18 percent water content is greater than in the samples compacted at 22 percent water content for specimens tested under the same effective confining stresses.

As shown in Figures 3.2 and 3.3, the stress-strain behavior observed for all fiber-reinforced silty sand specimens is a strain-hardening response with no noticeable peak stress at strains up to 30 percent. This has been noted in numerous previous investigations. At small strains (less than 5 percent), the deviatoric stress observed for the fiber-reinforced specimens is generally similar to the stresses observed for the unreinforced specimens tested at the same confining stresses. In contrast, at moderate strains (5 to 15 percent), the reinforced specimens tested at higher effective confining stresses (greater than or equal to 20-psi) showed slightly lower deviatoric stresses than the unreinforced specimens tested under the same conditions. The difference in terms of unreinforced and reinforced specimens tends to increase with increasing effective confining stresses, as demonstrated in Figures 3.2 (c), (d), and (e). At large strains, the deviatoric stresses observed for fiber-reinforced specimens are consistently larger than those observed for unreinforced specimens tested at the same effective confining stresses. However, the level of strain when the deviatoric stresses of the fiber-reinforced silty sand specimens became significantly greater than those of the unreinforced specimens appeared to vary along with the effective confining stresses.

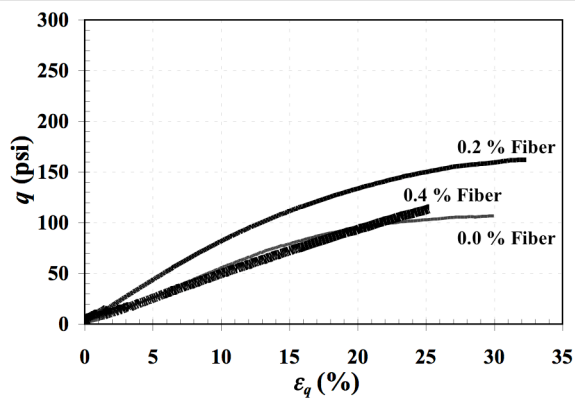

a) 5-psi effective consolidation stress

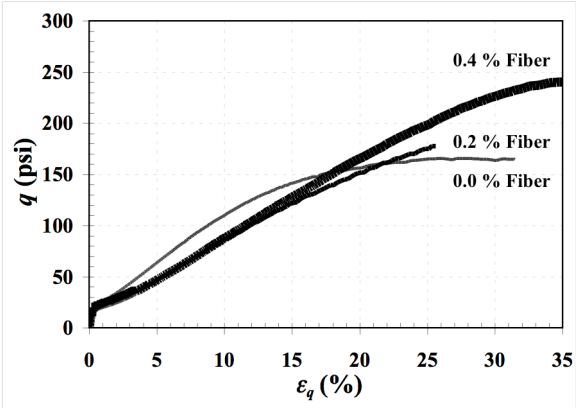

d) 40-psi effective consolidation stress

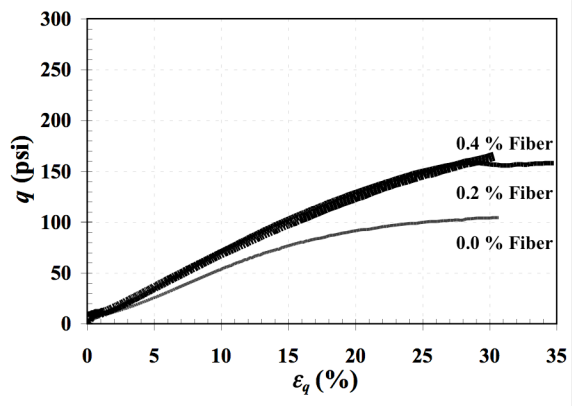

b) 10-psi effective consolidation stress

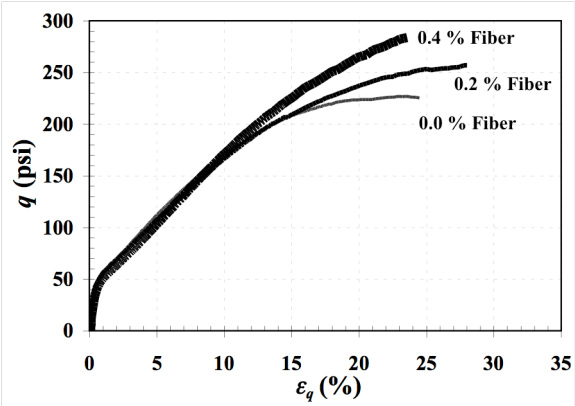

e) 80-psi effective consolidation stress

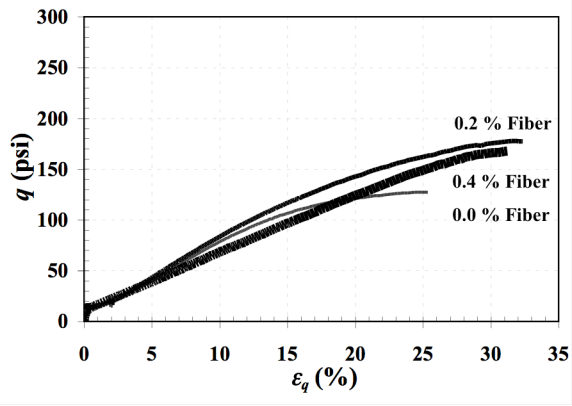

c) 20-psi effective consolidation stress

Figure 3.2 Deviatoric stress (q) versus triaxial shear strain (ε_q) curves from $\overline{CU}$ tests for silty sand specimens compacted at 18 percent water content and consolidated to: a) 5-psi effective stress, b) 10-psi effective stress, c) 20-psi effective stress, d) 40-psi effective stress, and e) 80-psi effective stress.

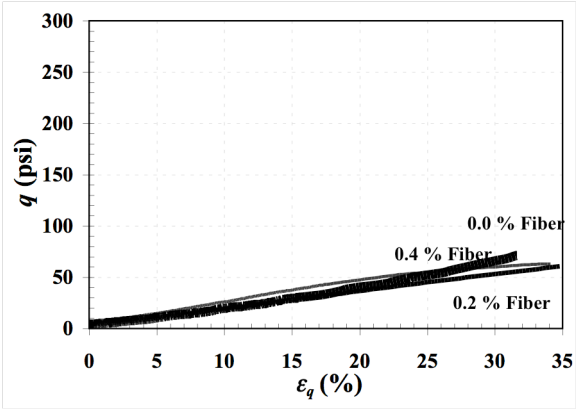

a) 5-psi effective consolidation stress

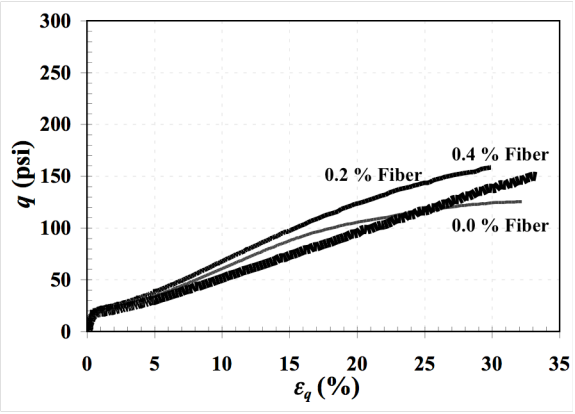

d) 40-psi effective consolidation stress

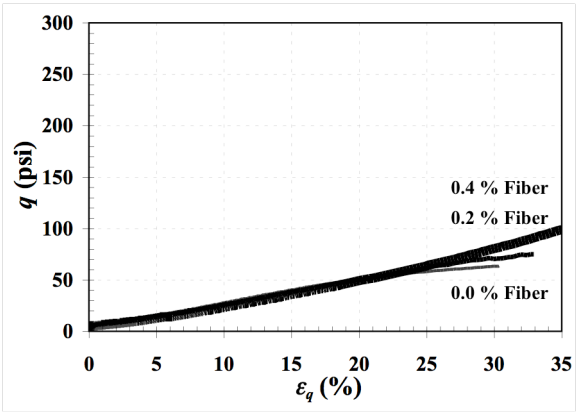

b) 10-psi effective consolidation stress

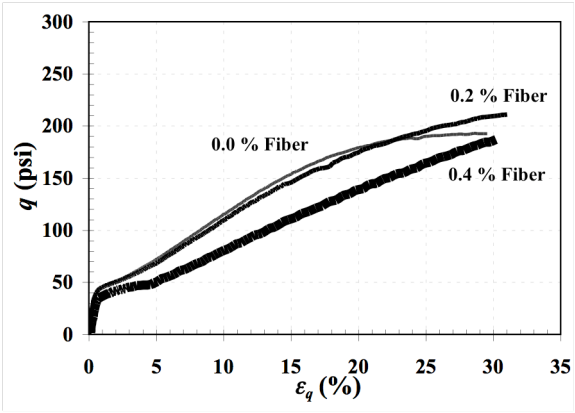

e) 80-psi effective consolidation stress

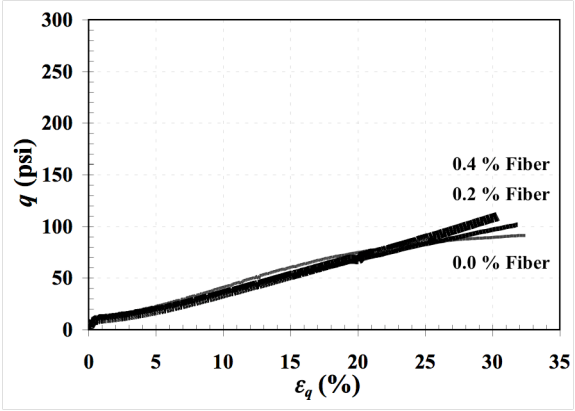

c) 20-psi effective consolidation stress

Figure 3.3 Deviatoric stress (q) versus triaxial shear strain (ε_q) curves from $\overline{CU}$ tests for silty sand specimens compacted at 22 percent water content and consolidated to: a) 5-psi effective stress, b) 10-psi effective stress, c) 20-psi effective stress, d) 40-psi effective stress, and e) 80-psi effective stress.

Figure 3.2 reveals that for specimens compacted at 18 percent water content with low effective confining stresses (less and equal to 10-psi), the deviatoric stresses of the reinforced specimens tend to become significantly greater than those of the unreinforced specimens at 5 percent strains. In contrast, at higher effective confining stresses (greater than or equal to 20-psi), the stress-strain curves begin to deviate at strains greater than 10 to 20 percent for unreinforced and reinforced specimens compacted at 18 percent water content. This occurred, in part, because the reinforcing fibers in the specimens need extra shear strain to mobilize resistance under undrained loading conditions. Furthermore, the level of strain required to begin mobilizing resistance in the fibers depends on the effective confining stress (Romero, 2003).

It is noticeable that specimens reinforced with 0.2 percent fibers consistently exhibited deviatoric stresses equal to or greater than specimens reinforced with 0.4 percent fibers at a moderate or larger strain (5 to 15 percent) for silty sand specimens at all confining stresses, as shown in Figures 3.2 and 3.3. This indicates that increasing the fiber content does not necessarily produce an increase in the deviatoric stresses for silty sand specimens. Except for the specimens reinforced with 0.4 percent fibers showed the greater deviatoric stresses than for those reinforced with 0.2 percent fibers content and compacted at 18 percent water content with higher confining stresses (grater than or equal to 40-psi). Finally, the stress-strain response of the unreinforced and fiber-reinforced specimens at all effective confining stresses began to deviate at 25 percent strain for specimens compacted at 22 percent water content.

Figure 3.4 shows the typical failure modes of the $\overline{CU}$ tests for the unreinforced and fiber-reinforced silty sand specimens compacted at 18 and 22 percent water contents. These photographs exhibit that the unreinforced specimens exhibited a budging deformation failure, while the reinforced specimens developed multiple failure plans. The random mix of fibers in the specimens tended to mobilize the shear stress in every direction among the reinforced samples, and finally deformed as multiples of failure plans when sheared to the large strains.

a) 18 % water content, 0.0 % fiber

c) 22 % water content, 0.0 % fiber

b) 18 % water content, 0.4 % fiber

d) 22 % water content, 0.4 % fiber

Figure 3.4 Typical failure modes of the $\overline{CU}$ tests at 20-psi effective consolidation stress for silty sand specimens compacted and mixed with: a) 18% water content, 0.0% fiber, b) 18% water content, 0.4% fiber, c) 22% water content, 0.0% fiber, and d) 22% water content, 0.4% fiber.

3.5.2 Effective Principal Stress Ratio-Strain Response

The effective principal stress ratio versus the shear strain response observed in the $\overline{CU}$ test results are shown for unreinforced and reinforced silty sand specimens in Figures 3.5 and 3.6 for specimens compacted at 18 percent and 22 percent water contents, respectively. In general, the effective principal stress ratios for the unreinforced specimens reach their peak at strains of 3 percent to 5 percent and remained essentially constant at a value of 3 with additional strain.

Both figures reveal a strain-hardening type of behavior for specimens reinforced with 0.4 percent fibers with no noticeable peak stresses, but for specimens reinforced with 0.2 percent fibers didn't show a strain-hardening behavior in both figures. When the effective consolidation stresses increased, however, the effective principal stress ratio decreased for the specimens reinforced with 0.4 percent fibers. In general, the effective principal stress ratios for specimens reinforced with 0.2 percent fibers reach their peak at strains 5 percent and remained essentially constant at a value of 5 with additional strain. Moreover, the effective principal stress ratio-strain response of the unreinforced and fiber-reinforced specimens begins to deviate at strains of 1 to 5 percent. The strain levels at which the effective principal stress ratio-strain curves for unreinforced and reinforced specimens began to deviate and increase with increasing effective confining stress. This occurred because the mobilization resistance in the fibers depended on the effective confining stresses, as observed in the stress-strain behavior of the fiber-reinforced specimens.

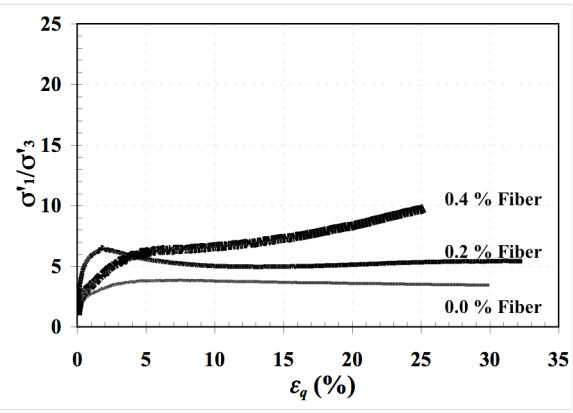

a) 5-psi effective consolidation stress

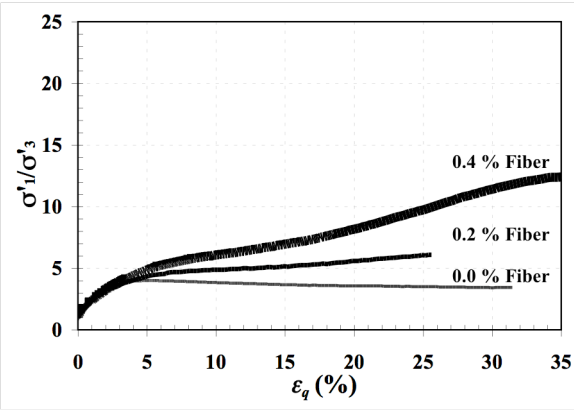

d) 40-psi effective consolidation stress

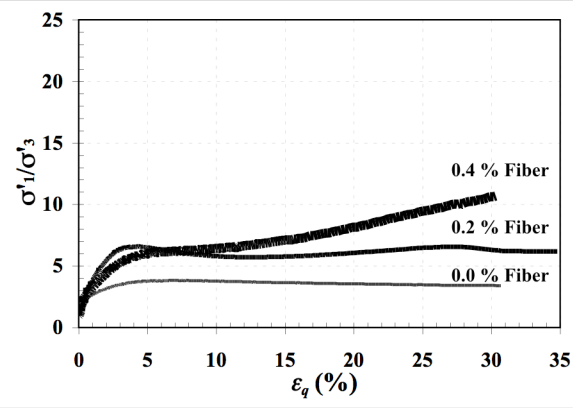

b) 10-psi effective consolidation stress

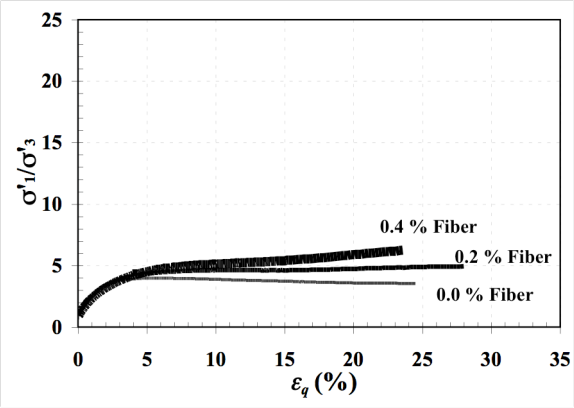

e) 80-psi effective consolidation stress

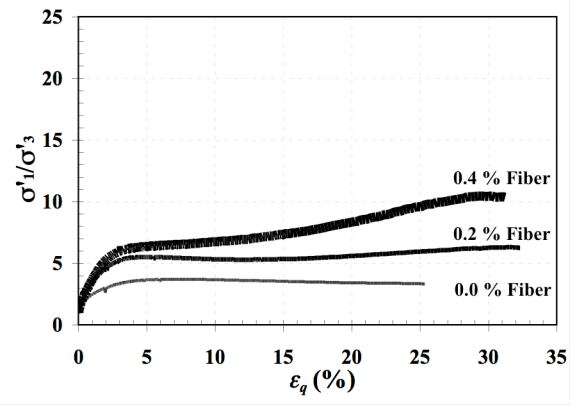

c) 20-psi effective consolidation stress

Figure 3.5 Effective principal stress ratio (σ'_1/σ'_3) versus triaxial shear strain (ε_q) curves from the $\overline{CU}$ tests for silty sand specimens compacted at 18 percent water content and consolidated to: a) 5-psi effective stress, b) 10-psi effective stress, c) 20-psi effective stress, d) 40-psi effective stress, and e) 80-psi effective stress.

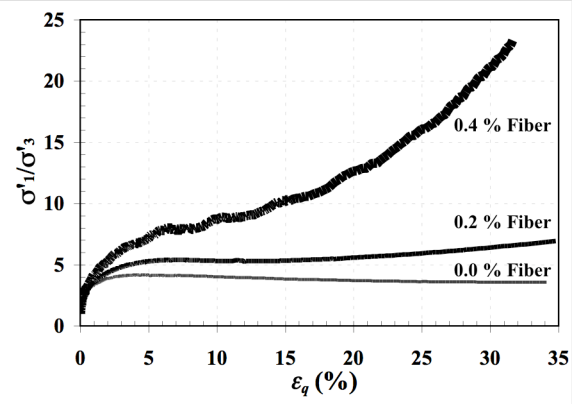

a) 5-psi effective consolidation stress

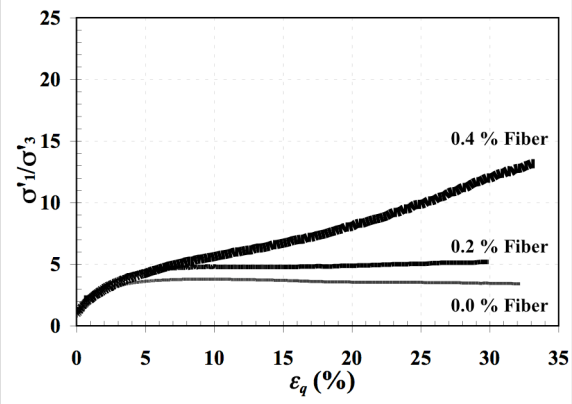

d) 40-psi effective consolidation stress

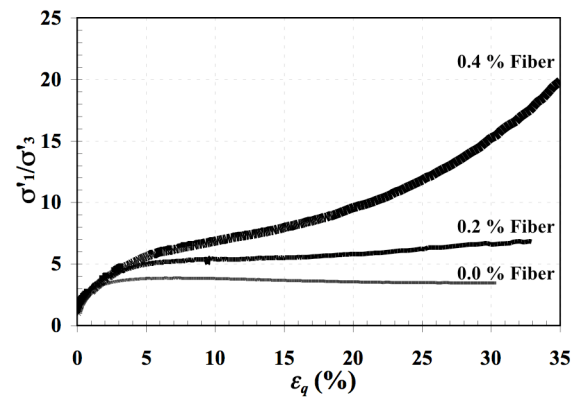

b) 10-psi effective consolidation stress

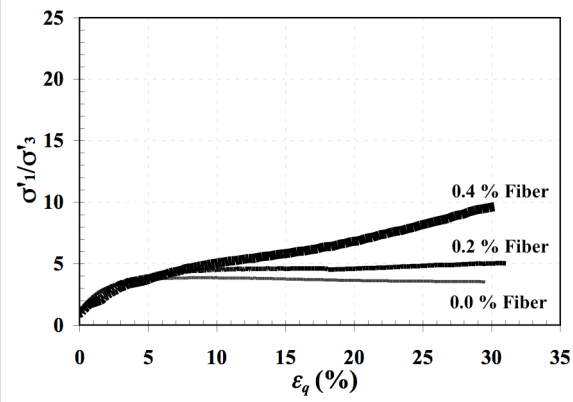

e) 80-psi effective consolidation stress

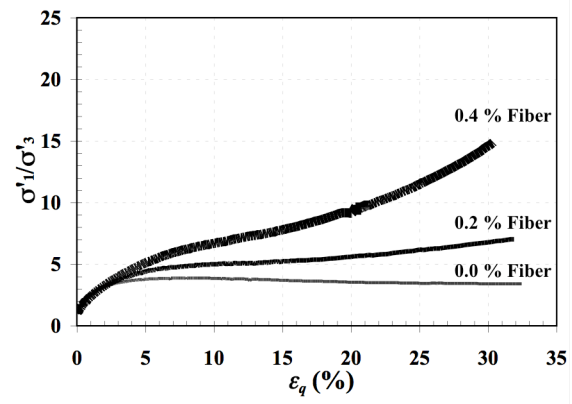

c) 20-psi effective consolidation stress

Figure 3.6 Effective principal stress ratio (σ'_1/σ'_3) versus triaxial shear strain (ε_q) curves from the $\overline{CU}$ tests for silty sand specimens compacted at 22 percent water content and consolidated to: a) 5-psi effective stress, b) 10-psi effective stress, c) 20-psi effective stress, d) 40-psi effective stress, and e) 80-psi effective stress.

3.5.3 Pore Pressure Response

In undrained loading conditions, the pore pressures in the soil specimens are known to change during shearing to maintain a zero volume change condition. The pore pressure change versus shear strain responses for the $\overline{CU}$ tests for unreinforced and reinforced silty sand specimens are shown in Figures 3.7 and 3.8 for specimens compacted at 18 percent and 22 percent water content, respectively. In general, the pore pressures increase at small strains (up to 2 percent), decrease with additional strains (from 2 percent to 20 percent), and tend to level off at very large strains for the unreinforced specimens. Unreinforced specimens compacted at 18 percent water content exhibited a greater reduction in pore pressure change at a large strains than unreinforced specimens compacted at 22 percent water content. This explains the higher deviatoric stresses observed in specimens compacted at 18 percent water content as compared to specimens compacted at 22 percent (e.g. Figure 3.2 versus Figure 3.3). In addition, the pore pressures generated during undrained shear increased with the effective confining stresses for the unreinforced specimens compacted at both 18 percent and 22 percent water content. All of this behavior is typical of most compacted soils.

Fiber-reinforced silty sand specimens also generally produced changes in pore pressure with initial increases at small strains and slight decreases with additional strain. As a result, the deviatoric stresses are similar at small strains and begin to deviate at moderate strains when comparing the unreinforced to the reinforced specimens. The initial increases in pore pressure at small strains are similar or slightly greater for reinforced specimens than for unreinforced specimens. The pore pressure change-strain responses of the fiber-reinforced specimens began to deviate from the behavior of

unreinforced specimens before the 5 percent strains. More importantly, the decrease in pore pressures observed for the reinforced specimens at intermediate strains was significantly less than that observed for the unreinforced specimens. This observation is consistent with those of Romero (2003), who postulated that the fibers create an "internal confining stress" (due to tension developed in the fibers) that, when added to the applied total stresses and actual pore pressures generated in the fiber-reinforced soil, produce additional effective stress to prevent volume change in undrained tests.

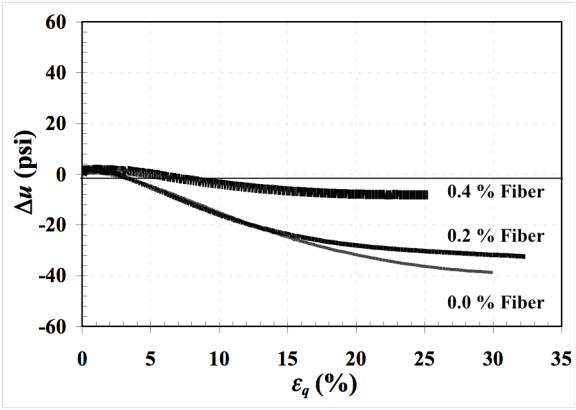

a) 5-psi effective consolidation stress

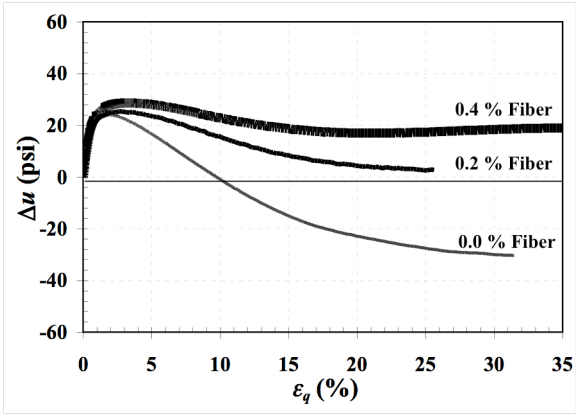

d) 40-psi effective consolidation stress

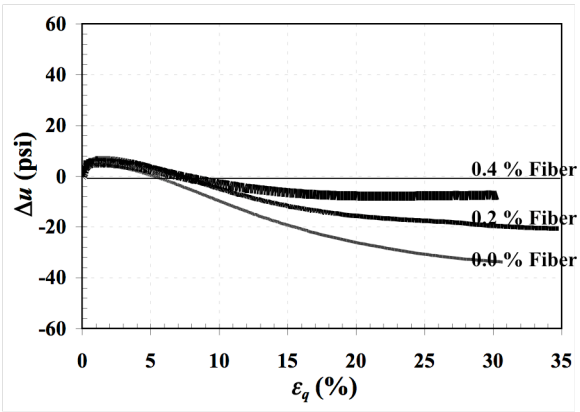

b) 10-psi effective consolidation stress

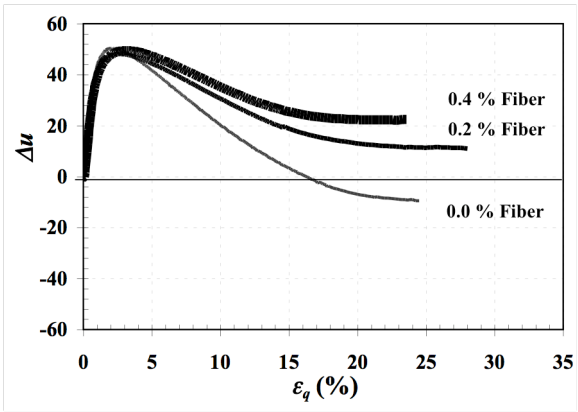

e) 80-psi effective consolidation stress

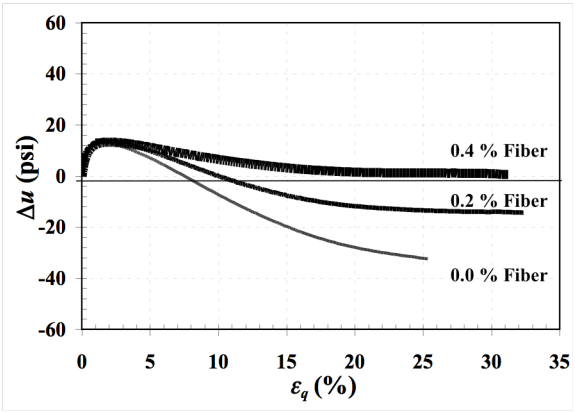

c) 20-psi effective consolidation stress

Figure 3.7 Pore pressure changes (Δu) versus triaxial shear strain (ε_q) curves from the $\overline{CU}$ tests for silty sand specimens compacted at an 18 percent water content and consolidated to: a) 5-psi effective stress, b) 10-psi effective stress, c) 20-psi effective stress, d) 40-psi effective stress, and e) 80-psi effective stress.

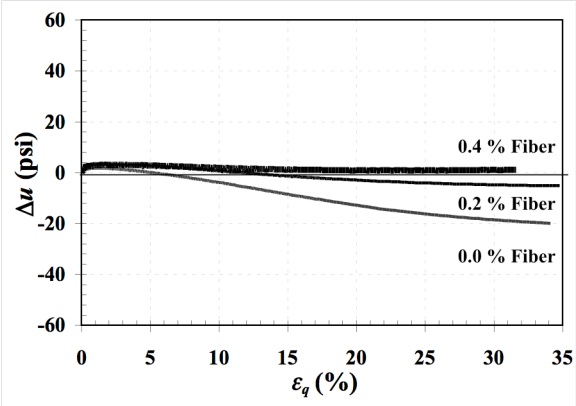

a) 5-psi effective consolidation stress

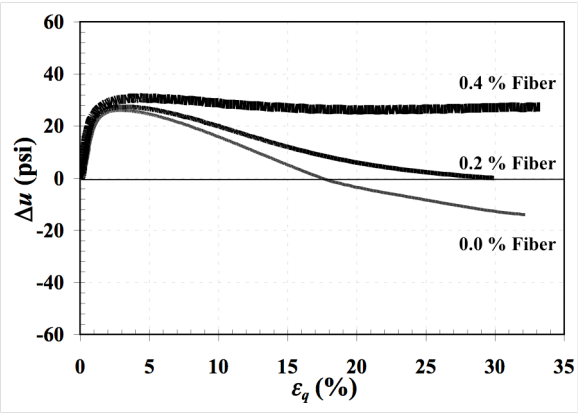

d) 40-psi effective consolidation stress

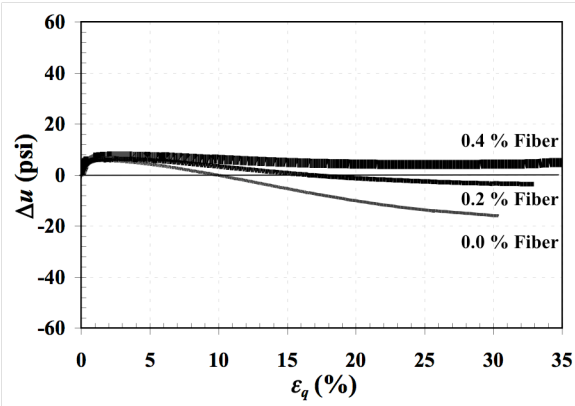

b) 10-psi effective consolidation stress

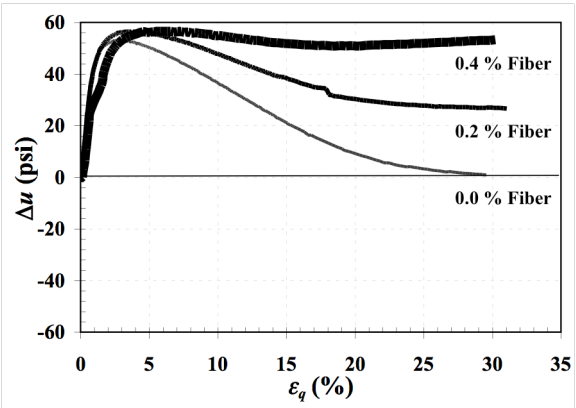

e) 80-psi effective consolidation stress

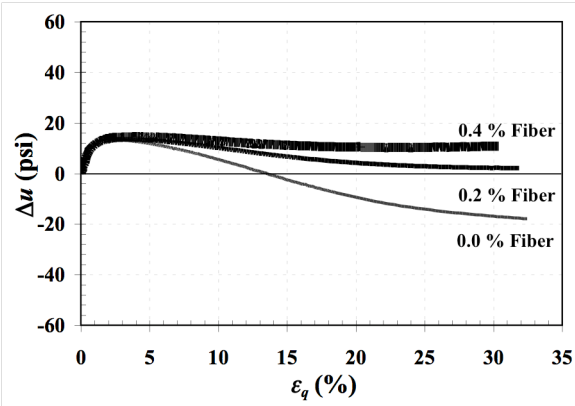

c) 20-psi effective consolidation stress

Figure 3.8 Pore pressure changes (Δu) versus triaxial shear strain (ε_q) curves from the $\overline{CU}$ tests for silty sand specimens compacted at 22 percent water content and consolidated to: a) 5-psi effective stress, b) 10-psi effective stress, c) 20-psi effective stress, d) 40-psi effective stress, and e) 80-psi effective stress.

3.5.4 Stress Paths

Figures 3.9 and 3.10 show the observed Cambridge stress path diagrams from $\overline{CU}$ tests in deviatoric stress ($q = \sigma_1' - \sigma_3'$) versus the mean effective stress ($p' = (\sigma_1' + 2\sigma_3')/3$) space for the unreinforced and reinforced silty sand specimens compacted at 18 percent and 22 percent water contents, respectively. The unreinforced specimens show typical stress paths for compacted soils with initial reductions in mean effective stresses followed by increases in mean effective stresses with increasing shear stress up to large strains.

The fiber-reinforced specimens exhibit a similar initial reduction in mean effective stresses as the unreinforced specimens. The stress paths begin to differ at greater shear stress, with the reinforced specimens generally having lower p' for a given level of q. This is a result of difference the pore pressures developed in the fiber-reinforced silty sand.

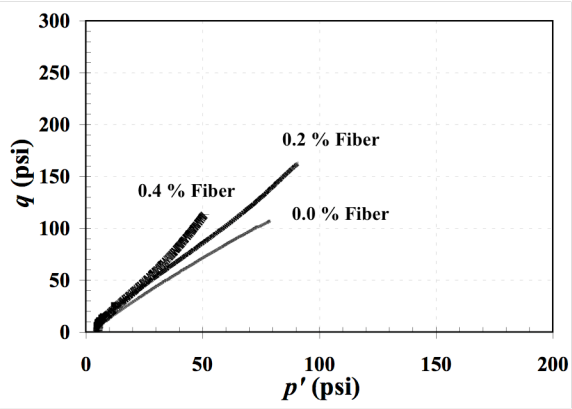

a) 5-psi effective consolidation stress

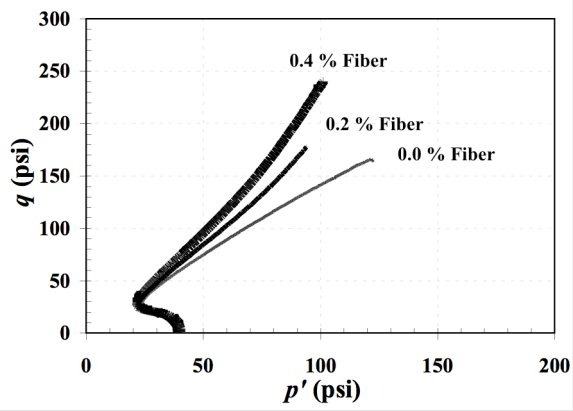

b) 10-psi effective consolidation stress

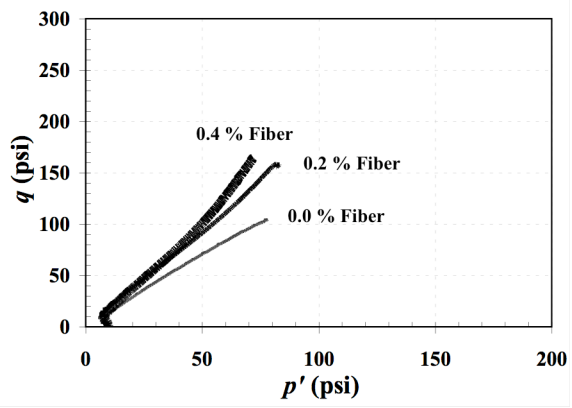

c) 20-psi effective consolidation stress

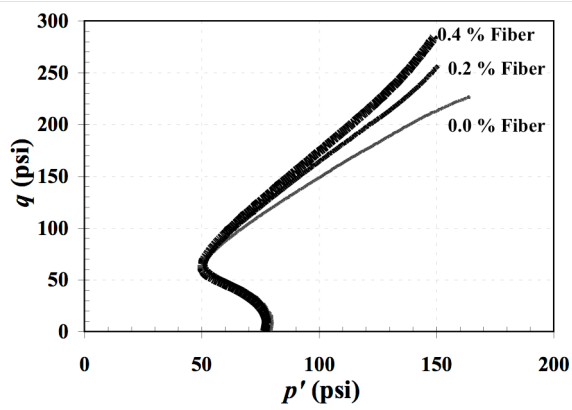

d) 40-psi effective consolidation stress

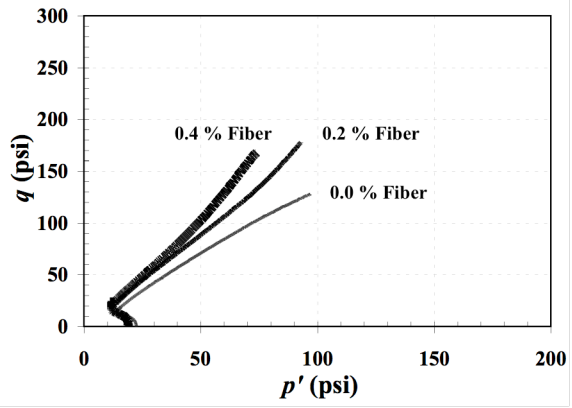

e) 80-psi effective consolidation stress

Figure 3.9 Cambridge stress paths (p':q) from the $\overline{CU}$ tests for silty sand specimens compacted at 18 percent water content and consolidated to: a) 5-psi effective stress, b) 10-psi effective stress, c) 20-psi effective stress, d) 40-psi effective stress, and e) 80-psi effective stress.

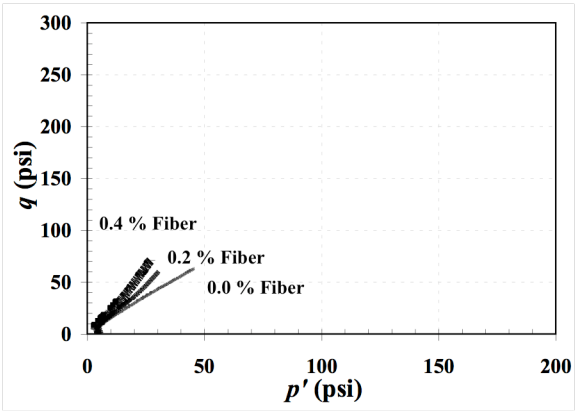

a) 5-psi effective consolidation stress

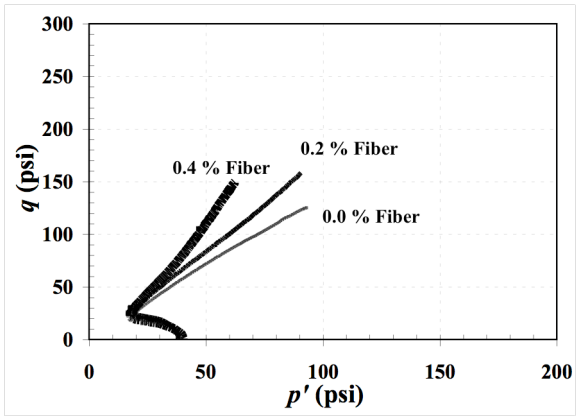

d) 40-psi effective consolidation stress

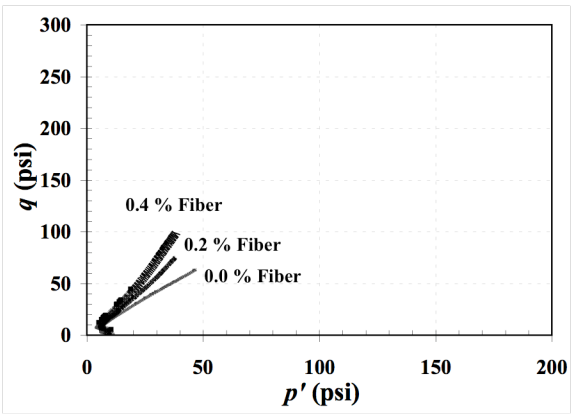

b) 10-psi effective consolidation stress

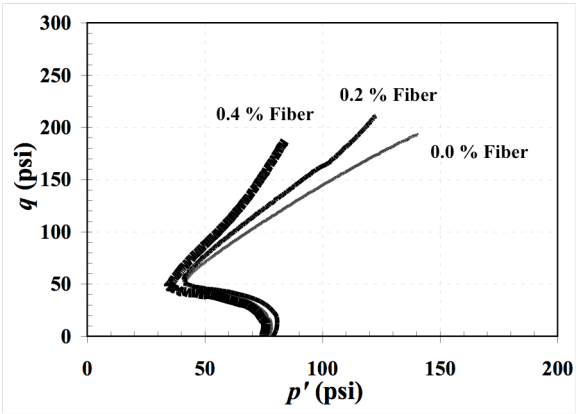

e) 80-psi effective consolidation stress

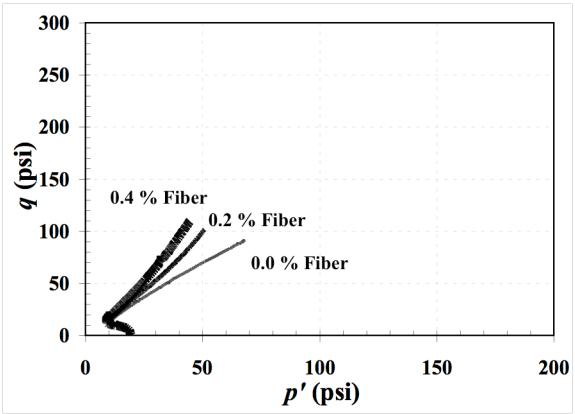

c) 20-psi effective consolidation stress

Figure 3.10 Cambridge stress paths (p':q) from the $\overline{CU}$ tests for silty sand specimens compacted at 22 percent water content and consolidated to: a) 5-psi effective stress, b) 10-psi effective stress, c) 20-psi effective stress, d) 40-psi effective stress, and e) 80-psi effective stress.

3.6 Results for Consolidation-Undrained ($\overline{CU}$) Triaxial Compression Tests for Ottawa Sand

A total of sixteen consolidation-undrained triaxial compression tests were performed (Table 3.2) on unreinforced and fiber-reinforced Ottawa sand specimens prepared at loose and medium-dense states and consolidated to 5, 20, 40, and 60-psi (35, 140, 280, 415-kPa) to evaluate the stress-strain-pore pressure change behavior under undrained loading conditions.

3.6.1 Stress-Strain Response

The stress-strain behavior observed in the $\overline{CU}$ tests for the unreinforced and reinforced Ottawa sand specimens are shown in Figures 3.11 and 3.12 for samples compacted to loose ($e_0 = 0.74$) and medium-dense ($e_0 = 0.60$) states, respectively. Loose unreinforced specimens consolidated to 5-psi effective stresses show no noticeable peak deviatoric stresses and tend to keep constant until large strains are reached. The rest of the loose unreinforced specimens consolidated at greater effective stresses (e.g. 20, 40, and 60-psi) reached a peak deviatoric stress at approximately 2 percent strains and then decreased with additional strain. In contrast, medium-dense unreinforced specimens at different effective consolidation stresses reached peak deviatoric stresses at strains of approximately 5 percent, but tended to level off or decrease slightly at large strains.

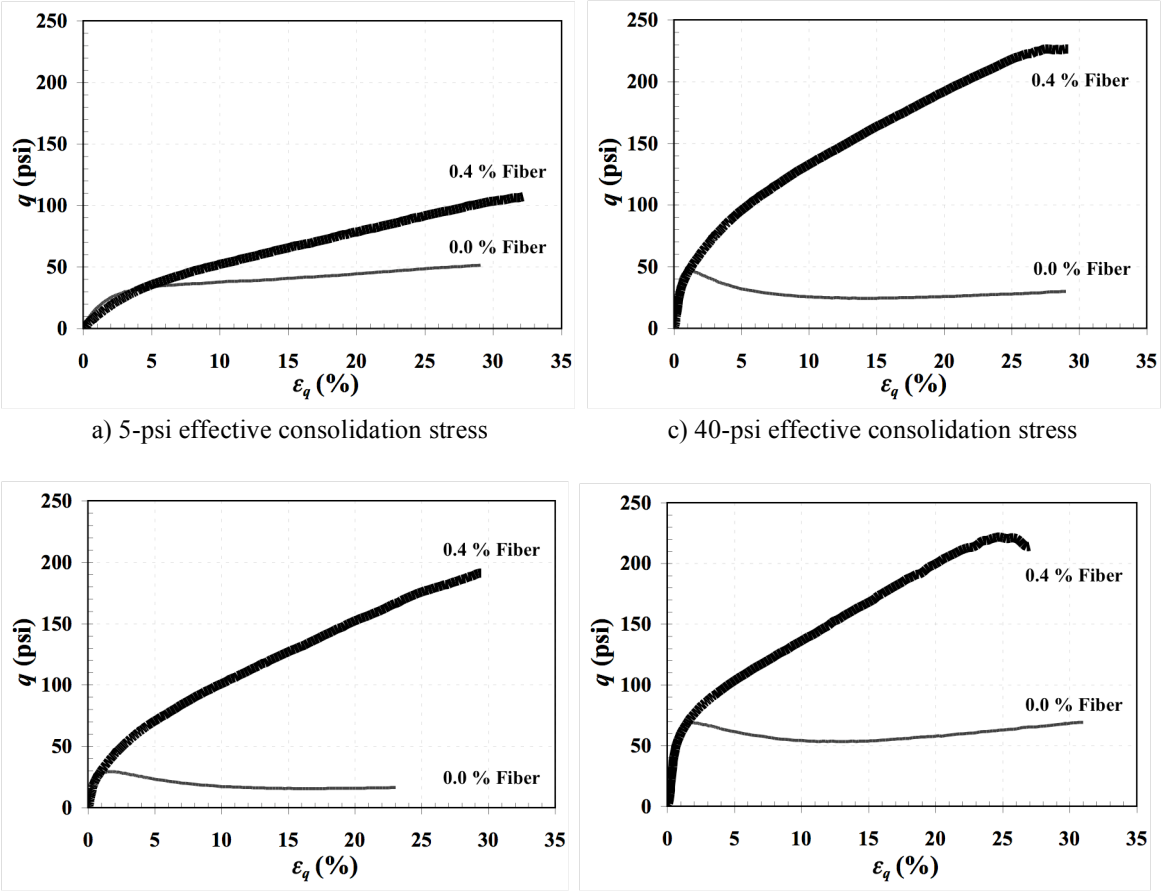

a) 5-psi effective consolidation stress

c) 40-psi effective consolidation stress

b) 20-psi effective consolidation stress

d) 60-psi effective consolidation stress

Figure 3.11 Deviatoric stress (q) versus the triaxial shear strain (ε_q) curves from the $\overline{CU}$ tests for loose Ottawa sand specimens ($e_0 = 0.74$) and consolidated to: a) 5-psi effective stress, b) 20-psi effective stress, c) 40-psi effective stress, and d) 60-psi effective stress.

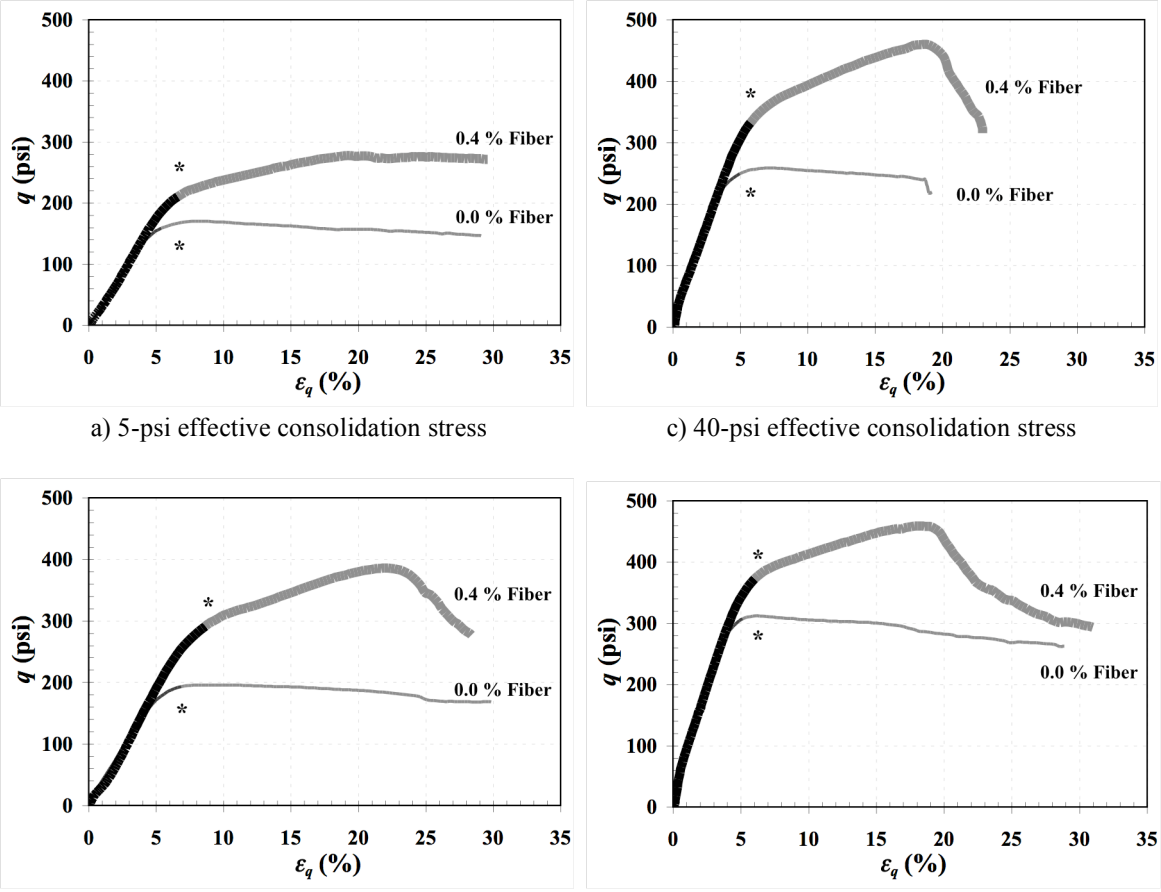

a) 5-psi effective consolidation stress

c) 40-psi effective consolidation stress

b) 20-psi effective consolidation stress

d) 60-psi effective consolidation stress

Figure 3.12 Deviatoric stress (q) versus the triaxial shear strain (ε_q) curves from the $\overline{CU}$ tests for medium-dense Ottawa sand specimens and consolidated to: a) 5-psi effective stress, b) 20-psi effective stress, c) 40-psi effective stress, and d) 60-psi effective stress.

*: Start point of suspicious measurement, the detail is shown in Section 3.6.3.

The loose fiber-reinforced specimens exhibited a strain-hardening behavior at low effective confining stresses (less than or equal to 20-psi), but noticeable peak stresses were observed at very large strains (more than 25 percent) for the loose reinforced specimens at high effective confining stresses (great than or equal to 40-psi). Medium-dense fiber-reinforced specimens also exhibited strain-hardening behavior, but revealed noticeable peak stresses at large strains (e.g. 20 percent) when consolidated to different effective confining stresses.

The stress-strain responses of the unreinforced and fiber-reinforced Ottawa sand specimens begin to deviate at strains of 2 to 6 percent for both the loose and medium-dense specimens. This is similar strains then was observed for the silty sand specimens.

Typical failure modes observed for the $\overline{CU}$ tests for the unreinforced and fiber-reinforced Ottawa sand specimens compacted at loose and medium-dense states and consolidated to 60-psi (415-kPa) are shown in Figure 3.13. The loose unreinforced Ottawa sand reveal a budging failure, while loose specimen reinforced with 0.4 percent fibers exhibited less budging than for loose unreinforced specimen. However, both medium-dense unreinforced and fiber-reinforced Ottawa sand specimens developed clearly defined failure plans when they reached the failure.

a) Loose state, 0.0 % fiber

c) Medium-dense state, 0.4 % fiber

b) Loose state, 0.4 % fiber

d) Medium-dense state, 0.4 % fiber

Figure 3.13 Typical failure modes of the $\overline{CU}$ tests at 60-psi effective consolidation stress for Ottawa sand specimens compacted at and mixed with: a) loose state, 0.0% fiber, b) dense state, 0.0% fiber, c) loose state, 0.4% fiber, and d) dense state, 0.4% fiber.

3.6.2 Effective Principal Stress Ratio-Strain Response

Figures 3.14 and 3.15 show the effective principal stress ratio versus shear strain observed in the $\overline{CU}$ tests for the unreinforced and reinforced Ottawa sand specimens. The effective principal stress ratio-strain curves generally reach their peak at about 1 to 2 percent strain for all unreinforced specimens and remained relatively constant at larger strains. Loose specimens peaked at a effective principal stress ratio of approximately 3, while medium-dense specimens peaked at a stress ratio of approximately 3.5.

As shown in Figure 3.14, a strain-hardening type of behavior was exhibited with no clear peak effective principal stress ratios for all loose fiber-reinforced specimens. No noticeable peak effective principal stress ratio was observed at effective consolidation stresses of 5-psi and 20-psi (35-kPa and 140-kPa), but clear peaks were observed at greater confining stress. As the effective consolidation stresses (σ_c') increased, the effective principal stress ratios generally decreased at any given strain. In contrast, the medium-dense fiber-reinforced specimens (Figure 3.15) consistently reached a local peak effective principal stress ratio at small strains. Effective principal stress ratio then decreased slightly with additional strain before increasing to a second peak at large strains. The magnitude of the first peak effective principal stress ratio decreases with effective consolidation stress for both loose and medium-dense reinforced specimens. The effective principal stress ratio-strain responses of the fiber-reinforced and unreinforced Ottawa sand specimens generally begin to deviate at about 1 percent strain, and the differences in stress ratio in terms of unreinforced and reinforced specimens tend to decrease with the increase in effective consolidation stress.

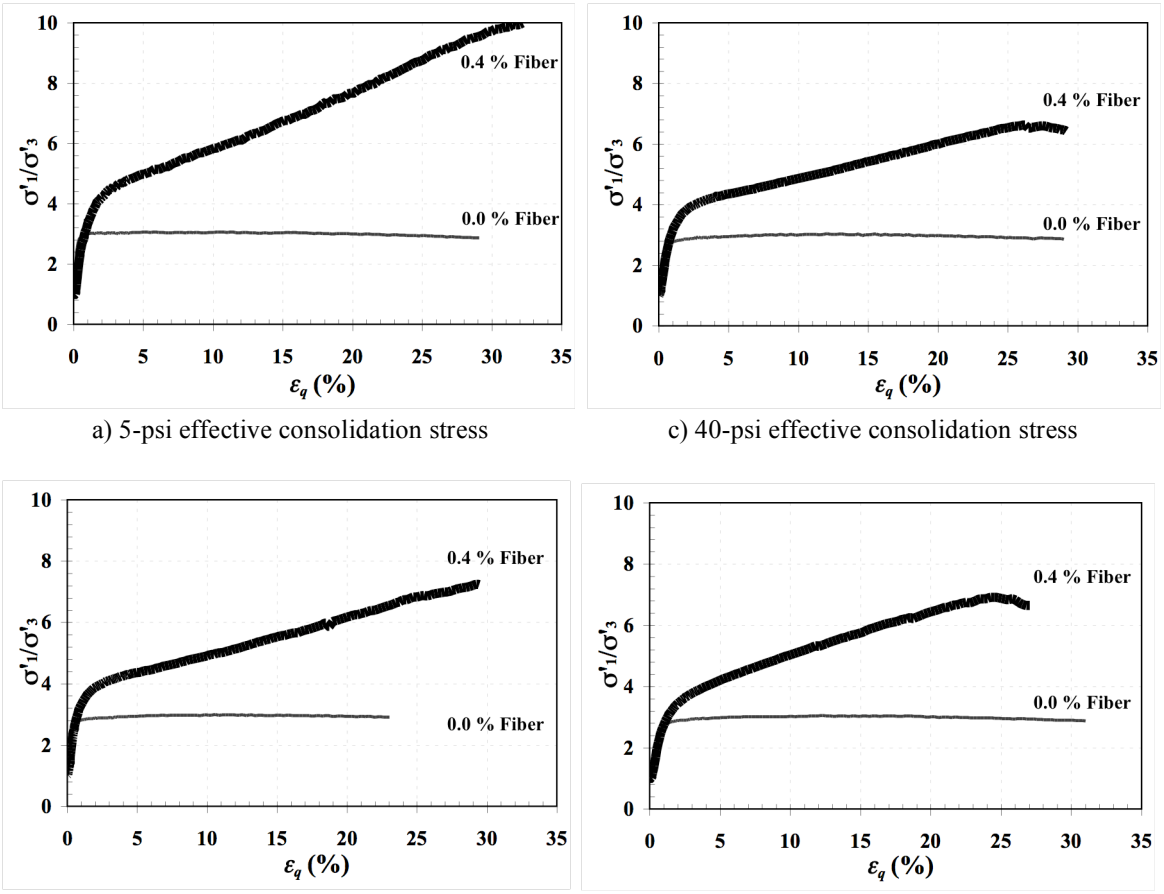

a) 5-psi effective consolidation stress

c) 40-psi effective consolidation stress

b) 20-psi effective consolidation stress

d) 60-psi effective consolidation stress

Figure 3.14 Effective principal stress ratio (σ'_1/σ'_3) versus triaxial shear strain (ε_q) curves from the $\overline{CU}$ tests for loose Ottawa sand specimens ($e_0 = 0.74$) and consolidated to: a) 5-psi effective stress, b) 20-psi effective stress, c) 40-psi effective stress, and d) 60-psi effective stress.

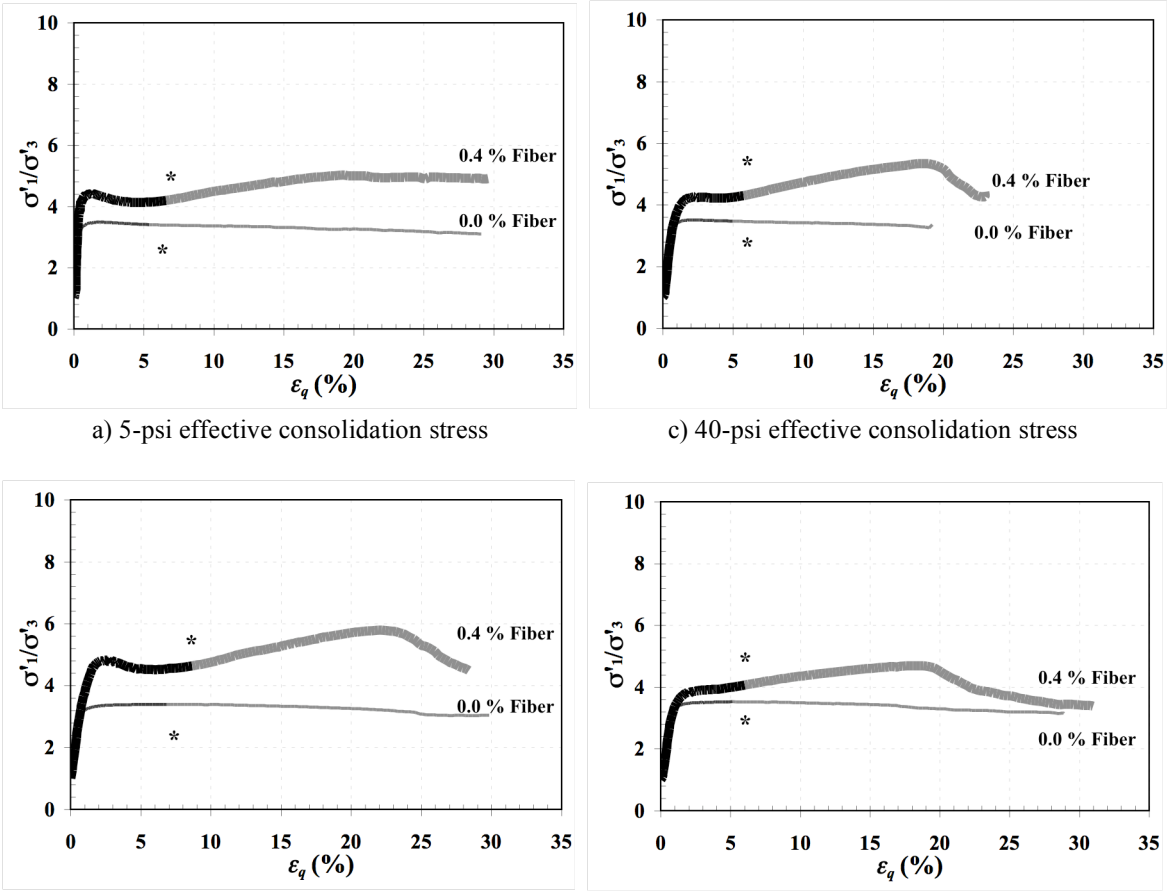

a) 5-psi effective consolidation stress

c) 40-psi effective consolidation stress

b) 20-psi effective consolidation stress

d) 60-psi effective consolidation stress

Figure 3.15 Effective principal stress ratio (σ'_1/σ'_3) versus triaxial shear strain (ε_q) curves from the $\overline{CU}$ tests for medium-dense Ottawa sand specimens ($e_0 = 0.60$) and consolidated to: a) 5-psi effective stress, b) 20-psi effective stress, c) 40-psi effective stress, and d) 60-psi effective stress.

*: Start point of suspicious measurement, the detail is shown in Section 3.6.3.

3.6.3 Pore Pressure Response

Figures 3.16 and 3.17 show the change in pore pressure versus shear strain for the $\overline{CU}$ tests for both unreinforced and reinforced Ottawa sand specimens for samples compacted to loose ($e_0 = 0.74$) and medium-dense ($e_0 = 0.60$) states, respectively. The loose unreinforced specimens consolidated to lower effective stresses (e.g. 5-psi) exhibited typical "dense sand" behavior with the change in pore pressure decreasing rapidly at small strains and subsequently slowly decreasing until the end of the test. Unreinforced specimens consolidated at higher effective confining stresses (greater than or equal to 20-psi) exhibited typical "loose sand" behavior with pore pressures increasing throughout the end of test. The magnitude of change in pore pressure increased as the effective confining stresses increased for the loose unreinforced specimens consolidated at higher effective stresses, as shown in Figure 3.16 (b), (c), and (d).

In contrast, medium-dense unreinforced Ottawa sand specimens showed that the initial pore pressure changes increased within 1 percent, followed by significant decreases and the absolute pore pressure equal or less than zero before 10 percent strains. The amount of initial pore pressure changes increased with increases in effective confining stresses for the medium-dense unreinforced specimens, as shown in Figure 3.17. When pore pressure transducer measured less than the atmosphere pressure, cavitation has taken place. Pore pressure transducers cannot measure negative pressure accurately; therefore, the measured values do not represent the real readings in the soil when the absolute value of pore pressure is equal to or less than zero.

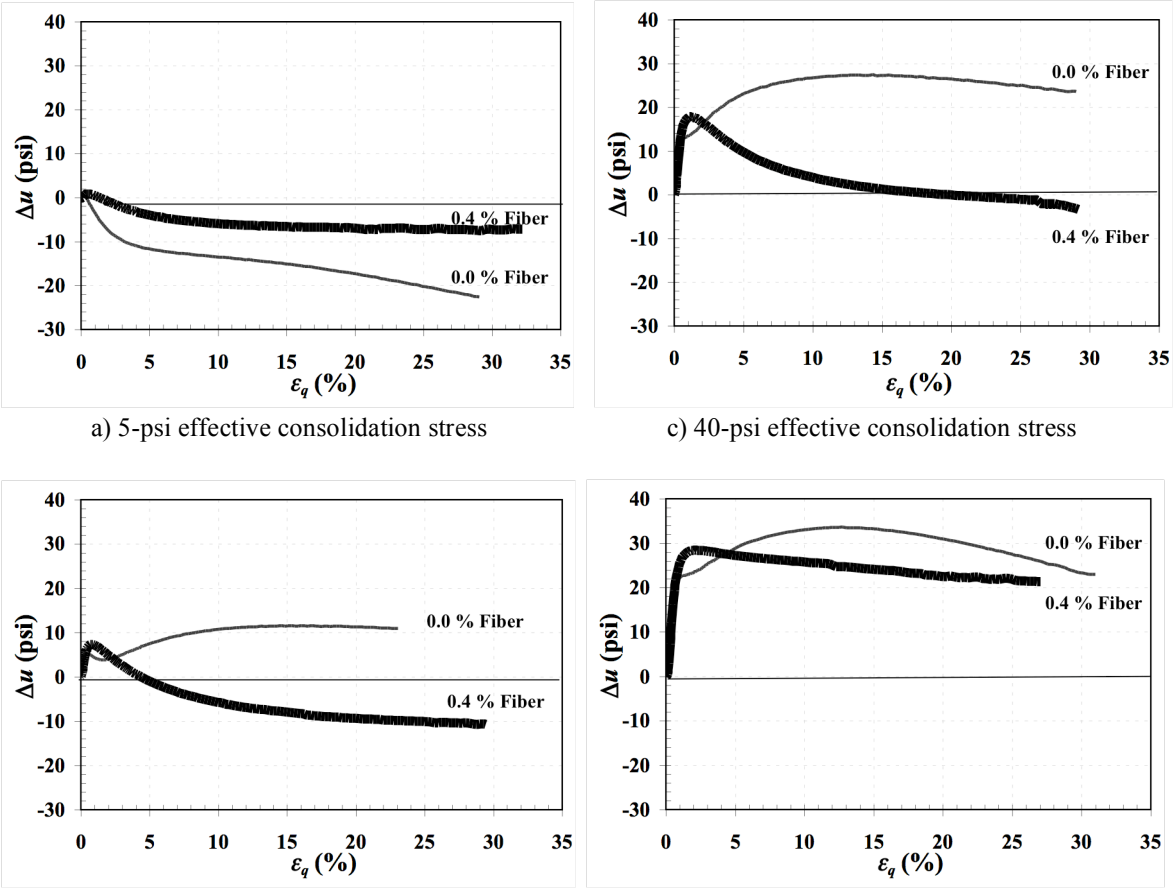

a) 5-psi effective consolidation stress

c) 40-psi effective consolidation stress

b) 20-psi effective consolidation stress

d) 60-psi effective consolidation stress

Figure 3.16 Change in pore pressures (Δu) versus triaxial shear strain (ε_q) curves from the $\overline{CU}$ tests for loose Ottawa sand specimens ($e_0 = 0.74$) and consolidated to: a) 5-psi effective stress, b) 20-psi effective stress, c) 40-psi effective stress, and d) 60-psi effective stress.

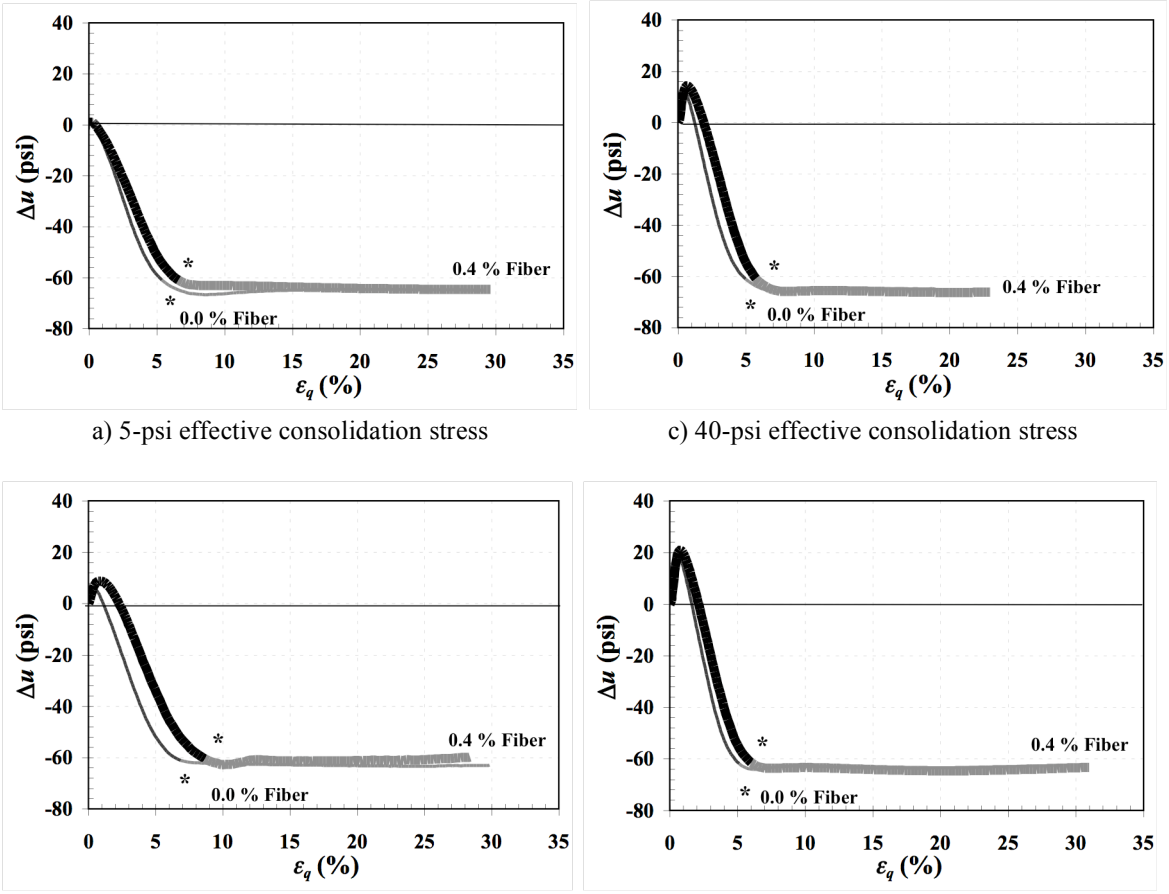

a) 5-psi effective consolidation stress

c) 40-psi effective consolidation stress

b) 20-psi effective consolidation stress

d) 60-psi effective consolidation stress

Figure 3.17 Change in pore pressures (Δu) versus triaxial shear strain (ε_q) curves from the $\overline{CU}$ tests for medium-dense Ottawa sand specimens ($e_0 = 0.60$) and consolidated to: a) 5-psi effective stress, b) 20-psi effective stress, c) 40-psi effective stress, and d) 60-psi effective stress.

*: Start point of suspicious measurement.

The loose reinforced specimens (Figure 3.16) generally show that the initial change in pore pressure increase at small strains (e.g. 2 percent), decrease with additional strains, and tend to level off at larger strains. The loose reinforced specimens consolidated to a 5-psi effective stress showed higher amounts of pore pressure than the unreinforced specimen at any given strain, while specimens consolidated to higher effective stresses (greater than or equal to 20-psi) showed lower pore pressure amounts than in unreinforced specimens at any given strain. Although the initial increases in pore pressure at lower strains are slightly higher for the reinforced specimens than for the unreinforced specimens, the differences in pore pressure change in terms of loose unreinforced and fiber-reinforced specimens became larger with increasing effective confining stresses up to 40-psi (280-kPa), and the differences became smaller for the specimens consolidated to 60-psi (415-kPa).

Medium-dense fiber-reinforced specimens showed that initial changes in pore pressure increased at small strains (2 percent) followed by a significant decrease at absolute pore pressures equal to or less than zero before 10 percent strains. The amount of initial pore pressure increased as the effective confining stresses increased for the unreinforced Ottawa sand specimens as well. Medium-dense reinforced specimens tended to have slightly higher pore pressures than unreinforced specimens before absolute pore pressure became equal to or less than zero.

3.6.4 Stress Paths

Figures 3.18 and 3.19 illustrate the observed Cambridge stress paths from the $\overline{CU}$ tests for the unreinforced and reinforced specimens of loose and medium-dense Ottawa sand. The loose unreinforced specimen consolidated to a 5-psi effective stress showed "dense sand" behavior, which is also revealed in the stress-strain response (Figure 3.11 (a)). However, the loose unreinforced specimens consolidated to higher effective stresses (greater than or equal to 20-psi) had stress paths exemplifying "loose sand" behavior. The medium-dense unreinforced specimens show a typical stress path response for compacted soils, with initial reductions in mean effective stresses (p') followed by an increase in mean effective stress up to large strains.

Significant differences in stress paths for the unreinforced and fiber-reinforced loose sand specimens are shown in Figure 3.18. The fiber-reinforced loose specimens have similar curves at different effective consolidation stresses. However, the response of the unreinforced specimens is quite different and varies from low to high effective confining stress. This signifies that the pore pressure response for loose reinforced specimens is unlike the unreinforced specimens. However, both the unreinforced and reinforced medium-dense sand specimens show overall similar stress paths. The slight differences shown are primarily due to differences in pore pressure between the unreinforced and fiber-reinforced medium-dense specimens.

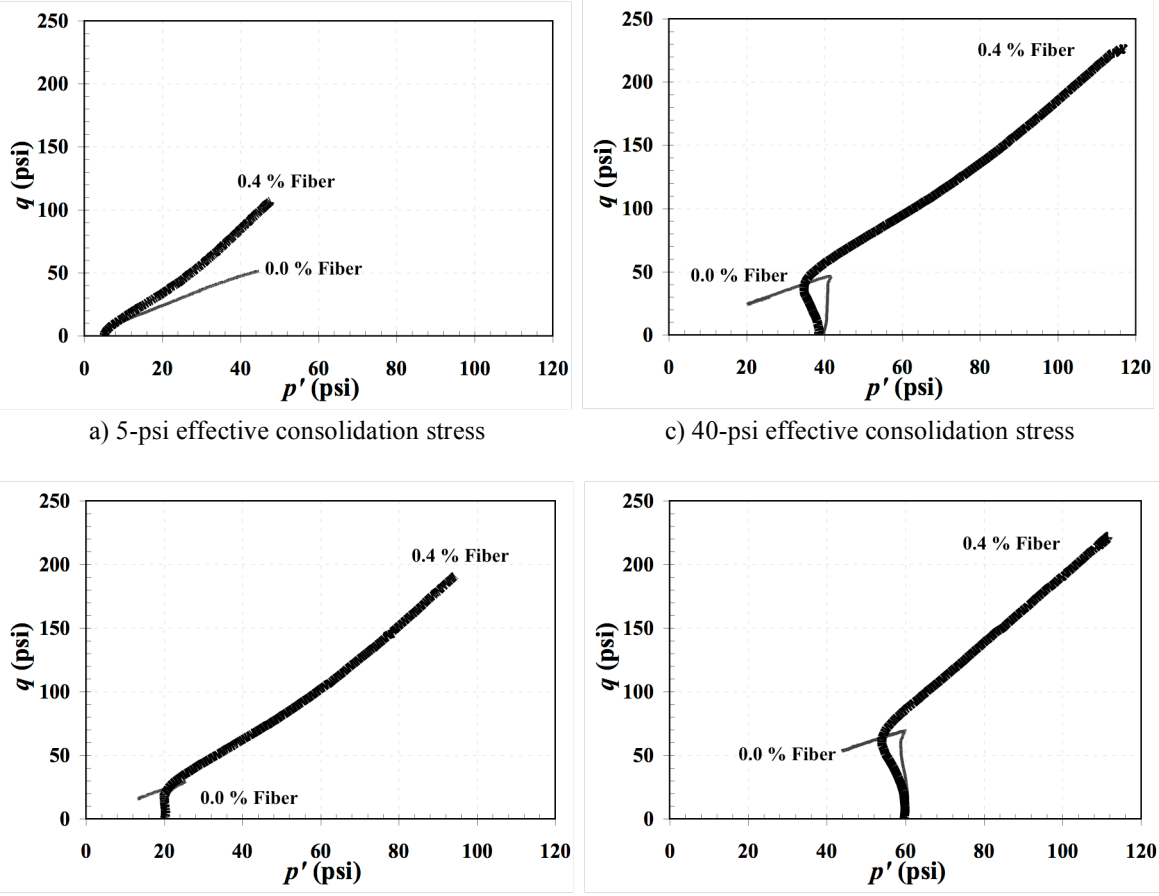

a) 5-psi effective consolidation stress

c) 40-psi effective consolidation stress

b) 20-psi effective consolidation stress

d) 60-psi effective consolidation stress

Figure 3.18 Cambridge stress paths (p': q) from the $\overline{CU}$ tests for loose Ottawa sand specimens ($e_0 = 0.74$) and consolidated to: a) 5-psi effective stress, b) 20-psi effective stress, c) 40-psi effective stress, and d) 60-psi effective stress.

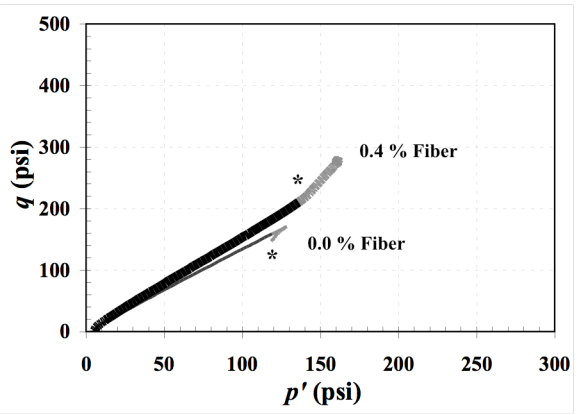

a) 5-psi effective consolidation stress

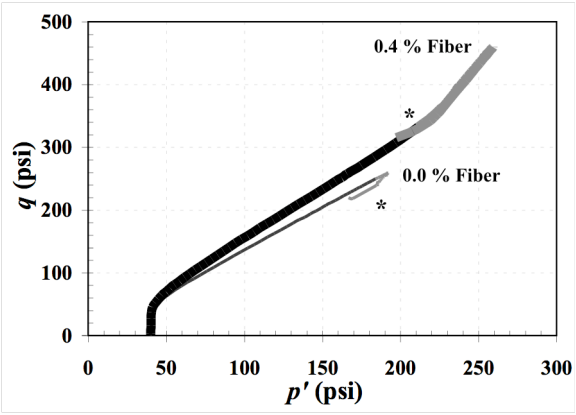

c) 40-psi effective consolidation stress

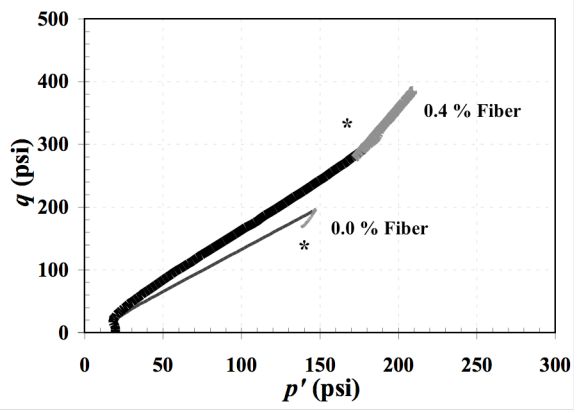

b) 20-psi effective consolidation stress

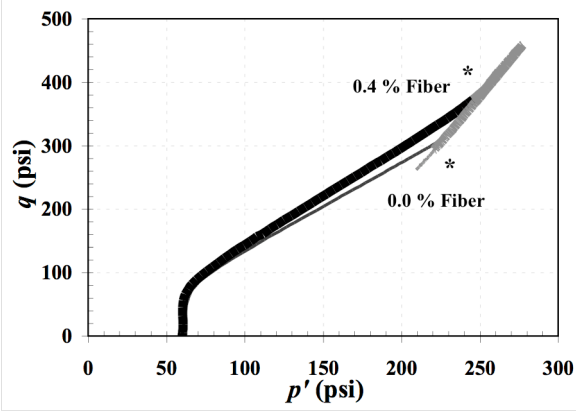

d) 60-psi effective consolidation stress

Figure 3.19 Cambridge stress paths (p': q) from the $\overline{CU}$ tests for medium-dense Ottawa sand specimens ($e_0 = 0.60$) and consolidated to: a) 5-psi effective stress, b) 20-psi effective stress, c) 40-psi effective stress, and d) 60-psi effective stress.

*: Start point of suspicious measurement.

3.7 Failure Envelopes for Consolidation-Undrained ($\overline{CU}$) Triaxial Compression Tests

Mohr-Coulomb strength parameters determined for unreinforced and reinforced silty sand and Ottawa sand specimens in the $\overline{CU}$ tests are presented and discussed in the following sections.

3.7.1 Undrained Failure Envelopes for Silty Sand

Two failure criterions can be used in the $\overline{CU}$ tests: one is the peak deviator stress (PDS), and the other is the peak effective principal stress ratio (PSR). Values of the effective stress cohesion intercept, c', and the effective stress friction angle, ϕ', for these envelopes are summarized in Table 3.4. The results point out the shear strength of the unreinforced silty sand specimens compacted at 18 percent and 22 percent water contents can be represented by an effective stress cohesion intercept of 0-psi and angle of internal friction of 36° (PSR). The effective stress friction angle at PSR for the unreinforced specimens is slightly greater than for those determined at the peak deviator stress (PDS).

Table 3.4 Mohr-Coulomb Strength Parameters, c' and ϕ', for Unreinforced and Reinforced Silty Sand Specimens from the $\overline{CU}$ Tests

Water Content (%)	0.0% Fiber Content		0.2% Fiber Content		0.4% Fiber Content	
	PDS		PDS		PDS	
	c' (psi)	ϕ' (deg)	c' (psi)	ϕ' (deg)	c' (psi)	ϕ' (deg)
18	0	33.7	0	45.7	0	55.5
22	0	33.8	0	48.5	7.4	54.4
Water Content (%)	PSR		PSR		PSR	
	c' (psi)	ϕ' (deg)	c' (psi)	ϕ' (deg)	c' (psi)	ϕ' (deg)
18	0	36.5	0.2	46.5	0	55.6
22	0.2	35.8	0	48.5	7.4	54.4

The effectives stress strength parameter values for these envelopes are summarized in Table 3.4. Comparing the failure envelopes for unreinforced and reinforced silty sand specimens show that the inclusion of fibers had a significant effect on increasing both the effective cohesion intercept and the effective friction angle. As the fiber content increased from 0.2 percent to 0.4 percent for the fiber-reinforced specimens, both the effective stress cohesion intercept and the effective stress friction angle increased as well. The data indicate that reinforced specimens compacted at 22 percent water content tended to have similar effective stress friction angles, but higher effective stress cohesion intercepts than the specimens compacted at 18 percent water content. In addition, the results of effective stress cohesion intercept and effective stress internal friction angle of the PDS failure criterion have similar values to the PSR failure criterion.

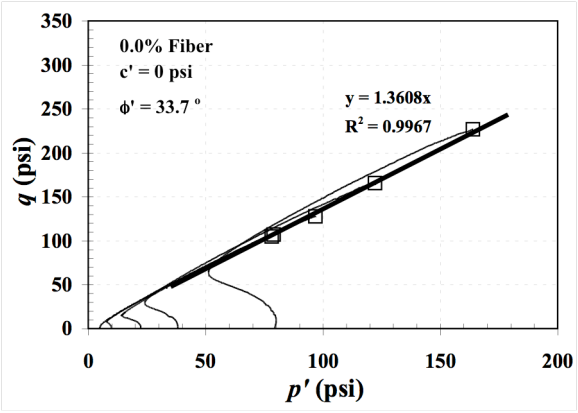

a) PDS failure envelop for 0.0% fiber

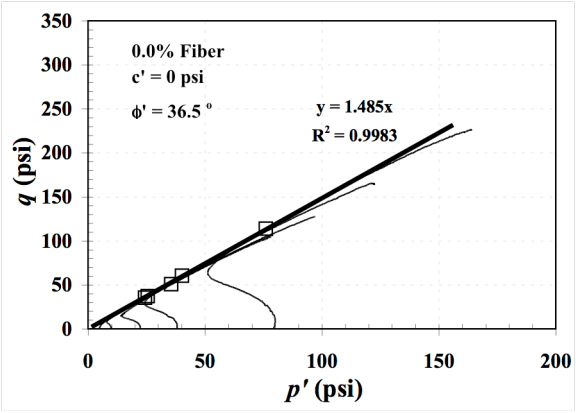

b) PSR failure envelop for 0.0% fiber

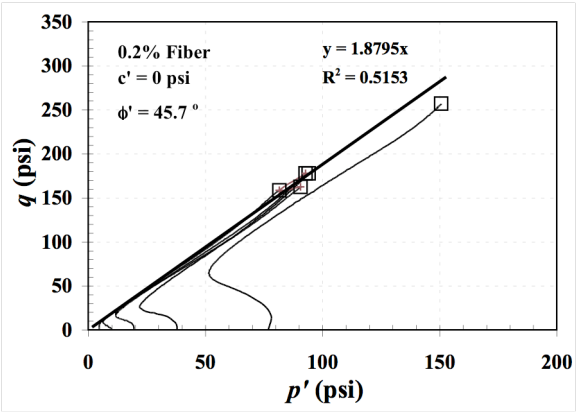

c) PDS failure envelop for 0.2% fiber

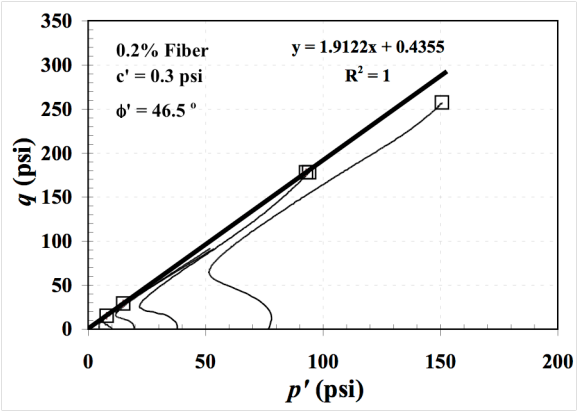

d) PSR failure envelop for 0.2% fiber

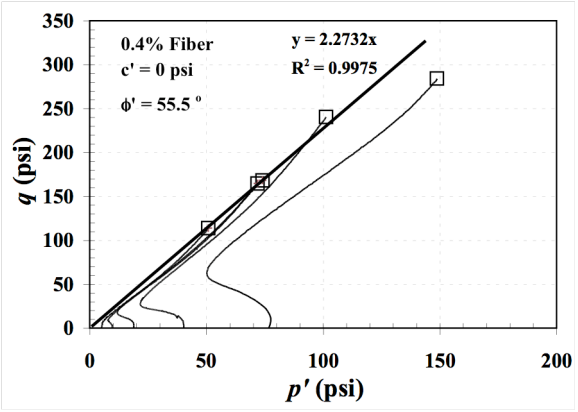

e) PDS failure envelop for 0.4% fiber

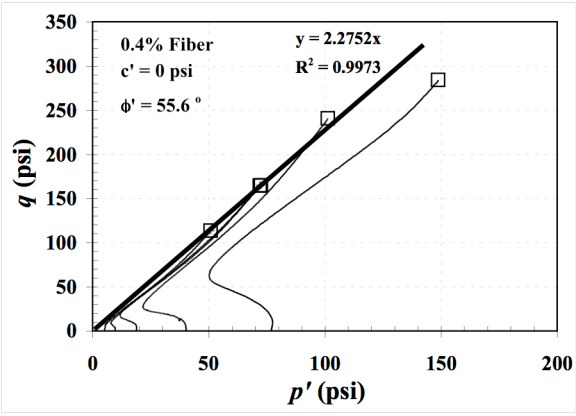

f) PSR failure envelop for 0.4% fiber

Figure 3.20 Failure envelopes of peak deviator stress (PSD) and peak effective principal stress ratio (PSR) from the $\overline{CU}$ tests for silty sand specimens compacted at 18 percent water content and mixed with: a) 0.0% fiber (PDS), b) 0.0% fiber (PSR), c) 0.2% fiber (PDS), d) 0.2% fiber (PSR), e) 0.4% fiber (PDS), and f) 0.4% fiber (PSR).

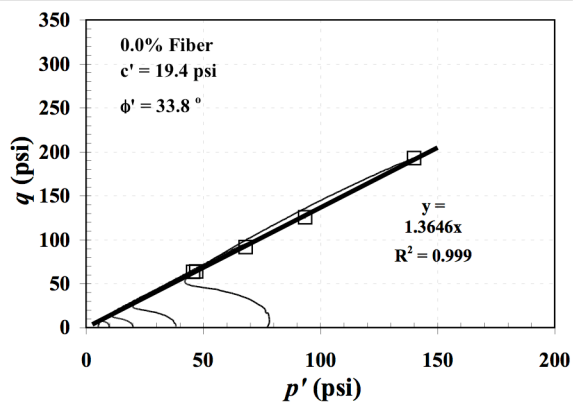

a) PDS failure envelop for 0.0% fiber

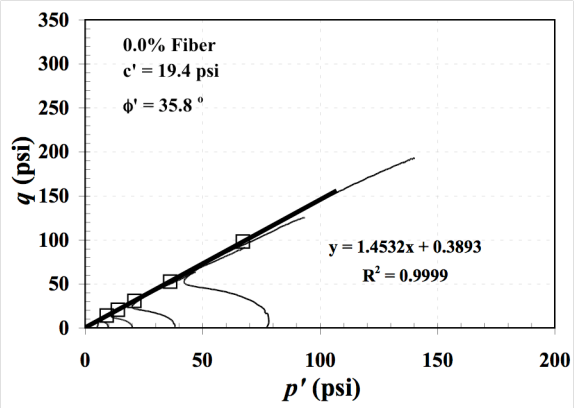

b) PSR failure envelop for 0.0% fiber

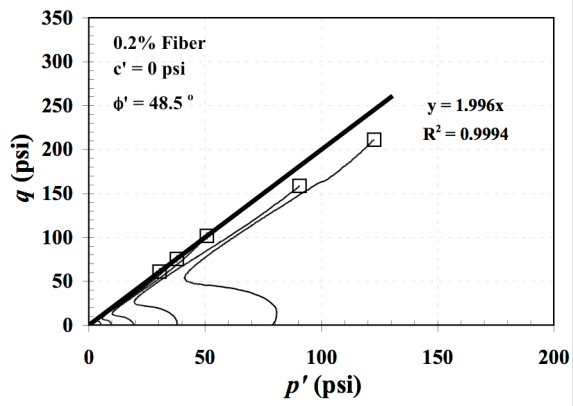

c) PDS failure envelop for 0.2% fiber

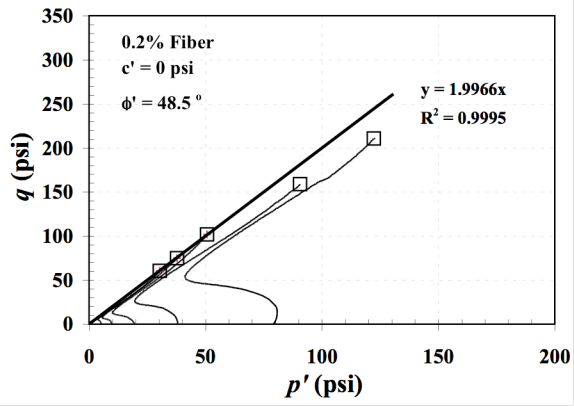

d) PSR failure envelop for 0.2% fiber

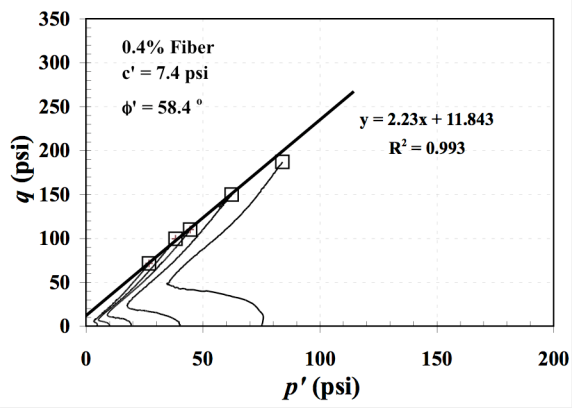

e) PDS failure envelop for 0.4% fiber

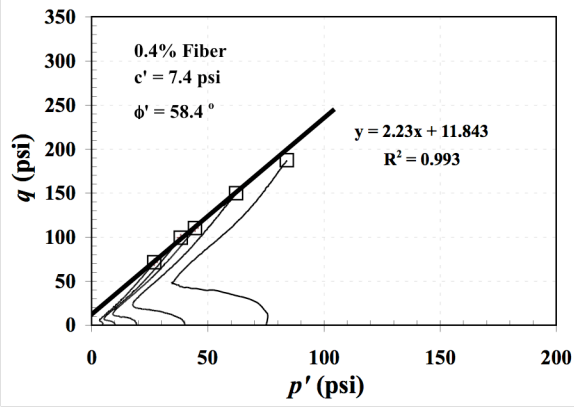

f) PSR failure envelop for 0.4% fiber

Figure 3.21 Failure envelopes of the peak deviator stress (PSD) and the peak effective principal stress ratio (PSR) from the $\overline{CU}$ tests for silty sand specimens compacted at 22 percent water content and mixed with: a) 0.0% fiber (PDS), b) 0.0% fiber (PSR), c) 0.2% fiber (PDS), d) 0.2% fiber (PSR), e) 0.4% fiber (PDS), and f) 0.4% fiber (PSR).

Figures 3.20 and 3.21 show the observed Cambridge stress paths for all $\overline{CU}$ tests on unreinforced specimens for the silty sand samples along with the two failure criteria. As shown in the figures, the failure envelopes for specimens reinforced with 0.2 percent and 0.4 percent fibers based on the first 3 points, not including the last two points. It is because that may not have reached actual failure, but just limit of strain that is reasonable for tests. Alternatively, it may be an indication of non-linearity in failure envelope at high mean effective stress (e.g. fiber yield). As such values shown in Table 3.5 will be representative of behavior at relatively low effective confining stress. The failure envelopes presented in Figures 3.20 and 3.21 correspond to the maximum stress experienced during the undrained loading conditions. However, these stresses in the fiber-reinforced silty sand specimens were often not mobilized until reaching strains as large as 30 percent. Since such large strains are seldom tolerable, failure envelopes were also established at limiting strains of 5, 15, and 25 percent to evaluate the effects of the fibers inclusion on mobilized resistance at small strains.

Figure 3.22 shows failure envelopes and the chosen limiting strains for the unreinforced and reinforced silty sand specimens compacted at 18 percent and 22 percent water contents. In all cases, the stress used to establish the failure envelopes were the maximum stresses at strains equal to the limiting strains. Mohr-Coulomb strength parameters, c' and ϕ' for the unreinforced and reinforced specimens at the limiting strains are summarized in Table 3.5.

Table 3.5 Mohr-Coulomb Strength Parameters, c' and ϕ', for Unreinforced and Reinforced Silty Sand Specimens from the $\overline{CU}$ Tests When Peak Strength is Taken as Peak Stress Experienced at Limiting Strains of 5, 15, and 25 Percent

Water Content (%)	Fiber Content	Limit Strain					
		5% Strain		15% Strain		25% Strain	
		c' (psi)	ϕ' (deg)	c' (psi)	ϕ' (deg)	c' (psi)	ϕ' (deg)
18%	0.0%	0.0	36.6	0.0	35.0	0.0	33.7
	0.2%	3.7	36.0	8.1	37.2	16.5	36.3
	0.4%	3.2	37.2	8.6	40.7	17.5	41.9
22%	0.0%	0.3	34.7	0.0	35.3	0.0	34.1
	0.2%	1.1	35.9	2.1	39.1	4.8	39.3
	0.4%	1.9	33.1	3.8	42.4	6.5	48.1

The strength parameters for unreinforced silty sand specimens are essentially identical for the chosen limiting strains. This occurs because the peak stresses are generally experienced at relatively low strains. However, the strength parameters determined from the reinforced silty sand specimens at different limiting strains are significantly different. In general, both the effective stress cohesion intercept and the effective stress friction angle increase with the increasing chosen limiting strains. This indicates the strain hardening behavior for the fiber-reinforced silty sand specimens. Moreover, this suggests that the consideration of the tolerable level of strains in selecting appropriate strength parameters for a given engineering application of the fiber-reinforced silty sand is critical.

Table 3.5 reveals a comparison of the different failure envelopes for the specimens compacted at 18 percent and 22 percent water contents. The values shown in the table, the reinforced specimens compacted at 18 percent water content indicate

increases in both the effective stress cohesion intercept and the effective stress friction angle, whereas specimens compacted at 22 percent water content show extensively large increases in the effective stress friction angle, but only small increases in the effective stress cohesion intercept as the limiting strains increase.

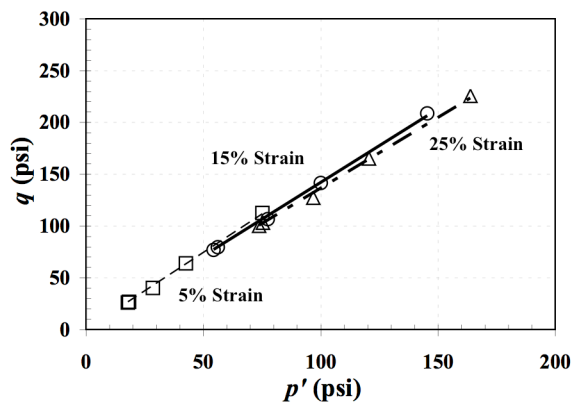

a) 18% water content, 0.0% fiber content

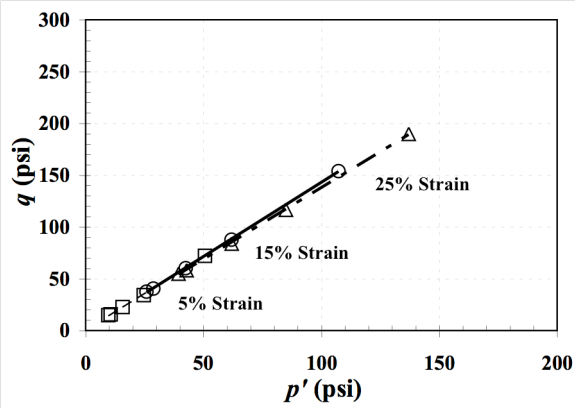

d) 22% water content, 0.0% fiber content

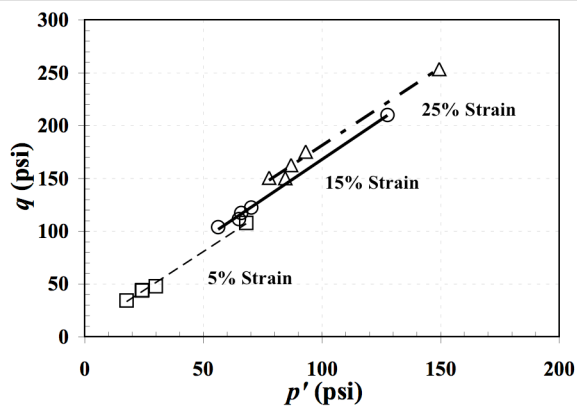

b) 18% water content, 0.2% fiber content

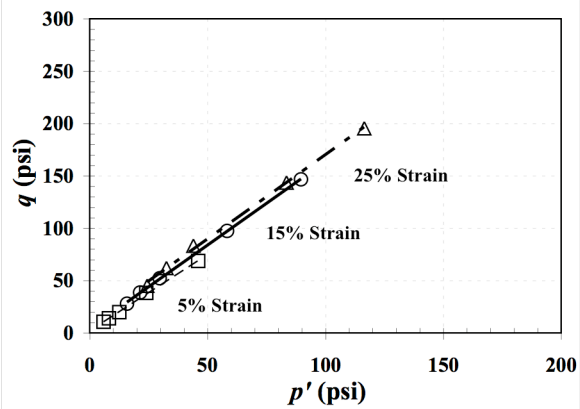

e) 22% water content, 0.2% fiber content

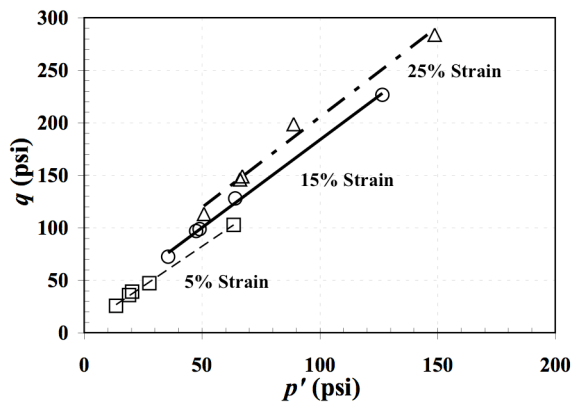

c) 18% water content, 0.4% fiber content

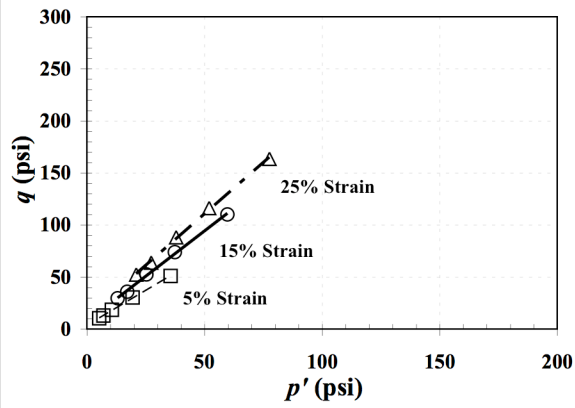

f) 22% water content, 0.4% fiber content

Figure 3.22 Failure Envelopes from the $\overline{CU}$ tests for limiting strains of 5,15, and 25 percent shear strain on unreinforced and reinforced silty sand specimens compacted at and mixed with: a) 18% water content, 0.0% fiber, b) 18% water content, 0.2% fiber, c) 18% water content, 0.4% fiber, d) 22% water content, 0.0% fiber, e) 22% water content, 0.2% fiber, and f) 22% water content, 0.4% fiber.

3.7.2 Undrained Failure Envelopes for Ottawa Sand

The resulting of shear strength parameters from these envelopes are summarized in Table 3.6. The shear strength of the unreinforced Ottawa sand specimens compacted at loose state can be represented by an effective friction angle of 30°, and those compacted at medium-dense state can be interpreted by an effective friction angle of 34° for both failure criterions with zero effective cohesion intercept. Again, the effective stress friction angles using the PSR criteria are slightly greater than those computed using the PSD criteria for all unreinforced Ottawa sand specimens. The data show the effective cohesion intercepts of 13-psi (90-kPa) and the effective friction angle of 43° for loose reinforced Ottawa sand specimens. In addition, the results indicate that inclusion fibers in the loose specimens tend to have a pronounced effect on increasing the effective stress friction angle. This is consistently seen in the behavior of fiber-reinforced silty sand.

Table 3.6 Mohr-Coulomb Strength Parameters, c' and ϕ', for Unreinforced and Reinforced Ottawa Sand Specimens from the $\overline{CU}$ Tests

Initial Void Ratio	0.0% Fiber Content		0.4% Fiber Content	
	PDS		PDS	
	c' (psi)	ϕ' (deg)	c' (psi)	ϕ' (deg)
0.74	0	28.8	12.7	42.7
0.60	0	33.5	0[a]	43.5[a]
Initial Void Ratio	PSR		PSR	
	c' (psi)	ϕ' (deg)	c' (psi)	ϕ' (deg)
0.74	0	30.4	12.6	42.8
0.60	0	33.7	0[a]	43.5[a]

[a]: Suspicious result due to equipment limitation for pore pressure measurements.

Cambridge stress paths for the $\overline{CU}$ tests on unreinforced Ottawa sand specimens along with the PDS and PSR failure criteria used to establish the failure envelopes are shown in Figures 3.23 and 3.24. In the figures, the failure envelopes for fiber-reinforced specimens only based on the first 3 points, not including the last point. As described in previous section (3.7.1), it is strain limited, instead of strength limited for fiber-reinforced specimens. A comparison of failure envelopes for the unreinforced and reinforced Ottawa sand specimens show that fiber inclusion has a significant effect in improving not only the effective stress friction angles, but also the effective stress cohesion intercepts.

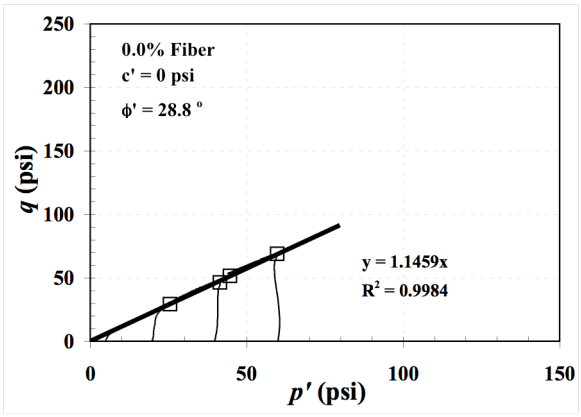

a) 0.0% fiber (PSD failure envelop)

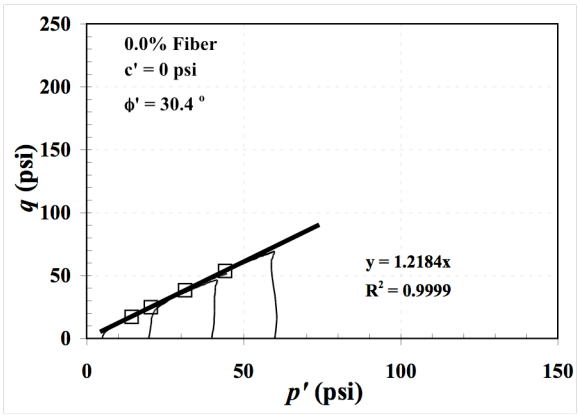

b) 0.0% fiber (PSR failure envelop)

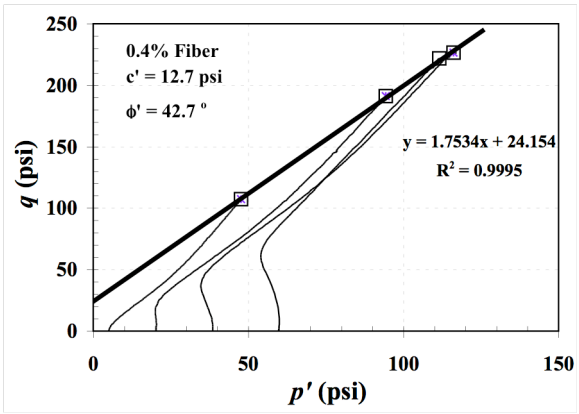

c) 0.4% fiber (PSD failure envelop)

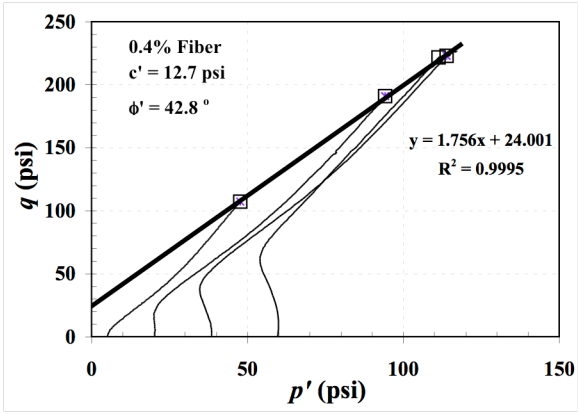

d) 0.4% fiber (PSR failure envelop)

Figure 3.23 Failure envelopes of peak deviator stress (PDS) and peak effective principal stress ratio (PSR) from the $\overline{CU}$ tests for the Ottawa sand specimens compacted at loose state ($e_0 = 0.74$) and mixed with: a) 0.0% fiber (PDS), b) 0.0% fiber (PSR), c) 0.4% fiber (PDS), and d) 0.4% fiber (PSR).

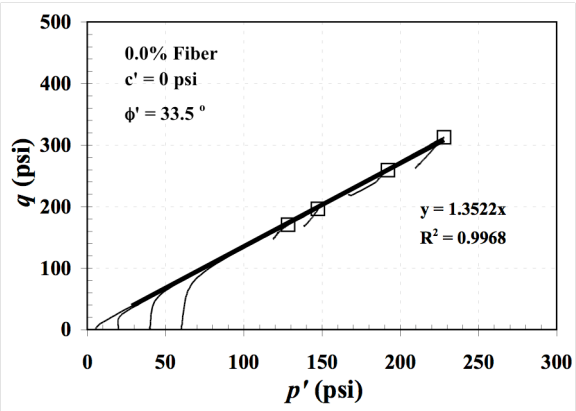

a) 0.0% fiber (PSD failure envelop)

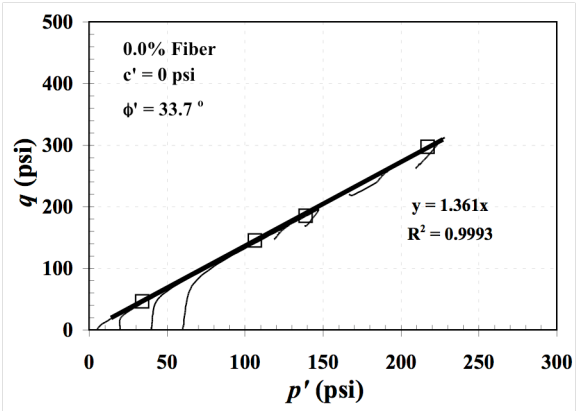

b) 0.0% fiber (PSR failure envelop)

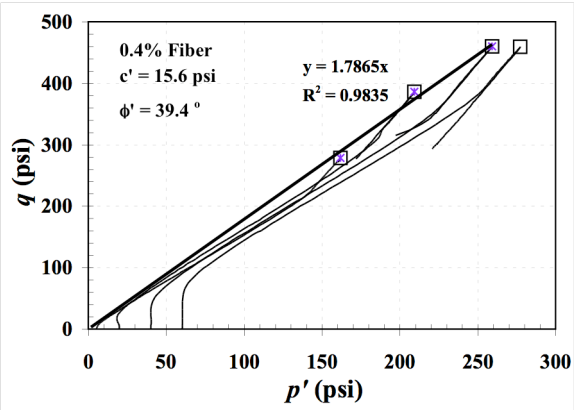

c) 0.4% fiber (PSD failure envelop)

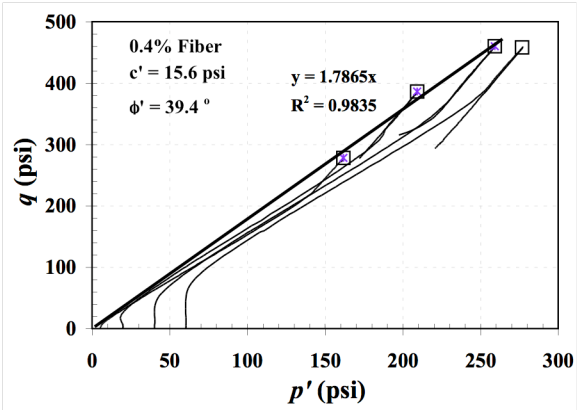

d) 0.4% fiber (PSR failure envelop)

Figure 3.24 Failure envelopes of peak deviator stress (PSD) and peak effective principal stress ratio (PSR) from the $\overline{CU}$ tests for the Ottawa sand specimens compacted at medium-dense state ($e_0 = 0.60$) and mixed with: a) 0.0% fiber (PSD), b) 0.0% fiber (PSR), c) 0.4% fiber (PSD), and d) 0.4% fiber (PSR).

Figure 3.25 shows the failure envelopes for the $\overline{CU}$ tests with the chosen limiting strains for the unreinforced and reinforced Ottawa sand prepared as loose and medium-dense specimens. The Mohr-Coulomb strength parameters, c' and ϕ' for the unreinforced and reinforced Ottawa sand specimens at limiting strains are summarized in Table 3.7. Since peak stresses generally occurred at relatively low strains and maintain strength up to large strains, the effective stress friction angles for the unreinforced Ottawa sand specimens are identical for the chosen limiting strains. In contrast, the shear strength parameters computed for the reinforced specimens at chosen limiting strains are all different. For loose reinforced specimens in particular, both the effective stress cohesion intercepts and friction angles increased with increasing strains. This also indicates the strain hardening response for the loose fiber-reinforced Ottawa sand.

Table 3.7 Mohr-Coulomb Strength Parameters, c' and ϕ', for Unreinforced and Reinforced Ottawa Specimens from the $\overline{CU}$ Tests When Peak Strength is Taken as Peak Stress Experienced at Limiting Strains of 5, 15, and 25 Percent

Initial Void Ratio	Fiber Content	Limit Strain					
		5% Strain		15% Strain		25% Strain	
		c' (psi)	ϕ' (deg)	c' (psi)	ϕ' (deg)	c' (psi)	ϕ' (deg)
0.74	0.0%	0.0	29.9	0.0	30.2	0.0	29.6
	0.4%	2.3	36.7	4.0	42.0	7.0	44.9
0.60	0.0%	0.0	33.6	0[a]	33.0[a]	0[a]	31.3[a]
	0.4%	8.1	35.6	9.4[a]	39.6[a]	0[a]	39.1[a]

[a]: Suspicious result due to equipment limitation for pore pressure measurements.

A comparison of the different failure envelopes for the Ottawa sand specimens compacted at loose and medium-dense states is exemplified in Table 3.7. Since the absolute pore pressure of the medium-dense reinforced specimens reached zero before 10 percent strain, the Mohr-Coulomb strength parameters are only reached at 5 percent strain. The results indicate that the medium-dense reinforced specimens show increases in both the effective stress cohesion intercept and the effective stress friction angle, whereas loose specimens show dominant large increases in the effective friction angle, but only limited increases in the effective stress cohesion intercept with increasing limiting strains.

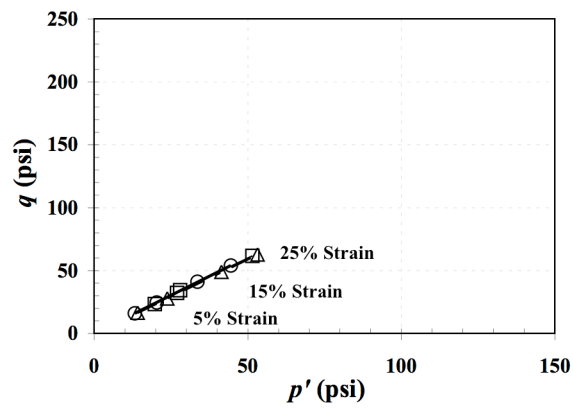

a) loose specimen, 0.0% fiber

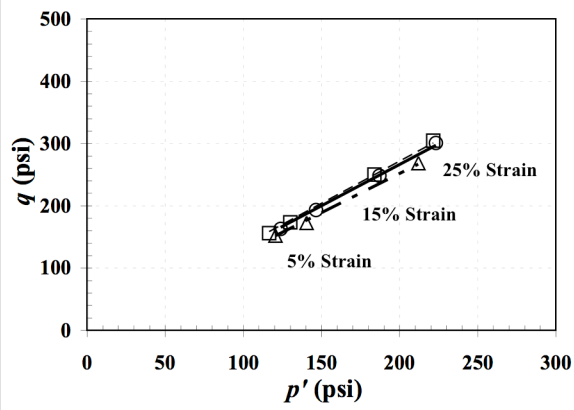

c) medium-dense specimen, 0.0% fiber

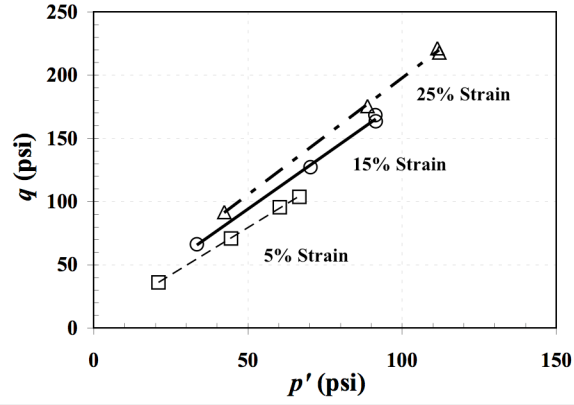

b) loose specimen, 0.4% fiber

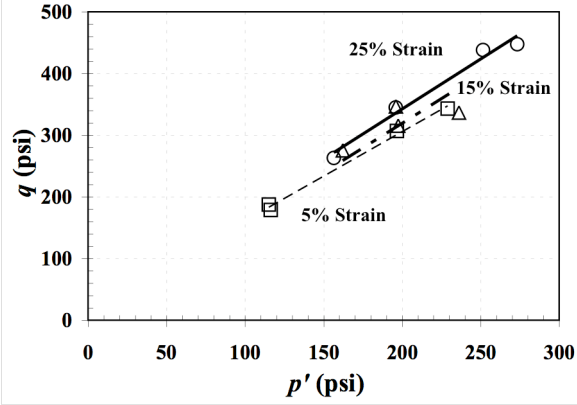

d) medium-dense specimen, 0.4% fiber

Figure 3.25 Failure envelopes from the $\overline{CU}$ tests for limiting strains of 5,15, and 25 percent shear strain on unreinforced and reinforced Ottawa sand specimens compacted at and mixed with: a) loose state, 0.0% fiber, b) loose state, 0.4% fiber, c) medium-dense state, 0.0% fiber, and d) medium-dense state, 0.4% fiber.

3.8 Summary

Test materials and preparation methods for the laboratory work were described in this chapter, as was the research programs performed for this research. Results of the undrained tests show that the silty sand and Ottawa sand reinforced with fibers can improve the strength of soils in terms of the effective stress cohesion intercept and friction angle under undrained loading conditions. In addition, fiber-reinforced soils can increase the strength parameters when the chosen limiting strains are increased (e.g. 5, 15, and 25 percent strains). Increasing fiber content does not affect the increase in the deviator stress for silty sand. Furthermore, the silty sand needs more triaxial shear strains (e.g. 20 percent) to mobilize the fiber resistance than the Ottawa sand specimens (e.g. 5 percent) do.

The results presented in Figures 3.7 and 3.8 show that the fiber-reinforced silty sand specimens required a higher pore pressure to maintain the zero volume change during the $\overline{CU}$ tests. According to Romero (2003), the fibers interact with silty clay to create an "internal confining stress" when added to the applied total stresses and the actual pore pressures generated in the fiber-reinforced silty clay specimens. The fibers produce the additional effective stress to prevent the volume change during undrained loading conditions are observed for the fiber-reinforced silty sand specimens as well.

However, the fibers in the loose Ottawa sand specimens did not need the extra pore pressure to prevent the zero volume change in the $\overline{CU}$ tests (Figure 3.16). The inclusion of fibers generated a negative “internal confining stress” and produced a negative effective stress to prevent the zero volume change within the loose Ottawa sand specimens.

CHAPTER 4: DRAINED BEHAVIOR OF FIBER-REINFORCED SOILS

4.1 Introduction

In this chapter, the results of conventional consolidation-drained (*CD*) type triaxial compression tests conducted to evaluate the stress-strain-volume change behavior of fiber-reinforced soils under drained loading conditions are presented. Results of isotropic consolidation tests performed on unreinforced and fiber-reinforced silty and Ottawa sand specimens are also presented and discussed.

4.2 Results of the Consolidation-Drained (*CD*) Triaxial Compression Tests for Silty Sand

A total of twenty *CD* type triaxial compression tests were performed on unreinforced and fiber-reinforced silty sand specimens compacted at 18 percent and 22 percent water contents (Table 3.1). The silty sand specimens were consolidated to 5, 10, 20, 40, and 80-psi (35, 70, 140, 280, 350-kPa) to evaluate their stress-strain-volume change behavior under drained loading conditions at a range of consolidation stresses. All fiber-reinforced specimens were prepared with 0.4 percent fibers.

4.2.1 Stress-Strain Response

The stress-strain behavior observed in the *CD* tests for the unreinforced and fiber-reinforced silty sand specimens is shown in Figures 4.1 and 4.2 for samples compacted at 18 percent and 22 percent water contents, respectively. Unreinforced specimens consolidated to low effective stresses of about 10-psi (70-kPa) or less showed peak stresses at 5 percent strain or less, while those consolidated to higher effective stresses

required greater strain to reach the peak stress. The fiber-reinforced silty sand specimens show a strain-hardening behavior similar to that of the undrained tests for the reinforced specimens. In these tests, there was generally no noticeable peak stress observed except at the highest effective confining stresses, where peak stresses were observed at approximately 25 percent strain.

As seen in Figures 4.1 and 4.2, the stress-strain responses of fiber-reinforced silty sand specimens begin to deviate from that of the unreinforced specimens at 3 to 7 percent strains for specimens compacted at 18 percent water content, and at 5 to 12 percent strains for those compacted at 22 percent water content. Note that the level of strain at which the stress-strain response for unreinforced and reinforced specimens is much lower for drained (CD) tests than for undrained ($\overline{CU}$) tests (Section 3.5.1). This suggests that fibers in the specimen mobilize resistance at lower strains in drained tests. This is presumably due to the volume change that is allowed in drained tests. In addition, the strain levels at which the stress-strain curves for unreinforced and reinforced specimens begin to deviate tends to increase as the effective confining stress increases, which is also presumably due to differences in volume change in tests performed at higher effective confining stress.

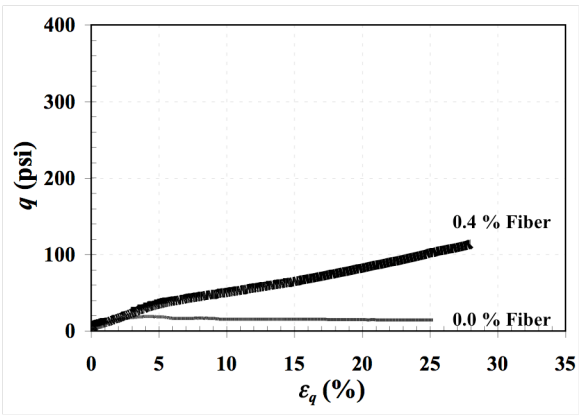

a) 5-psi effective consolidation stress

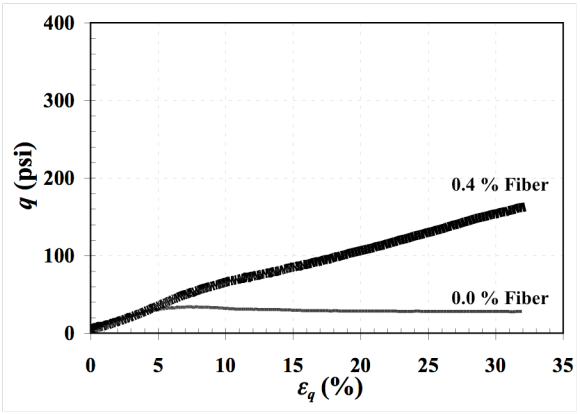

b) 10-psi effective consolidation stress

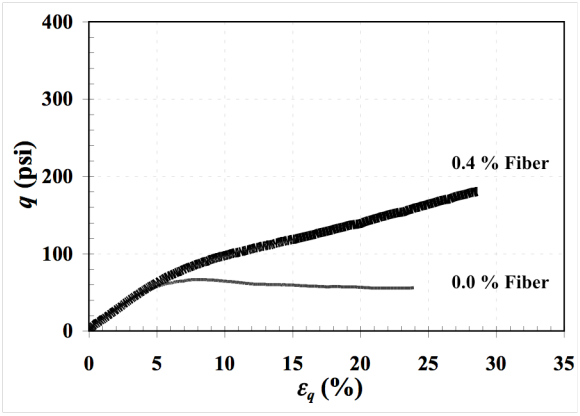

c) 20-psi effective consolidation stress

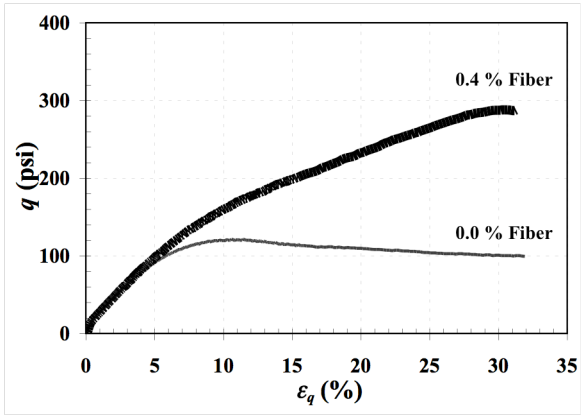

d) 40-psi effective consolidation stress

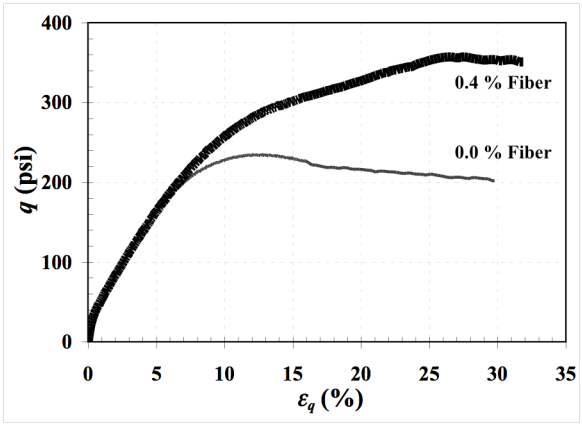

e) 80-psi effective consolidation stress

Figure 4.1 Deviatoric stress (q) versus triaxial shear strain (ε_q) curves from CD tests for the silty sand specimens compacted at 18 percent water content and consolidated to: a) 5-psi effective stress, b) 10-psi effective stress, c) 20-psi effective stress, d) 40-psi effective stress, and e) 80-psi effective stress.

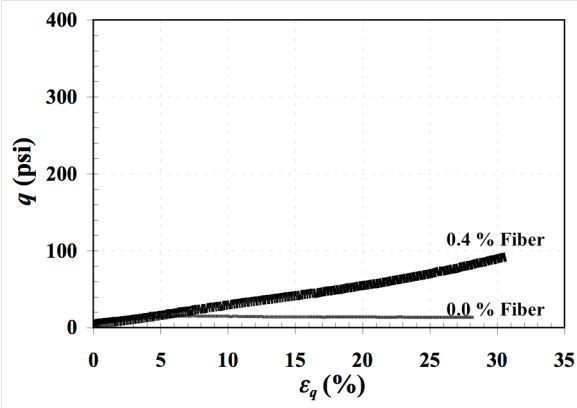

a) 5-psi effective consolidation stress

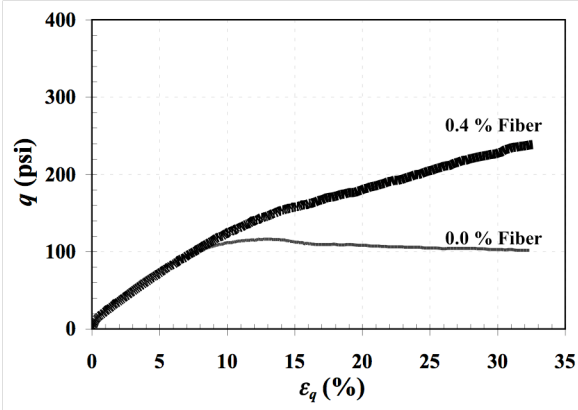

d) 40-psi effective consolidation stress

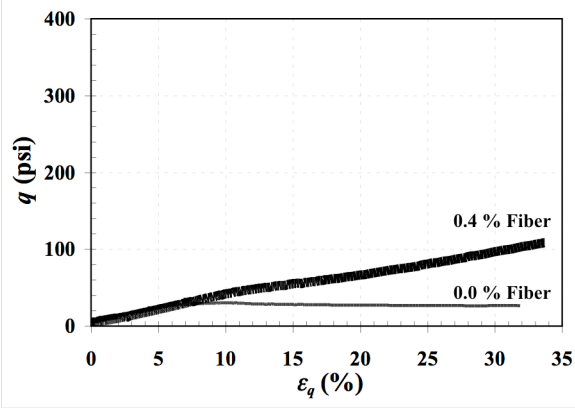

b) 10-psi effective consolidation stress

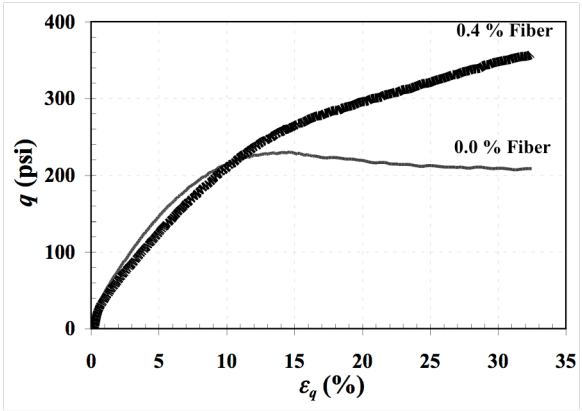

e) 80-psi effective consolidation stress

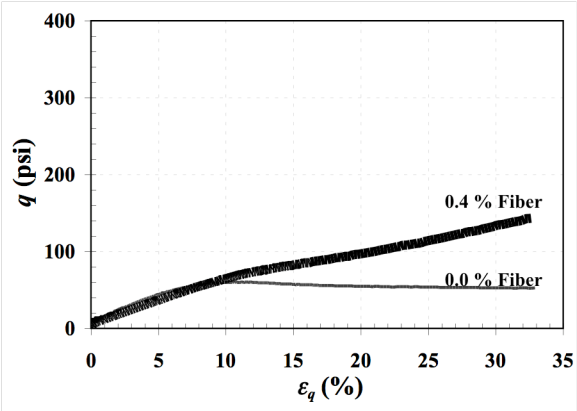

c) 20-psi effective consolidation stress

Figure 4.2 Deviatoric stress (q) versus triaxial shear strain (ε_q) curves from CD tests for the silty sand specimens compacted at 22 percent water content and consolidated to: a) 5-psi effective stress, b) 10-psi effective stress, c) 20-psi effective stress, d) 40-psi effective stress, and e) 80-psi effective stress.

Typical failure modes for the *CD* tests for unreinforced and fiber-reinforced silty sand specimens compacted at 18 percent and 22 percent water contents and consolidated to 20-psi (140-kPa) are shown in Figure 4.3. These photographs reveal that the unreinforced specimens exhibited a budging deformation type of failure, while the reinforced specimens developed multiple failure plans. The randomly placed fibers within the specimens tend to mobilize the shear stress in every direction, producing multiple failure planes when sheared to large strains.

a) 18 % water content, 0.0 % fiber

c) 22 % water content, 0.0 % fiber

b) 18 % water content, 0.4 % fiber

d) 22 % water content, 0.4 % fiber

Figure 4.3 Typical failure modes of the *CD* tests at 20-psi effective consolidation stress for the silty sand specimens compacted at and mixed with: a) 18% water content, 0.0% fiber, b) 18% water content, 0.4% fiber, c) 22% water content, 0.0% fiber, and d) 22% water content, 0.4% fiber.

4.2.2 Effective Principal Stress Ratio-Strain Response

Figures 4.4 and 4.5 show the effective principal stress ratio versus strain responses in the *CD* tests for the silty sand specimens compacted at 18 percent and 22 percent water contents, respectively. The unreinforced specimens exhibited effective principal stress ratio-strain curves where reached a peak at about 5 to 10 percent strain and kept an essentially constant stress ratio of about 3 until they reached larger strains. Specimens consolidated to lower effective stresses reached peak strains at lower strains than specimens consolidated to higher effective stresses.

In general, the effective principal stress ratio versus strain behavior observed for fiber-reinforced silty sand specimens tested under drained loading conditions was similar to specimens tested in undrained tests. The reinforced specimens showed a strain-hardening behavior with no observable peak effective principal stress ratio over the range of strains tested. A clear trend of decreasing ultimate effective principal stress ratios with increases effective confining stress is observed, with maximum effective principal stress ratio of 20 to 25 observed at low confining stress while the maximum effective principal stress ratio at higher confining stress was around 5.

The effective principal stress ratio-strain response of fiber-reinforced specimens began to deviate from that of unreinforced specimens at strains of 4 to 10 percent. The strain levels at which the effective principal stress ratio-strain curves for both unreinforced and reinforced specimens began to deviate tended to increase as the effective confining stresses increased. The magnitude of the effective principal stress ratio for both unreinforced and reinforced specimens tended to decrease as the effective confining stress increased.

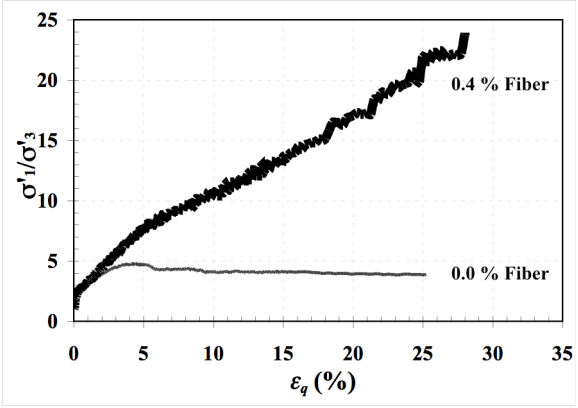

a) 5-psi effective consolidation stress

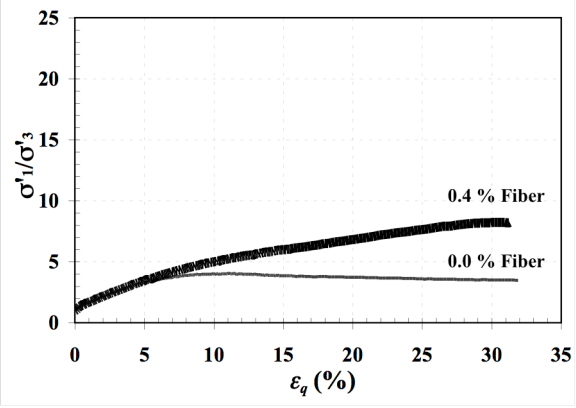

d) 40-psi effective consolidation stress

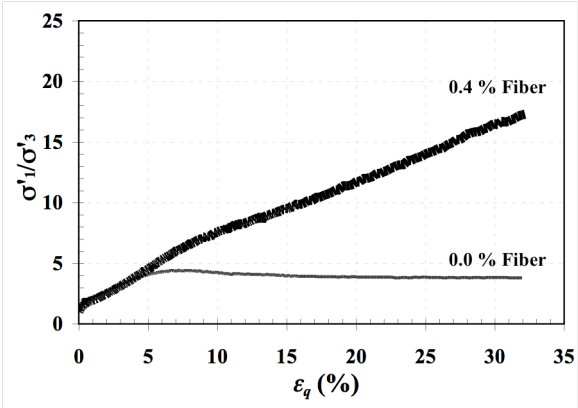

b) 10-psi effective consolidation stress

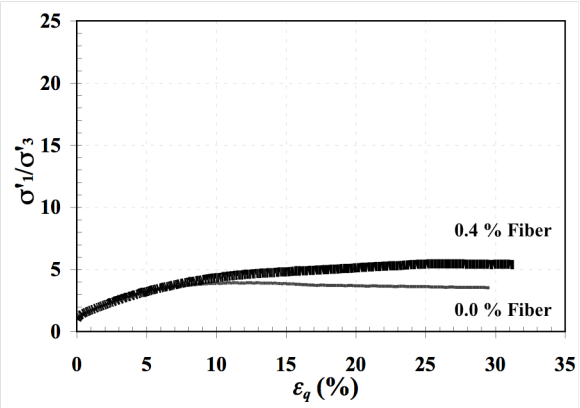

e) 80-psi effective consolidation stress

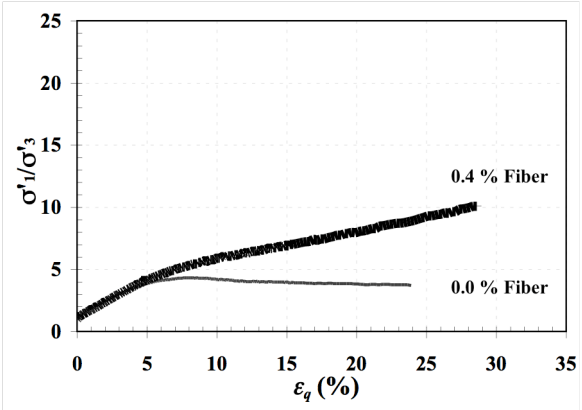

c) 20-psi effective consolidation stress

Figure 4.4 Effective principal stress ratio (σ'_1/σ'_3) versus the triaxial shear strain (ε_q) curves from the *CD* tests for silty sand specimens compacted at 18 percent water content and consolidated to: a) 5-psi effective stress, b) 10-psi effective stress, c) 20-psi effective stress, d) 40-psi effective stress, and e) 80-psi effective stress.

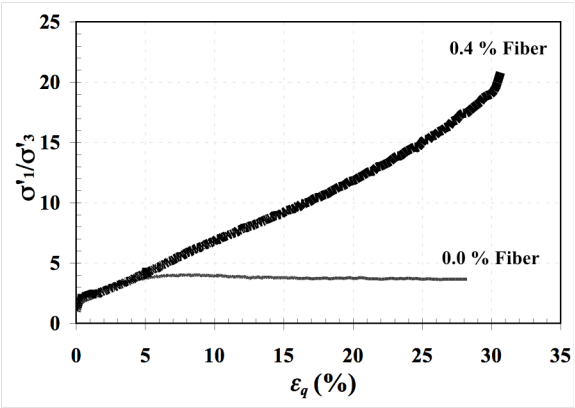

a) 5-psi effective consolidation stress

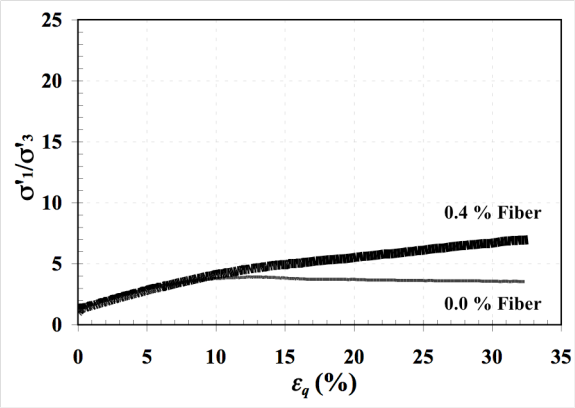

d) 40-psi effective consolidation stress

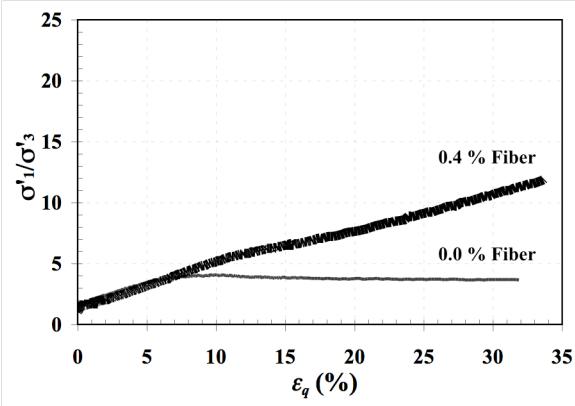

b) 10-psi effective consolidation stress

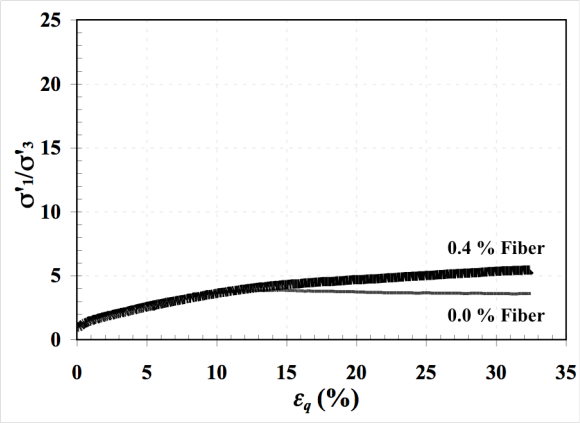

e) 80-psi effective consolidation stress

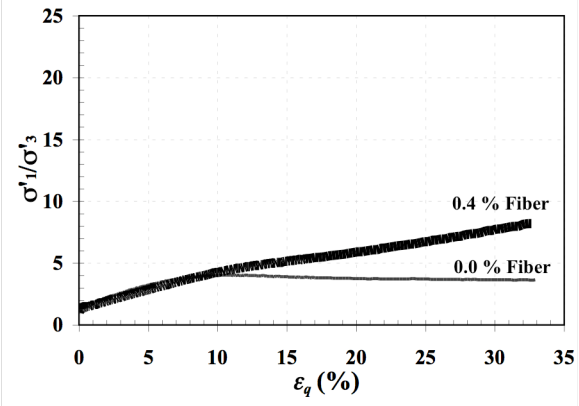

c) 20-psi effective consolidation stress

Figure 4.5 Effective principal stress ratio (σ'_1/σ'_3) versus the triaxial shear strain (ε_q) curves from the *CD* tests for silty sand specimens compacted at 22 percent water content and consolidated to: a) 5-psi effective stress, b) 10-psi effective stress, c) 20-psi effective stress, d) 40-psi effective stress, and e) 80-psi effective stress.

4.2.3 Volumetric Strain-Stain Response

Volumetric strain versus the triaxial shear strain responses observed in the *CD* test for unreinforced and reinforced silty sand specimens are shown in Figures 4.6 and 4.7, respectively. The unreinforced specimens revealed classical response for compacted soils compression at small strains followed by significant dilation as they reached larger strains. The amount of dilation was observed to decrease with increasing effective confining stresses. Fiber-reinforced silty sand specimens revealed similar volumetric strain response with initial compression at small strains followed by dilation. However, the amount of dilation observed for the reinforced specimens was significantly less than that of the unreinforced specimens. The differences in volumetric strain for unreinforced and reinforced specimens tended to decrease with increasing effective confining stresses. The volumetric strain for fiber-reinforced silty sand specimens began to deviate from that of the unreinforced specimens at strains of 1 to 5 percent. The strain levels at which the volumetric strain curves for both the unreinforced and reinforced specimens began to deviate tended to increase as the effective confining stresses increased, which suggests greater mobilization of fiber resistance at lower effective confining stress. This, in turn, again suggests that volumetric strain plays an important role in mobilization of fiber resistance.

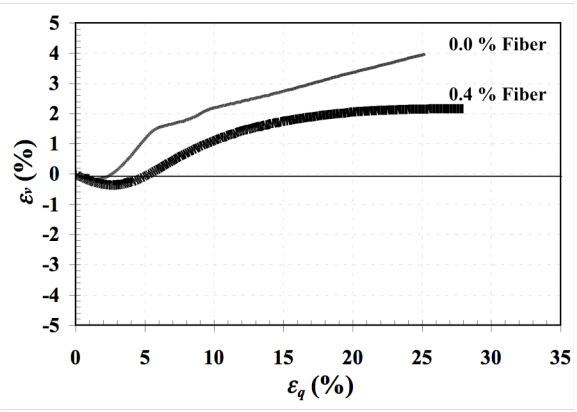

a) 5-psi effective consolidation stress

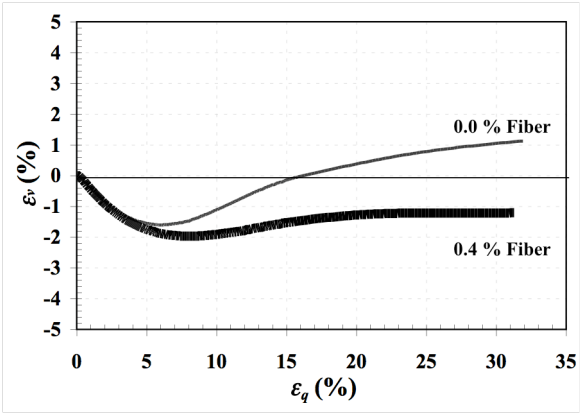

d) 40-psi effective consolidation stress

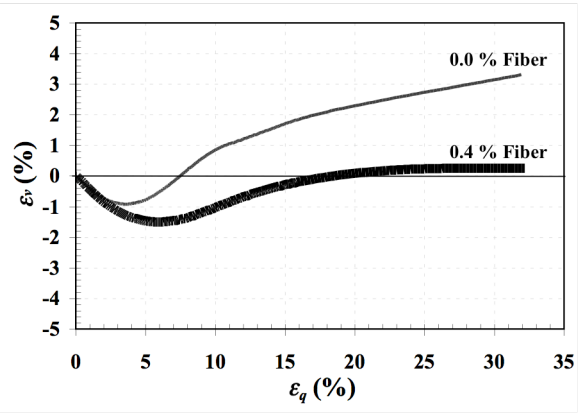

b) 10-psi effective consolidation stress

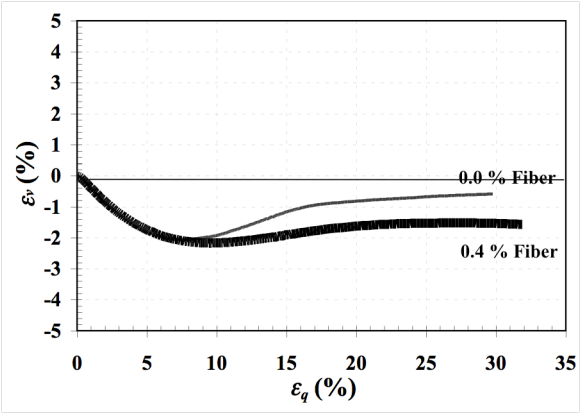

e) 80-psi effective consolidation stress

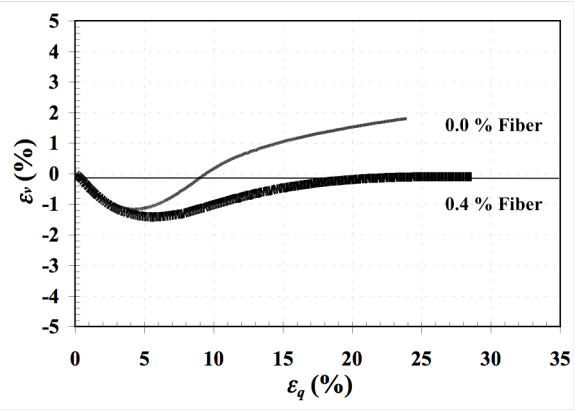

c) 20-psi effective consolidation stress

Figure 4.6 Volumetric Strain (ε_v) versus triaxial shear strain (ε_q) curves from the *CD* tests for silty sand specimens compacted at 18 percent water content and consolidated to: a) 5-psi effective stress, b) 10-psi effective stress, c) 20-psi effective stress, d) 40-psi effective stress, and e) 80-psi effective stress.

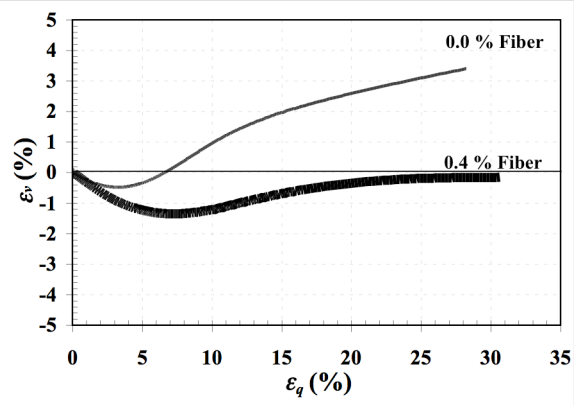

a) 5-psi effective consolidation stress

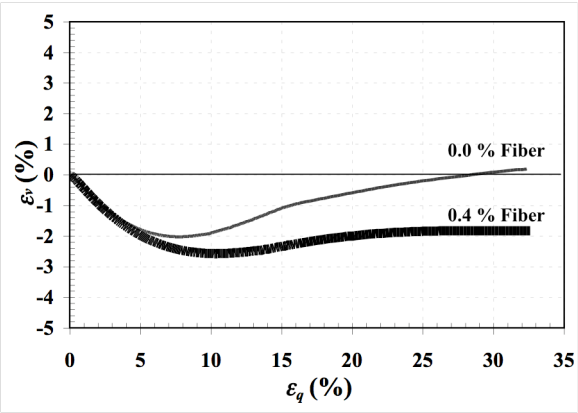

d) 40-psi effective consolidation stress

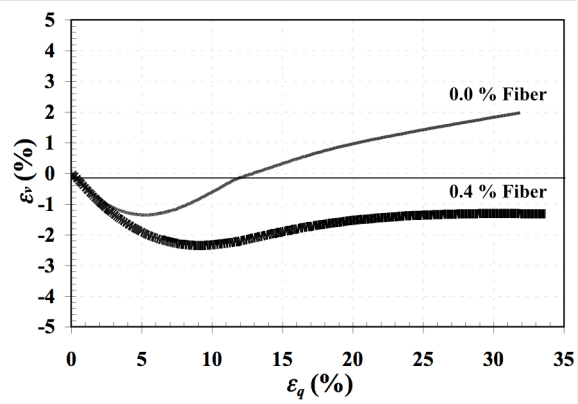

b) 10-psi effective consolidation stress

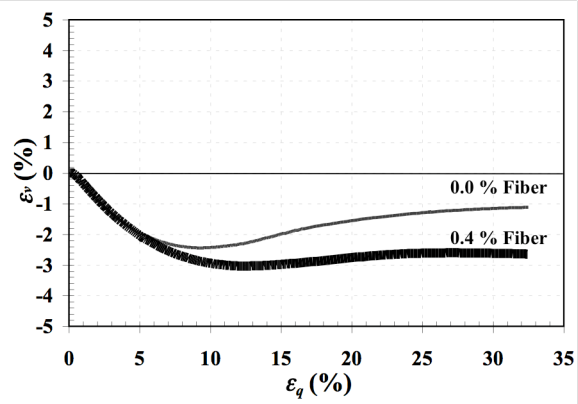

e) 80-psi effective consolidation stress

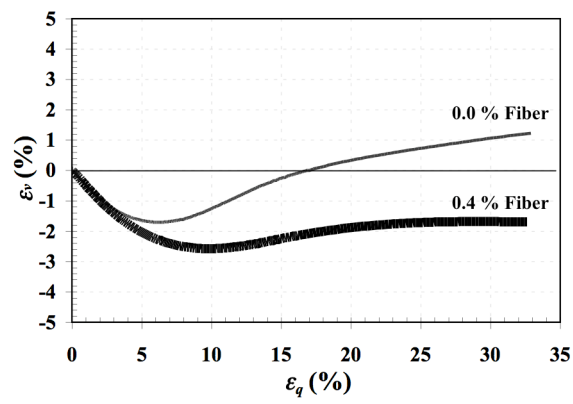

c) 20-psi effective consolidation stress

Figure 4.7 Volumetric Strain (ε_v) versus triaxial shear strain (ε_q) curves from the *CD* tests for silty sand specimens compacted at 18 percent water content and consolidated to: a) 5-psi effective stress, b) 10-psi effective stress, c) 20-psi effective stress, d) 40-psi effective stress, and e) 80-psi effective stress.

4.3 Results of Consolidated-Drained (*CD*) Triaxial Compression Tests for Ottawa Sand

A total of sixteen *CD* type triaxial compression tests were performed on unreinforced and fiber-reinforced Ottawa sand specimens compacted at loose ($e_0 = 0.74$) and medium-dense ($e_0 = 0.60$) states and consolidated to 5, 20, 40, and 60-psi (35, 140, 280, and 415-kPa) to evaluate the stress-strain-volume change behavior under drained loading conditions. Table 3.2 summarized the conditions for these tests.

4.3.1 Stress-Strain Response

The stress-strain behavior observed in the *CD* tests for the unreinforced and reinforced Ottawa sand specimens is shown in Figures 4.8 and 4.9. In general, the unreinforced specimens consolidated to different confining stresses tended to reach peak deviatoric stress levels at a very small strain of 1 percent and maintained stresses until large strains were reached.

The reinforced specimens again exhibit strain-hardening response for all tests. At higher effective confining stresses (e.g. greater than or equal to 20-psi) reinforced specimens also exhibited a peak stress at strains of 20 percent or greater. The stress-strain responses for fiber-reinforced loose and dense specimens began to deviate from those of unreinforced specimens before 2 percent strain at all effective consolidation stresses. Again, the mobilization of the fibers in drained loading conditions is observed to be faster than in undrained loading cases.

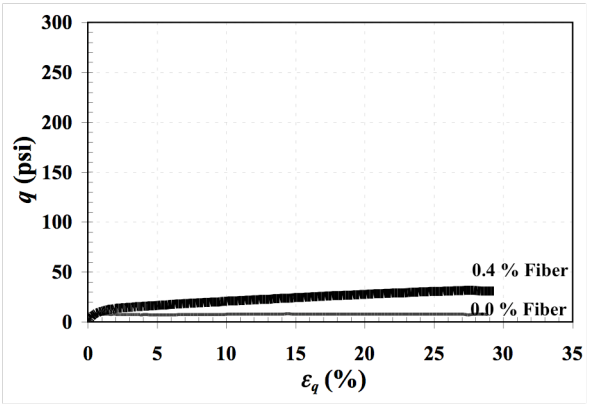

a) 5-psi effective consolidation stress

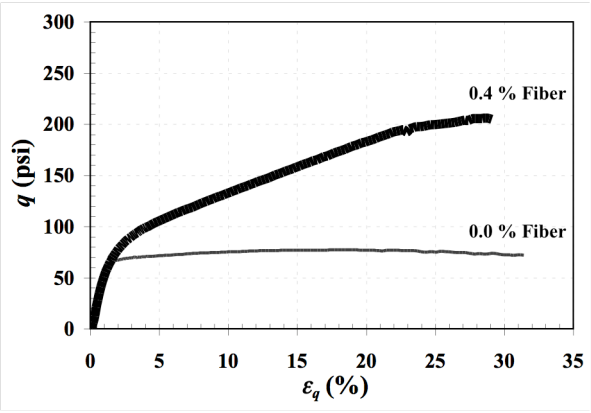

c) 40-psi effective consolidation stress

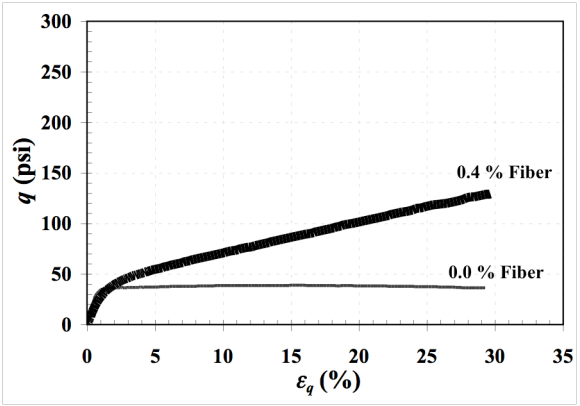

b) 20-psi effective consolidation stress

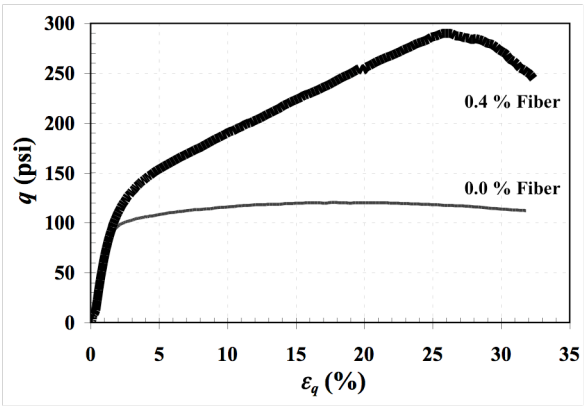

d) 60-psi effective consolidation stress

Figure 4.8 Deviatoric stress (q) versus triaxial shear strain (ε_q) curves from the CD tests for loose Ottawa sand specimens ($e_0 = 0.74$) and consolidated to: a) 5-psi effective stress, b) 20-psi effective stress, c) 40-psi effective stress, and d) 60-psi effective stress.

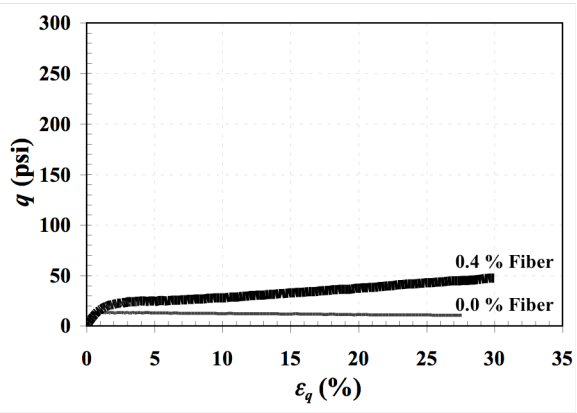

a) 5-psi effective consolidation stress

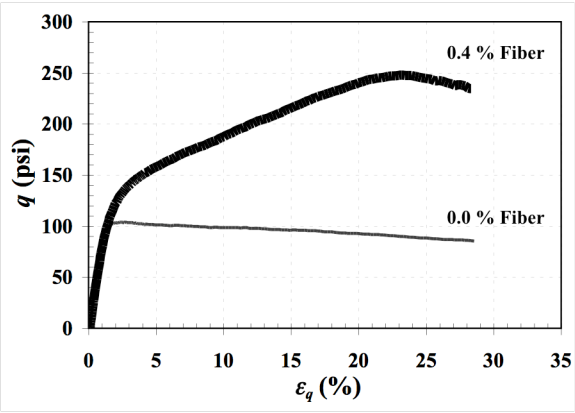

c) 40-psi effective consolidation stress

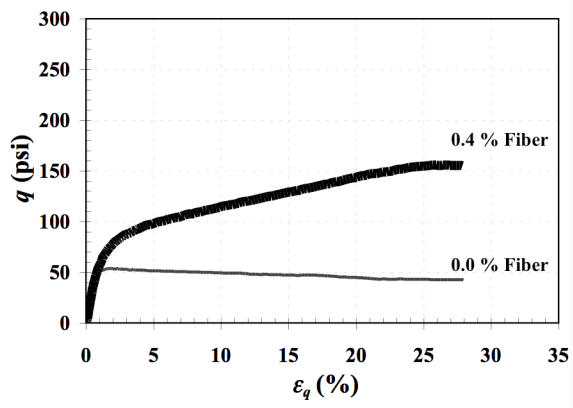

b) 20-psi effective consolidation stress

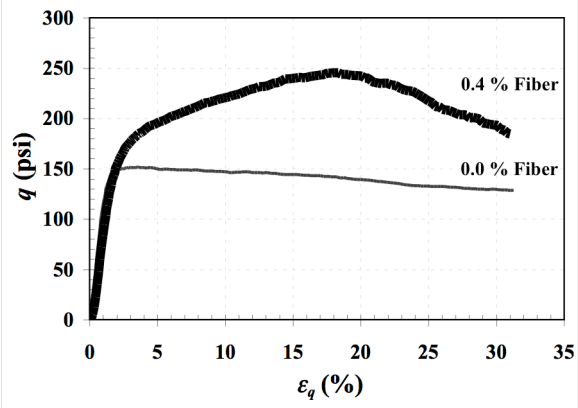

d) 60-psi effective consolidation stress

Figure 4.9 Deviatoric stress (q) versus triaxial shear strain (ε_q) curves from the CD tests for medium-dense Ottawa sand specimens ($e_0 = 0.60$) and consolidated to: a) 5-psi effective stress, b) 20-psi effective stress, c) 40-psi effective stress, and d) 60-psi effective stress.

Typical *CD* test failure modes for the unreinforced and fiber-reinforced Ottawa sand specimens compacted at loose and medium-dense states and consolidated to 60-psi (415-kPa) are shown in Figure 4.10. These photographs reveal that the unreinforced loose and medium-dense specimens exhibited a budging failure, and medium-dense unreinforced specimen exhibited larger budging than for loose unreinforced specimens tested under the same conditions. The reinforced loose specimens also demonstrated a budging failure, whereas the reinforced medium-dense specimens revealed clearly defined multiple failure plans when they reached the failure.

a) loose state, 0.0 % fiber

c) medium-dense state, 0.0 % fiber

b) loose state, 0.4 % fiber

d) medium-dense state, 0.4 % fiber

Figure 4.10 Typical failure modes of the *CD* tests at 60-psi effective consolidation stress for Ottawa specimens prepared at and mixed with: a) loose state, 0.0% fiber, b) loose state, 0.4% fiber, c) medium-dense state, 0.0% fiber, and d) medium-dense state, 0.4% fiber.

4.3.2 Effective Principal Stress Ratio-Stress Response

Figures 4.11 and 4.12 show the effective principal stress ratio versus the shear strain in the *CD* tests for the unreinforced and fiber-reinforced Ottawa sand specimens compacted at loose and medium-dense states, respectively. The effective principal stress ratio-strain curves for unreinforced specimen peak at about 1 percent strain and remained relatively constant up to large strains. The peak effective principal stress ratio for loose specimens was about 3, and for medium-dense specimens was about 3.5. The effective principal stress ratio-strain curves are similar to the results of undrained tests, which are shown in Figures 4.11 and 4.12.

The loose and medium-dense reinforced specimens showed a strain-hardening behavior for specimens consolidated to 5-psi and 20-psi (35-kPa and 140-kPa) with no observable peak effective principal stress over the range of strains tested. However, the maximum effective principal stress ratio of 5 to 8 was observed when reached very large strains (up to 25 percent) at higher confining stress. A clear trend of decreasing ultimate effective principal stress ratios with increasing effective confining stress is observed, which can be seen for fiber-reinforced silty sand specimen in drained tests.

The effective principal stress ratio-strain responses for reinforced specimens began to deviate from that of unreinforced specimens before reached 2 percent strains under different consolidation stresses. The effective principal stress ratio differences in terms of unreinforced and reinforced Ottawa sand specimens tended to decrease with increasing effective confining stress at any given strain.

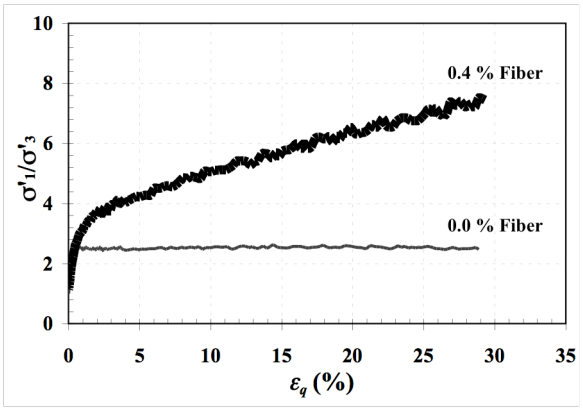

a) 5-psi effective consolidation stress

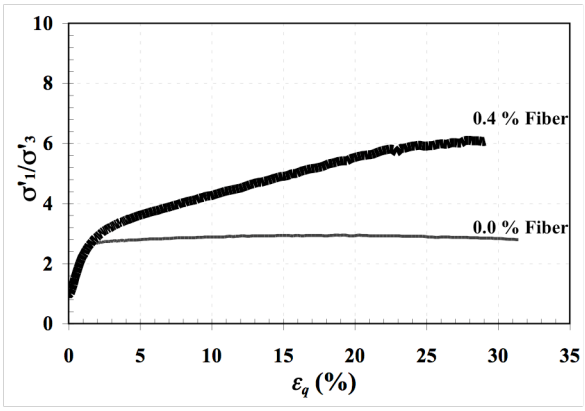

c) 40-psi effective consolidation stress

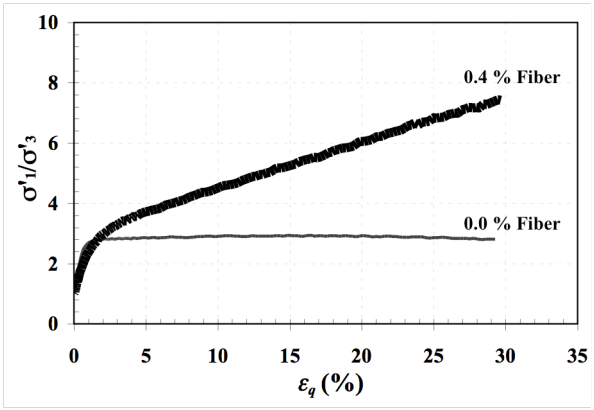

b) 20-psi effective consolidation stress

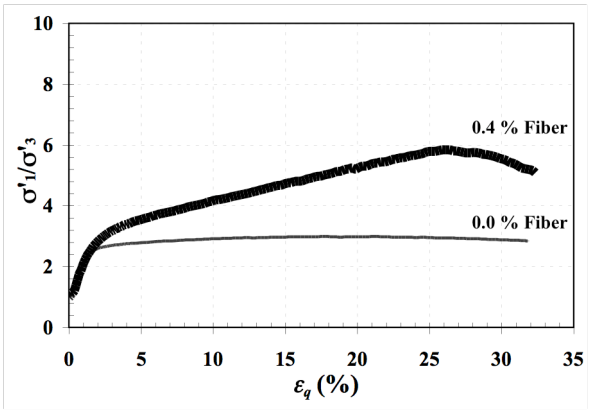

d) 60-psi effective consolidation stress

Figure 4.11 Effective principal stress ratio (σ'_1/σ'_3) versus triaxial shear strain (ε_q) curves from the CD tests for loose Ottawa sand specimens ($e_0 = 0.74$) and consolidated to: a) 5-psi effective stress, b) 20-psi effective stress, c) 40-psi effective stress, and d) 60-psi effective stress.

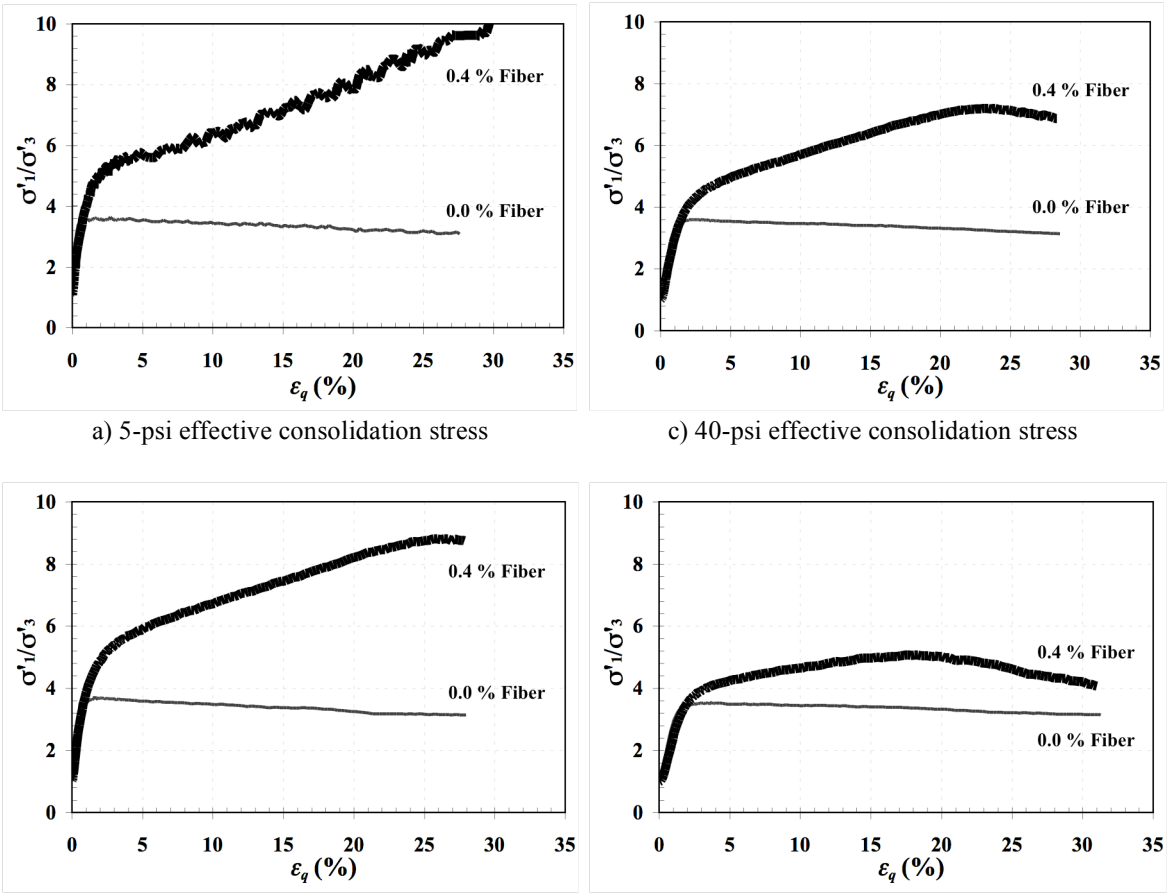

Figure 4.12 Effective principal stress ratio (σ'_1/σ'_3) versus triaxial shear strain (ε_q) curves from the CD tests for medium-dense Ottawa sand specimens ($e_0 = 0.60$) and consolidated to: a) 5-psi effective stress, b) 20-psi effective stress, c) 40-psi effective stress, and d) 60-psi effective stress.

4.3.3 Volumetric Strain Response

The volumetric strain versus shear strain responses for the unreinforced and reinforced Ottawa sand specimens are shown in Figures 4.13 and 4.14 for samples compacted in loose and medium-dense states. The loose unreinforced specimens consolidated at low effective stress (5-psi) showed an little volumetric strain throughout shear. While the loose specimens consolidated to higher effective stresses showed increasing compression with increasing consolidation stress. In contrast, the medium-dense unreinforced specimens showed initial compression at small strains followed by a significant dilation up to large strains. The initial compression increased with increasing effective confining stress; however, the amount of dilation decreased with increasing effective confining stress.

The loose and medium-dense reinforced specimens generally showed similar volumetric strain response to the unreinforced specimens. In same tests, reinforced specimens exhibited slightly more or less volumetric strain than unreinforced specimens, but the differences are small and appear to follow no consistent trend.

The volumetric strain response observed for the reinforced silty sand is different from that observed for the reinforced Ottawa sand. The amount of dilation observed in the reinforced silty sand specimens was significantly less than the dilation observed in the unreinforced specimens. However, the reinforced Ottawa sand specimens tended to compress less (dilate more) than the unreinforced specimens when specimens were consolidated to higher effective stresses (e.g. greater than or equal to 20-psi), which is a consistent observation for the silty and Ottawa sand in undrained tests.

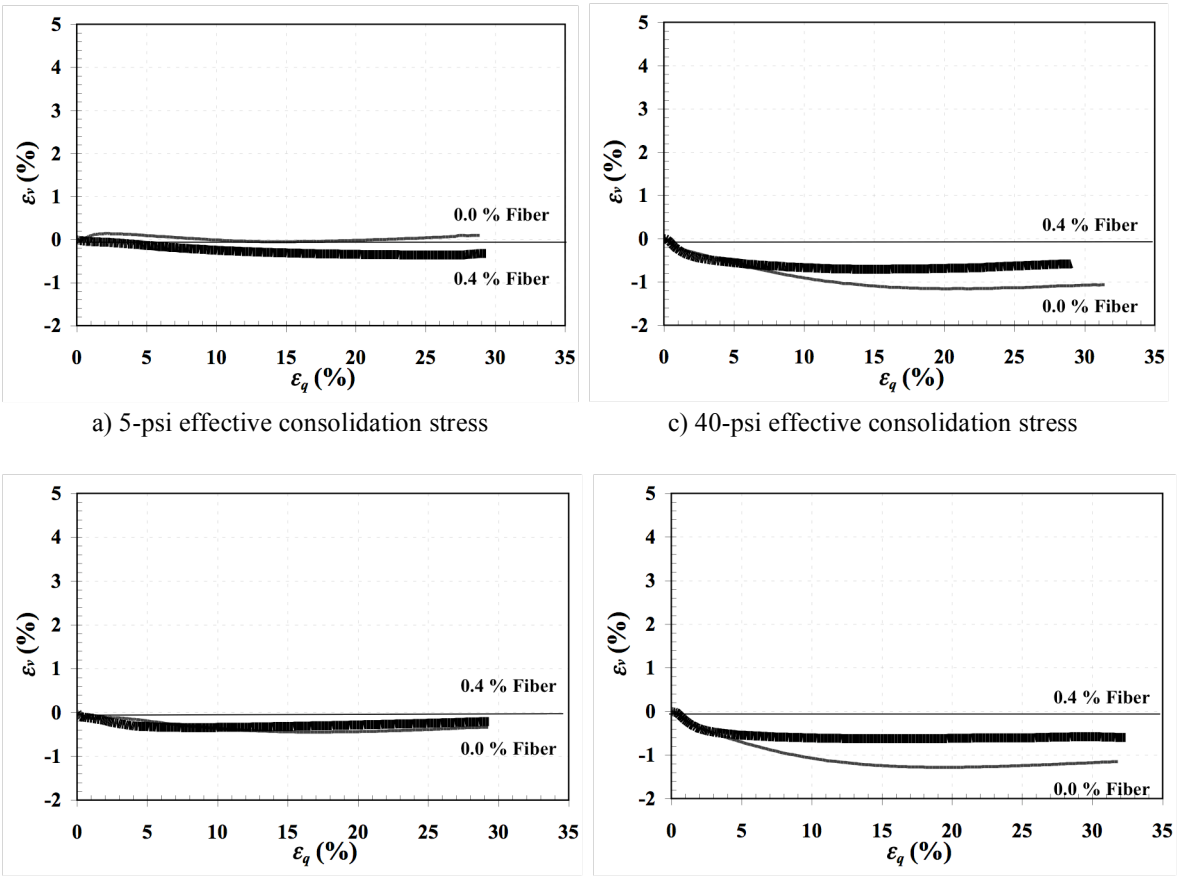

a) 5-psi effective consolidation stress

c) 40-psi effective consolidation stress

b) 20-psi effective consolidation stress

d) 60-psi effective consolidation stress

Figure 4.13 Volumetric Strain (ε_v) versus triaxial shear strain (ε_q) curves from the *CD* tests for loose Ottawa sand specimens ($e_0 = 0.74$) and consolidated to: a) 5-psi effective stress, b) 20-psi effective stress, c) 40-psi effective stress, and d) 60-psi effective stress.

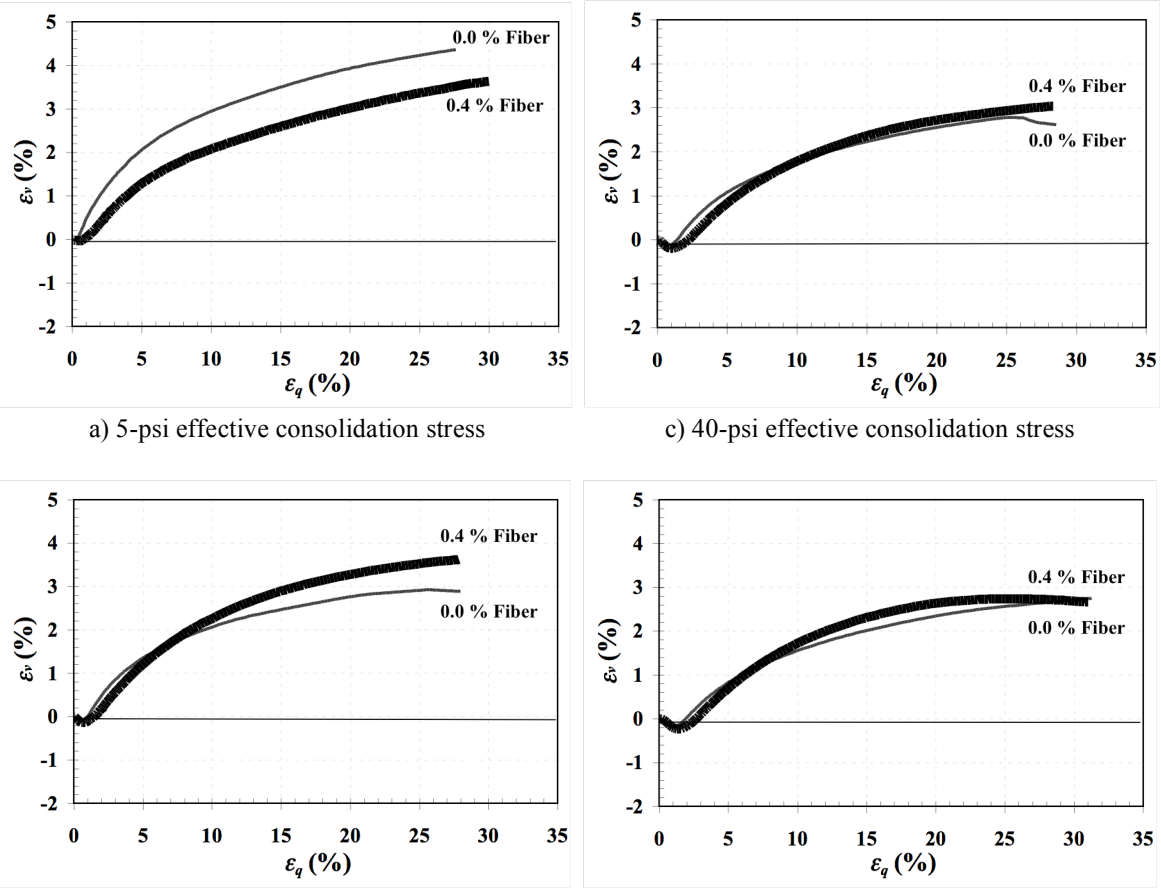

Figure 4.14 Volumetric Strain (ε_v) versus the triaxial shear strain (ε_q) curves from the *CD* tests for medium-dense Ottawa sand specimens ($e_0 = 0.60$) and consolidated to: a) 5-psi effective stress, b) 20-psi effective stress, c) 40-psi effective stress, and d) 60-psi effective stress.

4.4 Failure Envelopes for Consolidated-Drained (*CD*) Triaxial Compression Tests

Mohr-Coulomb strength parameters determined for unreinforced and reinforced silty and Ottawa sand specimens from the *CD* tests are presented and discussed in the following sections.

4.4.1 Drained Failure Envelopes for Silty Sand

Stress paths for all *CD* tests on unreinforced and fiber-reinforced specimens along with the failure envelopes established from these tests are shown in Figure 4.15. Mohr-Coulomb strength parameters, c' and ϕ', in terms of effective stresses for these envelopes are summarized in Table 4.1. The two failure criteria considered for undrained tests in Chapter 3 occur simultaneously in drained tests, so only the PSR criterion is considered here. The results indicate that the effective stress cohesion intercept and the friction angle of unreinforced specimens compacted at both 18 percent and 22 percent water content can be represented by 1-psi (7-kPa) and 36°, respectively. When comparing failure envelopes for the unreinforced specimens acquired from the *CD* tests with those acquired from the $\overline{CU}$ tests (Figure 3.20 and 3.21), the effective strength parameters determined from both sets of tests are similar under the PSR failure criteria. Again, the failure envelopes for specimens reinforced with 0.4 percent fibers based on the first 3 points, not including the last two points.

Table 4.1 Mohr-Coulomb Strength Parameters, c' and ϕ', for Unreinforced and Reinforced Silty Sand Specimens from the CD Tests

Water Content (%)	0.0% Fiber Content		0.4% Fiber Content	
	PSR		PSR	
	c' (psi)	ϕ' (deg)	c' (psi)	ϕ' (deg)
18	1.7	36.1	20.6	44.5
22	0.6	36.0	18.1	39.0

As shown in Table 4.1, the comparison of strength parameters for unreinforced and reinforced silty sand specimens reveal that the inclusion of fibers can improve the effective stress cohesion intercept by increasing it on average from 1-psi to 20-psi (7-kPa and 140-kPa). Inclusion fibers also improve the effective stress friction angle by increasing it on average from 36° to 42° in the CD tests.

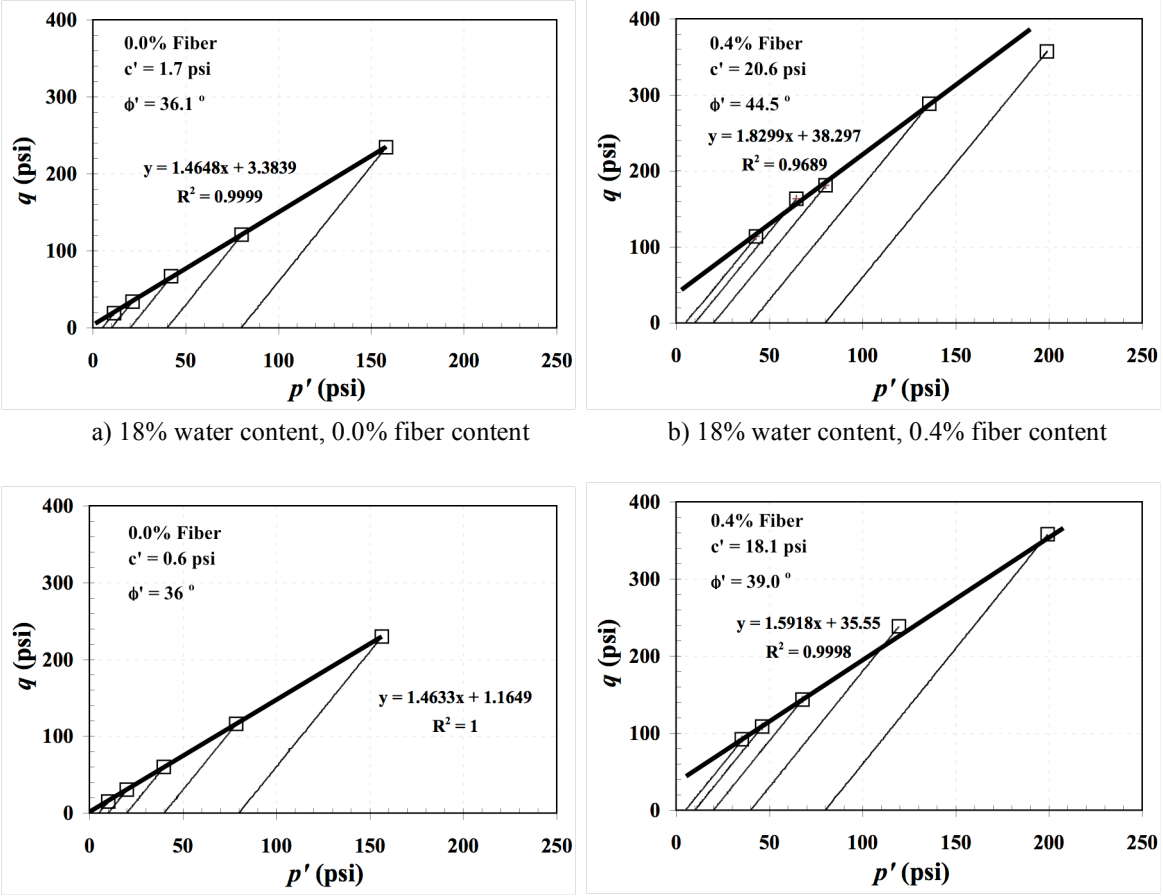

a) 18% water content, 0.0% fiber content

b) 18% water content, 0.4% fiber content

c) 22% water content, 0.0% fiber content

d) 22% water content, 0.4% fiber content

Figure 4.15 Failure envelopes of peak effective principal stress ratio (PSR) from the *CD* tests for silty sand specimens compacted at and mixed with: a) 18% water content, 0.0% fiber, b) 18% water content, 0.4% fiber, c) 22% water content, 0.0% fiber, and d) 22% water content, 0.4% fiber.

Figure 4.16 shows the failure envelopes at several limiting strains for the reinforced silty sand specimens compacted at 18 percent and 22 percent water contents. The failure envelopes for reinforced specimens tend to increase as the triaxial shear strains increase and are higher than the failure envelopes of the unreinforced specimens. The effective stress Mohr-Coulomb strength parameters, c' and ϕ', for the unreinforced and reinforced specimens at limiting strains are summarized in Table 4.2.

Table 4.2 Mohr-Coulomb Strength Parameters, c' and ϕ', for Unreinforced and Reinforced Silty Sand Specimens from the CD Tests When Peak Strength is Taken as Peak Stress Experienced at Limiting Strains of 5, 15, and 25 Percent

Water Content (%)	Fiber Content	Limit Strain					
		5% Strain		15% Strain		25% Strain	
		c' (psi)	ϕ' (deg)	c' (psi)	ϕ' (deg)	c' (psi)	ϕ' (deg)
18	0.0%	3.5	30.7	0.5	35.9	0.6	34.4
	0.4%	7.3	29.6	13.0	38.4	22.5	39.5
22	0.0%	1.9	29.4	0.0	35.9	0.2	34.7
	0.4%	2.9	26.8	6.4	37.6	12.3	39.6

As seen in the table, both the effective stress cohesion intercepts and the effective stress friction angles for the fiber-reinforced silty sand specimens increased with the increasing chosen limiting strains. In addition, a significant increase in the effective stress cohesion intercept was observed for the reinforced specimens as compared to the unreinforced specimens, but the effective stress friction angles determined at a 5 percent strain decreased for the unreinforced specimens. Again, the effective stress cohesion intercept for the failure envelopes determined at all levels of limiting shear strain is higher for reinforced specimens than for unreinforced specimens. Furthermore, a more

pronounced effect was produced when the effective stress cohesion intercepts increased than when the effective friction angle increased as a result of the inclusion of fibers.

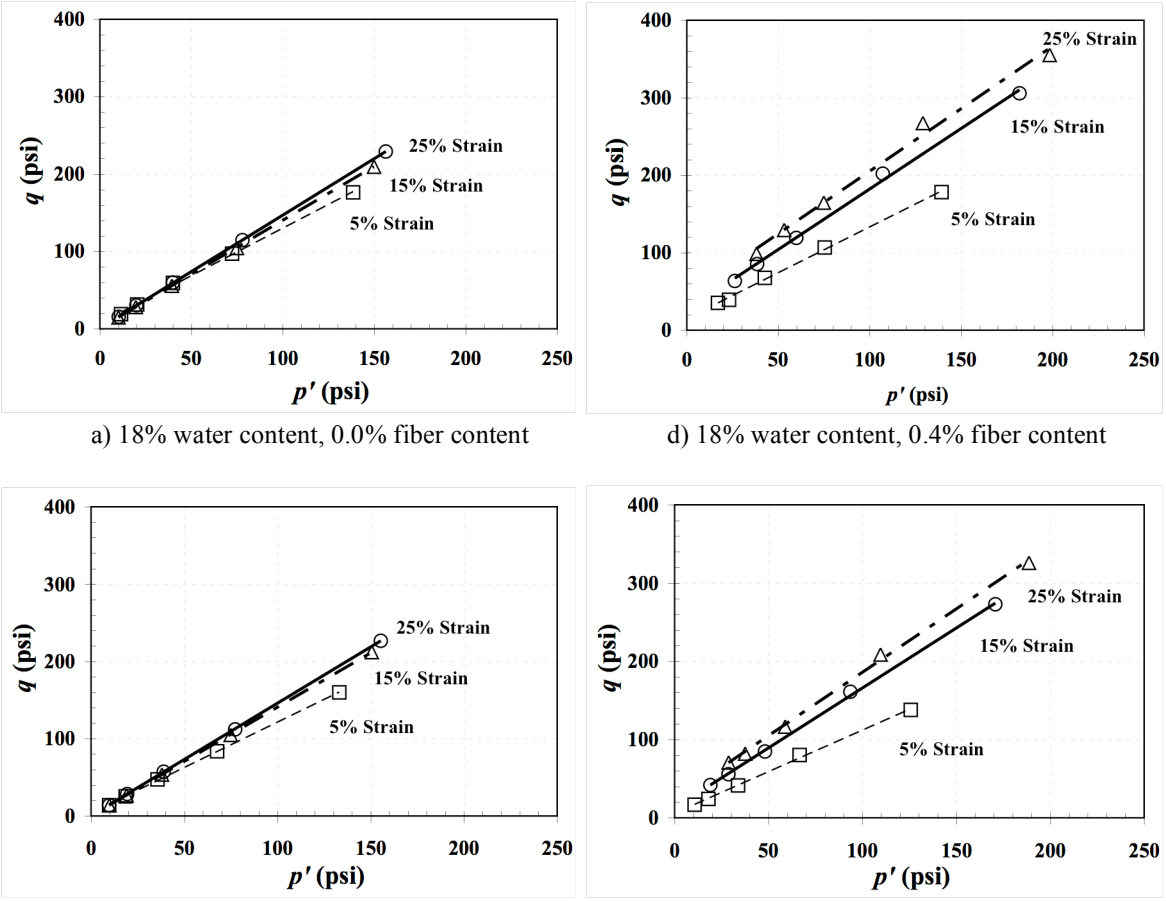

a) 18% water content, 0.0% fiber content

d) 18% water content, 0.4% fiber content

b) 22% water content, 0.4% fiber content

d) 22% water content, 0.4% fiber content

Figure 4.16 Failure envelopes from the *CD* tests for limiting strains of 5, 15, and 25 percent shear strain on unreinforced and reinforced silty sand specimens compacted at and mixed with: a) 18% water content, 0.0% fiber content, b) 22% water content, 0.0% fiber content, c) 18% water content, 0.4% fiber content, and d) 22% water content, 0.4% fiber content.

4.4.2 Drained Failure Envelopes for Ottawa Sand

Mohr-Coulomb strength parameters, c' and ϕ', for the Ottawa sand are summarized in Table 4.3. The shear strength of the unreinforced Ottawa sand specimens compacted at a loose state is represented by an effective stress friction angle of 30°, while the shear strength at a medium-dense state is represented by an effective stress friction angle of 34°. These envelopes are similar to those determined for the $\overline{CU}$ tests. In contrast, the failure envelopes for reinforced specimens determined from the CD tests compared with those determined from the $\overline{CU}$ tests (Table 3.7) under the same preparation and compaction, show that both the effective stress cohesion intercepts and the effective stress friction angles are not the same for reinforced specimens compacted at either loose or medium-dense states. The effective stress cohesion intercepts from the $\overline{CU}$ tests are higher than those from the CD tests, whereas the effective stress friction angle from the $\overline{CU}$ tests are slightly lower than those from the CD tests.

Table 4.3 Mohr-Coulomb Strength Parameters, c' and ϕ', for Unreinforced and Reinforced Ottawa Sand Specimens from the CD Tests

Initial Void Ratio	0.0% Fiber Content		0.4% Fiber Content	
	PSR		PSR	
	c' (psi)	ϕ' (deg)	c' (psi)	ϕ' (deg)
0.74	0.0	29.8	3.1	45.3
0.60	0.0	34.2	4.9	47.9

Compared with Table 3.7 from undrained tests

Initial Void Ratio	0.0% Fiber Content		0.4% Fiber Content	
	PSR		PSR	
	c' (psi)	ϕ' (deg)	c' (psi)	ϕ' (deg)
0.74	0	30.4	12.6	42.8
0.60	0	33.7	0 [a]	43.5 [a]

[a]: Suspicious result due to equipment limitation for pore pressure measurements.

The stress paths for all CD tests on unreinforced and reinforced Ottawa sand specimens along with failure envelopes established from these tests are shown in Figure 4.17. In the figures, the failure envelopes for fiber-reinforced specimens only based on the first 3 points, not including the last point. Overall, the failure envelopes of reinforced specimens tend to have greater effective stress cohesion intercept and the effective stress friction angle than unreinforced specimens.

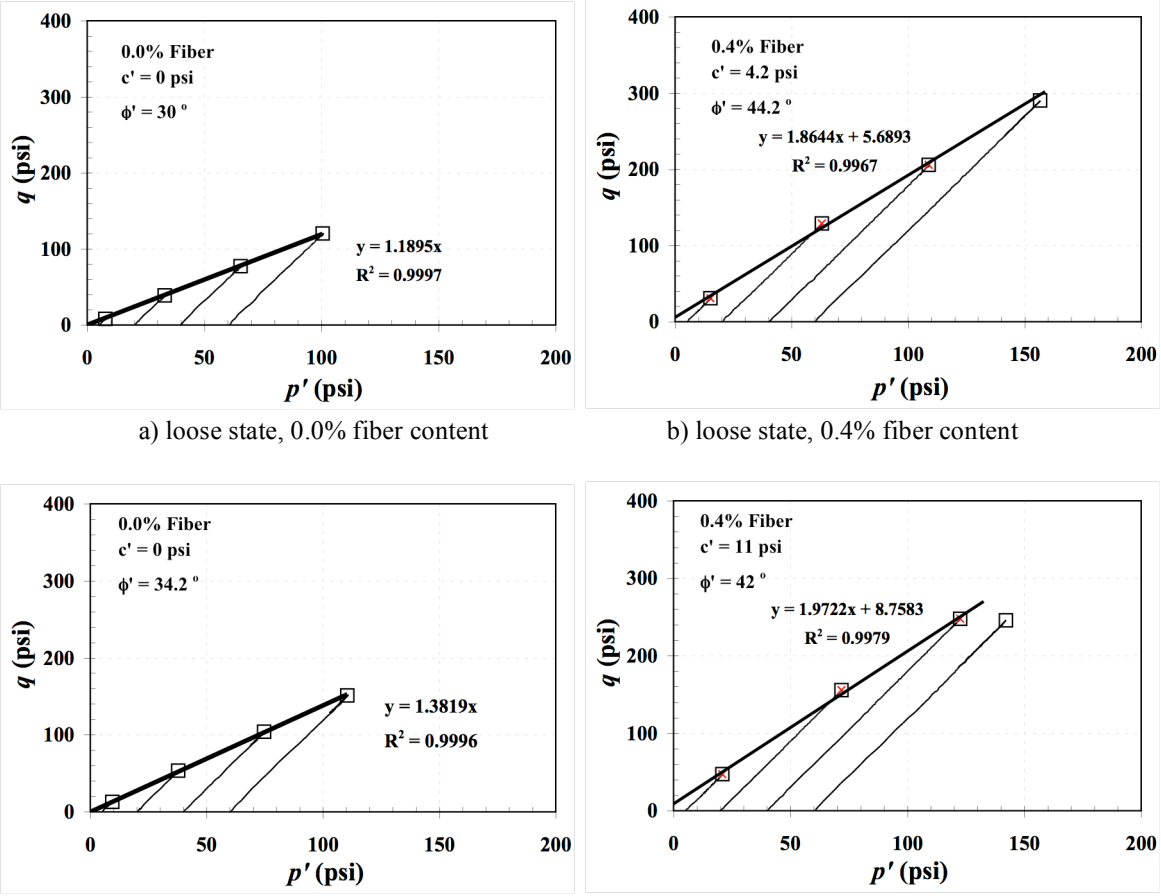

a) loose state, 0.0% fiber content

b) loose state, 0.4% fiber content

c) medium-dense state, 0.0% fiber content

d) medium-dense state, 0.4% fiber content

Figure 4.17 Failure envelopes of peak effective principal stress ratio (PSR) from the *CD* tests for Ottawa sand specimens compacted at and mixed with: a) loose state, 0.0% fiber content, b) loose state, 0.4% fiber, content c) medium-dense state, 0.0% fiber content, and d) medium-dense state, 0.4% fiber content.

Figure 4.18 shows the failure envelopes for the CD tests at several limiting strains for both unreinforced and reinforced Ottawa sand prepared at loose and medium-dense states. The effective stress strength parameters, c' and ϕ', for these envelopes are summarized in Table 4.4. Since the peak stress was observed at relatively small strains, the effective stress friction angles of the unreinforced specimens are essentially identical at the chosen limiting strains. Furthermore, the effective stress strength parameters at the limiting strains in the $\overline{CU}$ tests are very close to the results of the CD tests. For the loose reinforced specimens, both the effective stress cohesion and the effective stress friction angles increased as the limiting strains increased. In contrast, for the medium-dense reinforced specimens, the effective stress strength parameters determined at moderate strains (e.g. 15 percent) were similar with those computed at large strains (e.g. 25 percent). This is because the peak stress was reached at moderate strains for medium-dense reinforced specimens in the CD tests.

Table 4.4 Mohr-Coulomb Strength Parameters, c' and ϕ', for Unreinforced and Reinforced Ottawa Sand Specimens from the CD Tests When Peak Strength is Taken as Peak Stress Experienced at Limiting Strains of 5, 15, and 25 Percent

Initial Void Ratio	Fiber Content	Limit Strain					
		5% Strain		15% Strain		25% Strain	
		c' (psi)	ϕ' (deg)	c' (psi)	ϕ' (deg)	c' (psi)	ϕ' (deg)
0.74	0.0%	0.0	28.3	0.0	29.7	0.0	29.4
	0.4%	1.2	33.8	2.2	40.2	3.0	44.2
0.60	0.0%	0.0	33.9	0.0	33.1	0.0	31.8
	0.4%	5.2	37.4	6.6	41.5	9.8	41.5

Compared with Table 3.8 from undrained tests

Initial Void Ratio	Fiber Content	Limit Strain					
		5% Strain		15% Strain		25% Strain	
		c' (psi)	ϕ' (deg)	c' (psi)	ϕ' (deg)	c' (psi)	ϕ' (deg)
0.74	0.0%	0.0	29.9	0.0	30.2	0.0	29.6
	0.4%	2.3	36.7	4.0	42.0	7.0	44.9
0.60	0.0%	0.0	33.6	0[a]	33.0[a]	0[a]	31.3[a]
	0.4%	8.1	35.6	9.4[a]	39.6[a]	0[a]	39.1[a]

[a]: Suspicious result due to equipment limitation for pore pressure measurements.

Comparing the failure envelopes for reinforced specimens determined from the CD tests with those determined in the $\overline{CU}$ tests (Table 3.8), under the same preparation and compaction, shows that both the effective stress cohesion intercept and the effective stress friction angle in the $\overline{CU}$ tests are larger than for those in the CD test at given limiting strains for loose reinforced Ottawa sand specimens. The range of differences is from 1-psi to 4-psi (7-kPa and 28-kPa) and from 1° to 3° for effective cohesion intercepts and effective friction angles. In contrast, the effective stress friction angles determined from the $\overline{CU}$ tests are smaller than for those determined by the CD tests for medium-

dense reinforced specimens at a limiting strain of 5 percent. The difference in terms of the effective stress friction angle is about 2°.

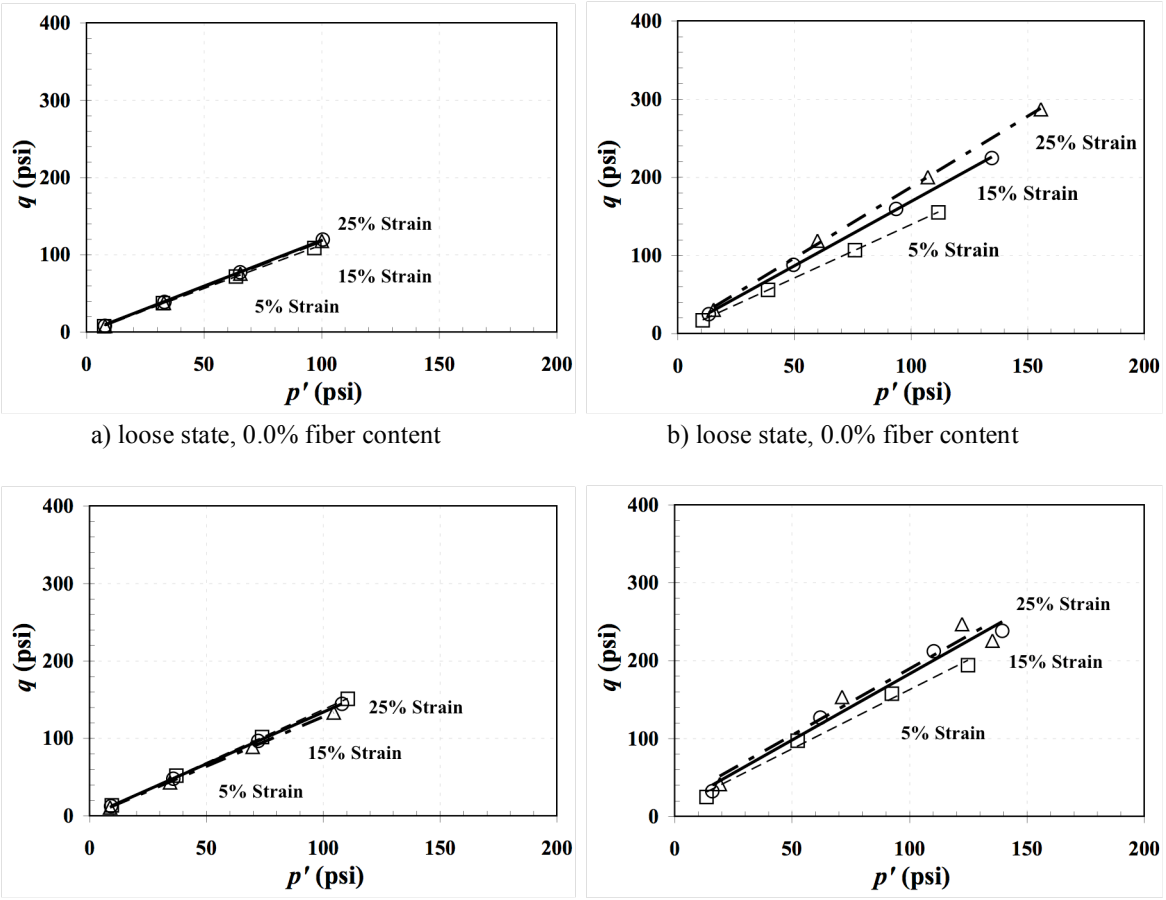

a) loose state, 0.0% fiber content

b) loose state, 0.0% fiber content

c) medium-dense state, 0.4% fiber content

d) medium-dense state, 0.4% fiber content

Figure 4.18 Failure envelopes from the *CD* tests for limiting strains of 5, 15, and 25 percent shear strain on unreinforced and reinforced Ottawa sand specimens prepared at and mixed with: a) loose state, 0.0% fiber content, b) loose state, 0.4% fiber content, c) medium-dense state, 0.0% fiber content, and d) medium-dense state, 0.4% fiber content.

4.5 Stress-Strain Response from Isotropic Consolidation Tests

A total of eight isotropic consolidation tests were carried out on unreinforced and fiber-reinforced silty sand and Ottawa sand specimens. The results were interpreted by directly comparing the consolidation parameters and the stress-deformation relationship to evaluate differences in deformation behavior under varying consolidation pressures. The compression parameters, index properties, and bulk moduli for the unreinforced and fiber-reinforced silty sand and Ottawa sand were calculated and used subsequently for prediction of the volumetric strain of fiber-reinforced specimens.

4.5.1 Silty Sand

Figure 4.19 shows the typical change in void ratio (Δe) versus the effective consolidation stress (σ'_c) response observed in isotropic consolidation tests for the unreinforced and reinforced silty sand specimens compacted at 18 percent and 22 percent water contents. As seen in the figures, the overall change in void ratio for specimens compacted at 18 percent water content was smaller (0.1) than for the specimens compacted at 22 percent water content (0.15). Plus, the fiber-reinforced specimens were slightly more compressible than the unreinforced specimens prepared in similar conditions.

The results for the compression parameters, consolidation index, and bulk modulus for both the unreinforced and reinforced silty sand specimens compacted at the 18 and 22 percent water contents are summarized in Table 4.5. The apparent maximum past consolidation pressure (σ'_p) decreases from approximately 20-psi (140-kPa) for the specimens compacted at 18 percent water content to approximately 15-psi (100-kPa) for

the specimens compacted at 22 percent water content. The parameters, λ and κ, are respectively slopes of the normal compression line and the unloading-reloading lines when plotted in a compression plane of υ versus $ln\, p'$ (Wood, 1990), and υ_λ and υ_κ, are the intercepts of the normal compression line and the unloading-reloading line at $p'=1$. In isotropic consolidation test, where porewater pressure equal to zero, at end of each loading stage $\sigma_c' = p = p'$ (Atkinson & Bransby, 1978). Often, the normal consolidation line is known as the λ-line, and a swelling line denoted as the κ-line. Thus, the equation for the λ-line is

$$\upsilon = \upsilon_\lambda - \lambda ln\, p' \tag{4.1}$$

in which υ is the specific volume, which is defined as the volume of the soil sample containing the unit volume of soil grains ($\upsilon = 1 + e$). υ_λ is the specific volume of a normally consolidated soil at $p'=1$. Similarly, the κ-line equation is

$$\upsilon = \upsilon_\kappa - \kappa ln\, p' \tag{4.2}$$

in which υ_κ is the specific volume for the overconsolidated of soil at $p'=1$. Note that λ, κ, υ_λ, and υ_κ depend on the particular soil and must be determined from laboratory testing.

For an ideal isotropic elastic soil, the increment in volumetric strain is given

$$\delta\varepsilon_v = \frac{1}{K}\delta p' \tag{4.3}$$

in which K is known as the bulk modulus, and $\delta p'$ is an increment of mean effective stress. Therefore, the parameters, K_c and K_r, in Table 4.5 are bulk moduli, which are slopes of the normal compression line and unloading-reloading line, respectively, when plotted as effective consolidation stress (σ'_c) versus volumetric strain (ε_v). The bulk

modulus of the silty sand specimens under the unloading-reloading (K_r) is about 11,500-psi (79,300-kPa), which is almost 6 times greater than the bulk modulus under the virgin loading condition (K_c) of 2,300-psi (15,860-kPa). These bulk moduli will be used subsequently for predicting the volumetric strain of fiber-reinforced soil in the proposed constitutive model.

Table 4.5 Compression Parameters Obtained from the Isotropic Consolidation Tests for the Silty Sand Specimens

Water content (%)	Fiber Content	σ_p' (psi)	λ	κ	υ_λ [a]	υ_κ [a]	K_c (psi)	K_r (psi)
18	0.0%	22	0.048	0.012	1.698	1.519	2567	11048
	0.4%	18	0.051	0.011	1.719	1.523	2478	11870
22	0.0%	14	0.060	0.011	1.769	1.527	2149	12324
	0.4%	15	0.066	0.013	1.785	1.521	1954	11527

[a]: Although υ_λ, υ_κ are themselves dimensionless, the values will depend on the units chosen for σ'_p

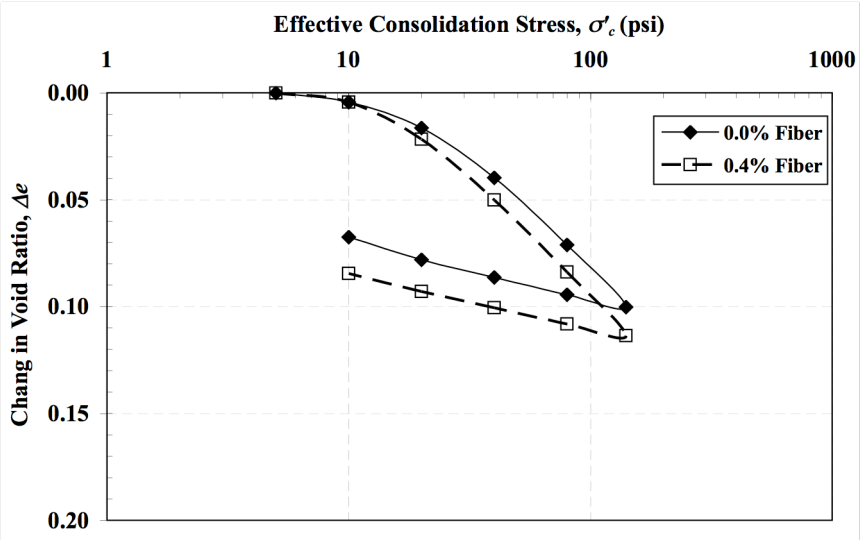

a) 18 percent water content

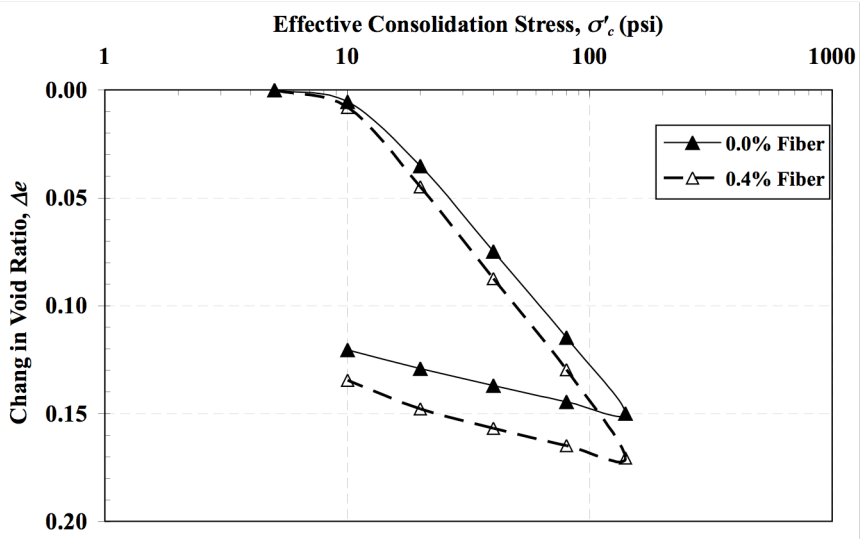

b) 22 percent water content

Figure 4.19 Change in void ratio (Δe) versus the effective consolidation stress (p') curves from the isotropic consolidation tests for the silty sand specimens compacted at: a) 18 percent water content, and b) 22 percent water content.

4.5.2 Ottawa Sand

Typical changes in void ratio (Δe) versus the effective consolidation stress (σ_c') observed in the isotropic consolidation test results for both the unreinforced and reinforced Ottawa sand specimens at loose and medium-dense states are shown in Figure 4.20. The overall changes in void ratio of the medium-dense specimens (0.017) were smaller than for the loose specimens (0.024). In addition, the fiber-reinforced specimens were slightly more compressible than the unreinforced specimens.

Results for the compression parameters, the consolidation index, and the bulk modulus for the unreinforced and reinforced Ottawa sand specimens are summarized in Table 4.6. The apparent maximum past consolidation pressure (σ'_p) decreased from approximately 35-psi (240-kPa) for the medium-dense specimens to approximately 30-psi (210-kPa) for the loose specimens. In general, the apparent maximum past consolidation pressure for the Ottawa sand specimens was larger than for the silty sand specimens. The bulk modulus under unloading-reloading (K_r) was about 23,000-psi (158,580-kPa), and the bulk modulus under the virgin loading condition (K_c) was 15,000-psi (103,420-kPa) for the Ottawa sand specimens. It was noted that the bulk moduli for Ottawa sand were significantly larger than for silty sand in terms of normal loading and unloading-reloading conditions.

Table 4.6 Compression Parameters Obtained from the Isotropic Consolidation Tests for the Ottawa Sand Specimens

Initial Void Ratio	Fiber Content	σ_p' (psi)	λ	κ	υ_λ*	υ_κ*	K_c (psi)	K_r (psi)
0.74	0.0%	30	0.007	0.005	1.624	1.610	17483	25603
	0.4%	31	0.009	0.005	1.713	1.694	15740	24990
0.66	0.0%	35	0.009	0.005	1.732	1.715	15623	23409
	0.4%	32	0.011	0.006	1.759	1.733	12595	21988

*: Although υ_λ, υ_κ are themselves dimensionless, the values will depend on the units chosen for σ'_p

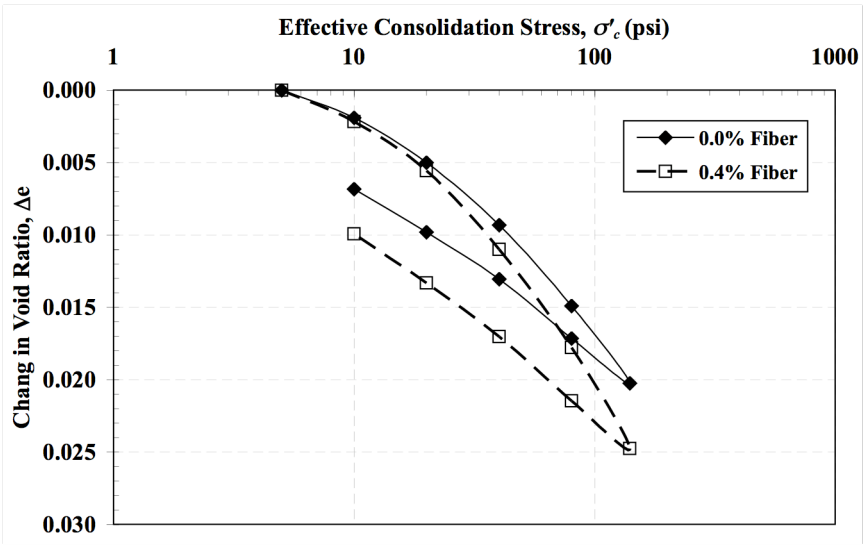

a) loose state

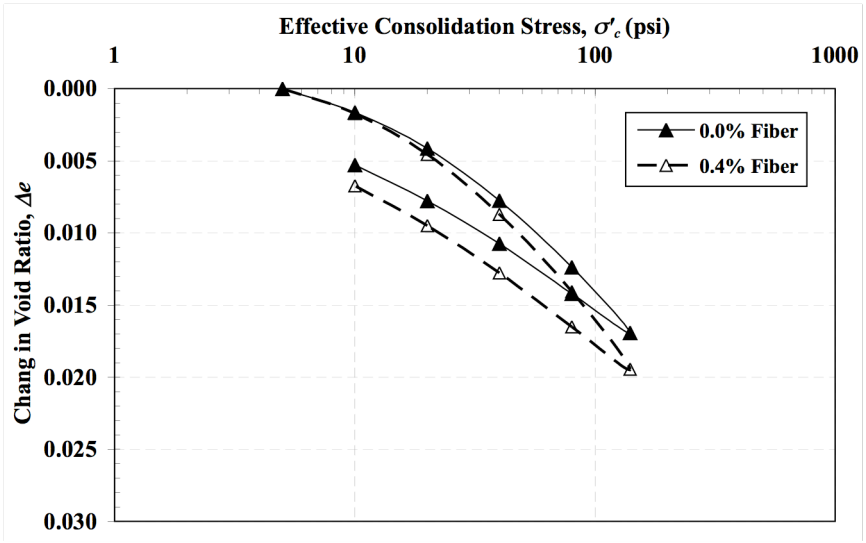

b) medium-dense state

Figure 4.20 Change in void ratio (Δe) versus the effective consolidation stress (p') curves from the isotropic consolidation tests for the Ottawa sand specimens compacted at: a) loose and b) medium-dense states.

4.6 Summary

Results of consolidated-drained (CD) triaxial compression tests performed on compacted silty sand and Ottawa sand show that fiber reinforcement can improve soil strength in terms of the effective stress cohesion intercept and the effective stress friction angle under drained loading condition.

The volumetric strain versus the triaxial shear strain behavior of the reinforced silty sand is different from the reinforced Ottawa sand. The amount of dilation observed for the reinforced silty sand specimens was significantly less than what was observed for the unreinforced specimens. However, the reinforced Ottawa sand specimens tended to compress less (dilate more) than the unreinforced specimens when they were consolidated to higher effective stresses (e.g. greater than or equal to 20-psi).

The volumetric strain versus the triaxial shear stress behavior of the fiber-reinforced silty sand specimens differs from the reinforced Ottawa sand specimens. The amount of dilation observed for the reinforced silty sand specimens was significantly less than what was observed for the unreinforced specimens. However, the reinforced Ottawa sand specimens tended to compress less (dilate more) than the unreinforced specimens when they were consolidated to higher effective stresses (e.g. greater than or equal to 20-psi).

CHAPTER 5: INTERPRETATION OF RESULTS FOR TRIAXIAL COMPRESSION TESTS

5.1 Introduction

Results from the triaxial compression tests presented in Chapters 3 and 4 showed several unique behaviors for fiber-reinforced soils. In addition, several differences response during undrained and drained tests were observed, and the overall behavior was shown to be consistent in the silty sand and Ottawa sand specimens. In this chapter, analyses and interpretations of the results are in terms of contributions made to the response by the inclusion of fibers. Also presented here is a series of key features needed to construct a constitutive model for fiber-reinforced soils.

5.2 Basis of Interpretation

Results from both the $\overline{CU}$ and CD tests on replicate fiber-reinforced and unreinforced soil specimens suggest that fiber-reinforcement provides both a deviatoric and a hydrostatic contribution to the stresses in the specimens. Stress paths for the unreinforced and reinforced silty sand specimens compacted at 18 percent water content, consolidated at 10-psi (70-kPa), and tested under undrained and drained conditions are shown in Figure 5.1. For the purposed of this work, the deviatoric contribution of the fibers, denoted q_f, taken to be the difference in measured deviatoric stress ($q = \sigma_1 - \sigma_3$) at equal shear strains for the fiber-reinforced and unreinforced specimens:

$$q_f = q_{0.4\%} - q_{0.0\%} \tag{5.1}$$

in which $q_{0.4\%}$ is the deviatoric stress of the specimen reinforced with 0.4 percent fiber content and $q_{0.0\%}$ is the deviatoric stress of the unreinforced specimen at the same triaxial

shear strain. The magnitude of the hydrostatic contribution of the fibers, denoted p_f, is similarly calculated from the difference in the mean effective stress ($p' = (\sigma'_1 + 2\sigma'_3)/3$) at points of equal triaxial shear strain in comparable tests on reinforced and unreinforced specimens:

$$p_f = p'_{0.4\%} - p'_{0.0\%} \tag{5.2}$$

in which $p'_{0.4\%}$ is the mean effective stress of the specimens reinforced with 0.4 percent fiber content and $p'_{0.0\%}$ is the mean effective stress of the replicate unreinforced specimen.

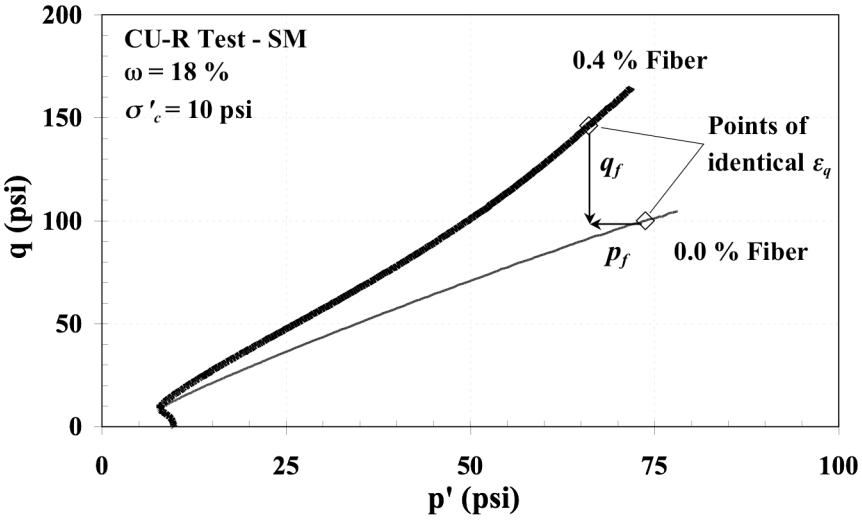

a) undrained loading conditions ($\overline{CU}$ tests)

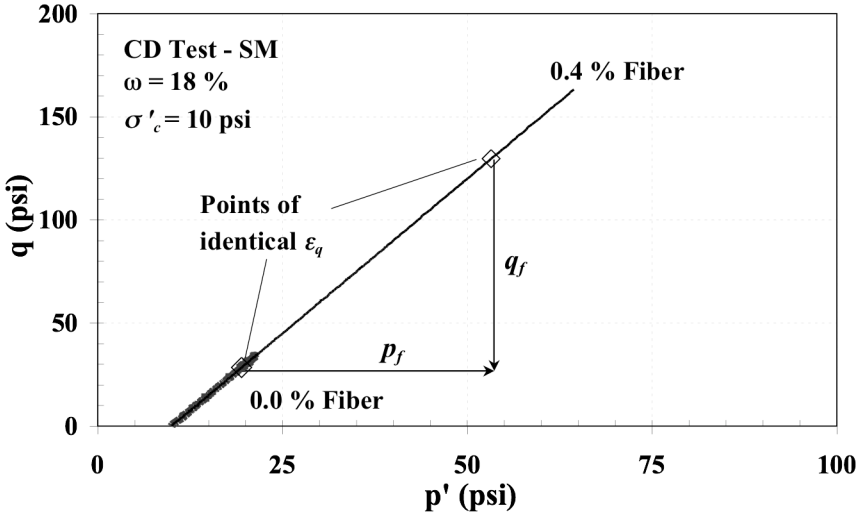

b) drained loading conditions (CD tests)

Figure 5.1 Method used to establish q_f and p_f from experimental results on replicate unreinforced and reinforced silty sand specimens under: a) undrained loading conditions ($\overline{CU}$ tests), and b) drained loading conditions (CD tests).

5.2.1 Evaluation of Deviatoric Contributions of Fibers (q_f)

The typical deviatoric contribution (q_f) of the fiber reinforcment for both $\overline{CU}$ and CD tests is shown in Figure 5.2. The response can be modeled as a bi-linear function with an initial constant contribution (q_{f0}) at small strains and a linear load transfer contribution at greater strains. It can be shown that the linear contribution at large strain is three times the shear modulus attributed to fibers ($3G_f$) contribution (Wood, 1990). The value of the initial contribution of fibers (q_{f0}) is dependent on the compaction conditions and the effective consolidation stress of the specimens (Romero, 2003). Since the unreinforced and reinforced specimens were prepared and tested under the same conditions, the magnitude q_{f0} relies primarily on the variations in effective consolidation stress. Additional analysis and discussion is presented subsequently Section 5.3.

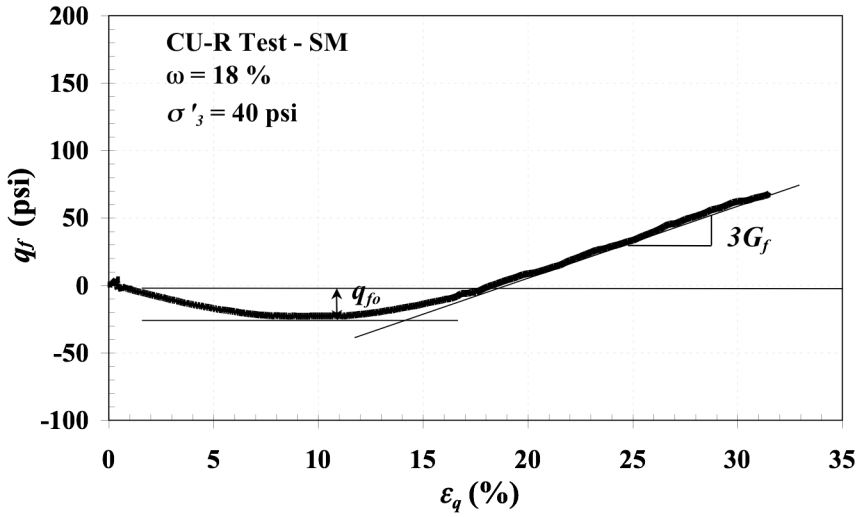

Figure 5.2 Typical fiber resistance (q_f) versus triaxial shear strain response showing the definition of initial fiber stress (q_{f0}) and the shear modulus due to fibers (G_f) from the $\overline{CU}$ tests for silty sand specimens compacted at 18% water content and consolidated to 40-psi effective stress.

5.2.2 Evaluation of Hydrostatic Contributions of Fibers (p_f)

The typical hydrostatic contribution of the fibers (p_f) versus the shear strain for both $\overline{CU}$ and *CD* tests is shown in Figure 5.3. The hydrostatic contribution of fibers seem to have an initial constant contribution (p_{f0}) followed by a linear change in hydrostatic stress at moderate strains, which is followed by a noticeable decrease at large shear strains. The magnitude of the initial contribution (p_{f0}) is observed to vary with the effective confining stress at the end of consolidation. Additional analysis and discussion is presented in Section 5.4.

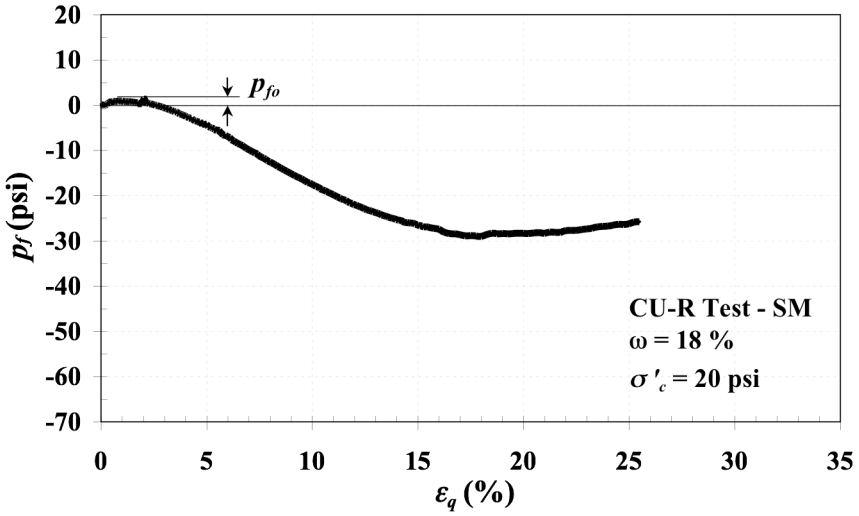

Figure 5.3 Typical hydrostatic contribution of fibers (p_f) versus triaxial shear from the $\overline{CU}$ tests for silty sand specimens compacted at 18% water content and consolidated to 20-psi effective stress.

5.3 Deviatoric Contribution of Fibers (q_f)

The deviatoric contribution of fibers from the undrained and drained triaxial tests for silty sand specimens consolidated at 5, 10, 20, 40, and 80-psi (35, 70, 140, 280, and 550-kPa) and for Ottawa sand specimens consolidated at 5, 20, 40, and 60-psi (35, 140, 280, and 415-kPa) are presented and evaluated to determine the level of strains required to begin mobilizing the resistance in the fibers.

5.3.1 Silty Sand

The results shown in Chapters 3 and 4 for unreinforced and unreinforced silty sand specimens in the $\overline{CU}$ and CD tests clearly indicate that some strain is required to begin mobilizing the fiber resistance. The deviatoric contribution of fibers for reinforced specimens is plotted as a function of the triaxial shear strain for the undrained tests on silty sand specimens in Figures 5.4 and 5.5. Each of theses graphs reveals a consistent trend that indicates the mobilization of fibers resistance. At small strains, the fibers provide a relatively small and essentially constant resistance to shearing, which is defined here as the initial deviatoric contribution of fibers (q_{f0}). Then, at greater strain levels, the deviatoric contribution of fibers increased linearly with additional shear. Note that negative values of the initial deviatoric contribution are frequently observed, which appear to depend on the effective consolidation stresses.

Generally, the specimens compacted at 18 percent water content had a tendency to mobilize positive shear resistance of fibers at lower strains than specimens compacted at 22 percent water content. Most specimens compacted at 18 percent water content started to mobilize the fibers shear resistance at moderate strains (10 to 15 percent).

However, specimens compacted at 22 percent did not mobilize the fiber shear resistance until they reached large strains (up to 20 percent).

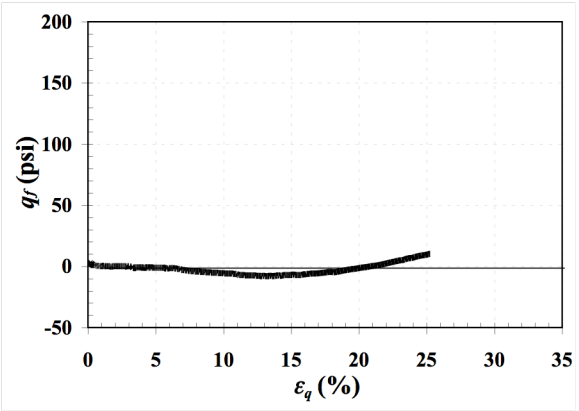

a) 5-psi effective consolidation stress

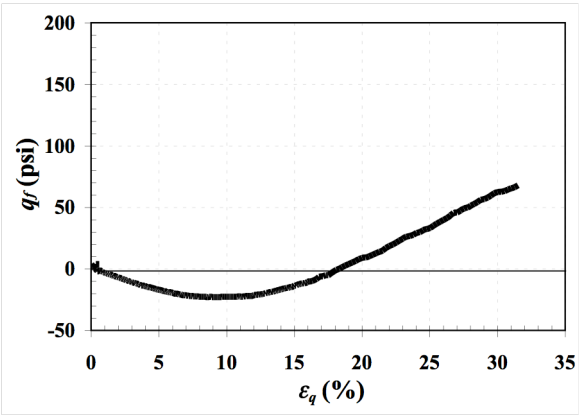

d) 40-psi effective consolidation stress

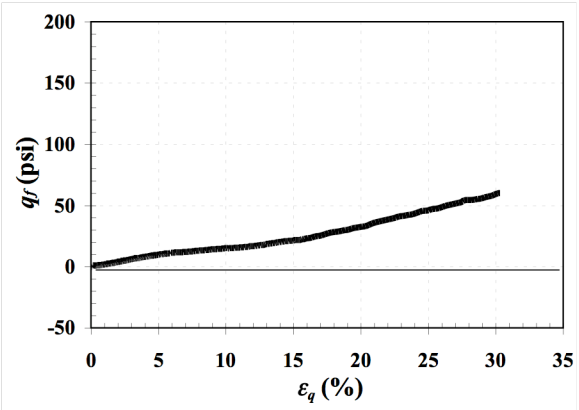

b) 10-psi effective consolidation stress

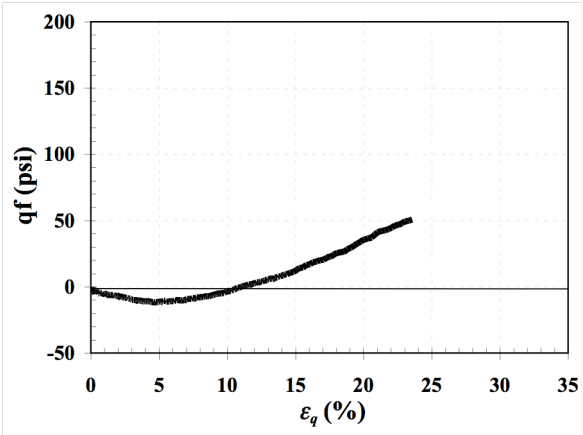

e) 80-psi effective consolidation stress

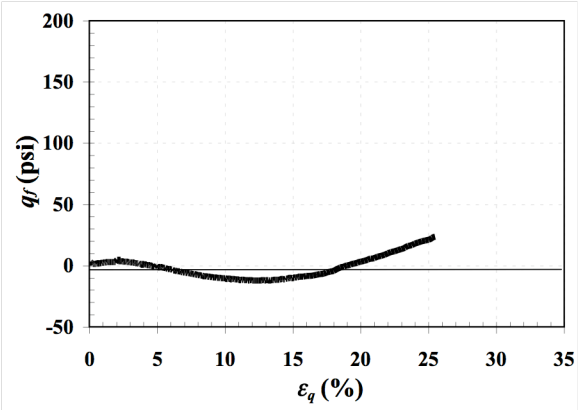

c) 20-psi effective consolidation stress

Figure 5.4 Deviatoric contributions of fibers (q_f) versus triaxial shear strain (ε_q) from the $\overline{CU}$ tests for silty sand specimens compacted at 18 percent water content and consolidated to: a) 5-psi effective stress, b) 10-psi effective stress, c) 20-psi effective stress, d) 40-psi effective stress, and e) 80-psi effective stress.

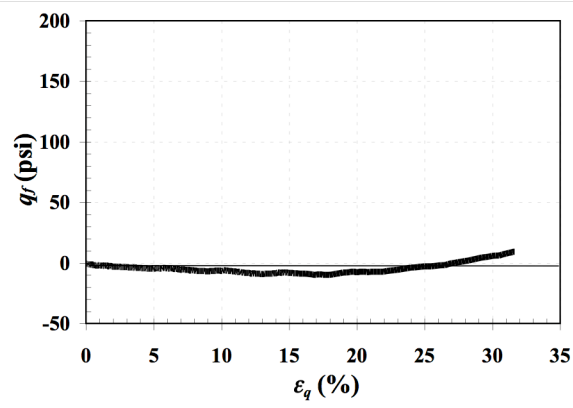

a) 5-psi effective consolidation stress

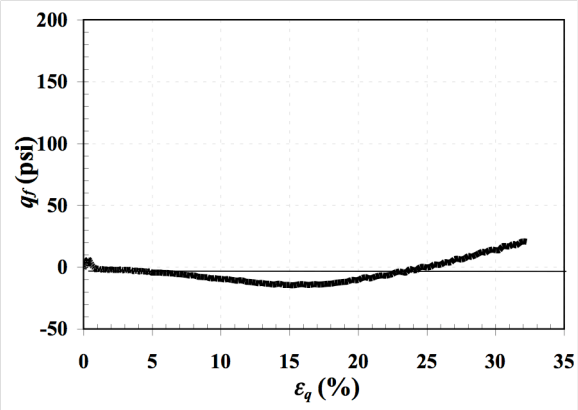

d) 40-psi effective consolidation stress

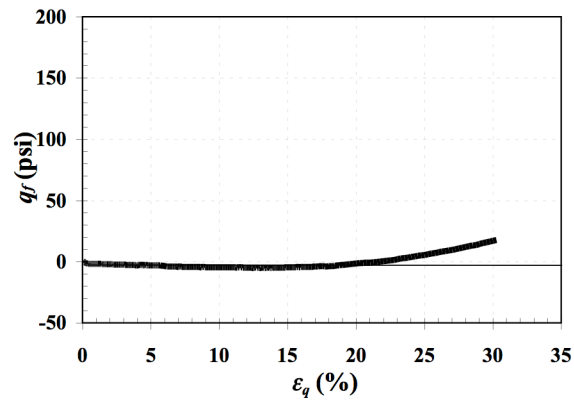

b) 10-psi effective consolidation stress

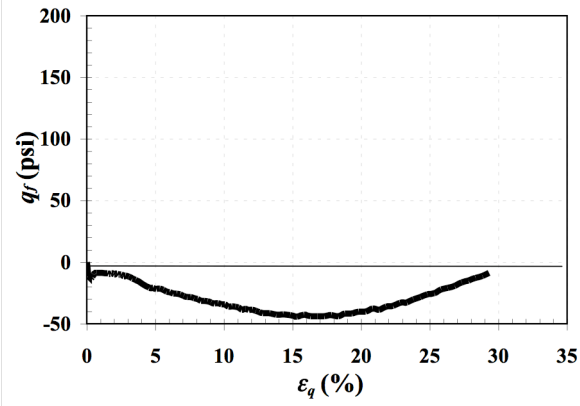

e) 80-psi effective consolidation stress

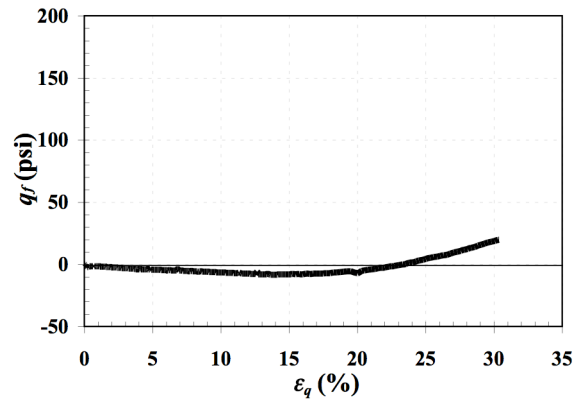

c) 20-psi effective consolidation stress

Figure 5.5 Deviatoric contributions of fibers (q_f) versus triaxial shear strain (ε_q) from the $\overline{CU}$ tests for silty sand specimens compacted at 22 percent water content and consolidated to: a) 5-psi effective stress, b) 10-psi effective stress, c) 20-psi effective stress, d) 40-psi effective stress, and e) 80-psi effective stress.

Figures 5.6 and 5.7 show the deviatoric contribution of fibers obtained from the comparable CD tests on unreinforced and reinforced specimens compacted at 18 percent and 22 percent water contents, respectively. Again, these graphs show the deviatoric contribution of fibers as a function of the triaxial shear strains and effective consolidation stresses. The curves determined from the drained tests are similar to those observed in undrained tests, in which the initial deviatoric contribution is small or even negative and then increased linearly with additional shear strains. Similarly, when comparing the curves in Figures 5.6 and 5.7, the silty sand specimens compacted at 18 percent water content reveal the tendency to mobilize positive shear resistance of fibers at lower strains than specimens compacted at 22 percent water content. However, the slopes of the linear response portion of the curves ($3G_f$) in the CD tests tended to be larger than those in the $\overline{CU}$ tests. The observed differences in mobilized fiber resistance in the undrained and drained tests are believed to result from the volume changes that occur in specimens tested under drained conditions. It was observed that the mobilization of shear fiber resistance during drained tests occurred at smaller strains than under undrained loading for the fiber-reinforced silty sand.

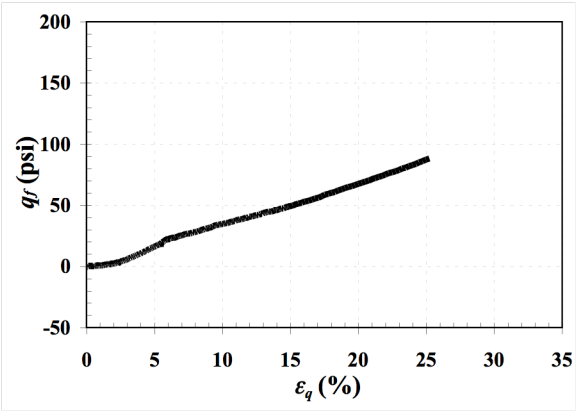

a) 5-psi effective consolidation stress

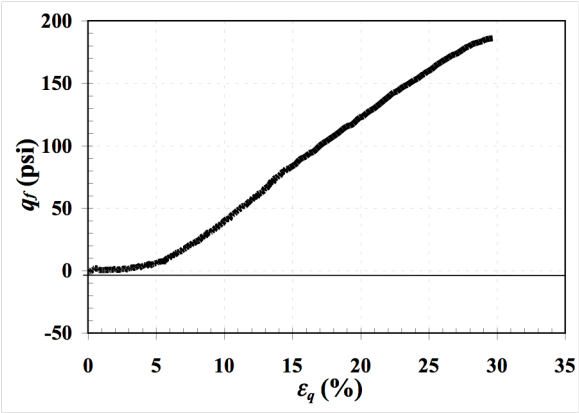

d) 40-psi effective consolidation stress

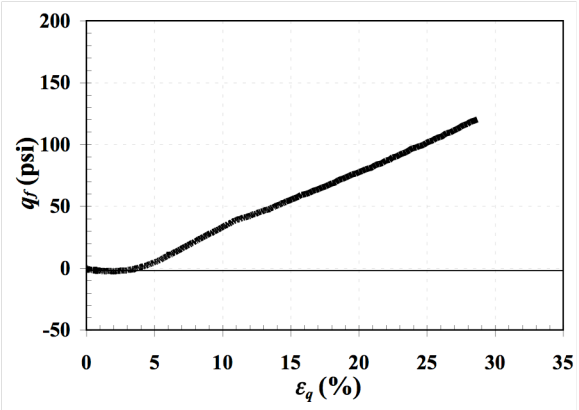

b) 10-psi effective consolidation stress

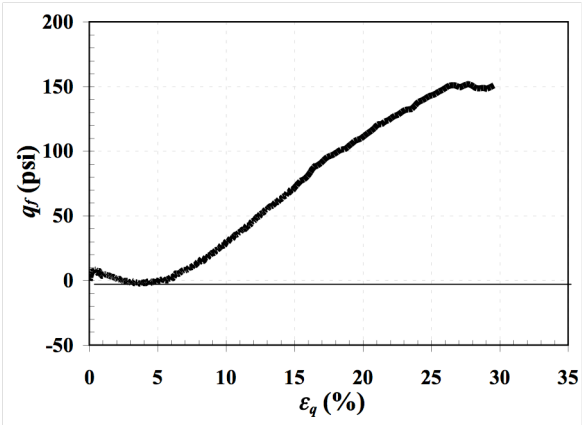

e) 80-psi effective consolidation stress

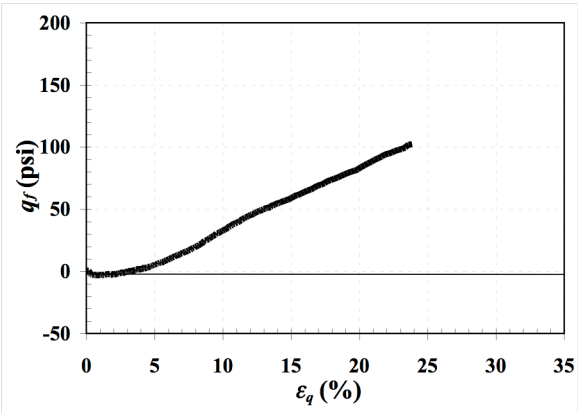

c) 20-psi effective consolidation stress

Figure 5.6 Deviatoric contributions of fibers (q_f) versus triaxial shear strain (ε_q) from the *CD* tests for silty sand specimens compacted at 18 percent water content and consolidated to: a) 5-psi effective stress, b) 10-psi effective stress, c) 20-psi effective stress, d) 40-psi effective stress, and e) 80-psi effective stress.

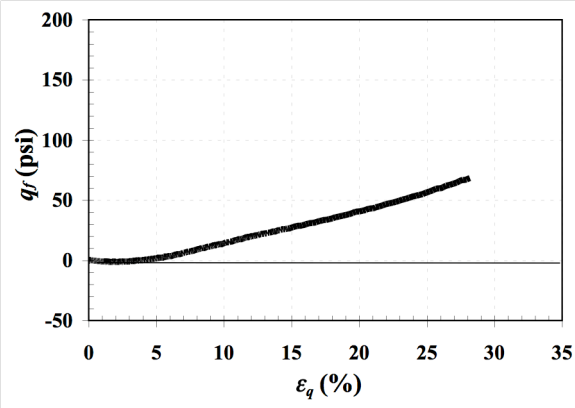

a) 5-psi effective consolidation stress

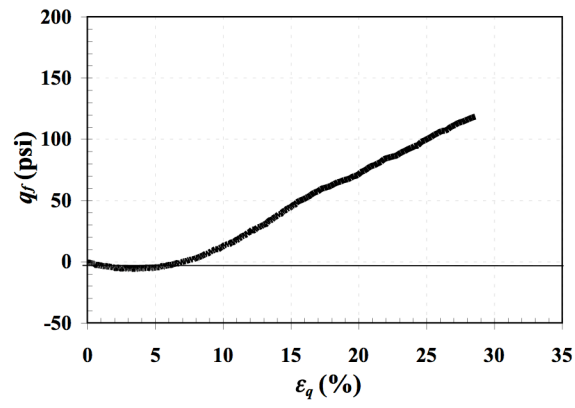

b) 10-psi effective consolidation stress

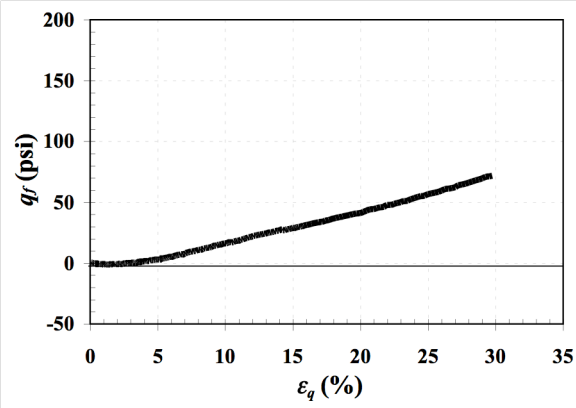

c) 20-psi effective consolidation stress

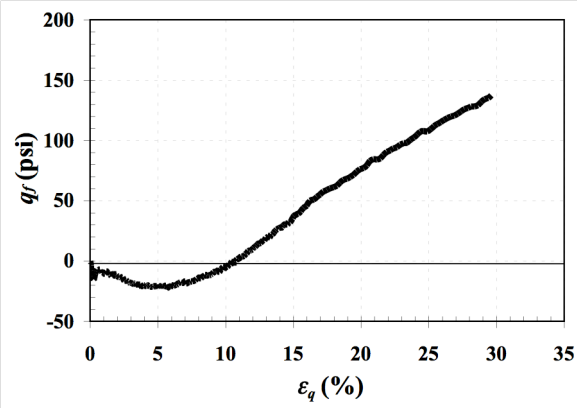

d) 40-psi effective consolidation stress

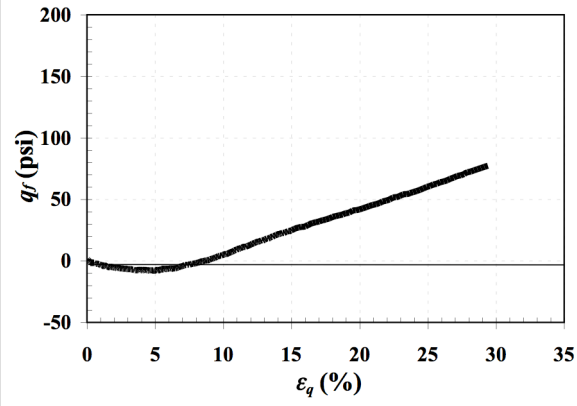

e) 80-psi effective consolidation stress

Figure 5.7 Deviatoric contributions of fibers (q_f) versus triaxial shear strain (ε_q) from the *CD* tests for silty sand specimens compacted at 22 percent water content and consolidated to: a) 5-psi effective stress, b) 10-psi effective stress, c) 20-psi effective stress, d) 40-psi effective stress, and e) 80-psi effective stress.

5.3.2 Ottawa Sand

The deviatoric contributions of fibers computed from the $\overline{CU}$ tests on unreinforced and reinforced loose and medium-dense Ottawa sand specimens are shown in Figures 5.8 and 5.9, respectively. In general, it was observed that the deviatoric contributions of fibers are similar to those observed for the silty sand specimens. The deviatoric contribution of fibers also yielded a relatively small negative value of q_f at small strains, which increased with additional shear strains. This was followed by a noticeable decrease in slope at large strains, especially when specimens were consolidated at higher effective stress. The medium-dense Ottawa sand specimens tended to mobilize the fiber shear resistance at greater shear strain than the loose specimens under undrained loading conditions. Observed was the fact that the Ottawa sand specimens mobilized shear resistance from the reinforcement faster than the silty sand specimens. In addition, the magnitude of the deviatoric contributions of fibers in Ottawa sand is larger than those in silty sand at any given shear strain.

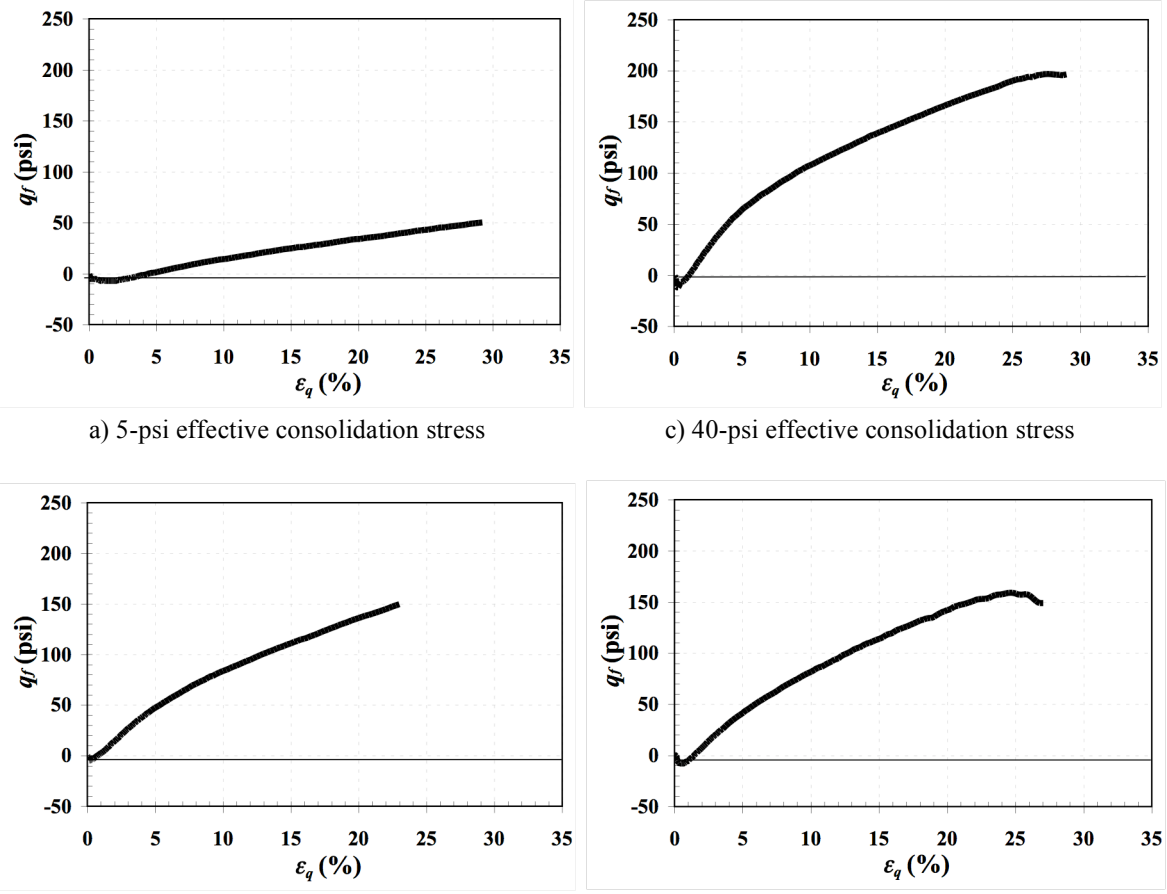

a) 5-psi effective consolidation stress

c) 40-psi effective consolidation stress

b) 20-psi effective consolidation stress

d) 60-psi effective consolidation stress

Figure 5.8 Deviatoric contributions of fibers (q_f) versus triaxial shear strain (ε_q) from the $\overline{CU}$ tests for loose Ottawa sand specimens and consolidated to: a) 5-psi effective stress, b) 20-psi effective stress, c) 40-psi effective stress, and d) 60-psi effective stress.

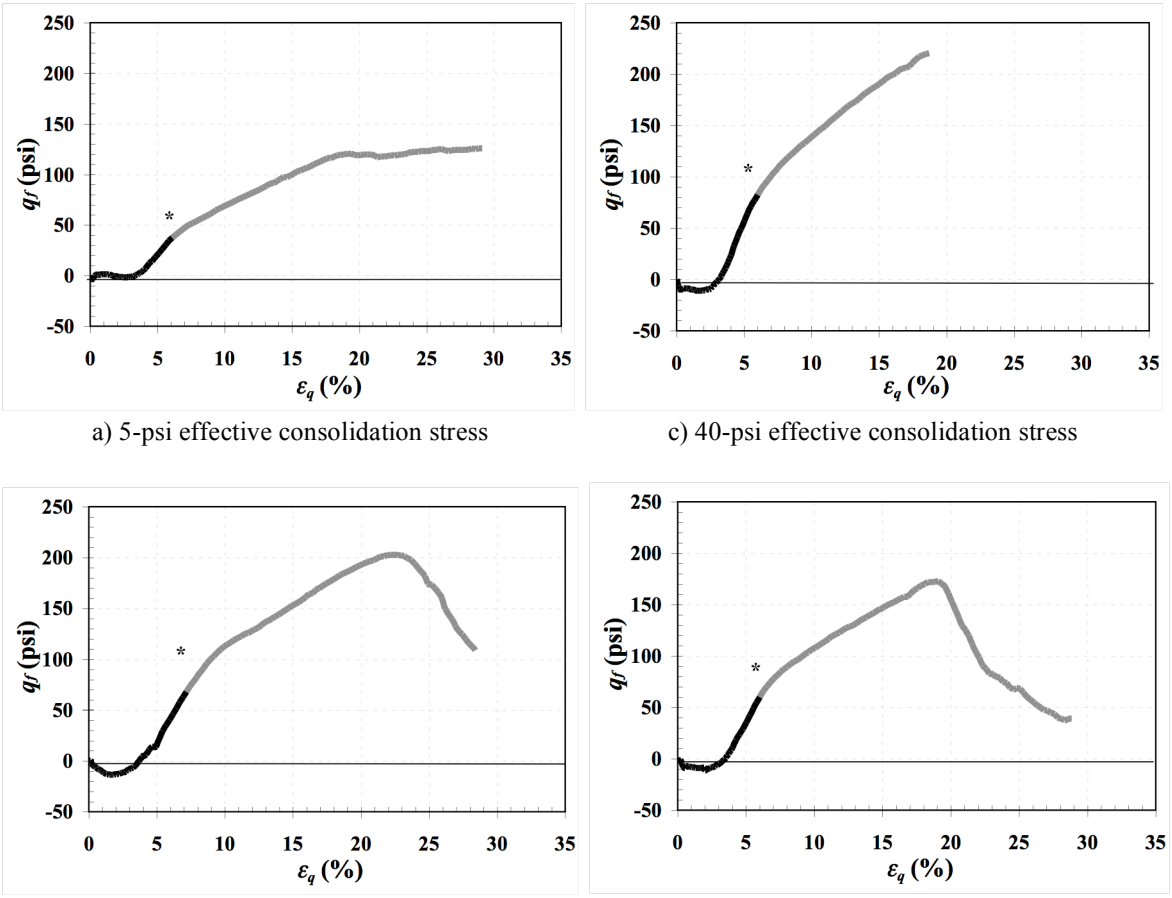

a) 5-psi effective consolidation stress

c) 40-psi effective consolidation stress

b) 20-psi effective consolidation stress

d) 60-psi effective consolidation stress

Figure 5.9 Deviatoric contributions of fibers (q_f) versus triaxial shear strain (ε_q) from the $\overline{CU}$ tests for medium-dense Ottawa sand specimens and consolidated to: a) 5-psi effective stress, b) 20-psi effective stress, c) 40-psi effective stress, and d) 60-psi effective stress.

*: Start point of suspicious measurement.

Figures 5.10 and 5.11 show the deviatoric contribution of fibers calculated from the comparable *CD* tests for both loose and medium-dense Ottawa sand specimens, respectively. The responses determined from the drained tests are similar to those observed in the undrained tests, in which a negative value of initial deviatoric contribution is small and then increases linearly with additional shear strain. Again, the drained tests mobilized the fiber shear resistance at lower stresses than was observed in undrained tests for the fiber-reinforced Ottawa sand, but the difference in mobilization strains was smaller than for the fiber-reinforced silty sand.

The plots of deviatoric contribution of fibers versus shear strain response can be used to explain load-transfer mechanism of inclusion fibers for both silty sand and Ottawa sand. At large strains, the linear increases portion of the load transfer is relatively easy to understand since the shear strains lead to elongation of the reinforcement and the development of stress in the fibers. The initial deviatoric contribution of fibers (q_{f0}), however, is harder to understand since it is not currently possible to directly measure the stresses in the fibers. As hypothesized by Romero (2003), the load-transfer mechanism includes some initial stress created in the fibers during the compaction, saturation, and consolidation process, in addition to stress produced by the fiber-reinforced specimens when subjected to undrained and drained tests and increasing shear strains. Since all specimens were prepared and compacted under the same conditions, the magnitude of the initial deviatoric contribution of fibers is believed to be primarily dependent on the differing effective consolidation stresses. The testing program's evidence for the Ottawa sand suggests the existence of the negative initial deviatoric fiber contributions. Additional discussion and illustration of this relationship is described in Section 5.5.1.

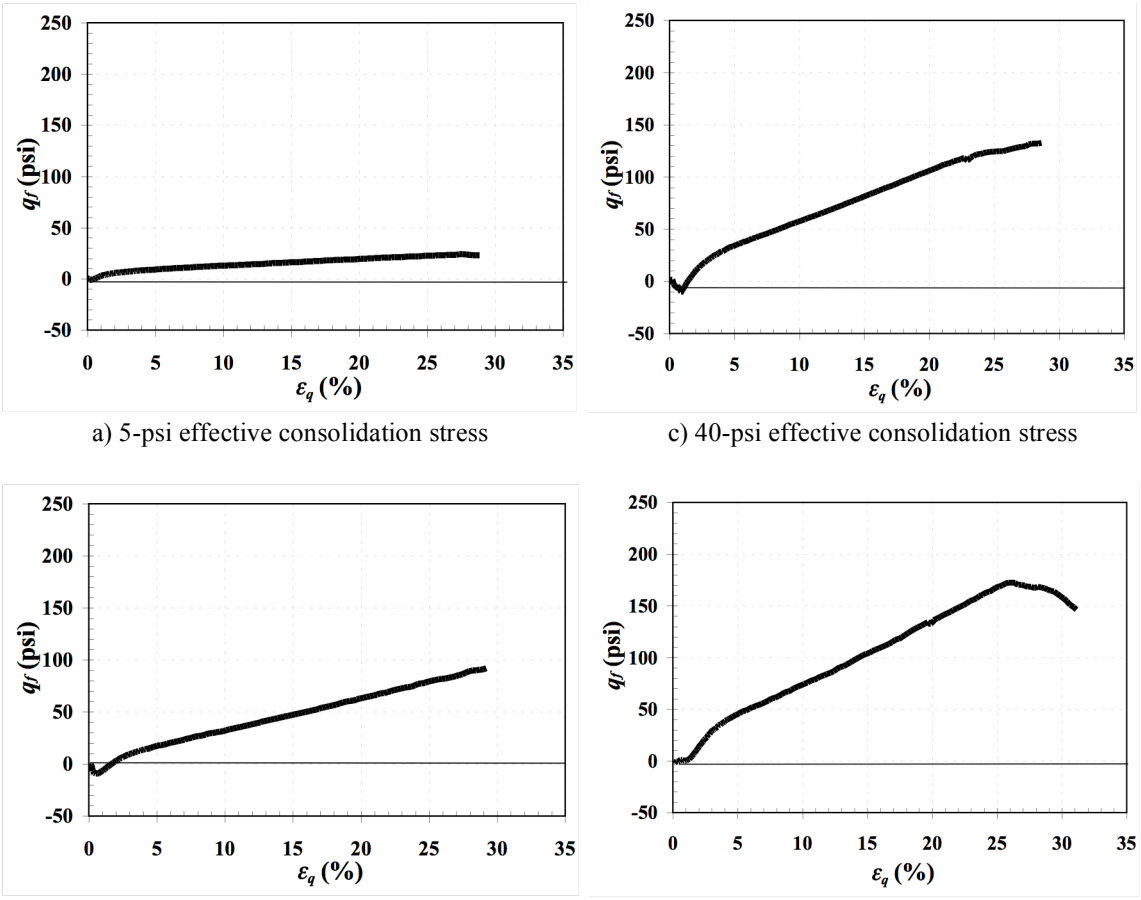

a) 5-psi effective consolidation stress

c) 40-psi effective consolidation stress

b) 20-psi effective consolidation stress

d) 60-psi effective consolidation stress

Figure 5.10 Deviatoric contributions of fibers (q_f) versus triaxial shear strain (ε_q) from the CD tests for loose Ottawa sand specimens and consolidated to: a) 5-psi effective stress, b) 20-psi effective stress, c) 40-psi effective stress, and d) 60-psi effective stress.

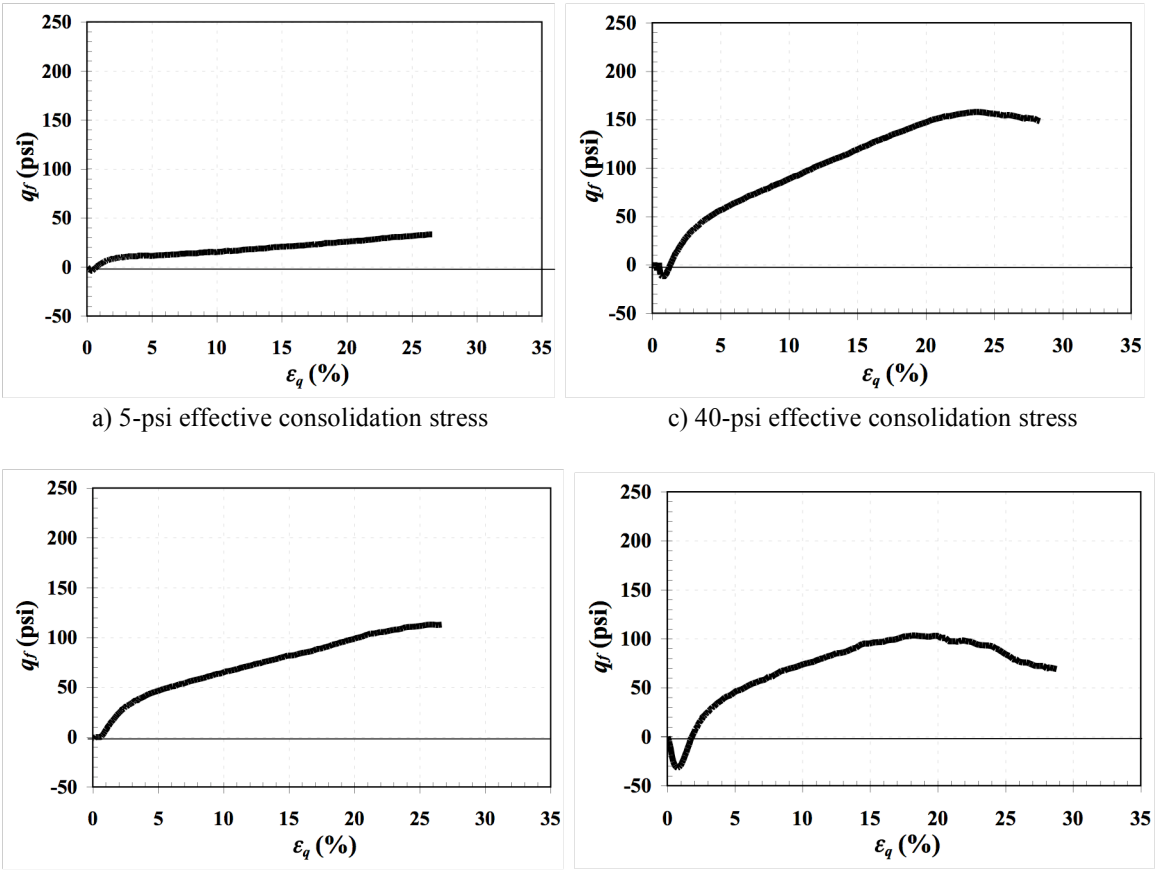

a) 5-psi effective consolidation stress

c) 40-psi effective consolidation stress

b) 20-psi effective consolidation stress

d) 60-psi effective consolidation stress

Figure 5.11 Deviatoric contributions of fibers (q_f) versus the triaxial shear strain (ε_q) from the CD tests for medium-dense Ottawa sand specimens and consolidated to: a) 5-psi effective stress, b) 20-psi effective stress, c) 40-psi effective stress, and d) 60-psi effective stress.

5.4 Hydrostatic Contributions of Fibers (p_f)

The hydrostatic contribution of fibers determined from the $\overline{CU}$ and CD tests for the silty sand specimens consolidated at 5, 10, 20, 40, and 80-psi (35, 70, 140, 280, and 550-kPa), and for Ottawa sand specimens consolidated at 5, 20, 40, and 60-psi (35, 140, 280, and 415-kPa) are presented and evaluated in terms of an "internal confining stress" due to the inclusion of fibers to both specimens.

5.4.1 Silty Sand

Figures 5.12 and 5.13 show the hydrostatic contribution of fibers determined from comparable $\overline{CU}$ tests on unreinforced and reinforced silty sand specimens compacted at 18 percent and 22 percent water contents. Each of these graphs illustrates the mobilization of confining stress due to the fibers as a consistent trend. As visible in the figures, small strains are required to begin mobilizing the additional confining stress provided by the inclusion of fibers under undrained loading conditions. The reinforcing fibers produced a small amount of positive initial hydrostatic contribution stress (p_{f0}) followed by a significant decrease in to the negative range caused by additional shear strains. As shown in the figures (5.12 and 5.13), the hydrostatic contribution of fibers remains level at large strains or even slightly increases again before reaching 20 percent, which is contrary to what was observed previously in terms of the deviatoric contribution of fibers (q_{f0}).

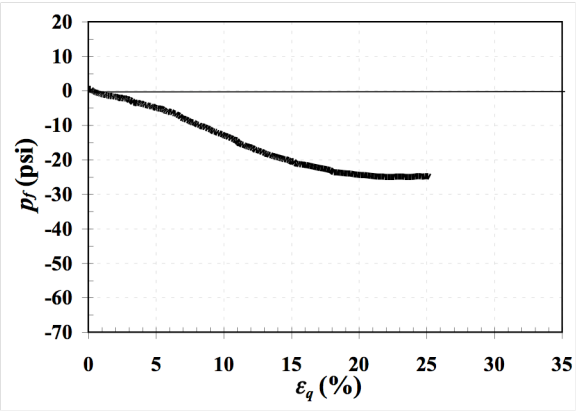

a) 5-psi effective consolidation stress

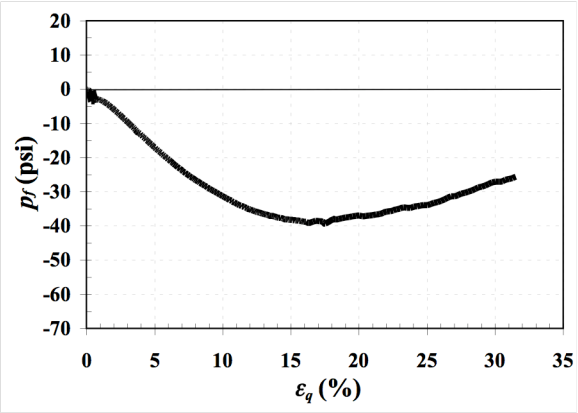

d) 40-psi effective consolidation stress

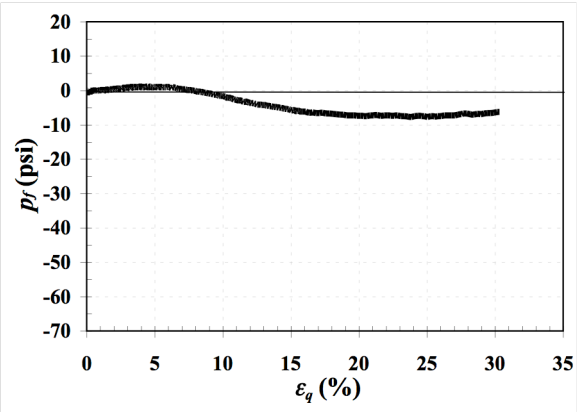

b) 10-psi effective consolidation stress

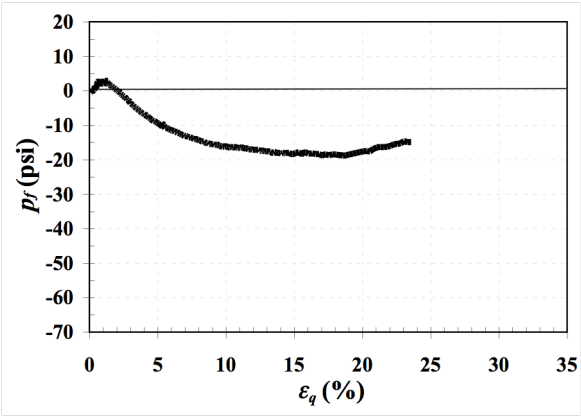

e) 80-psi effective consolidation stress

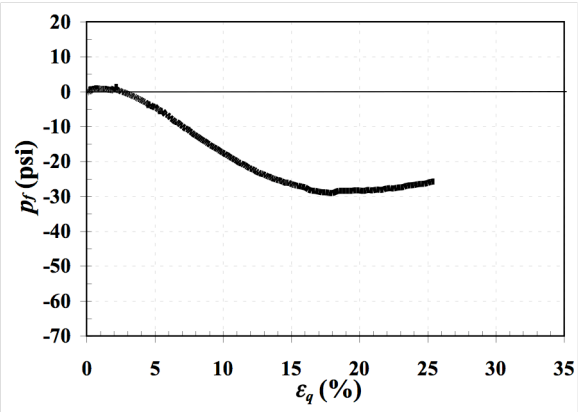

c) 20-psi effective consolidation stress

Figure 5.12 Hydrostatic contributions of fibers (p_f) versus triaxial shear strain (ε_q) from the $\overline{CU}$ tests for silty sand specimens compacted at 18 percent water content and consolidated to: a) 5-psi effective stress, b) 10-psi effective stress, c) 20-psi effective stress, d) 40-psi effective stress, and e) 80-psi effective stress.

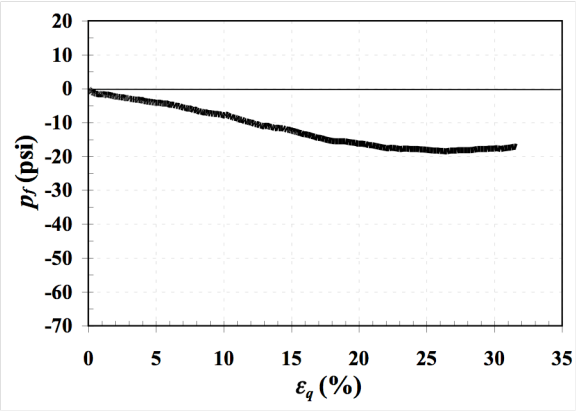

a) 5-psi effective consolidation stress

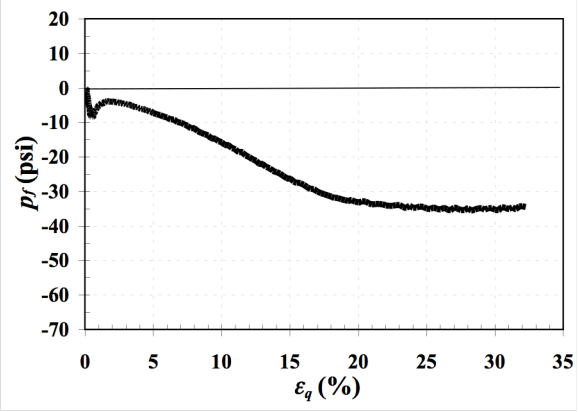

d) 40-psi effective consolidation stress

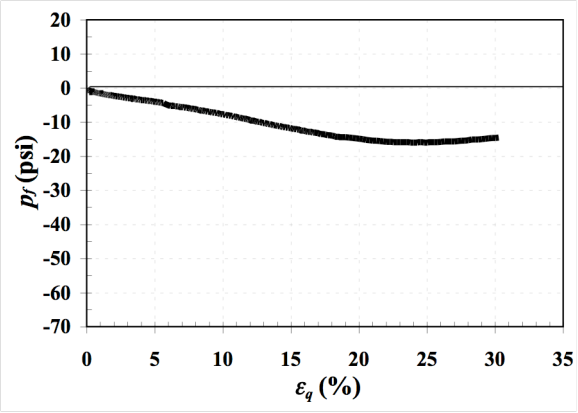

b) 10-psi effective consolidation stress

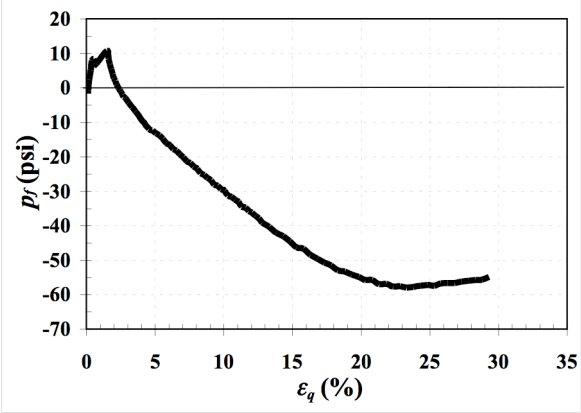

e) 80-psi effective consolidation stress

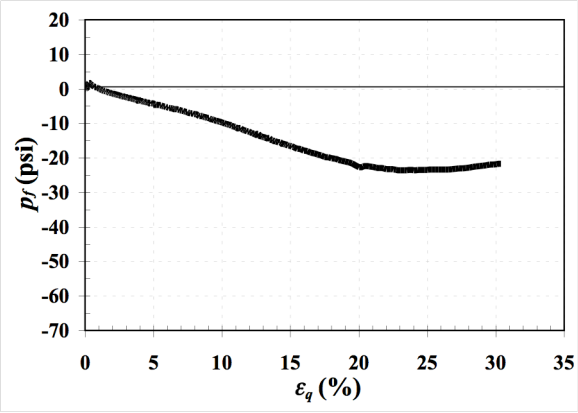

c) 20-psi effective consolidation stress

Figure 5.13 Hydrostatic contributions of fibers (p_f) versus triaxial shear strain (ε_q) from the $\overline{CU}$ tests for silty sand specimens compacted at 22 percent water content and consolidated to: a) 5-psi effective stress, b) 10-psi effective stress, c) 20-psi effective stress, d) 40-psi effective stress, and e) 80-psi effective stress.

The hydrostatic contribution of fibers determined from comparable *CD* tests on unreinforced and reinforced silty sand specimens compacted at 18 percent and 22 percent water contents are shown in Figures 5.14 and 5.15. Again, the graphs reveal that the mobilization of confining stress in the fibers is a consistent trend. The observed behavior in the *CD* tests is similar to what was observed for the deviatoric contribution of fibers (q_f) under the same loading conditions (Figures 5.6 and 5.7). Relatively small strains were required to begin mobilizing the additional confining stresses provided by the inclusion of fibers under drained loading conditions. At certain strain levels, the contribution attributed to the fibers increased along with the additional strains in an approximately linear fashion as well. However, the magnitude of this contribution (p_{f0}) is relatively smaller than the deviatoric contribution of fibers at any given shear strain under drained loading conditions.

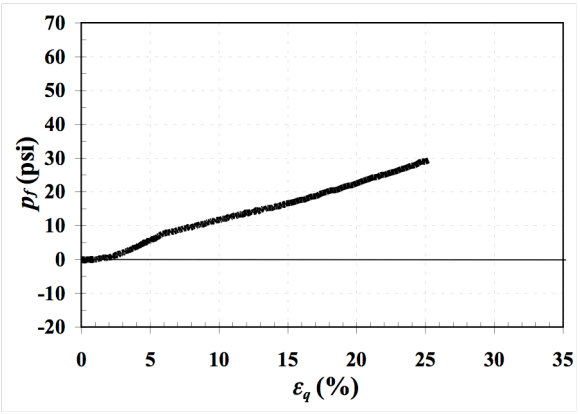

a) 5-psi effective consolidation stress

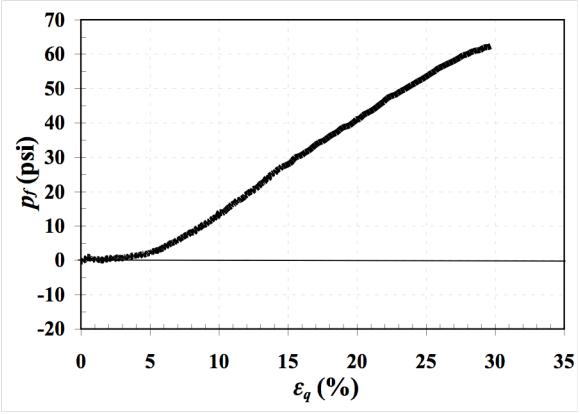

d) 40-psi effective consolidation stress

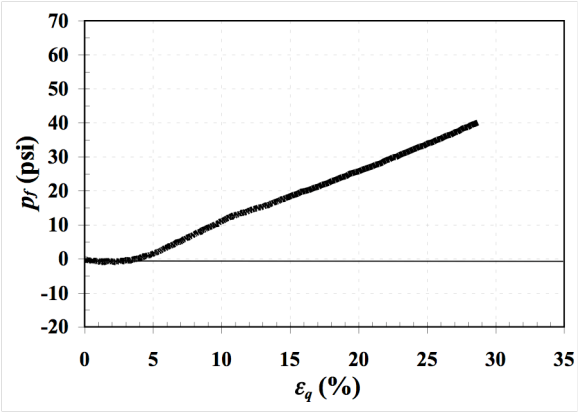

b) 10-psi effective consolidation stress

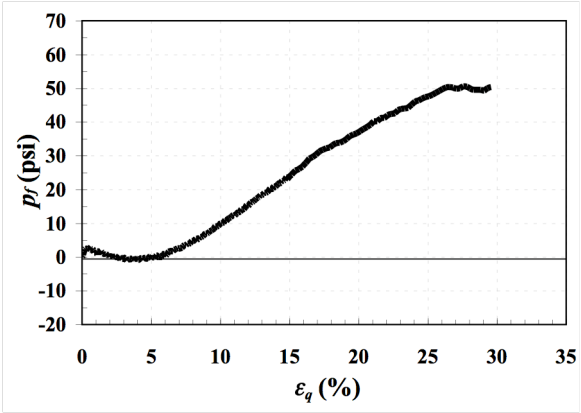

e) 80-psi effective consolidation stress

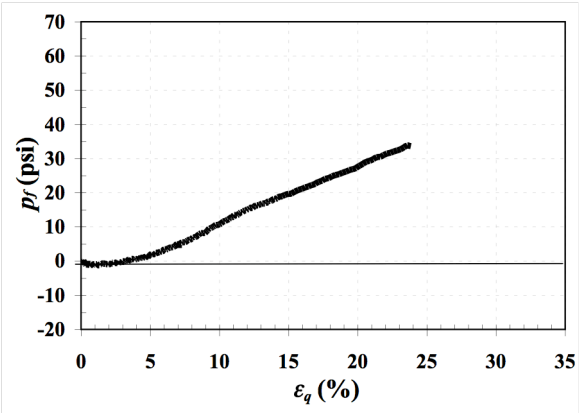

c) 20-psi effective consolidation stress

Figure 5.14 Hydrostatic contributions of fibers (p_f) versus triaxial shear strain (ε_q) from the *CD* tests for silty sand specimens compacted at 18 percent water content and consolidated to: a) 5-psi effective stress, b) 10-psi effective stress, c) 20-psi effective stress, d) 40-psi effective stress, and e) 80-psi effective stress.

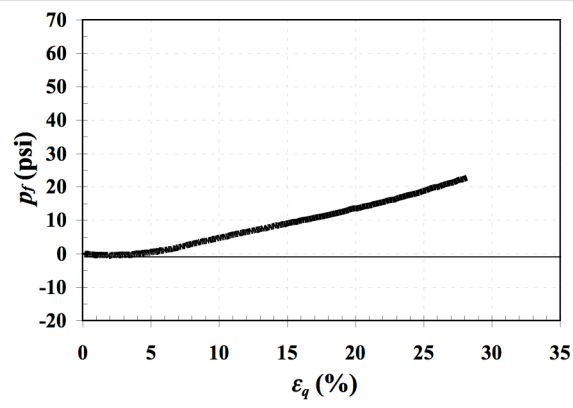

a) 5-psi effective consolidation stress

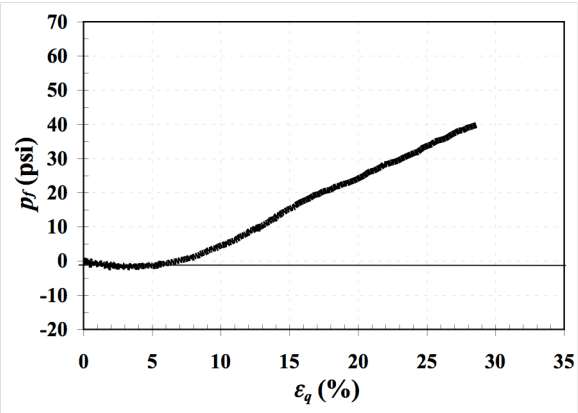

d) 40-psi effective consolidation stress

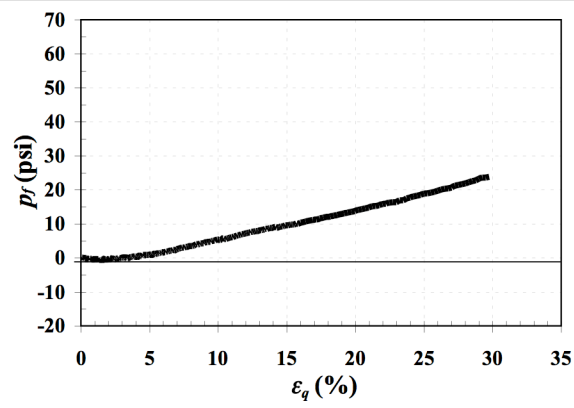

b) 10-psi effective consolidation stress

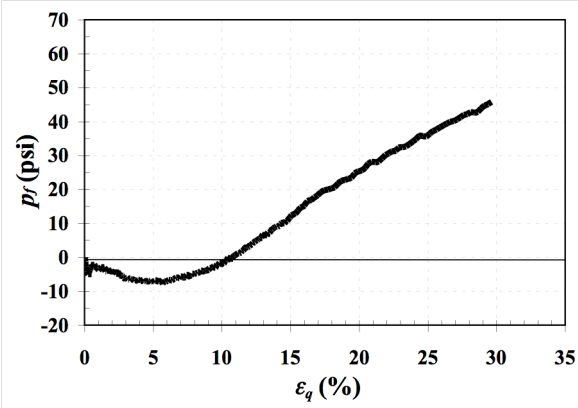

e) 80-psi effective consolidation stress

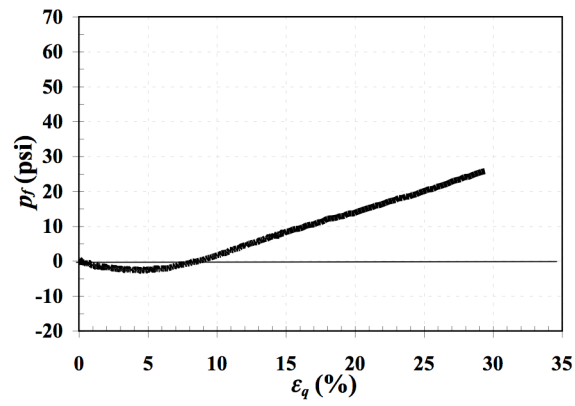

c) 20-psi effective consolidation stress

Figure 5.15 Hydrostatic contributions of fibers (p_f) versus triaxial shear strain (ε_q) from the *CD* tests for silty sand specimens compacted at 22 percent water content and consolidated to: a) 5-psi effective stress, b) 10-psi effective stress, c) 20-psi effective stress, d) 40-psi effective stress, and e) 80-psi effective stress.

5.4.2 Ottawa Sand

Figures 5.16 and 5.17 show the hydrostatic contribution of fibers versus the triaxial shear strain determined from the $\overline{CU}$ tests on unreinforced and reinforced loose and medium-dense Ottawa sand specimens, respectively. The observed behavior indicates that small strains are required to mobilize the additional confining stress produced by the reinforcing fibers under undrained loading, and in general, the same amount of shear strain was required to mobilize the fiber shear resistance as well. At certain strain levels, the hydrostatic contribution of fibers increased with increasing shear strain.

When the loose and medium-dense reinforced Ottawa sand specimens tested under undrained condition were compared, the medium-dense specimens had a much smaller initial hydrostatic fiber contribution (p_{f0}) than the loose specimens. In addition, the initial hydrostatic stress was smaller (more negative) than the initial deviatoric stress (q_{f0}) under undrained loading conditions. This response differs from the observed behavior for the reinforced specimens of silty sand.

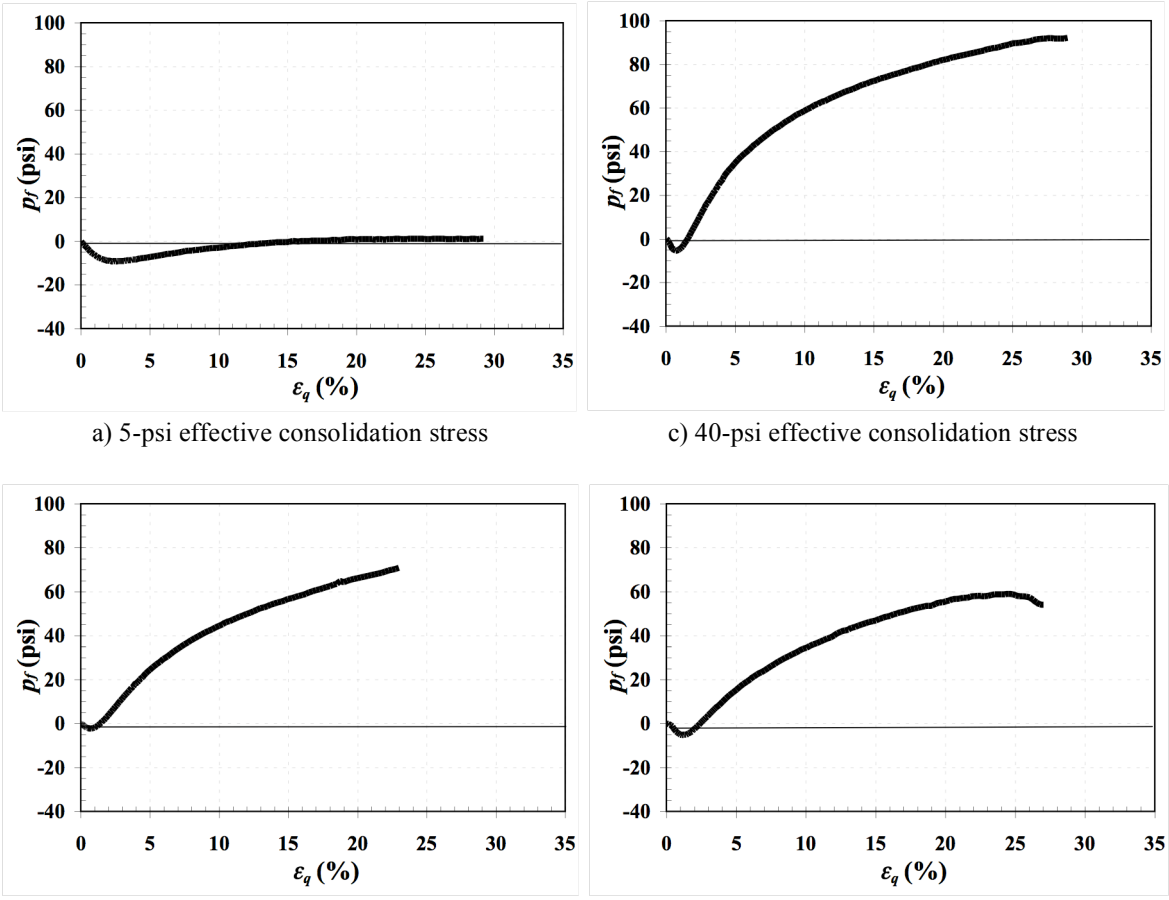

a) 5-psi effective consolidation stress

c) 40-psi effective consolidation stress

b) 20-psi effective consolidation stress

d) 60-psi effective consolidation stress

Figure 5.16 Hydrostatic contributions of fibers (p_f) versus triaxial shear strain (ε_q) from the $\overline{CU}$ tests for loose Ottawa sand specimens and consolidated to: a) 5-psi effective stress, b) 20-psi effective stress, c) 40-psi effective stress, and d) 60-psi effective stress.

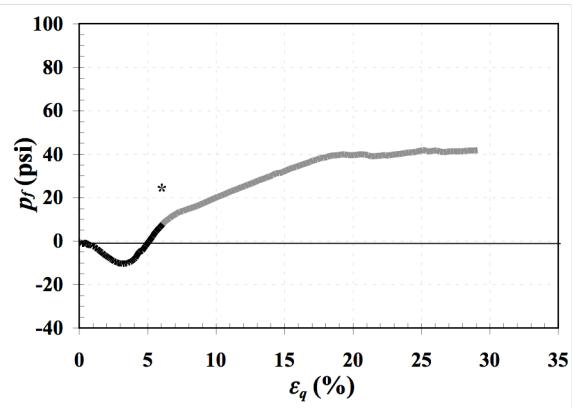

a) 5-psi effective consolidation stress

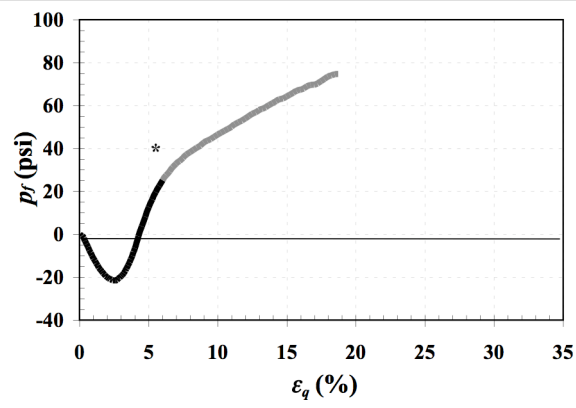

c) 40-psi effective consolidation stress

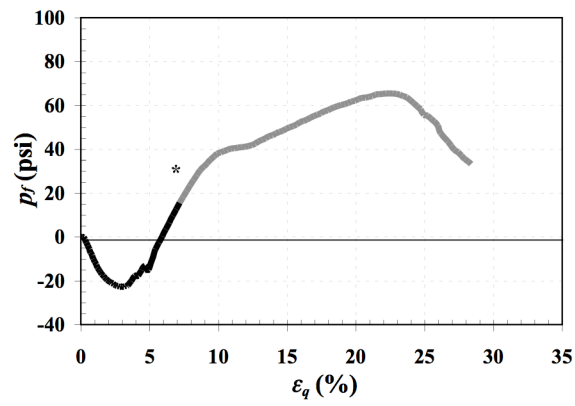

b) 20-psi effective consolidation stress

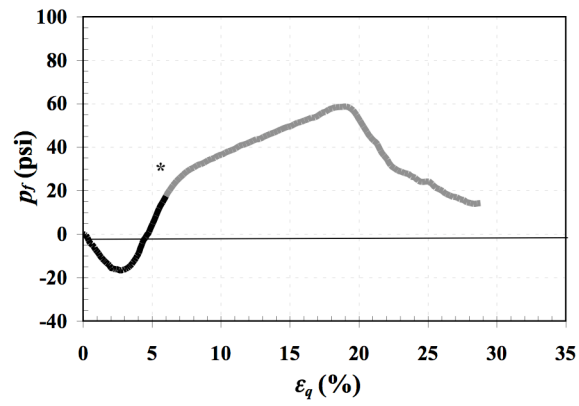

d) 60-psi effective consolidation stress

Figure 5.17 Hydrostatic contributions of fibers (p_f) versus triaxial shear strain (ε_q) from the $\overline{CU}$ tests for medium-dense Ottawa sand specimens consolidated to: a) 5-psi effective stress, b) 20-psi effective stress, c) 40-psi effective stress, and d) 60-psi effective stress.

*: Start point of suspicious measurement.

The hydrostatic contribution of fibers computed from the comparable *CD* tests on unreinforced and reinforced Ottawa sand specimens compacted at loose and medium-dense states are shown in Figures 5.18 and 5.19, respectively. The observed responses suggest that a consistent trend exists in the mobilization of the hydrostatic contribution in the reinforcing fibers, which is similar to what was observed in undrained tests (Figures 5.16 and 5.17). This behavior indicates that relatively small strains are required to mobilize the confining stress created by the inclusion of fibers. Again, the reinforced specimens tested under drained loading condition tended to mobilize the hydrostatic contribution at lower strains than specimens tested under undrained loading conditions.

Unlike silty sand and silty clay (Romero, 2003) specimens, the Ottawa sand specimens exhibited similar behavior in that both their deviatoric and hydrostatic contributions under undrained and drained tests. In general, the hydrostatic contribution of fibers tended to be much smaller than the deviatoric contribution of fibers at any given shear strain and at any given effective confining stress. The reason for the different mobilization responses of the deviatoric and hydrostatic contributions of fibers in silty sand and Ottawa sand is not clear. Soil type is believed to play an important role in determining the included fibers interaction in terms of the deviatoric and hydrostatic components of the fiber-reinforced soils. The evidence collected from the testing program suggests that a difference between the deviatoric and hydrostatic contribution of fibers under undrained loading conditions for silty sand and Ottawa sand does exist.

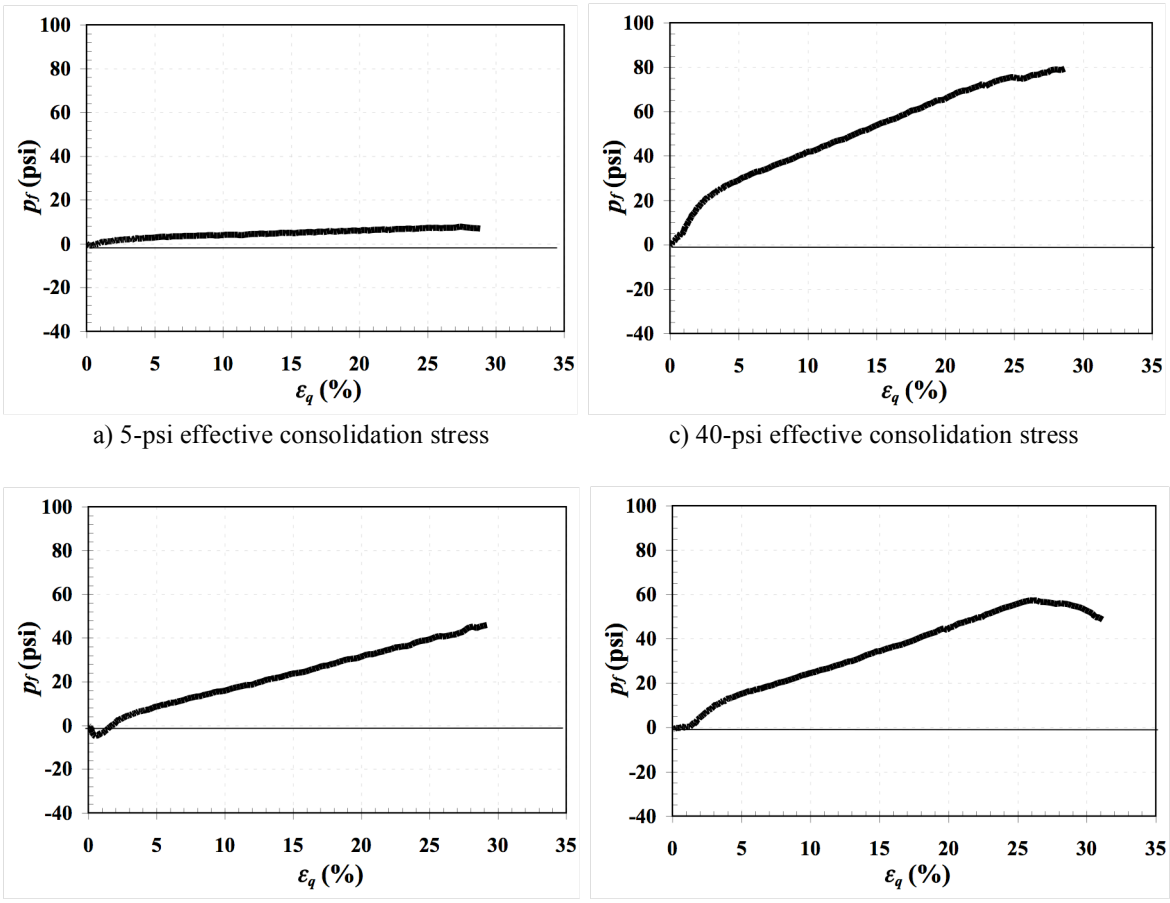

a) 5-psi effective consolidation stress

c) 40-psi effective consolidation stress

b) 20-psi effective consolidation stress

d) 60-psi effective consolidation stress

Figure 5.18 Hydrostatic contributions of fibers (p_f) versus triaxial shear strain (ε_q) from the *CD* tests for loose Ottawa sand specimens and consolidated to: a) 5-psi effective stress, b) 20-psi effective stress, c) 40-psi effective stress, and d) 60-psi effective stress.

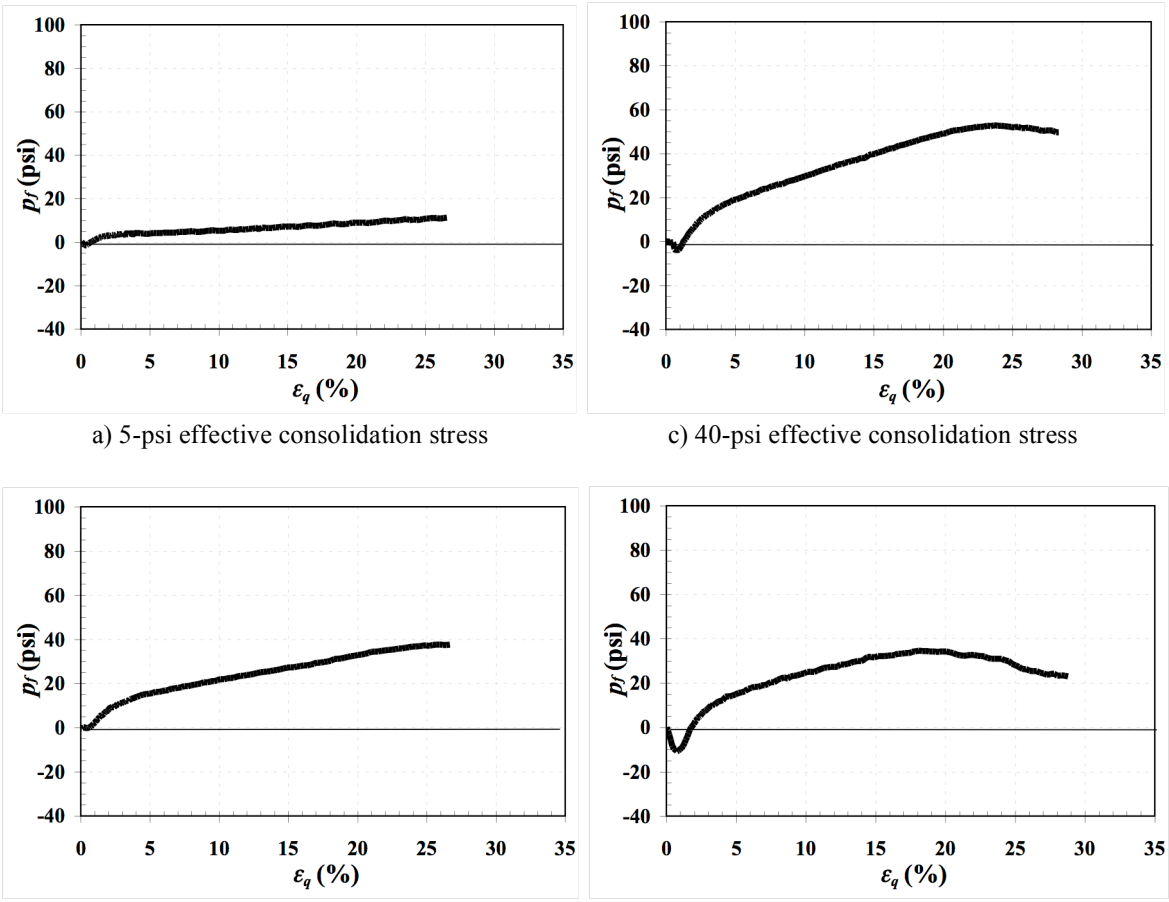

a) 5-psi effective consolidation stress

c) 40-psi effective consolidation stress

b) 20-psi effective consolidation stress

d) 60-psi effective consolidation stress

Figure 5.19 Hydrostatic contributions of fibers (p_f) versus triaxial shear strain (ε_q) from the *CD* tests for medium-dense Ottawa sand specimens consolidated to: a) 5-psi effective stress, b) 20-psi effective stress, c) 40-psi effective stress, and d) 60-psi effective stress.

5.5 Key Aspects of Behavior

The data presented above suggests that mobilization of fiber resistance in terms of the deviatoric and hydrostatic contribution of fibers is both a function of the shear strain and the effective confining stress. Additional discussion of this relationship as it is exhibited in silty sand and Ottawa sand is presented in this section. Both the fiber contributions due to shear resistance and internal confining stress can be modeled with an initial stress (q_{f0} and p_{f0}) and a bi-linear function of increasing shear strain.

5.5.1 Initial Deviatoric Contribution of Fibers (q_{f0})

Figure 5.20 shows the initial deviatoric contribution of fibers determined from Figures 5.4, 5.5, 5.6, and 5.7 and plotted as a function of effective consolidation stress from both undrained and drained tests for silty sand specimens compacted at 18 percent and 22 percent water contents. The values plotted are the minimum values for the deviatoric contribution of fibers (q_f) prior to reaching the linear portion of the q_f versus ε_q curve. The figure shows that the initial contribution of the fibers (q_{f0}) tends to decrease as the effective consolidation stress increases. The values range from slightly negative for low effective consolidation stress to significantly negative for high effective consolidation stress. Specimens consolidated to higher effective confining stresses would be expected to have low stress in the fibers and thus a lower initial deviatoric contribution of fibers, because higher effective confining stress will cause more compression of specimens during consolidation. In addition, the magnitude of the initial deviatoric contribution of fibers (q_{f0}) for silty sand specimens compacted at 22 percent water content is generally observed to be lower than for the specimens compacted at 18 percent

water content. The rate of change of q_{f0} is also greater for the specimens compacted at 22 percent water content as well.

It is noted that the initial deviatoric contribution of fibers from the *CD* tests is larger (less negative) than from the $\overline{CU}$ tests. The difference is believed to be due to volume changes occurring during drained loading conditions, which tends to compensate for volume changes that occur during consolidation.

The initial deviatoric contribution of fibers are plotted versus the effective consolidation stress from the $\overline{CU}$ and *CD* tests for Ottawa sand specimens compacted at loose and medium-dense states in Figure 5.21. The figures show that the initial deviatoric contribution of fibers tends to decrease as a function of increasing effective consolidation stress. However, the rate of change q_{f0} of the medium-dense reinforced Ottawa sand specimens is higher than that of the loose reinforced specimens.

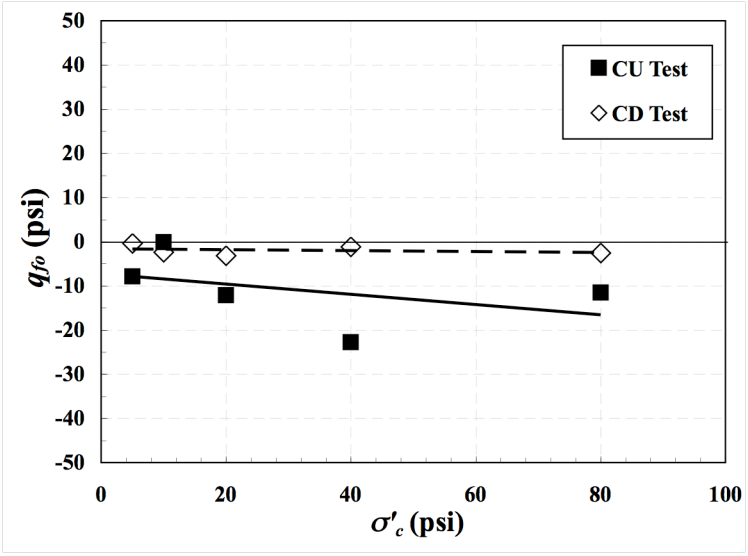

a) 18 percent water content

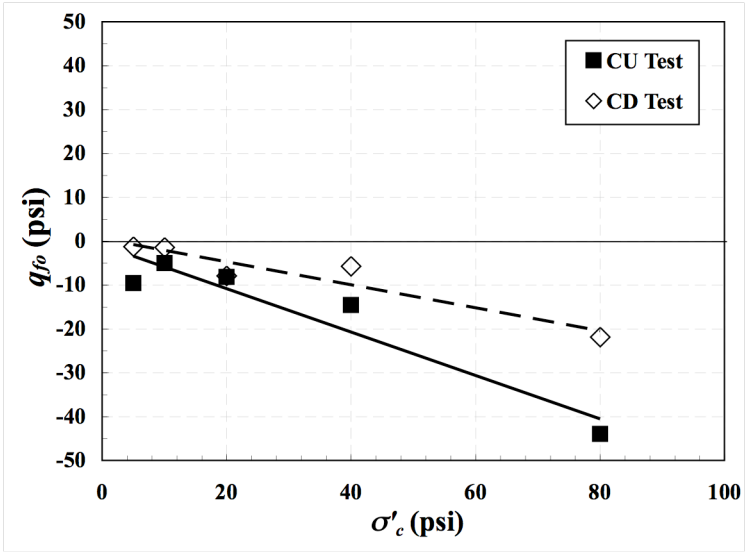

b) 22 percent water content

Figure 5.20 Initial deviatoric contribution of fibers (q_{f0}) versus effective consolidation stress (σ'_c) from the $\overline{CU}$ and CD tests for silty sand specimens compacted at: a) 18 percent water content, and b) 22 percent water content.

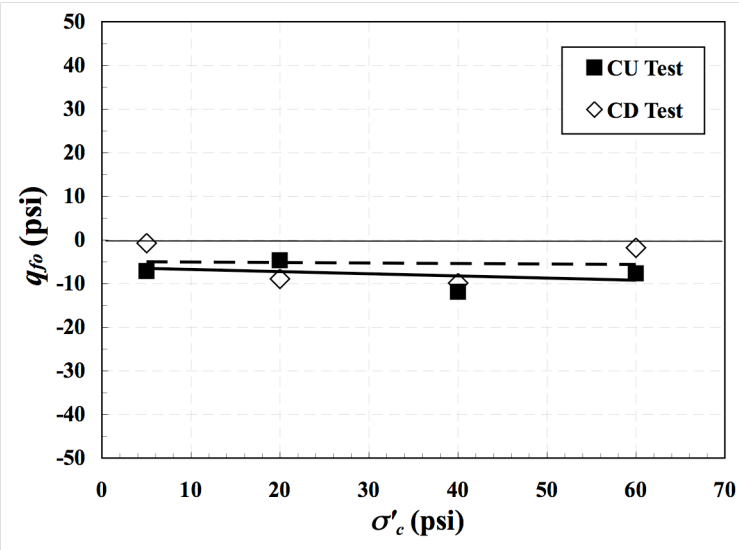

a) loose state

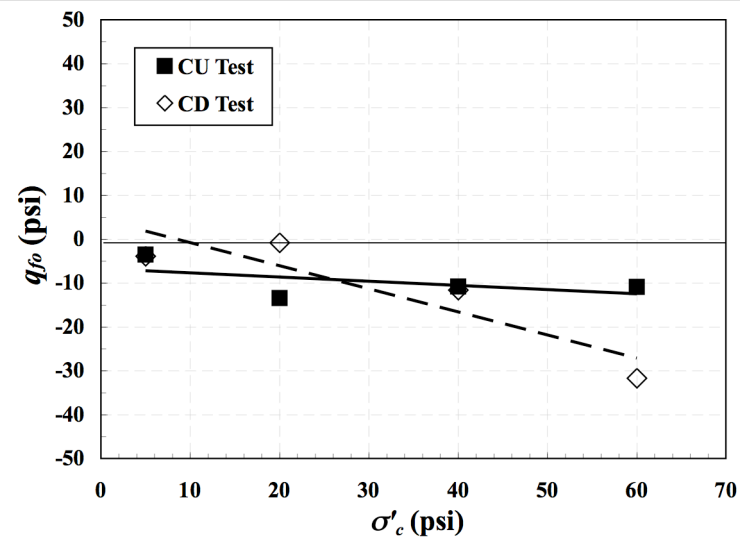

b) medium-dense state

Figure 5.21 Initial deviatoric contribution of fibers (q_{f0}) versus effective consolidation stress (σ'_c) from the $\overline{CU}$ and CD tests for the Ottawa sand specimens compacted at a: a) loose state, and b) medium-dense state.

5.5.2 Shear Modulus (G_f) due to Fibers

As illustrated in Figure 5.2, the slope of the linear portion of the fiber contribution is three times the shear modulus of the fiber shear contributions (Wood, 1990). This is "shear modulus" due to the fibers (q_f) is plotted as a function of effective consolidation stress for silty sand specimens compacted at 18 percent and 22 percent water contents in Figure 5.22. Although the results produce some scatter, the data suggests a linear relationship between q_f and the effective consolidation stress during each group of tests. Assuming that a linear relationship does exist, the slopes of the linear trends seem to be similar for the $\overline{CU}$ and CD tests for silty sand specimens compacted at both 18 percent and 22 percent water contents. For any given effective consolidation stress, the specimens compacted at an 18 percent water content consistently show higher values of q_f than those compacted at a 22 percent water content. The observed difference in G_f for specimens compacted at 18 percent and 22 percent water contents is believed to be due to the results of different initial stresses developed in the fibers during the compaction and consolidation process, which means that specimens compacted at different water contents will have different stress changes during test setups.

q_f values are also greater for specimens tested in the CD tests than in the $\overline{CU}$ tests, which is similar to the initial deviatoric contribution of fibers (Figure 5.20). Again, these differences are attributed to the fact that volume change during the CD tests may produce a different load transfer contribution than for the $\overline{CU}$ tests.

Figure 5.23 shows the q_f plotted as a function of effective consolidation stress from the undrained and drained tests for Ottawa sand specimens prepared at loose and

medium-dense state. The figure clearly reveals a linear relationship between q_f and the effective consolidation stress. Additionally, the slope of the linear trends seems to be similar for the undrained and drained loading conditions for both loose and medium-dense reinforced specimens. Only the medium-dense specimens tested under drained loading condition exhibited a much steeper slope of the linear trend than the loose Ottawa sand specimens. Note that the q_f values are similar for all loose Ottawa sand specimens in the $\overline{CU}$ and CD tests.

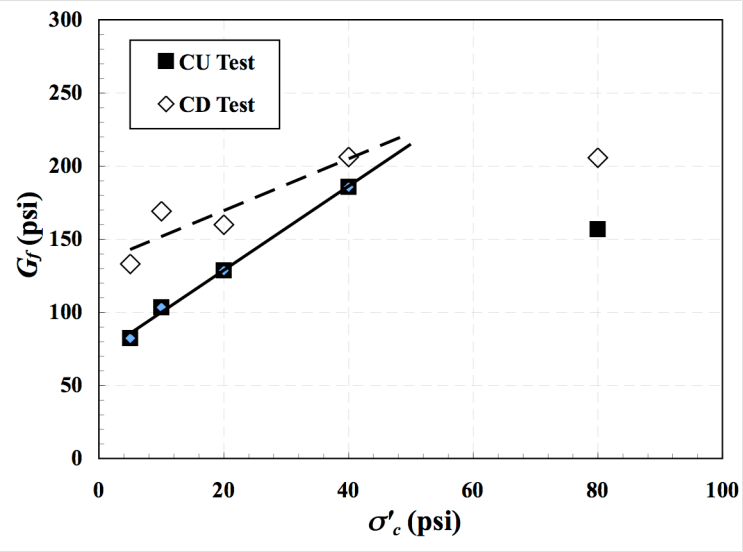

a) 18 percent water content

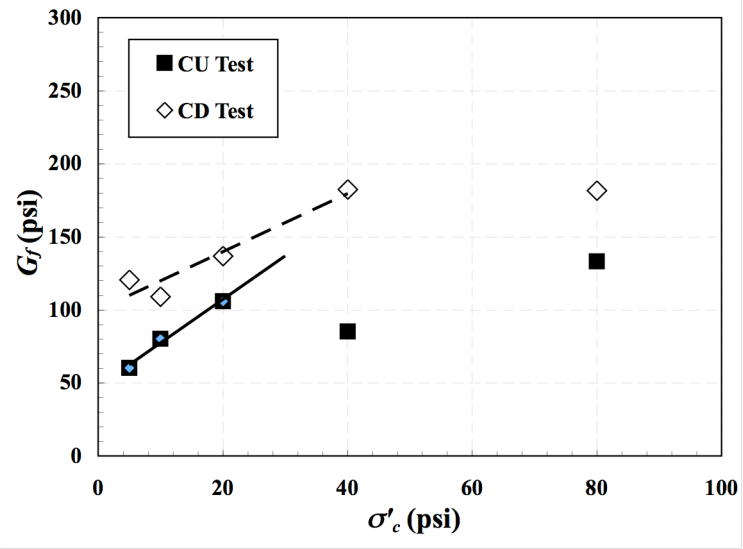

b) 22 percent water content

Figure 5.22 Shear modulus attributed to fibers (G_f) versus effective consolidation stress (σ'_c) from the $\overline{CU}$ and CD tests for silty sand specimens compacted at: a) 18 percent water content, and b) 22 percent water content.

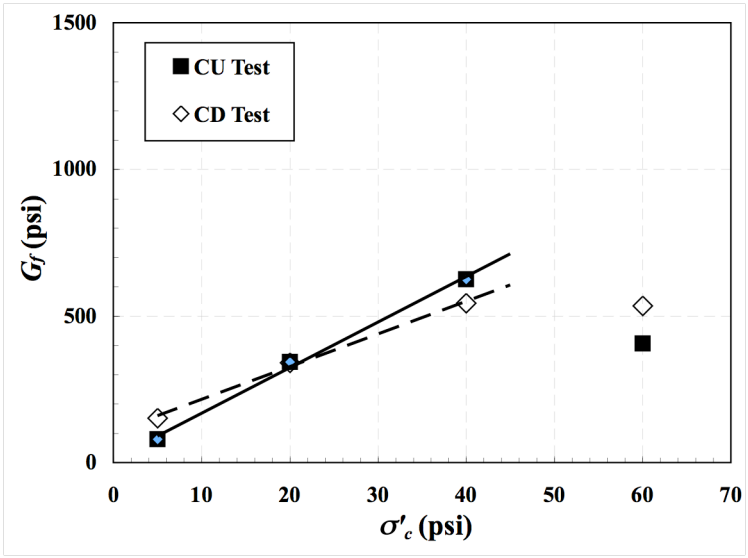

a) loose state

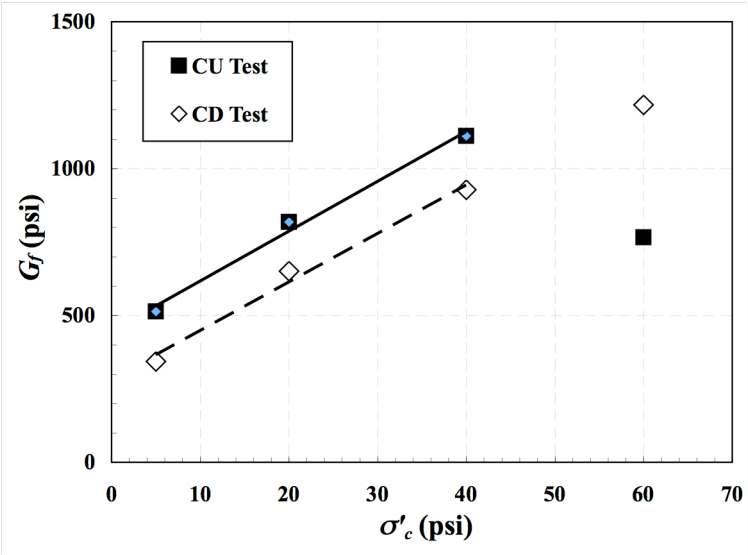

b) medium-dense state

Figure 5.23 Shear modulus due to fibers (G_f) versus effective consolidation stress (σ'_c) from the $\overline{CU}$ and CD tests for Ottawa sand specimens compacted at: a) loose state, and b) medium-dense state.

5.5.3 Hydrostatic Contributions of Fibers (p_f)

The initial hydrostatic contribution of fibers are plotted versus the effective consolidation stress for the silty sand specimens compacted at 18 percent and 22 percent water contents in Figure 5.24. The values plotted are either the maximum positive value or the minimum negative value for the hydrostatic contribution of fibers (p_f) determined by directly comparing the unreinforced and reinforced specimens in terms of mean effective stress (p') prior to reaching the linear portion of the curve (p_f versus ε_q).

The figures show two different kinds of relationships between the initial hydrostatic contribution of fibers and the effective consolidation stress. The first shows that the initial hydrostatic contribution of fibers (p_{f0}) decreasing with the increasing effective consolidation stress for the silty sand specimens tested under drained loading conditions. Values range from slightly negative for low values of consolidation stress to significantly negative values for high values of consolidation stress. This trend is consistent with observation of the initial deviatoric stresses (q_{f0} versus σ'_c) in the $\overline{CU}$ and CD tests for silty sand and Ottawa sand. The magnitude of p_{f0} is also observed to be lower for the silty sand specimens compacted at 22 percent water content, and the rate of change p_{f0} is higher for these specimens. However, the second relationship shows that the initial hydrostatic contribution of fibers (p_{f0}) increases with the increasing effective consolidation stress for the silty sand specimens tested under undrained loading conditions. Values range from small for low values of consolidation stress to large for high values of consolidation stresses under undrained loading conditions. This trend dramatically differs from the observed q_{f0} versus σ'_c relationships in the undrained and

drained tests. Conversely, the magnitude of p_{f0} is observed to be higher for specimens compacted at 22 percent water content, and the rate of change of p_{f0} is also greater for these specimens.

Figure 5.25 shows the initial hydrostatic contribution of fibers plotted as a function of effective consolidation stress for the Ottawa sand compacted at loose and medium-dense states. Although some scatter is apparent, the data clearly exhibits a linear relationship between the initial hydrostatic contribution (p_{f0}) and the effective consolidation stress for each group of tests. The loose Ottawa sand specimens show that the initial hydrostatic contribution of fibers slightly increases (or keep constant) with the increasing effective consolidation stress for both $\overline{CU}$ and CD tests. In contrast, the medium-dense Ottawa sand specimens demonstrate that the initial hydrostatic contribution of fibers slightly decreases with the increasing effective consolidation stress for both $\overline{CU}$ and CD tests. This agrees with the response relationship observed for q_{f0} versus σ'_c for same types of testing. Values of p_{f0} are greater for specimens tested in the CD type tests than for the $\overline{CU}$ tests for Ottawa sand. Conversely, values of p_{f0} are smaller than for specimens tested in the CD tests than for $\overline{CU}$ tests for silty sand at any given effective consolidation stress. Therefore, the behavior of the hydrostatic contribution (p_f) is affected by both varying soil types and loading conditions.

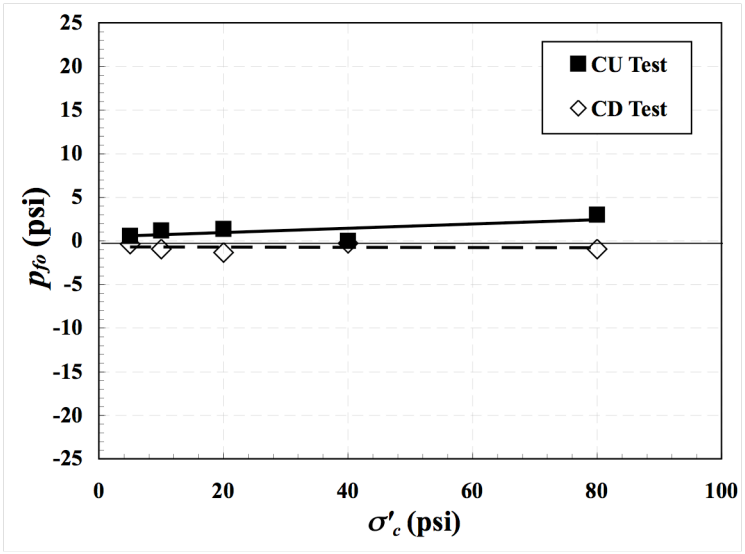

a) 18 percent water content

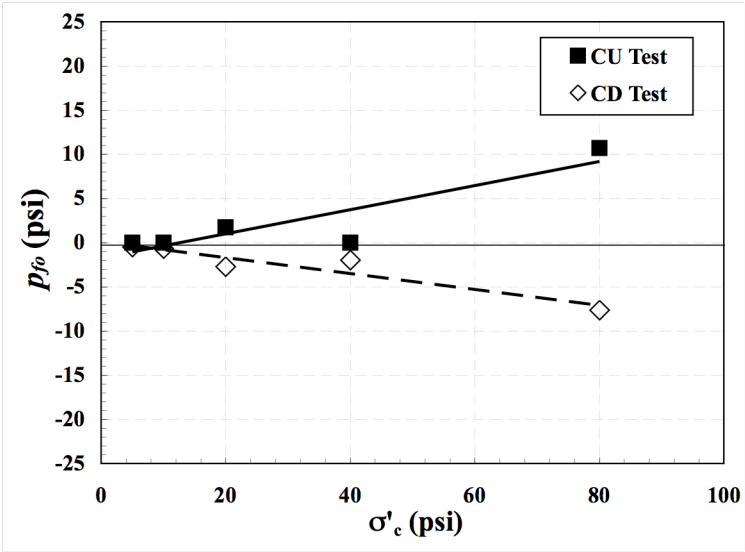

b) 22 percent water content

Figure 5.24 Initial hydrostatic contribution of fibers (p_{f0}) versus effective consolidation stress (σ'_c) from the $\overline{CU}$ and CD tests for silty sand specimens compacted at: a) 18 percent water content, and b) 22 percent water content.

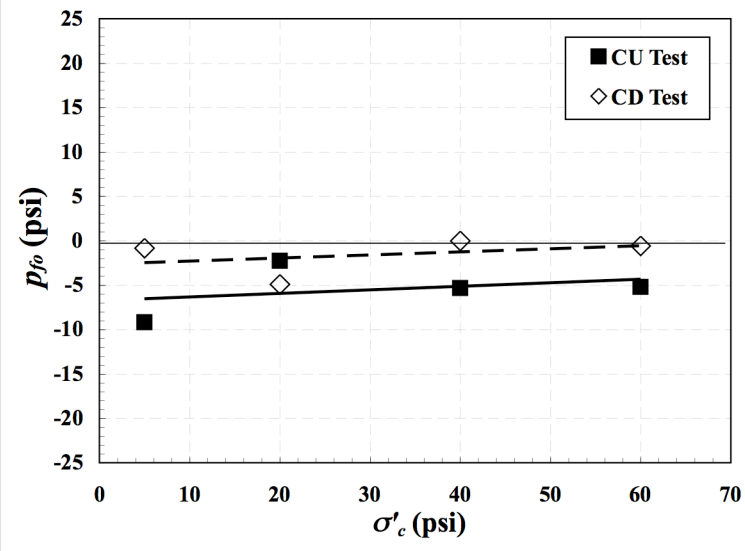

a) loose state

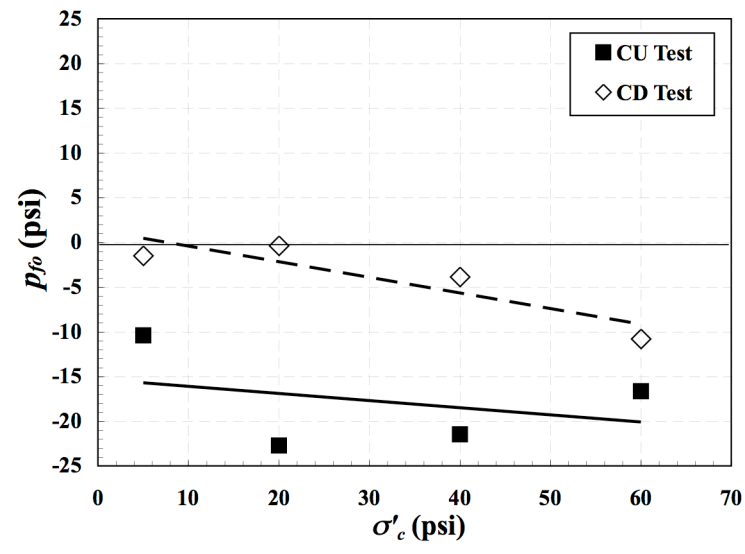

b) medium-dense state

Figure 5.25 Initial hydrostatic contribution of fibers (p_{f0}) versus effective consolidation stress (σ'_c) from the $\overline{CU}$ and CD tests for Ottawa sand specimens compacted at: a) loose state, and b) medium-dense state.

5.6 Summary

The analysis from the experimental data on fiber-reinforced soils suggests that the inclusion of fibers provides both a deviatoric (q_f) and a hydrostatic (p_f) contribution to the stresses in the specimens. Both contributions were compared in terms of either the equal shear strain for the deviatoric stresses (q) or the mean effective stress (p') for the reinforced and unreinforced specimens tested under identical conditions during undrained and drained tests. The deviatoric contribution of fibers can be modeled as a bi-linear function with an initial constant contribution (q_{f0}) plus a linear load transfer contribution ($3G_f$) that is three times the shear modulus due to fibers. The hydrostatic contribution of fibers can be modeled by an initial constant contribution (p_{f0}) plus the linear contribution of the hydrostatic stresses.

The analysis also reveals that the initial deviatoric contribution of fibers decreases (negative value) as the effective consolidation stress increases and suggests that the shear modulus attributed to fibers (G_f) also increases with the increase in effective consolidation stress. The initial hydrostatic contribution of fibers decreases with the increasing effective consolidation stress for the silty sand specimens tested in drained tests and for the Ottawa sand in both undrained and drained tests. Conversely, the initial hydrostatic contribution of fibers increases (a positive value) with increasing effective consolidation stress for the silty sand specimens tested in drained tests. Therefore, the soil types and loading conditions play an important role in determining the soils interaction with included fibers in terms of the deviatoric and hydrostatic components for fiber-reinforced soils.

CHAPTER 6: CONSTITUTIVE MODEL TO PREDICT THE EFFECTIVE STRESS BEHAVIOR

6.1 Introduction

The data analyzed in the previous chapter showed that fiber reinforcement provides both a deviatoric (q_f) and a hydrostatic (p_f) contribution to the stresses in fiber-reinforced specimens. Based on the hypothesis of this research, the effective stress behavior of fiber-reinforced soils can be predicted from the superposition of the response of unreinforced soil and the response attributed to the fibers. A constitutive model was developed to predict the stress-strain, pore pressure and volume change contributions of the fibers under undrained and drained loading. The model's basic components and terminologies are introduced and presented in this chapter.

6.2 Basis of Constitutive Model

6.2.1 Weight-Volume Definitions

The weight-volume relationships for fiber-reinforced soils as defined by Zornberg (2002) are fundamental to the construction of the model, and they are summarized in the following:

The volumetric fiber content, χ, used in this research work is defined as

$$\chi = \frac{V_f}{V} \tag{6.1}$$

in which V_f is the volume of fibers, and V is the volume of fiber-reinforced soil.

The gravimetric fiber content, χ_w, which is used in the experimental phase of this research is defined as

$$\chi_w = \frac{W_f}{W} \tag{6.2}$$

in which W_f is the weight of fibers, and W is the dry weight of the unreinforced soil. The definition above is consistent with the classic definition of gravimetric moisture content.

The dry unit weight of the fiber-reinforced specimen, γ_{df}, is defined as

$$\gamma_{df} = \frac{W_f + W_s}{V} \tag{6.3}$$

in which w_s is dry weight of soil in fiber-reinforced specimens. The specific gravity of fibers, G_{rf}, is defined as

$$G_{rf} = \frac{W_f}{V_f \gamma_w} \tag{6.4}$$

in which γ_w is the unit weight of water. This definition is analogous to the classic definition of specific gravity of solids. Substituting Equations 6.1, 6.2, and 6.3 into Equation 6.4, an expression for solves for the volumetric fiber content (χ) can be described:

$$\chi = \frac{\chi_w \gamma_d}{(1 + \chi_w) G_{rf} \gamma_w} \tag{6.5}$$

6.2.2 Relationship between fiber stain (ε_f) and axial strain (ε_a)

Assumed in the construction of the model is that the fibers are uniformly distributed in the specimens and that strains in the fibers produce the overall changes in

stress in the fiber-reinforced soil. If is necessary to establish a mean for relating in the fiber (really a fictitious average strain in the fibers) to strains in the fiber-reinforced soil composite. In triaxial compression tests, the axial strain is commonly and easily measured. Finding the fiber strains derived from the measured axial strain during the triaxial tests is critical for model calculations, which are discussed in the following sections.

In a three-dimensional system, the linear strain (Harr, 1966) between two points aliged in an arbitrary r direction can be written as

$$\varepsilon_f = \varepsilon_x l^2 + \varepsilon_y m^2 + \varepsilon_z n^2 + \gamma_{xy} lm + \gamma_{yz} mn + \gamma_{xz} l\, n \tag{6.6}$$

in which ε_x, ε_y,and ε_z are the normal strain in the x, y, and z direction, respectively; l, m, and n are direction cosines ($l = \cos(dr,dx)$, $m = \cos(dr,dy)$, $n = \cos(dr,dz)$), and γ_{xy}, γ_{yz}, and γ_{xz} are engineering shear strains in the xy, yz, and zx plans, which is twice the pure shear strain in terms of ε_{xy}, ε_{yz}, and ε_{xz} (Atkinson and Bransby, 1978). Equation 6.6 can be written as the matrix equation

$$\varepsilon_f = \begin{bmatrix} l & m & n \end{bmatrix} [D] \begin{bmatrix} l \\ m \\ n \end{bmatrix} \tag{6.7}$$

$$[D] = \begin{bmatrix} \varepsilon_x & \dfrac{1}{2\gamma_{xy}} & \dfrac{1}{2\gamma_{xz}} \\ \dfrac{1}{2\gamma_{xy}} & \varepsilon_y & \dfrac{1}{2\gamma_{yz}} \\ \dfrac{1}{2\gamma_{xz}} & \dfrac{1}{2\gamma_{yz}} & \varepsilon_x \end{bmatrix} \tag{6.8}$$

in which $[D]$ is a symmetric deformation matrix. Equation 6.7 is relative to the coordinate transformation as it transformed from the local coordinate along the r direction to the global coordinate.

The concept of principal strains from Mohr's Circle was utilized to represent the complete state of strains in a soil element. Strains in any given coordinate system can be transformed into a principal direction, as illustrated in Figure 6.1.

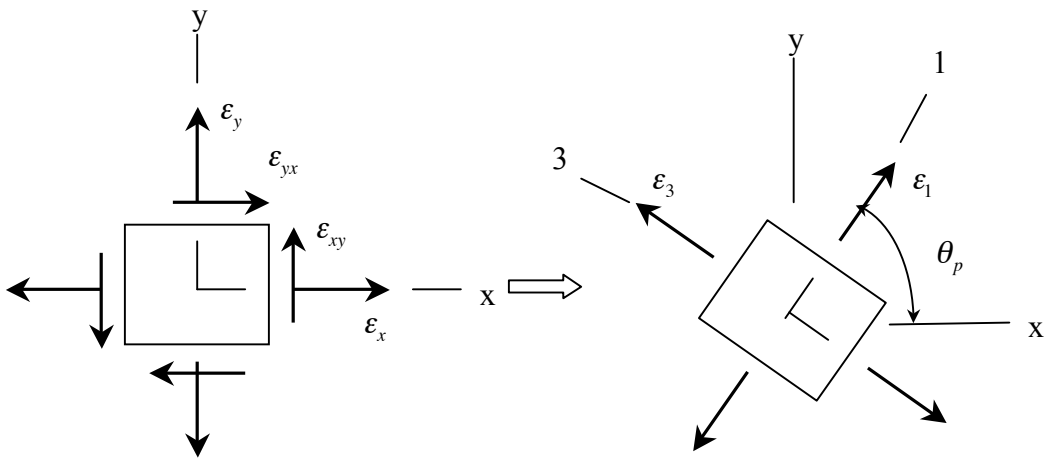

Figure 6.1 Soil element transformation coordinate system of plane strain.

The major and minor principle of strains can be expressed as

$$\varepsilon_1 = \frac{\varepsilon_x + \varepsilon_y}{2} + \sqrt{\left(\frac{\varepsilon_x - \varepsilon_y}{2}\right)^2 + \left(\frac{\gamma_{xy}}{2}\right)^2} \tag{6.9}$$

$$\varepsilon_3 = \frac{\varepsilon_x + \varepsilon_y}{2} - \sqrt{\left(\frac{\varepsilon_x - \varepsilon_y}{2}\right)^2 + \left(\frac{\gamma_{xy}}{2}\right)^2} \tag{6.10}$$

$$\tan 2\theta_p = \frac{\gamma_{xy}}{\varepsilon_x - \varepsilon_y} \tag{6.11}$$

in which ε_1 and ε_3 are the major and minor principal of strains, and θ_p is the angle of the principal plane axis (Gere and Timoshenko, 1972). The rearranged Equations 6.9, 6.10, and 6.11 are

$$\varepsilon_x = \frac{1}{2}(\varepsilon_1 + \varepsilon_3 + \frac{\varepsilon_1 - \varepsilon_3}{\sqrt{1 + (\tan 2\theta_p)^2}}) \tag{6.12}$$

$$\varepsilon_y = \frac{1}{2}(\varepsilon_1 + \varepsilon_3 - \frac{\varepsilon_1 - \varepsilon_3}{\sqrt{1 + (\tan 2\theta_p)^2}}) \tag{6.13}$$

$$\gamma_{xy} = \tan 2\theta_p \left(\varepsilon_x - \varepsilon_y\right) \tag{6.14}$$

Knowing the major and minor principle of strains (ε_1 and ε_3) and the angle to the principal plane (θ_p), allows the strains in the x and y direction (ε_x and ε_y), and the shear strain in the xy plane (γ_{xy}) to be computed.

In a two-dimensional system, the normal strain in z direction (ε_z) is equal to zero. Therefore, Equation 6.6 can be simplified as

$$\varepsilon_f = \varepsilon_x l^2 + \varepsilon_y m^2 + \gamma_{xy} lm \tag{6.15}$$

In undrained triaxial tests, no volume change occurs and the axial strain (ε_a) is equal to triaxial shear strain (ε_q). The volumetric strain (ε_v) is

$$\varepsilon_v = -\frac{\delta V}{V} = 0 = \varepsilon_a + 2\varepsilon_r \tag{6.16}$$

in which ε_r is the radial strain. Therefore, the radial strain for the zero volume change of undrained tests is $\varepsilon_r = -\frac{\varepsilon_a}{2}$. The axial strain measured in the triaxial tests is known to be the major principal of strain (ε_1), and the radial strain is known to be the minor principal of strain (ε_3).

In the present work, the strain in a fiber with the arbitrary orientation is taken as the linear strain defined in Equations 6.5 & 6.15. For any given angle of a principal plane (θ_p), plug into Equation 6.12, 6.13, and 6.14, the normal strain in the x and y direction (ε_x and ε_y), and shear strain in the xy plane (γ_{xy}) can be computed. The value of l and m can be calculated by knowing the angle from the fiber orientation to relative principal axis. Finally, the fiber strain (ε_f) is computed by inserting all information into Equation 6.15.

The relationship between the fiber orientation relative to the principal plane (θ_f) and the angle to the principal axis (θ_p) is illustrated in Figure 6.2 as a two-dimensional system.

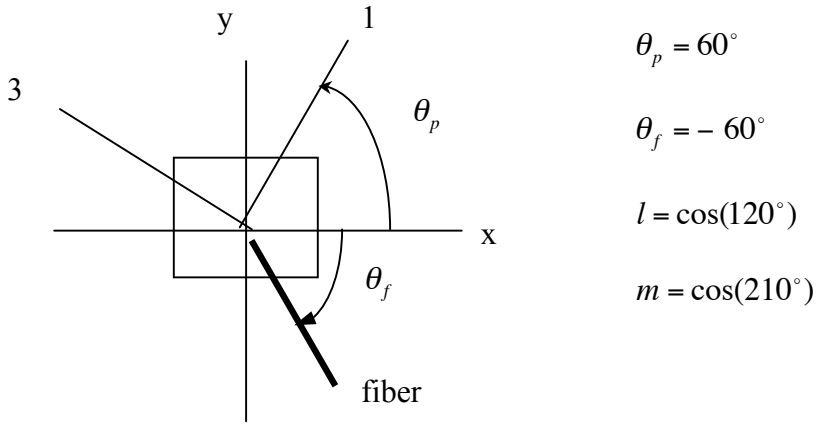

Figure 6.2 An example of the fiber angle (θ_f) in terms of transformation coordinate system of plain strain.

For given fiber orientation as illustrated in the figures, the linear strain in the fiber can be computed as follows. From the known angle to the principal axis (θ_p), fiber angle (θ_f),

and the measured axial and radial strain in the triaxial compression tests, the corresponding normal strains in the x and y direction (ε_x and ε_y), and the shear strain in the xy plane (γ_{xy}) can be computed from Equations 6.12, 6.13, and 6.14. For example, the fiber angle is equal to -60 degrees and the principal angle is equal to 60 degrees as shown in Figure 6.2. If the fiber orientation is fixed while the principal angle is rotated from -90 to 90 degrees, the predicted fiber strain can be plotted versus axial strain in the specimen, as shown in Figure 6.3. The ratio of predicted fiber strain to axial strain ($\varepsilon_f / \varepsilon_a$) can be observed in the figure. When the principal angles are 90, -60, and -90 degrees, the ratio equals to 0.625. For principal angles of 30, 0, and -30 degrees, the ratio becomes -0.125. Finally, if the principal angle is 60 degrees, the ratio is close to -0.5.

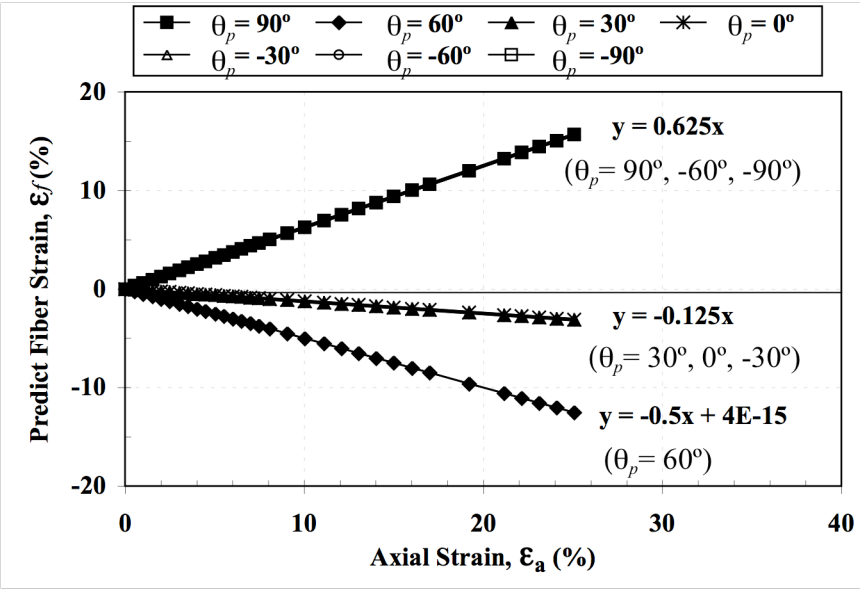

Figure 6.3 Predicted fiber strain versus axial strain for fiber angle equal to -60 degrees and the angle to the principal axis from 90 to -90 degrees.

To investigate the relationship between the measured axial strain in a triaxial compression test and the fiber strain for different fiber orientations, the calculation was extended by varying the angle to the principal plane (θ_p) from -90 to 90 degrees as the fiber angle is varied from -90 to 90 degrees. The results are plotted in Figure 6.4 As seen in the figure, the ratio of predicted fiber strain to axial strain is not unique. At any given angle to the principal planes, the ratio changes with the orientation of fiber angle. The ratios of predicted fiber strain to axial strain have values between -0.5 and 1.0. In all cases, but vary with orientation of fibers.

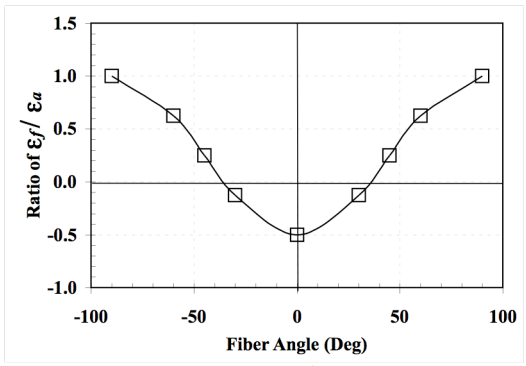

a) Principal angle, θ_p = 90 degree

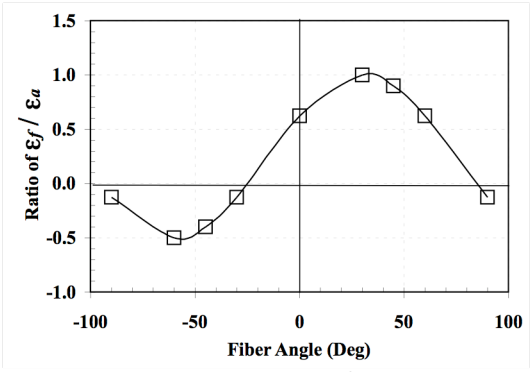

b) Principal angle, θ_p = 60 degree

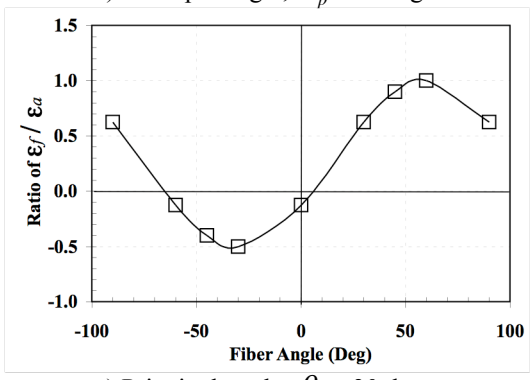

c) Principal angle, θ_p = 30 degree

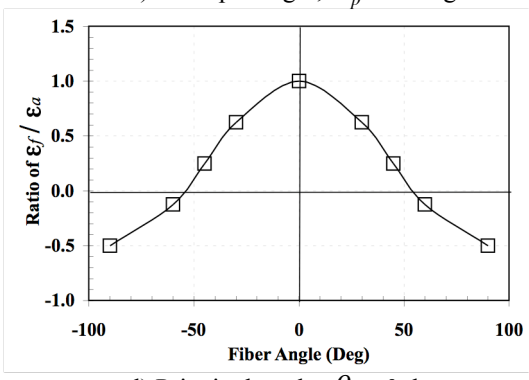

d) Principal angle, θ_p = 0 degree

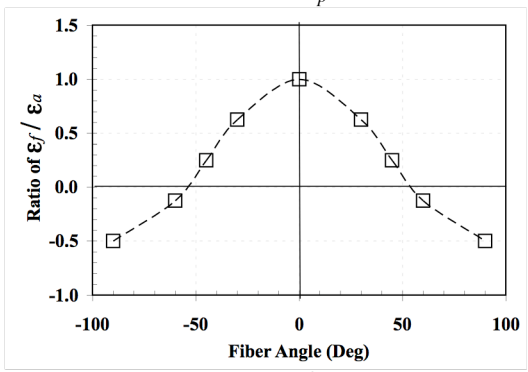

c) Principal angle, θ_p = -30 degree

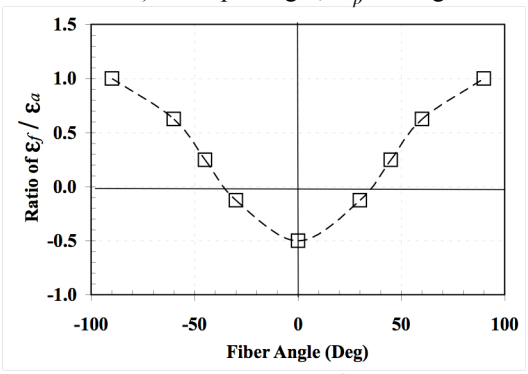

f) Principal angle, θ_p = -60 degree

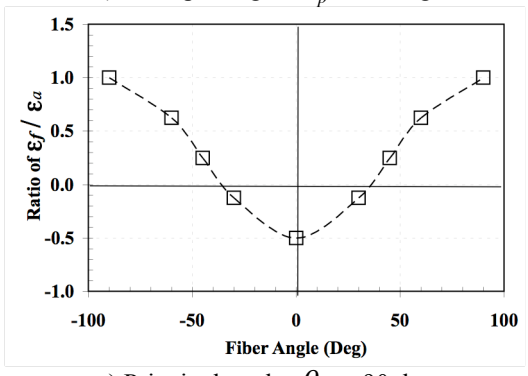

g) Principal angle, θ_p = -90 degree

Figure 6.4 Ratio of $\varepsilon_f / \varepsilon_a$ versus the fiber angle (θ_f) in undrained tests when the angle to the principal axis (θ_p) rotates from 90 degree to -90 degrees.

In general, the fibers in fiber-reinforced soils are assumed to be randomly oriented so that fibers are oriented in all directions. However, an "average" relation between fiber strain and axial strain can be established by considering Figure 6.5, which shows the compute $\varepsilon_f / \varepsilon_a$ ratio for principal planes oriented at ±45 degrees. The results show symmetrical behavior with an average ratio $\varepsilon_f / \varepsilon_a$ of 0.25. Therefore, the axial strain in the fibers due to axial strain in a triaxial compression test is assumed to be equal to

$$\varepsilon_{f-a} = 0.25 \times \varepsilon_a \tag{6.17}$$

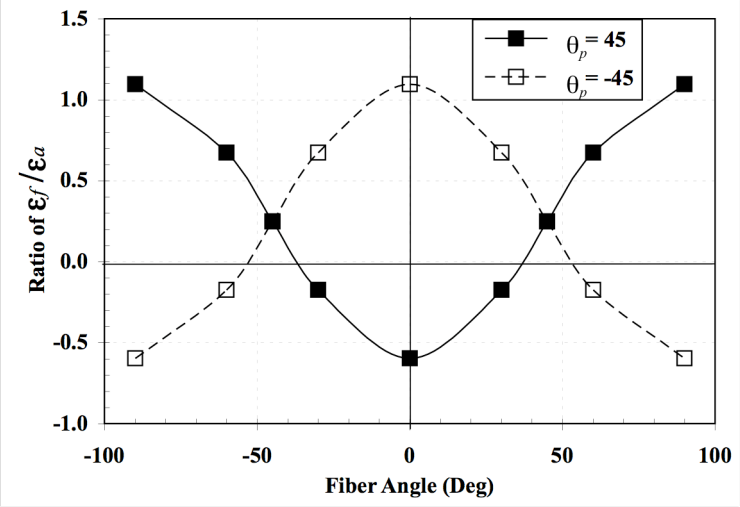

Figure 6.5 Ratio of $\varepsilon_f / \varepsilon_a$ versus the fiber angle (θ_f) in undrained tests when the angle to the principal axis equals to 45 and -45 degrees with fiber angles rotating from 90 to -90 degrees.

6.2.3 Relationship between fiber stain (ε_f) and volumetric strain (ε_v)

In drained triaxial tests, volume changes take place. As in Equation 6.16, the radial strain is

$$\varepsilon_r = \left(-\varepsilon_v + \varepsilon_a\right) \Big/ 2 \tag{6.18}$$

A set of calculations was performed similar to those shown in Figure 6.2 to predict the ratio of predicted fiber strain to volumetric strain ($\varepsilon_f \Big/ \varepsilon_v$). The results for the assigned fiber angle when the angles to the principal axis are rotated from -90 to 90 degrees are shown in Figure 6.6. To explore the relationship between the measured volumetric strain and the fiber strain, the calculation was expanded by assuming that the principal angle would rotate from -90 to 90 degrees as the fiber angle rotated from -90 to 90 degrees. The plotted results in Figure 6.6 show that the ratio of predicted fiber strain to volumetric strain is not unique. However, the curves are analogous in the figures show the ratios ranging from -3.3 to 5.7 as the angle to the principal axis are changed. It varies with the orientation of fibers in all cases.

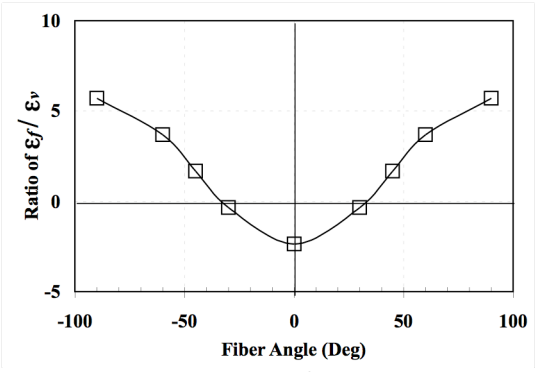

a) Principal angle, θ_p = 90 degree

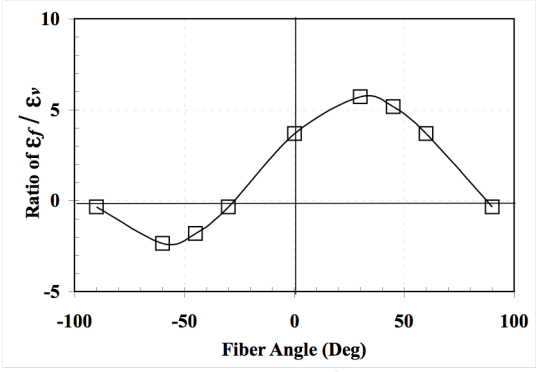

b) Principal angle, θ_p = 60 degree

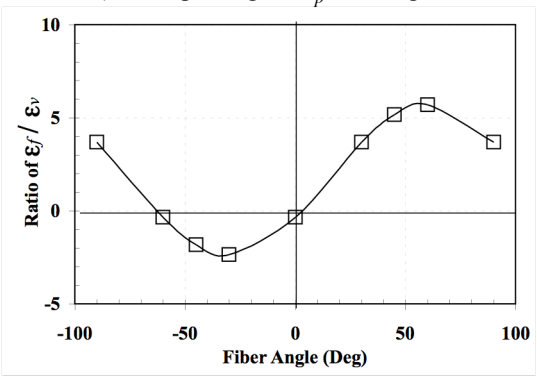

c) Principal angle, θ_p = 30 degree

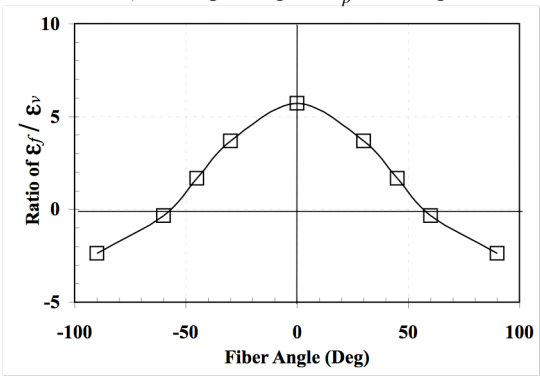

d) Principal angle, θ_p = 0 degree

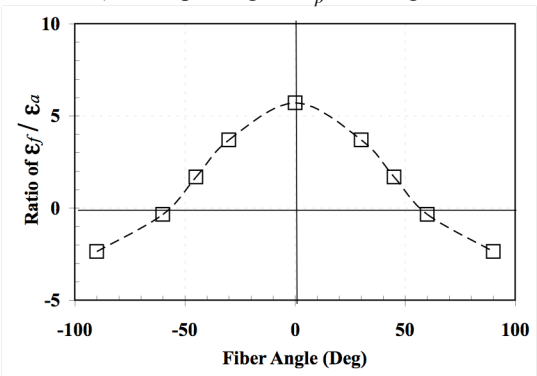

c) Principal angle, θ_p = -30 degree

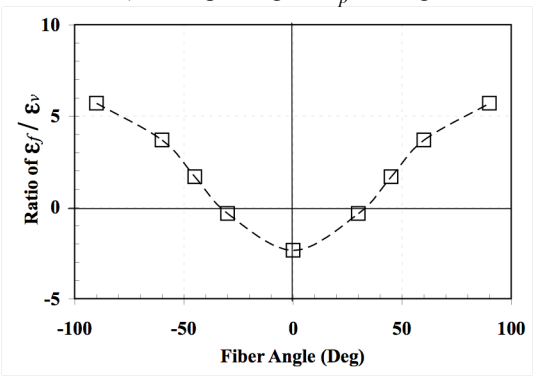

f) Principal angle, θ_p = -60 degree

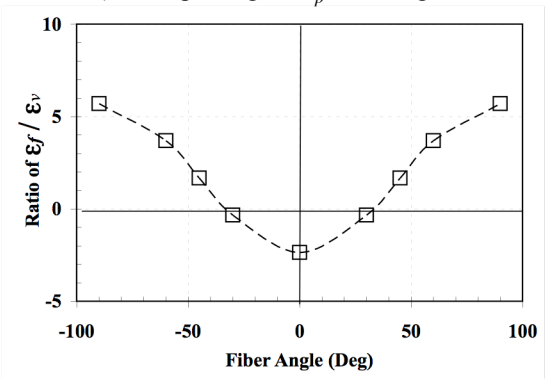

g) Principal angle, θ_p = -90 degree

Figure 6.6 Ratio of $\varepsilon_f / \varepsilon_v$ versus the fiber angle (θ_f) in undrained tests when the angle to the principal axis (θ_p) rotates from 90 to -90 degrees.

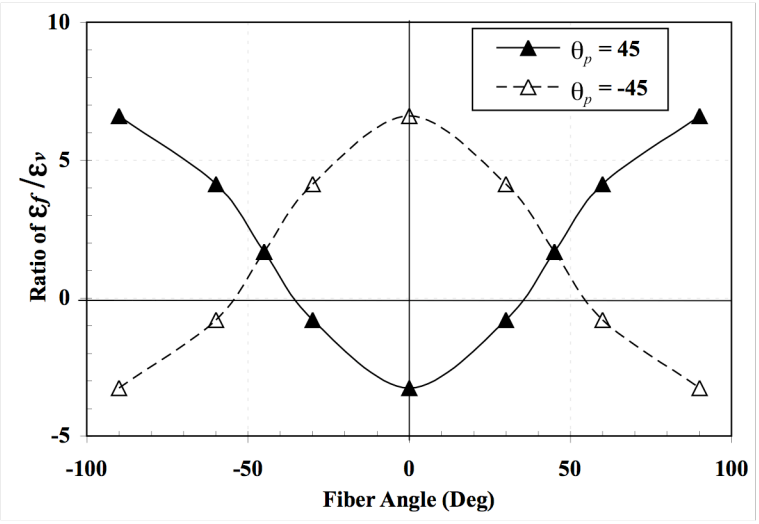

Figure 6.7 Ratio of $\varepsilon_f / \varepsilon_v$ versus the fiber angle (θ_f) in drained tests when the angle to the principal axis equals 45 and -45 degrees.

Again, the "average" relation between fiber strain and volumetric strain can be established by considering Figure 6.7, which shows the compute $\varepsilon_f / \varepsilon_v$ ratio for principal planes oriented at ± 45 degrees. The results also exhibited show symmetrical behavior with an average ratio $\varepsilon_f / \varepsilon_v$ of 1.68. Therefore, the axial strain in the fibers attributed to volumetric strain is assumed to be equal to

$$\varepsilon_{f-v} = 1.68 \times \varepsilon_v \tag{6.19}$$

The total strain in the fibers (ε_t) is assumed to the sum of the strain in the fibers induced by axial strain and the strain in the fibers induced by volumetric strains:

$$\varepsilon_t = 0.25 \times \varepsilon_a + 1.68 \times \varepsilon_v \tag{6.20}$$

6.3 Constitutive Model for the Research

6.3.1 Stress-Strain Relationships of the Fiber-Reinforced Soils

Gray and Ohashi (1983) represented the increase in shear strength (ΔS) due to fiber

$$\Delta S = t_f(\sin\theta + \cos\theta \times \tan\phi) \tag{6.21}$$

in which t_f is the mobilized tensile stress of fibers per unit area of soil, and θ is the angle of shear distortion in which the fibers contribute a normal and shear stress to the specimen (Gray and Ohashi, 1983). A similar concept is utilized in this research, where the perpendicular component of resistance is taken to be, p_f (hydrostatic contribution of the fibers), and the parallel component of resistance is taken to be, q_f (deviatoric contribution of the fibers). Thus, $\Delta S = q_f + p_f \tan\phi$, where

$$p_f = t_f \times \cos\theta \tag{6.22}$$

$$q_f = t_f \times \sin\theta \tag{6.23}$$

In the model, θ is assumed to be equal to the triaxial shear strain (ε_q) of the unreinforced samples. Therefore, the angle of shear distortion is the independent variable and is known in the constitutive model. The hydrostatic and deviatoric contribution of the fibers can be predicted if the mobilized tensile stress of fibers (t_f) can be calculated. The basis for predicting t_f in the model is described in the following section.

6.3.2 Prediction of Fiber Stress (t_f)

Young's modulus of the fibers (E_f) is a known property of the reinforcing fibers, and the total axial strain in the fibers (ε_t) is computed from Equations 6.20. The total mobilized tensile stress developed in the fibers at the shear plane (σ_t) can be computed as

$$\sigma_t = E_f \times \varepsilon_t \tag{6.24}$$

The mobilized tensile stress of the fibers per unit area of the soil (t_f) can be defined as the product of the total mobilized tensile stress in the fibers at the shear plane, the volumetric fiber content (χ), and a fiber mobilization factor (f_{mob})

$$t_f = \sigma_t \times \chi \times f_{mob} = E_f \times \varepsilon_t \times \chi \times f_{mob} \tag{6.25}$$

in which the fiber mobilization factor, f_{mob}, is taken as a constant value of 0.1 in the present work based on empirical observation. The f_{mob} is used to account for the reduction in fiber strain due to relative slip between the fibers and the soil. Yielding is considered in terms of the simple comparison of the total mobilized tensile stress in the fibers, σ_t, to the yield stress of the fibers (ultimate tensile strength is equal to 45-ksi). If the computed σ_t exceeds the yield stress, σ_t is simply set to equal the yield stress of the fibers. From Equations 6.22, 6.23, and 6.25, a predicted hydrostatic contribution of fibers, p_{pf}, and a predicted deviatoric contribution of fibers, q_{pf}, can be computed as

$$p_{pf} = t_f \times \cos\theta + p_{f0} \tag{6.26}$$

$$q_{pf} = t_f \times \sin\theta + q_{f0} \tag{6.27}$$

Again, the θ is the angle of shear distortion that is assumed to be equal to the triaxial shear strain (ε_q) in the samples. The initial hydrostatic stress (p_{f0}) and the initial

deviatoric stress (q_{f0}), as discussed in Chapter 5, were interpreted from the results of testing both the unreinforced and reinforced specimens in the undrained and drained tests. The initial hydrostatic and deviatoric stresses due to the fibers were used to account for the compaction, extrusion, and consolidation process, so that the overall magnitude of the stresses in the fibers could be adequately included in the model.

According to the hypothesis, the predicted deviator stress of the fiber-reinforced soil (q_r) can be estimated as the sum of the deviatoric stress of the unreinforced soil (q_s) and the additional deviatoric stress provided by fibers (q_{pf}). As a result, the total deviatoric stress for the fiber-reinforced soil can be defined as

$$q_r = q_s + q_{pf} \tag{6.28}$$

Prediction of mean effective stresses for fiber-reinforced soil (p'_r) is similarly estimated as

$$p'_r = p'_s + p_{pf} \tag{6.29}$$

6.4 Prediction of Effective Stress Behavior for Fiber-Reinforced Soils

6.4.1 Pore-Pressure-Change Prediction

According to Wood (1990), the pore pressure change during undrained loading can be predicted as

$$\Delta u = \Delta p + a \times \Delta q \tag{6.30}$$

for saturated specimens. Applying this same concept to the predicted changes in pore pressure due to fibers,

$$\Delta u_{pf} = \Delta p_{pf} + a \times \Delta q_{pf} \tag{6.31}$$

in which Δp_{pf} is the predicted change in hydrostatic stress due to the fibers, a is a pore pressure parameter for the unreinforced soil, and Δq_{pf} is the predicted change in deviatoric stress due to fibers.

The pore pressure parameter, a, is an indication of the current slope of the undrained effective stress path. It is not a constant value, but it depends on the current effective stress state in the soil. Therefore, it can be defined as

$$a = {-\Delta p'} \Big/ {\Delta q} \tag{6.32}$$

in which $\Delta p'$ is a change of mean effective stress, and Δq is a change of the deviatoric stress. For the current work, $\Delta p'$ and Δq are measured from unreinforced specimens sheared under undrained conditions. Again, based on the hypothesis, the predicted pore pressure change of the fiber-reinforced soil (Δu_p) can be computed as the sum of the pore

pressure change of the unreinforced soil (Δu_s) and the predicted pore pressure change provided by the fibers (Δu_f). This can be expressed as

$$\Delta u_p = \Delta u_s + \Delta u_{pf} \tag{6.33}$$

6.4.2 Volumetric-Strain Prediction

For isotropic elastic soil, the incremental change of volumetric strain is

$$\delta\varepsilon_v = \frac{1}{K}\delta p' \tag{6.34}$$

in which K is the bulk modulus of the soil, and $\delta p'$ is the incremental change of the mean effective stress (Wood, 1990). Based on the same concept, the change in volumetric strain due to the fibers ($\Delta\varepsilon_{vf}$) can be computed as

$$\Delta\varepsilon_{vf} = \frac{1}{K_f}\Delta p_{pf} \tag{6.35}$$

in which K_f is the bulk modulus of the fiber-reinforced soils, is calculated from the results of the isotropic consolidation test, and Δp_{pf} is the predicted change of hydrostatic stress due to the fibers. Finally, the total predicted volumetric strain (ε_p) of the fiber-reinforced specimen in drained loading can be expressed as

$$\varepsilon_p = \varepsilon_s + \Delta\varepsilon_{vf} \tag{6.36}$$

in which ε_s is the volumetric strain of the unreinforced specimen.

6.5 Behavior Predicted by Basic Model

The p_{pf} and q_{pf} can be predicted from the observed axial and volumetric strains in unreinforced specimens, the volumetric fiber content (χ), the shear distortion (θ), the initial hydrostatic and deviatoric stress due to the fibers (p_{f0} and q_{f0}), and Young's modulus for the fibers. The key assumptions in the basic model are: (1) the reductions in fiber strain due to the relative slip between the fibers and the soil is accounted for by applying f_{mob} with the assumption that it is a constant parameter, (2) yielding is considered in terms of the simple comparison of the average mobilized fiber stress, t_f, to the yield stress of the fibers (45-ksi), (3) shear distortion (θ) is equal to the triaxial shear strain (ε_q), (4) the total axial strain in the fibers (ε_t) is given by Equation 6.20, (5) the initial p_{f0} and q_{f0} were used to account for initial stresses induced during the compaction, extrusion, and consolidation process.

Figures 6.8 and 6.9 illustrate typical measured and predicted behavior for the fiber-reinforced silty sand and Ottawa sand specimens under undrained conditions. It can be seen that the basic model under estimates the shear stress at any given shear strain, especially for the Ottawa sand specimens. In addition, the predicted q_f versus ε_q curve (Figure 6.8d and 6.9d) shows a lower prediction than that of the observed behavior. The predicted Δu versus the ε_q behavior is in close agreement with the observed behavior up to large strains. However, the predicted p_f versus the ε_q curve (Figure 6.8e) for silty sand specimens increases with shear strains in contrast with the observed behavior. For Ottawa sand specimens, the predicted p_f was lower than the measured behavior as the

shear strains increased. Finally, the predicted stress paths from the basic model and observed stress paths for silty sand specimens closely matched for most tests, but the peak deviatoric stress was lower than the observed behavior at large strains. The predicted stress path departs significantly from the observed behavior at small strains for Ottawa sand specimens. This is in agreement with predicted deviatoric stresses, because the predicted deviatoric stresses were significantly lower than the observed responses. Ottawa sand specimens compacted at loose and dense state behaved similarly.

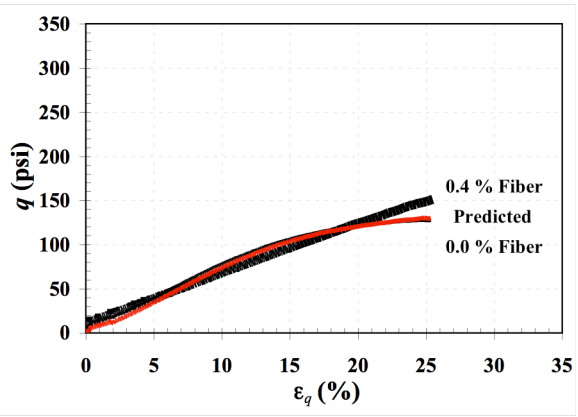

a) q versus ε_q

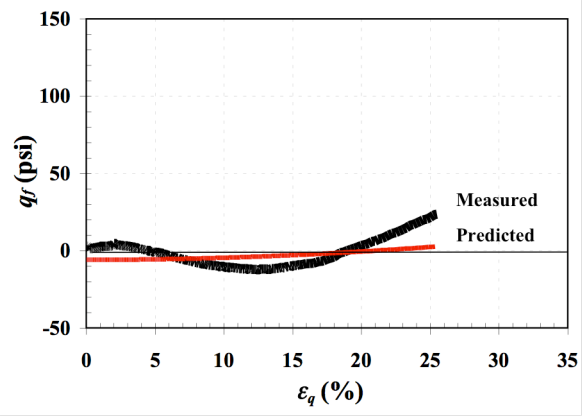

d) q_f versus ε_q

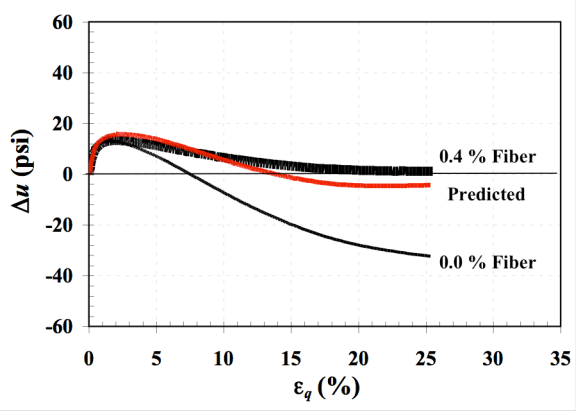

b) Δu versus ε_q

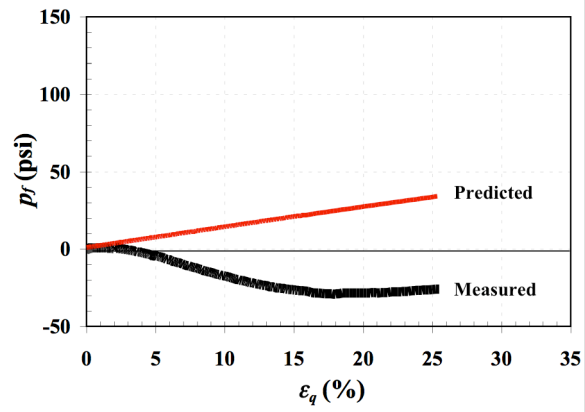

e) p_f versus ε_q

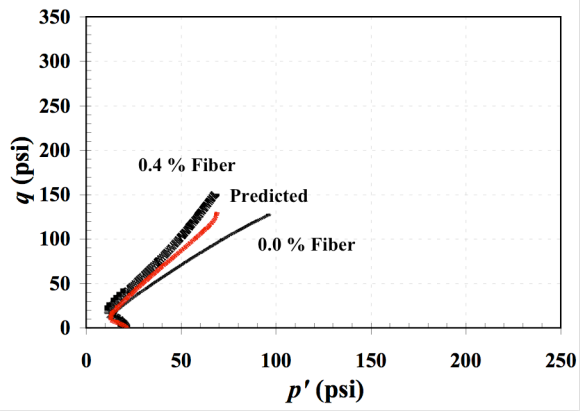

c) q versus p'

Figure 6.8 Measured and predicted behavior from the $\overline{CU}$ tests for silty sand specimens compacted at 18 percent water content, and consolidated to 20-psi effective stress: a) q versus ε_q, b) Δu versus ε_q, c) q versus p', d) q_f versus ε_q, and e) p_f versus ε_q.

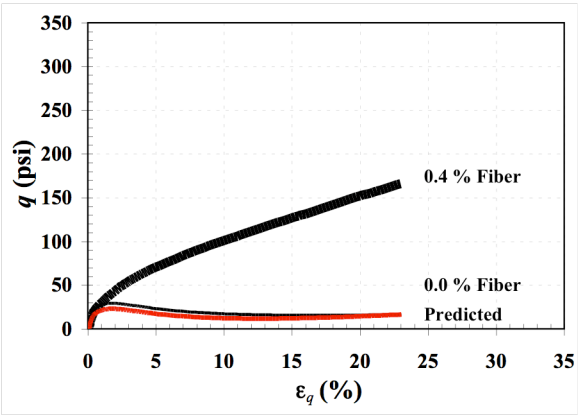

a) q versus ε_q

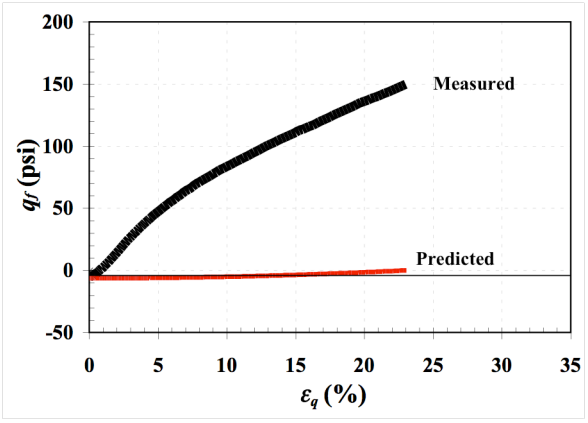

d) q_f versus ε_q

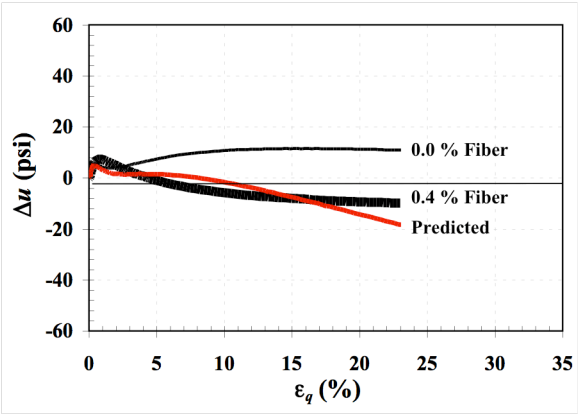

b) Δu versus ε_q

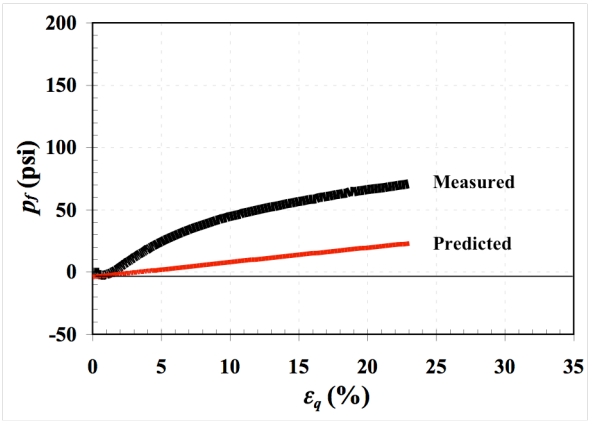

e) p_f versus ε_q

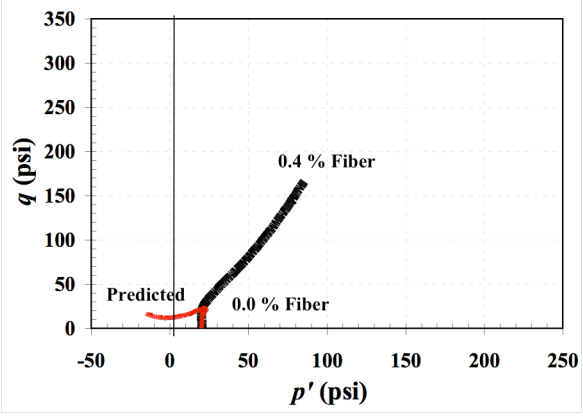

Figure 6.9 Measured and predicted behavior from the $\overline{CU}$ tests for Ottawa sand specimens compacted at a loose state and consolidated to 20-psi effective stress: a) q versus ε_q, b) Δu versus ε_q, c) q versus p', d) q_f versus ε_q, and e) p_f versus ε_q.

Typical measured and predicted behavior for the fiber-reinforced silty sand and Ottawa sand specimens tested under the CD conditions are illustrated in Figures 6.10 and 6.11, respectively. Note that the predicted q versus the ε_q behavior tends to under-predict the stress-strain response, particularly in small strains for both silty sand and Ottawa sand under drained conditions. Again, the predicted q_f versus the ε_q behavior is significantly lower than the observed responses for most of test. However, as seen in the $\overline{CU}$ tests, the predicted ε_p versus ε_q and predicted p_f versus ε_q behavior for the CD tests generally follows the same trend as the measured behavior up to high strains for both silty sand and Ottawa sand. Finally, the stress paths differ substantively due to the major underestimation of the predicted deviatoric stresses.

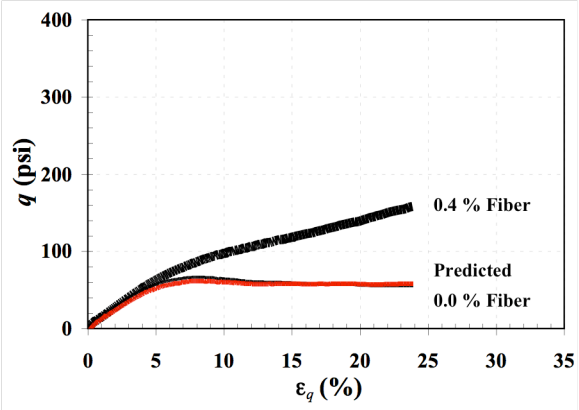

a) q versus ε_q

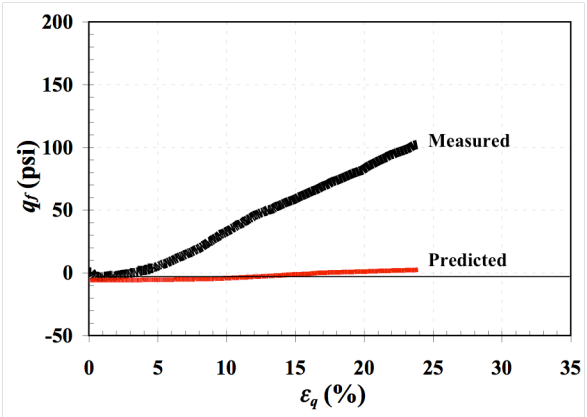

d) q_f versus ε_q

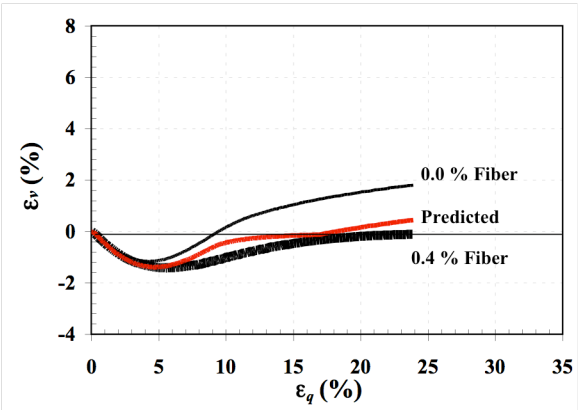

b) ε_v versus ε_q

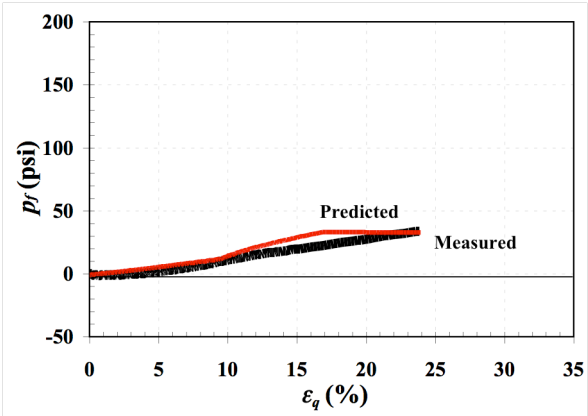

e) p_f versus ε_q

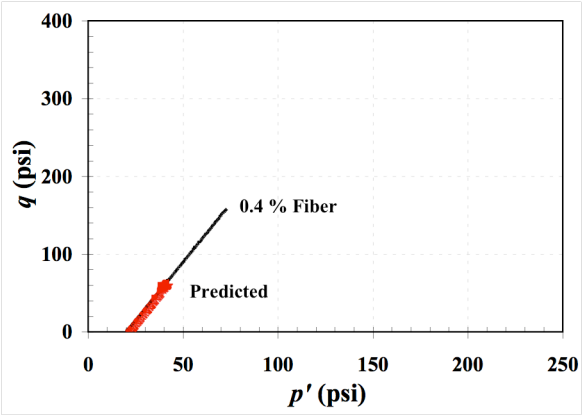

Figure 6.10 Measured and predicted behavior from the *CD* tests for silty sand specimens compacted at 18 percent water content, and consolidated to 20-psi effective stress: a) q versus ε_q, b) ε_v versus ε_q, c) q versus p', d) q_f versus ε_q, and e) p_f versus ε_q.

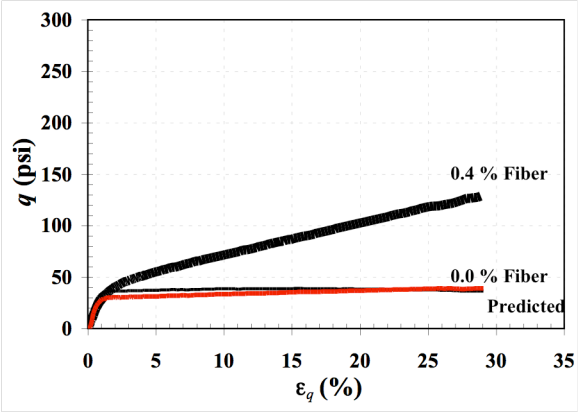

a) q versus ε_q

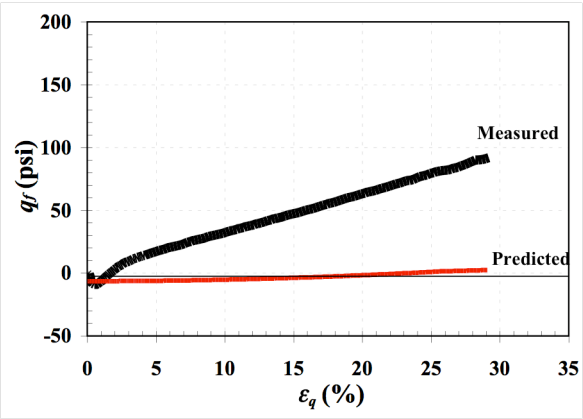

d) q_f versus ε_q

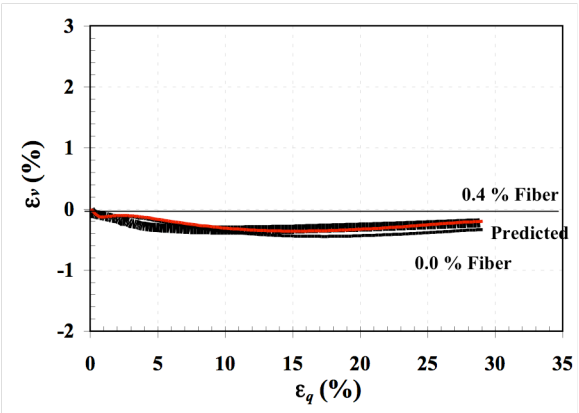

b) ε_v versus ε_q

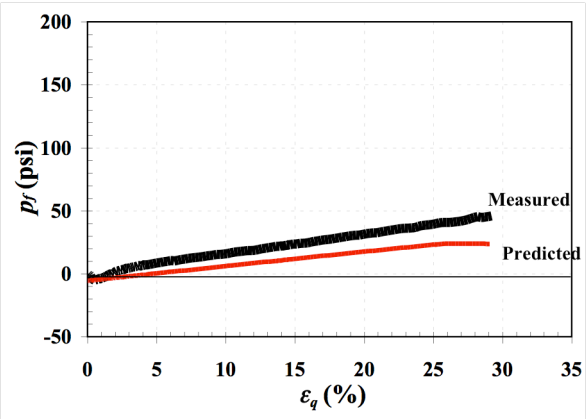

e) p_f versus ε_q

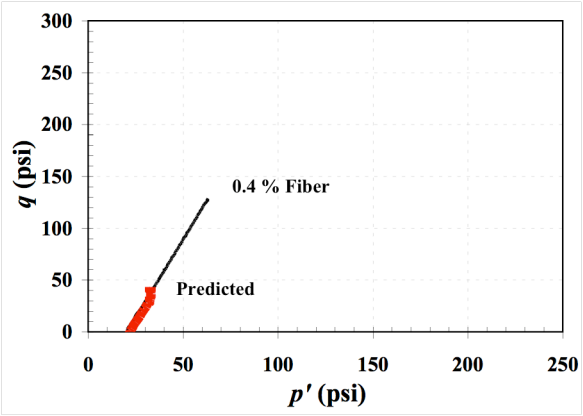

Figure 6.11 Measured and predicted behavior from the CD tests for Ottawa sand specimens prepared at a loose state and consolidated to 20-psi effective stress: a) q versus ε_q, b) ε_v versus ε_q, c) q versus p', d) q_f versus ε_q, and e) p_f versus ε_q.

The observed differences in predicted and observed behavior are due to the assumptions involved in the basic model, which include the perpendicular and parallel components ($\cos\theta$ and $\sin\theta$) of the mobilized fibers tensile stress (t_f), and the constant value of the fiber mobilization factor (f_{mob}). The basic model simply uses the perpendicular and parallel components to assign the mobilized tensile stress of fibers to the fibers hydrostatic and deviatoric contributions. Moreover, the fiber mobilization factor as a constant value does not take into consideration the changes with effective consolidation stress, the loading conditions, and the soil types. The basic model was therefore modified to account for these effects. Further investigation and discussion of the modifications is provided in the following section.

6.6 Modification and Calibration of the Basic Model

Two modifications were made to the basic model to account for the distribution functions of the mobilized tensile stress of fibers (t_f), the hydrostatic and deviatoric contribution of the fibers, and the fiber mobilization factor (f_{mob}).

6.6.1 New Distribution function of t_f

The predicted pore pressures and volumetric strains from the basic model had closely matched observed response for both silty sand and Ottawa sand. However, the predicted deviatoric contribution of fibers (q_f) under estimated the observed shear stress at any given shear strain for both silty sand and Ottawa sand reinforced specimens. For the predicted hydrostatic contribution of fibers (p_f), the basic model predicts that p_f increases with shear strains while observations showed decreases in hydrostatic stress for

silty sand specimens under undrained loading. The predicted hydrostatic contributions were lower than the measured response for the reinforced Ottawa sand specimens under both undrained and drained conditions.

One means to "correct" for these problems is to utilize different "distribution functions" (i.e. Equations 6.22 and 6.23) to relate the hydrostatic and deviatoric component of resistance to the nominal fiber stress. The approach used to search for distribution functions was to insert possible functions in the model calculation to more closely reproduce the behavior of the deviatoric and hydrostatic contribution of fibers. Many functions (i.e.: power, exponential, logarithmic, and polynomial) were considered and utilized in calculations to match the measured q_f and p_f versus ε_q behavior. The new distribution functions found to most closely reproduce observed behavior for silty sand, silty clay (Romero, 2003), and Ottawa sand are listed in Table 6.1. It was found that polynomial functions produced the best overall match of the observed load transfer results demonstrated in this study. Separate fiber distribution functions were developed for undrained and drained loading conditions. The new distribution functions for q_f are identical under both undrained and drained conditions and only vary with soil types (silty soil versus Ottawa sand). The new distribution functions for p_f vary along with the loading conditions for silty sand and silty clay, and have the same function under different loading conditions for Ottawa sand specimens.

Table 6.1 New Distribution Function for Mobilized Tensile Stress of Fibers (t_f) into Hydrostatic and Deviatoric Contribution of the Fibers for Testing Soils

Soil Types	Type of Triaxial Testing			
	$\overline{CU}$ Test		*CD* Test	
	Distribution Function for q_f	Distribution Function for p_f	Distribution Function for q_f	Distribution Function for p_f
Silty Sand	$0.2\,\varepsilon_q$	$-0.1\,\varepsilon_q+3$	$0.2\,\varepsilon_q$	$-0.001\,\varepsilon_q^2-0.01x+1$
Silty Clay	$0.2\,\varepsilon_q$	$-0.1\,\varepsilon_q+3$	$0.2\,\varepsilon_q$	$-0.001\,\varepsilon_q^2-0.01x+1$
Ottawa Sand	$0.1\,\varepsilon_q+7$	$-0.15\,\varepsilon_q+5$	$0.1\,\varepsilon_q+7$	$-0.15\,\varepsilon_q+5$

Figure 6.12 shows the new distribution functions for q_f and p_f for silty sand, silty clay and Ottawa sand under drained and undrained loading conditions as a function of triaxial shear strain in unreinforced samples. The distribution function q_f for silty sand and silty clay specimens exhibited increasing values as increasing the triaxial shear strains. In contrast, the distribution function for Ottawa sand showed slightly decreasing values at increasing the triaxial shear strains. As discussed in Chapter 3, the stress-strain behavior observed for silty soil fiber-reinforced specimens is a strain hardening type behavior with no noticeable peaks observed up to 30 percent strains for both $\overline{CU}$ and *CD* tests. However, the reinforced Ottawa sand specimens illustrated the peak strength yielded at large strains under undrained and drained conditions. The distribution function of p_f for silty sand, silty clay, and Ottawa sand specimens exhibited decreasing values the strains increased. Given these modifications, values of predicted p_f and q_f were computed as before from Equations 6.25 and 6.26 when replaced the $\cos\theta$ and $\sin\theta$ to the polynomial functions that shown in Table 6.1.

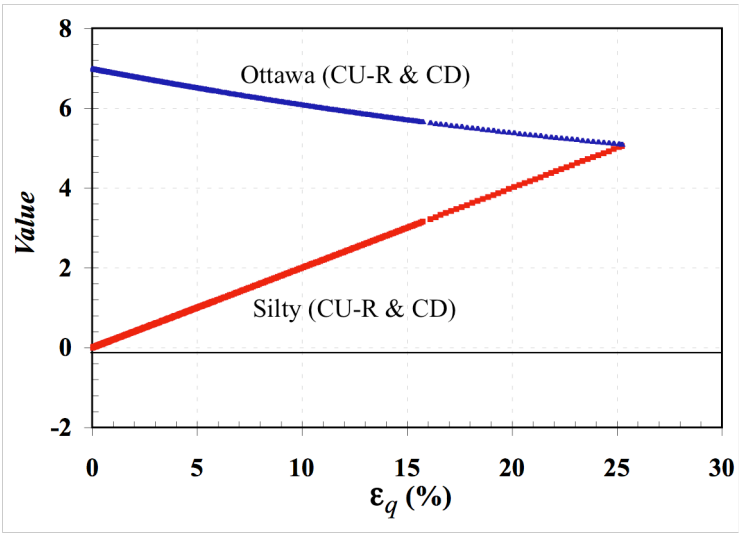

a) new distribution functions for q_f

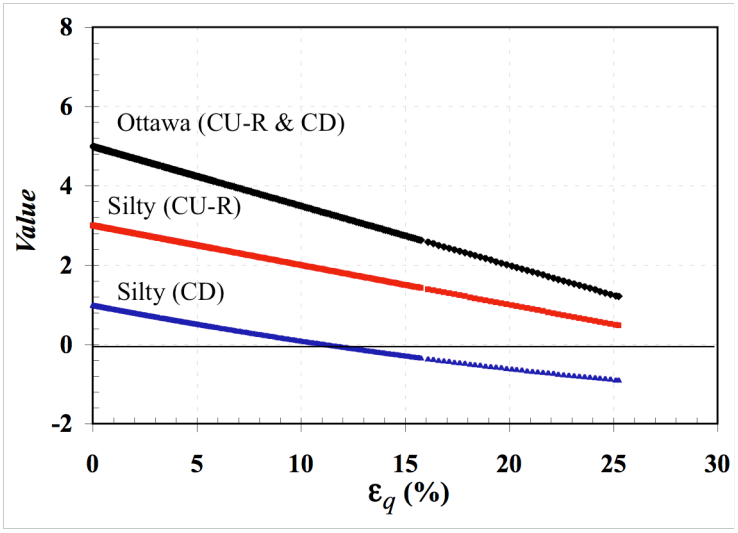

b) new distribution functions for p_f

Figure 6.12 New distribution functions for silty sand, silty clay, and Ottawa sand under drained and undrained loading conditions: a) for q_f, and b) for p_f.

6.6.2 New Fiber Mobilization Factor f_{mob}

Once the new distribution function for mobilized tensile stress of the fibers (t_f) were decided, the fiber mobilization factor (f_{mob}) were altered to identify an appropriate value. The resulting graphs were then analyzed after changing the values of f_{mob} in the mobilized tensile stress in the fibers from Equation 6.25. New mobilization factor versus the effective consolidation stress for silty sand, silt clay, and Ottawa sand specimens in both $\overline{CU}$ and CD tests are shown in Figure 6.13, which also reveals the best-fit results for measured behavior for the predicted p_f and q_f. The points plotted indicate that the new fiber mobilization factor (f_{mob}) is related to the effective consolidation stress (σ'_C), soil types, and shearing conditions. Overall, the modified f_{mob} increased as the effective confining stress increased in the fiber-reinforced soil tested in this study. The modified f_{mob} in the CD tests were generally greater than in the $\overline{CU}$ tests, except in Ottawa sand specimens. Comparisons of the predicted behavior and the observed response after implementing the modifications presented in this section are discussed in Chapters 7 and 8.

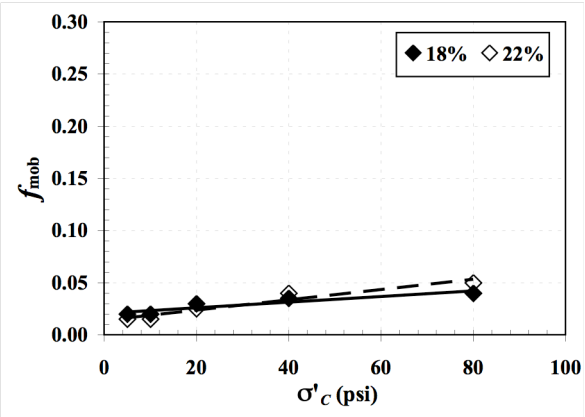

a) Silty sand (SM) in the $\overline{CU}$ tests

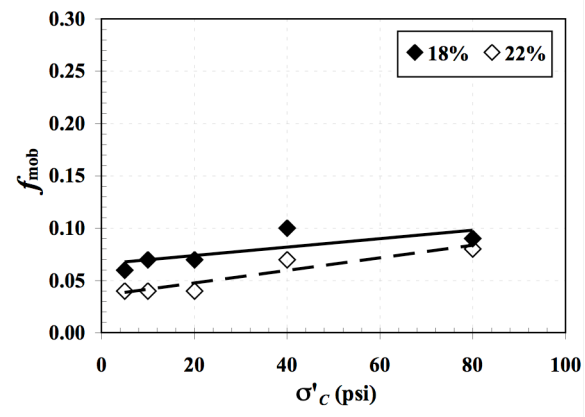

b) Silty sand (SM) in the CD tests

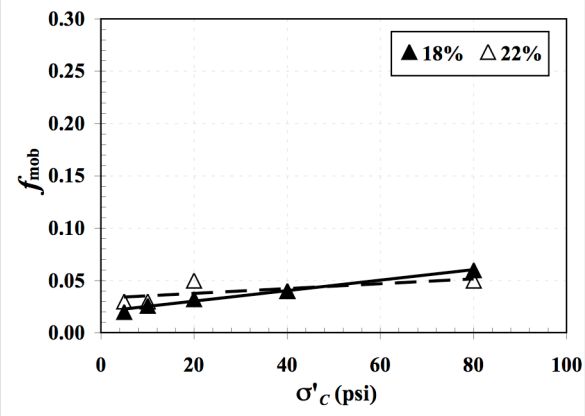

c) Silty clay (ML) in the $\overline{CU}$ tests

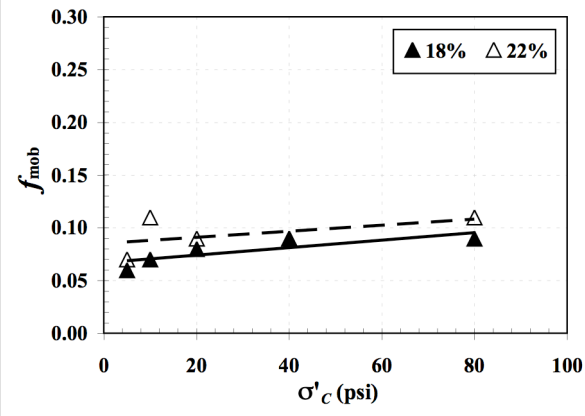

d) Silty sand (SM) in the CD tests

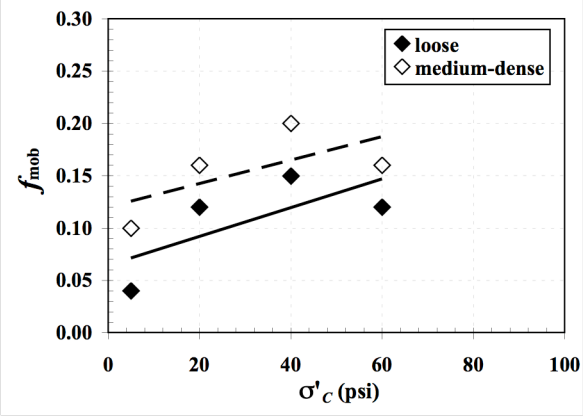

e) Ottawa sand in the $\overline{CU}$ tests

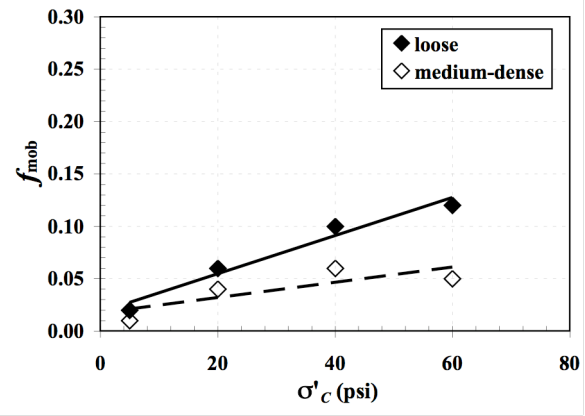

f) Ottawa sand in the CD tests

Figure 6.13 New fiber mobilization factor (f_{mob}) versus the effective consolidation stress (σ'_C) for: a) silty sand in the $\overline{CU}$ tests, b) silty sand in the CD tests, c) silty clay in the $\overline{CU}$ tests, d) silty clay in the CD tests, e) Ottawa sand in the $\overline{CU}$ tests, and f) Ottawa sand in the CD tests.

6.7 Summary

A constitutive model was proposed to predict the contributions of the reinforcing fibers in relation to the behavior of fiber-reinforced silty sand, silty clay, and Ottawa sand. In the model, the hydrostatic and deviatoric contribution of fibers is predicted from the axial and volumetric strain of unreinforced specimens, volumetric fiber content (χ), and the initial hydrostatic and deviatoric stresses of fibers (p_{f0} and q_{f0}). The key assumptions in the model include: (1) fibers are uniformly distributed in the specimens. (2) f_{mob} accounts for the reductions in fiber strain due to relative slip between the fibers and the soil, and varies with effective consolidation stress, soil types, and loading conditions, (3) yielding is considered by a simple comparison of the average mobilized fiber stress, t_f, to the yield stress of the fibers (45-ksi), (4) shear distortion (θ) is equal to triaxial shear strain (ε_q), (5) the total axial strain in the fibers (ε_t) is equal to 0.25 times the axial strain plus 1.68 times volumetric strain from tests on unreinforced specimens, and (6) the initial p_{f0} and q_{f0} are used to account for the compaction, extrusion, and consolidation process. The model parameters include fiber content (χ), Young's modulus of the fibers (E_f), initial stresses in the fibers (p_{f0} and q_{f0}), and the fiber mobilizations factor (f_{mob}). The parameters χ and E_f are known, and the remaining parameters along with distribution functions must be determined and interpreted from the results of tests on fiber-reinforced specimens.

CHAPTER 7: COMPARISON OF OBSERVED AND PREDICTED BEHAVIOR IN UNDRAINED ($\overline{CU}$) TRIAXIAL TESTS

7.1 Introduction

The constitutive model proposed to predict the effective stress-strain-pore pressure response of fiber-reinforced soil was introduced in Chapter 6. Here, the predicted behavior for the silty sand and Ottawa sand is compared to the observed responses previously described in Chapter 3.

7.2 Model Predictions

The model parameters used to predict the undrained behavior of the fiber-reinforced soil include the fiber content (χ), the Young's modulus of the fibers (E_f), the initial fiber stresses (p_{f0} and q_{f0}), the fiber mobilization factor (f_{mob}), and the pore pressure parameter (a). While the parameters χ and E_f were known, the remaining parameters were determined and interpreted from tests on fiber-reinforced specimens as described in Chapter 6.

p_{pf} and q_{pf} are predicted using the measured axial and volumetric strains from tests on replicable unreinforced specimens to produce p_f and q_f as a function of shear strain. This response is then added to the response of the unreinforced specimen to produce the predicted response of a fiber-reinforced specimen prepared and tested under similar conditions. This predicted response is then compared to the measured response of a fiber-reinforced specimen that was prepared and tested under similar conditions. The model itself predicts the contributions of the fibers alone, which must be added to

measured or predicted response due to the soil. This approach has advantage of isolating the response due to the fibers and eliminating the potential for compensating errors. However, it also has the disadvantage for comparisons like those presented here in that scatter in the response of the unreinforced soils, which is included along with scatter in the predicted response of the reinforced soils.

7.3 Comparison of Measured and Predicted Response from $\overline{CU}$ Tests for the Silty Sand Specimens

The predicted stress-strain-pore pressure change behavior of the fiber-reinforced silty sand is presented along with the observed undrained response of the reinforced specimens. The predicted deviatoric and hydrostatic contributions of the fibers are then compared to the measured responses. Finally, the stress paths of the predicted results are demonstrated in this section as well.

7.3.1 Comparison of Stress-Strain Response from the $\overline{CU}$ Tests

The measured and predicted deviatoric stresses versus the triaxial shear strains for all undrained triaxial tests for silty sand samples compacted at 18 and 22 percent water contents are shown in Figures 7.1 and 7.2. The model was generally capable of reproducing the deviatoric stress-strain response well for all effective consolidation stresses tested in this study, except for the specimens compacted at 22 percent water content and consolidated to stresses greater than 40-psi. In these cases, the predictions exceeded and tended to deviate from the measured behavior at large strains.

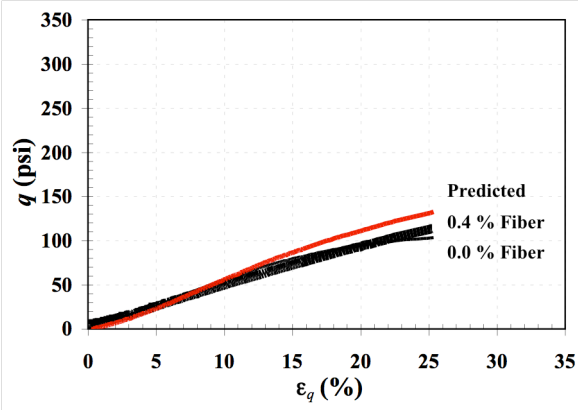

a) 5-psi effective consolidation stress

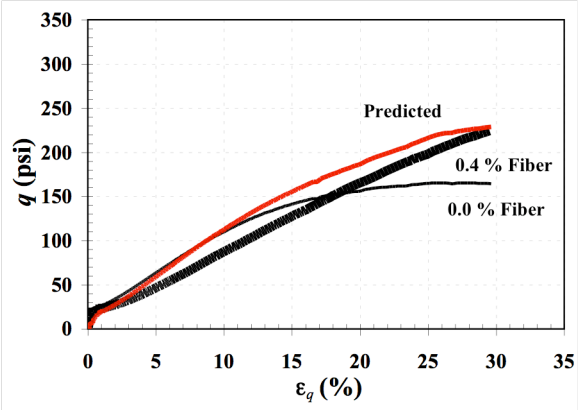

d) 40-psi effective consolidation stress

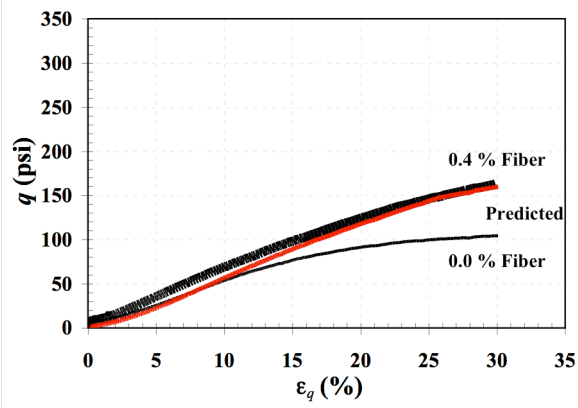

b) 10-psi effective consolidation stress

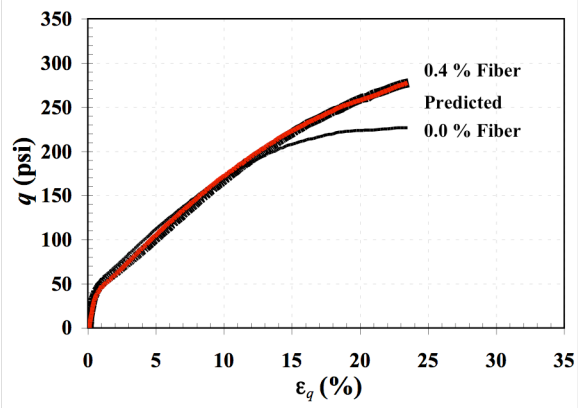

e) 80-psi effective consolidation stress

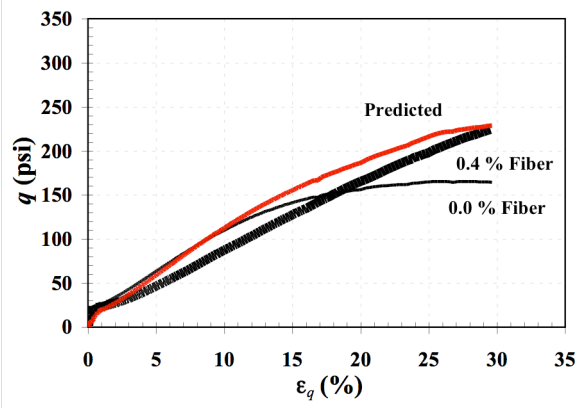

c) 20-psi effective consolidation stress

Figure 7.1 Measured and predicted q versus triaxial shear strain (ε_q) curves from the $\overline{CU}$ tests for silty sand specimens compacted at 18 percent water content and consolidated to: a) 5-psi effective stress, b) 10-psi effective stress, c) 20-psi effective stress, d) 40-psi effective stress, and e) 80-psi effective stress.

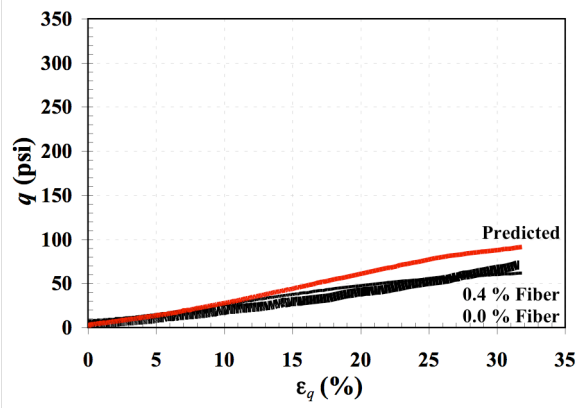

a) 5-psi effective consolidation stress

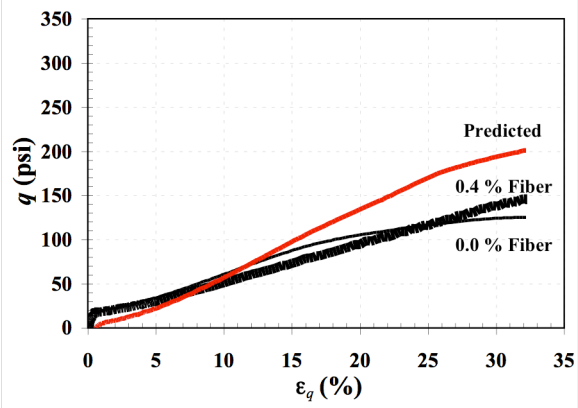

d) 40-psi effective consolidation stress

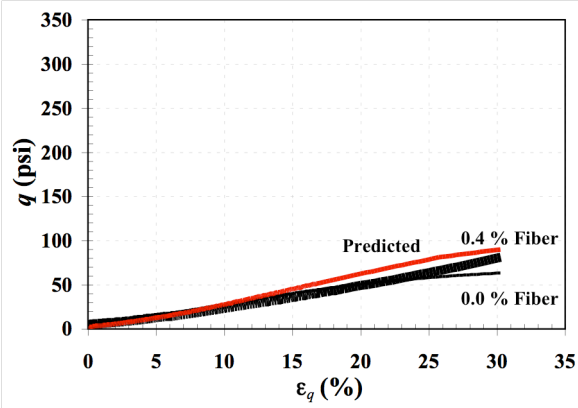

b) 10-psi effective consolidation stress

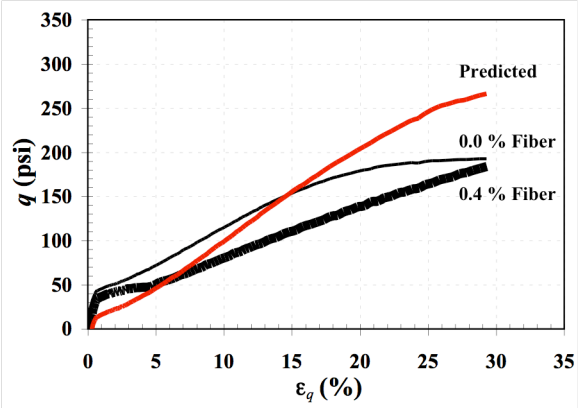

e) 80-psi effective consolidation stress

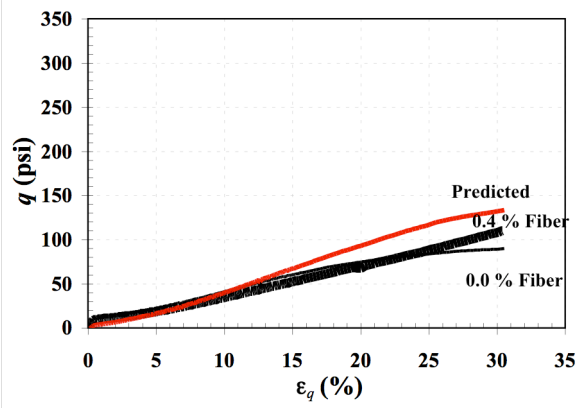

c) 20-psi effective consolidation stress

Figure 7.2 Measured and predicted q versus triaxial shear strain (ε_q) curves from the $\overline{CU}$ tests for silty sand specimens compacted at 22 percent water content and consolidated to: a) 5-psi effective stress, b) 10-psi effective stress, c) 20-psi effective stress, d) 40-psi effective stress, and e) 80-psi effective stress.

7.3.2 Comparison of Changing Pore Pressure Response from the $\overline{CU}$ Tests

Figures 7.3 and 7.4 show measured and predicted changes in pore pressure (Δu) versus the triaxial shear strain for silty sand specimens compacted at 18 and 22 percent water contents, respectively. Overall, the predicted behavior is in close agreement with the observed behavior up to large strains at all effective consolidation stresses tested in this study.

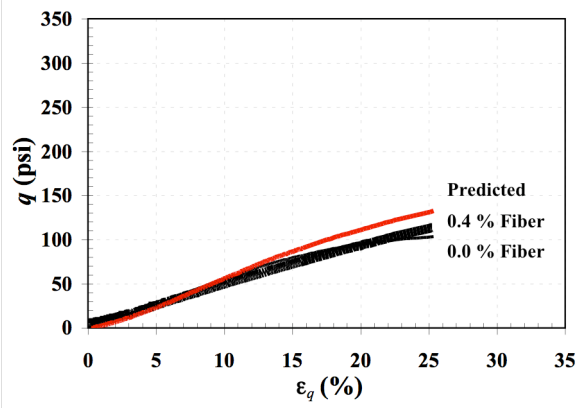

a) 5-psi effective consolidation stress

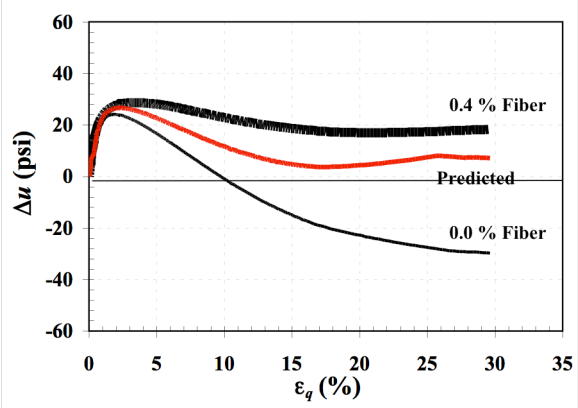

d) 40-psi effective consolidation stress

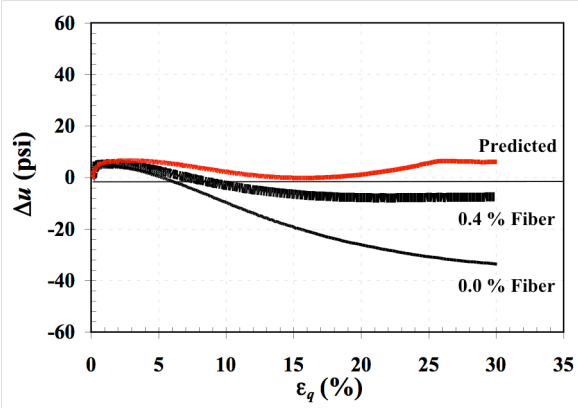

b) 10-psi effective consolidation stress

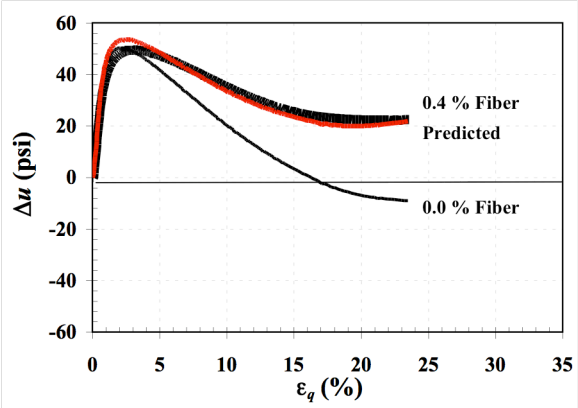

e) 80-psi effective consolidation stress

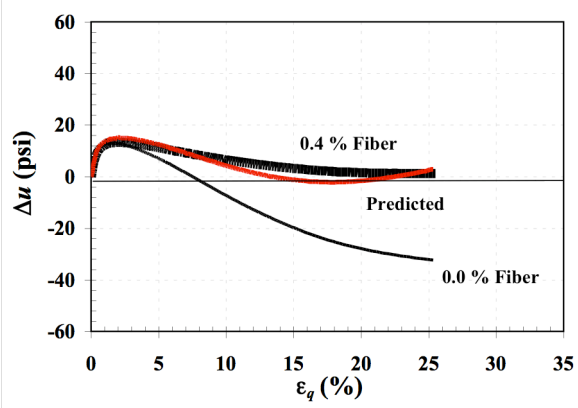

c) 20-psi effective consolidation stress

Figure 7.3 Measured and predicted Δu versus triaxial shear strain (ε_q) curves from the $\overline{CU}$ tests for silty sand specimens compacted at 18 percent water content and consolidated to: a) 5-psi effective stress, b) 10-psi effective stress, c) 20-psi effective stress, d) 40-psi effective stress, and e) 80-psi effective stress.

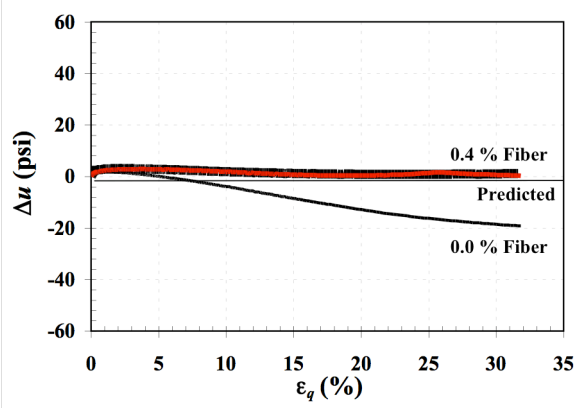

a) 5-psi effective consolidation stress

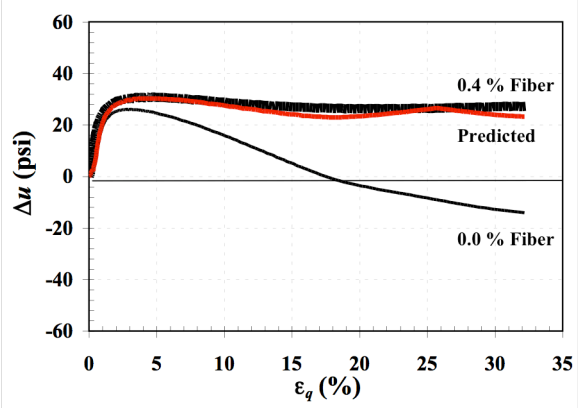

d) 40-psi effective consolidation stress

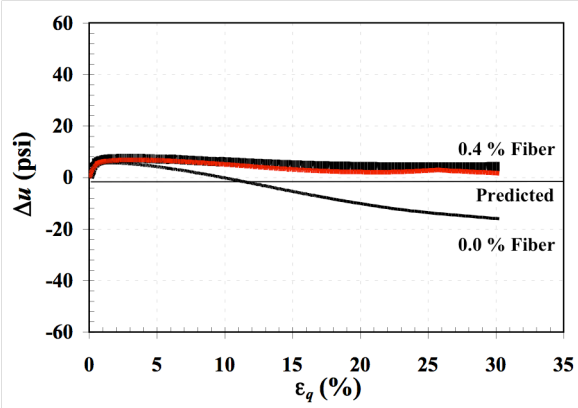

b) 10-psi effective consolidation stress

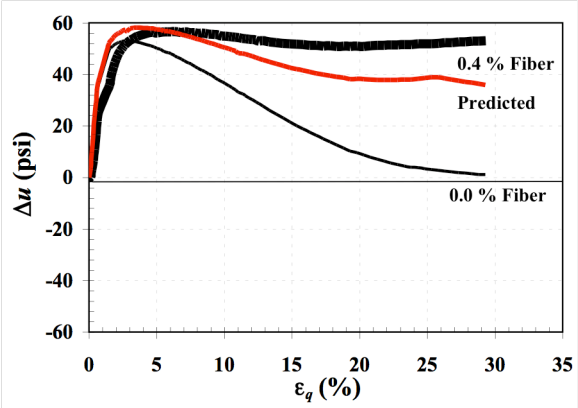

e) 80-psi effective consolidation stress

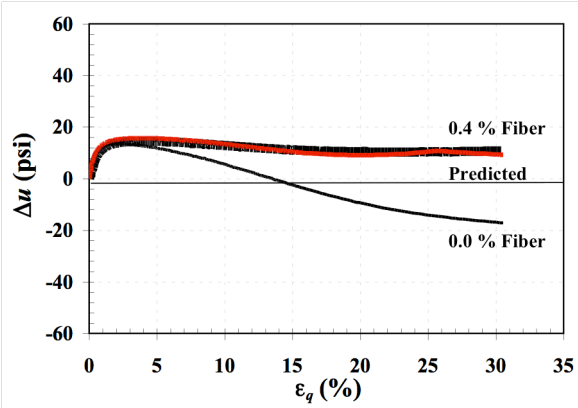

c) 20-psi effective consolidation stress

Figure 7.4 Measured and predicted Δu versus triaxial shear strain (ε_q) curves from the $\overline{CU}$ tests for silty sand specimens compacted at 22 percent water content and consolidated to: a) 5-psi effective stress, b) 10-psi effective stress, c) 20-psi effective stress, d) 40-psi effective stress, and e) 80-psi effective stress.

7.3.3 Comparison of Fiber Contributions for the $\overline{CU}$ Tests

The measured and predicted deviatoric contribution of fibers versus the triaxial shear strain from the $\overline{CU}$ tests are shown in Figures 7.5 and 7.6 for silty sand specimens compacted at 18 and 22 percent water contents, respectively. In general, the model slightly over-predicts the fiber deviatoric stress among all tested effective consolidation stresses, except for the specimens compacted at 22 percent water content and for consolidated stresses greater than 40-psi where the predicted values substantially exceeded the measured values. The difference between the measured and predicted fiber deviatoric stresses appears to be primarily due to the initial deviatoric contribution of fibers (q_{f0}) since the shapes of the predicted and measured responses are quite similar.

Figures 7.7 and 7.8 show the measured and predicted hydrostatic contribution of fibers versus the triaxial shear strain for the silty sand specimens. As before, in terms of the prediction of pore pressures, the model was capable of predicting the hydrostatic contributions of the fibers in close agreement with the observed behavior at moderate strains and tended to slightly deviate from the measured behavior at large strains.

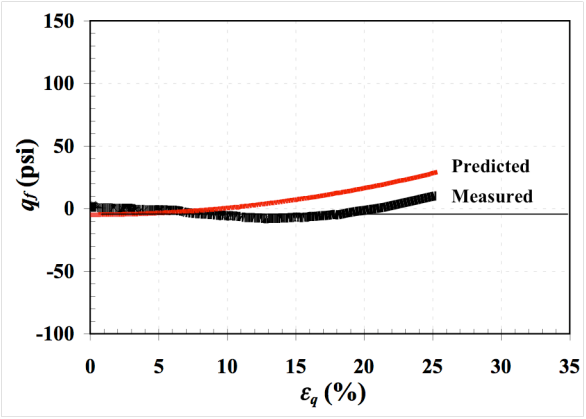

a) 5-psi effective consolidation stress

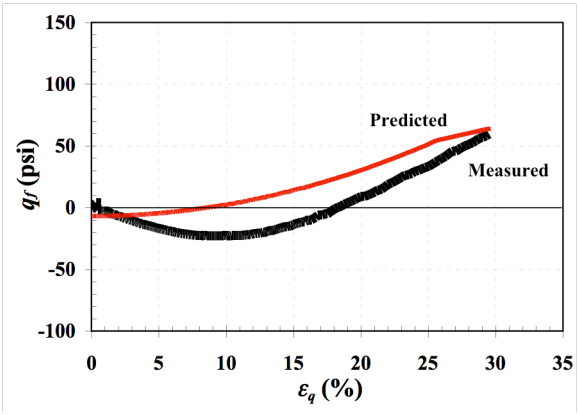

d) 40-psi effective consolidation stress

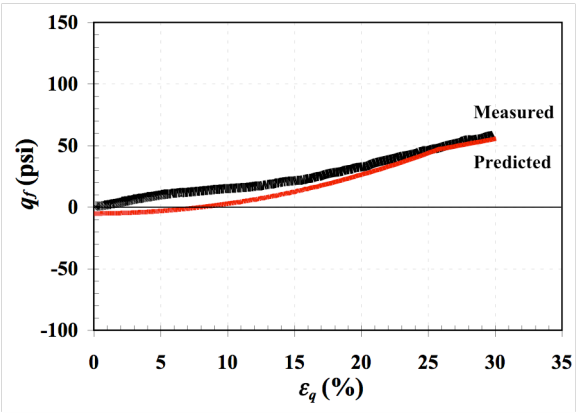

b) 10-psi effective consolidation stress

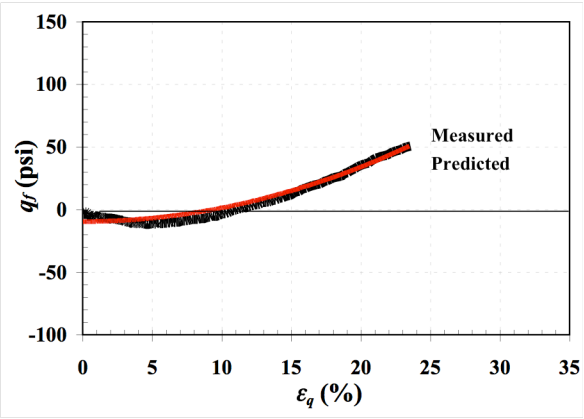

e) 80-psi effective consolidation stress

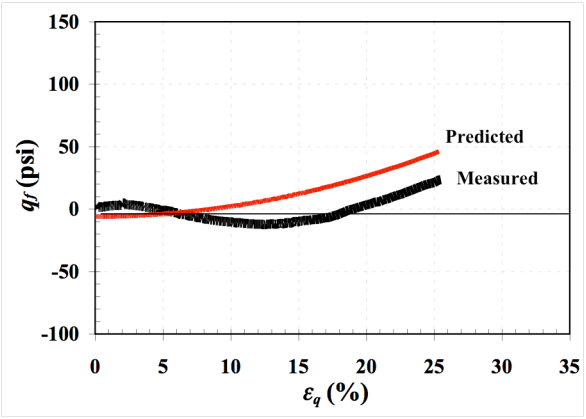

c) 20-psi effective consolidation stress

Figure 7.5 Measured and predicted deviatoric contribution of fibers (q_f) versus triaxial shear strain (ε_q) curves from the $\overline{CU}$ tests for silty sand specimens compacted at 18 percent water content and consolidated to: a) 5-psi effective stress, b) 10-psi effective stress, c) 20-psi effective stress, d) 40-psi effective stress, and e) 80-psi effective stress.

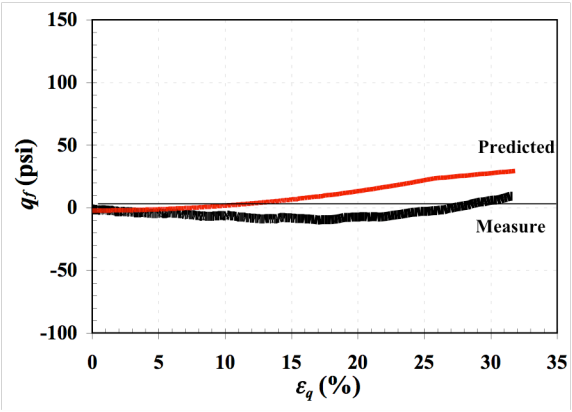

a) 5-psi effective consolidation stress

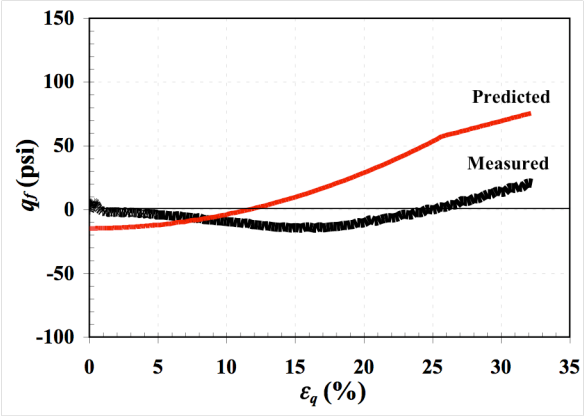

d) 40-psi effective consolidation stress

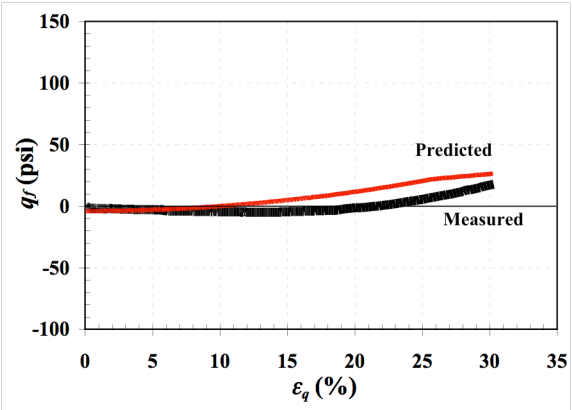

b) 10-psi effective consolidation stress

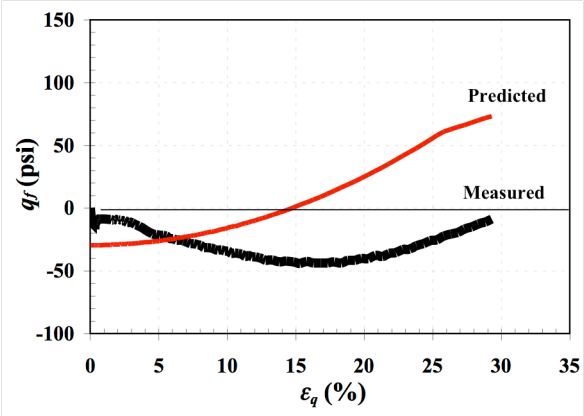

e) 80-psi effective consolidation stress

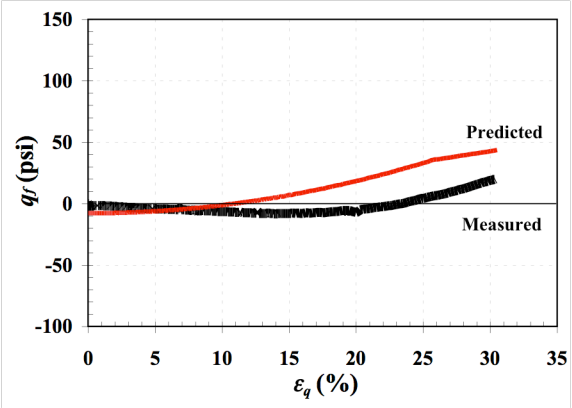

c) 20-psi effective consolidation stress

Figure 7.6 Measured and predicted deviatoric contribution of fibers (q_f) versus triaxial shear strain (ε_q) curves from the $\overline{CU}$ tests for silty sand specimens compacted at 22 percent water content and consolidated to: a) 5-psi effective stress, b) 10-psi effective stress, c) 20-psi effective stress, d) 40-psi effective stress, and e) 80-psi effective stress.

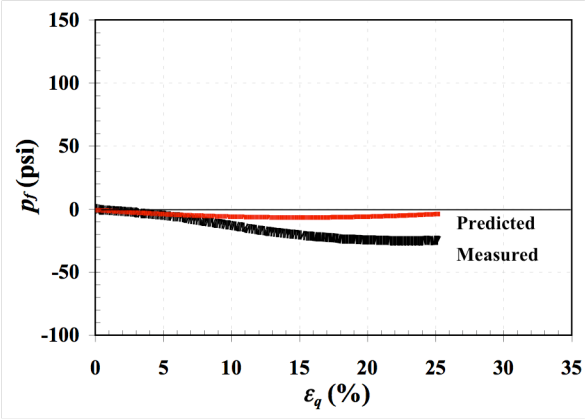

a) 5-psi effective consolidation stress

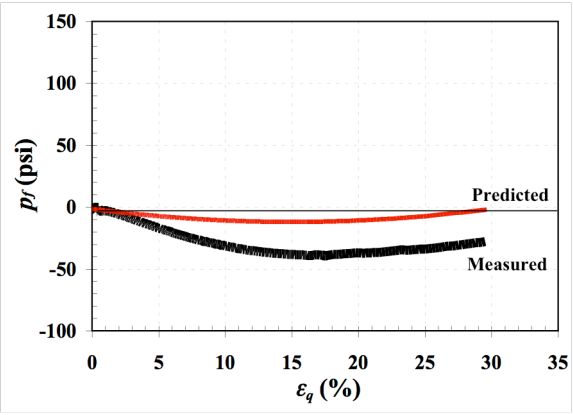

d) 40-psi effective consolidation stress

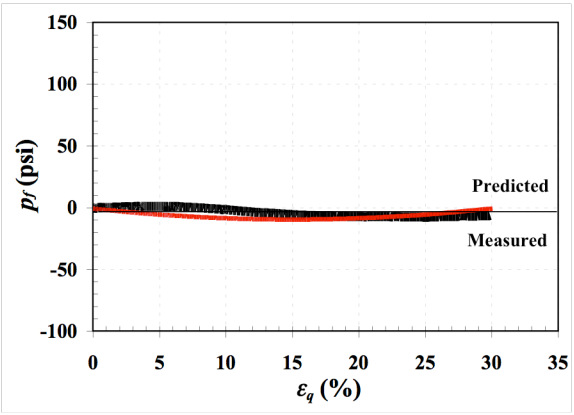

b) 10-psi effective consolidation stress

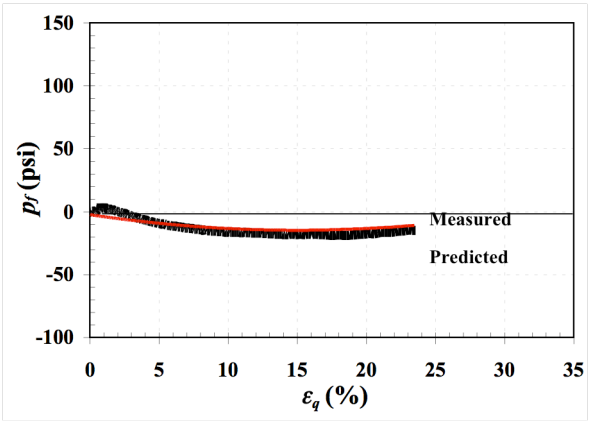

e) 80-psi effective consolidation stress

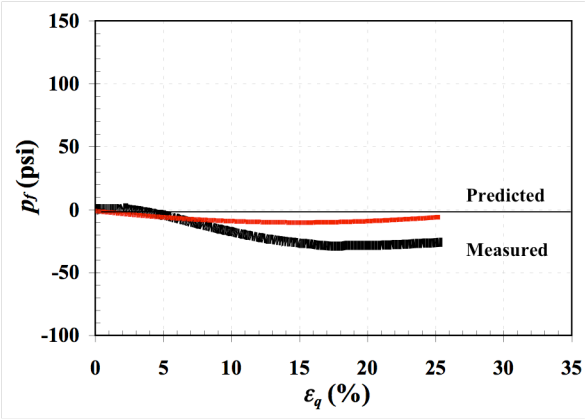

c) 20-psi effective consolidation stress

Figure 7.7 Measured and predicted hydrostatic contribution of fibers (p_f) versus triaxial shear strain (ε_q) curves from the $\overline{CU}$ tests for silty sand specimens compacted at 18 percent water content and consolidated to: a) 5-psi effective stress, b) 10-psi effective stress, c) 20-psi effective stress, d) 40-psi effective stress, and e) 80-psi effective stress.

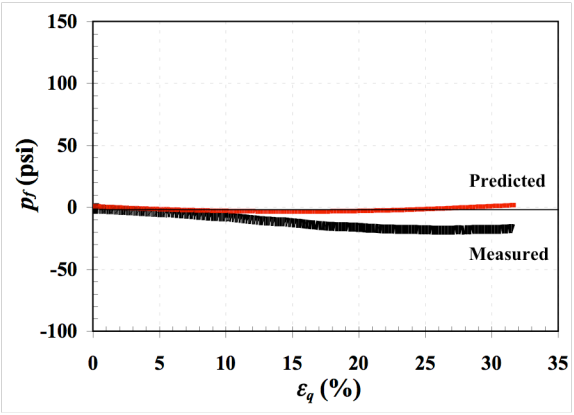

a) 5-psi effective consolidation stress

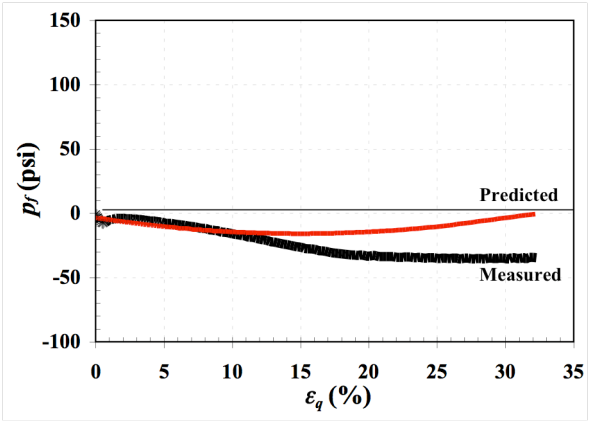

d) 40-psi effective consolidation stress

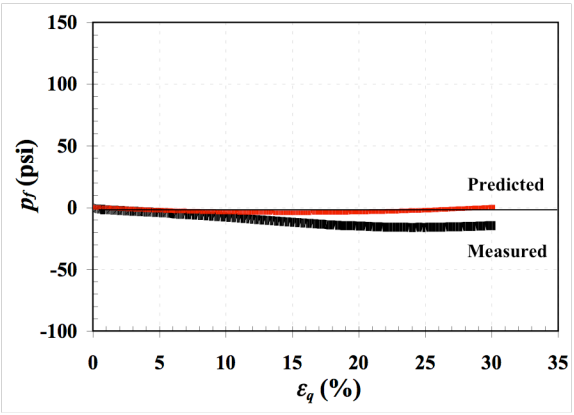

b) 10-psi effective consolidation stress

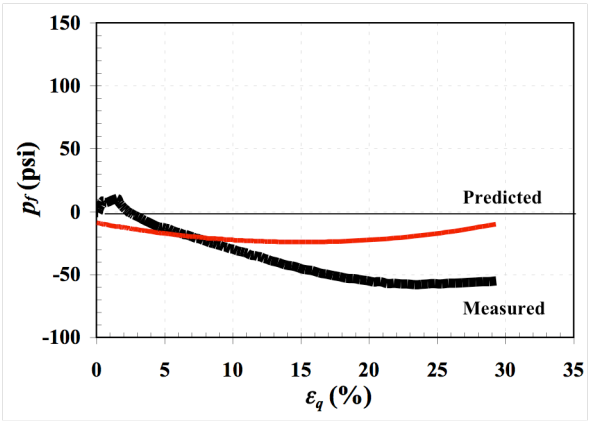

e) 80-psi effective consolidation stress

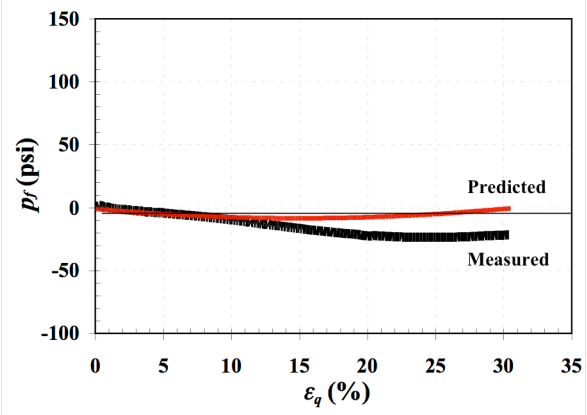

c) 20-psi effective consolidation stress

Figure 7.8 Measured and predicted hydrostatic contribution of fibers (p_f) versus triaxial shear strain (ε_q) curves from the $\overline{CU}$ tests for silty sand specimens compacted at 22 percent water content and consolidated to: a) 5-psi effective stress, b) 10-psi effective stress, c) 20-psi effective stress, d) 40-psi effective stress, and e) 80-psi effective stress.

7.3.4 Comparison of Stress Paths from $\overline{CU}$ Tests

The measured and predicted stress paths for the $\overline{CU}$ tests are shown in Figures 7.9 and 7.10 for the silty sand specimens compacted at 18 and 22 percent water contents, respectively. These figures reveal that the predicted stress paths match the measured stress paths reasonably well when consolidated collectively. In general, the predicted stress paths tend to lie on, or slightly below the measured stress paths for all comparisons.

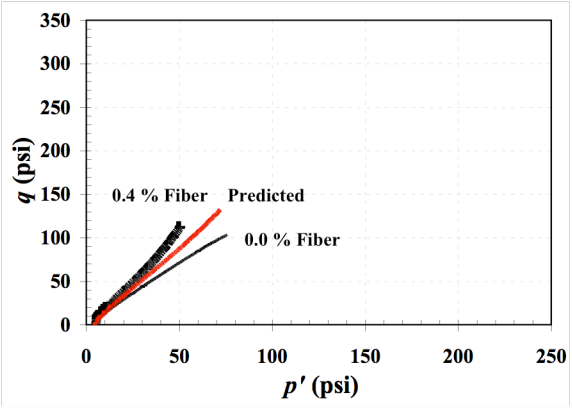

a) 5-psi effective consolidation stress

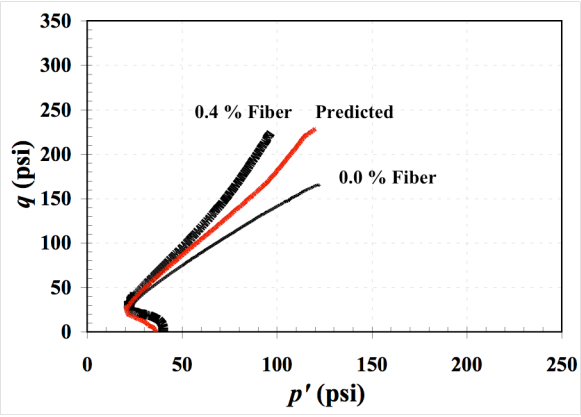

d) 40-psi effective consolidation stress

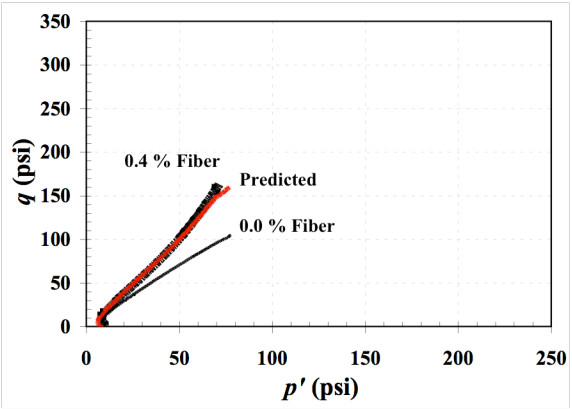

b) 10-psi effective consolidation stress

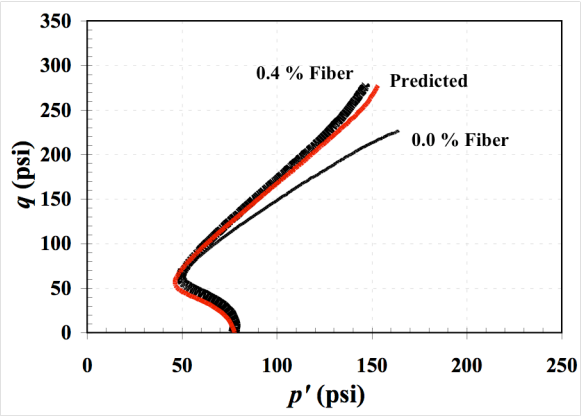

e) 80-psi effective consolidation stress

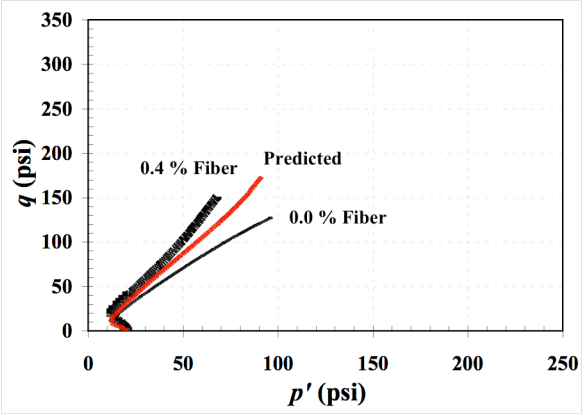

c) 20-psi effective consolidation stress

Figure 7.9 Measured and predicted stress paths from the $\overline{CU}$ tests for silty sand specimens compacted at 18 percent water content and consolidated to: a) 5-psi effective stress, b) 10-psi effective stress, c) 20-psi effective stress, d) 40-psi effective stress, and e) 80-psi effective stress.

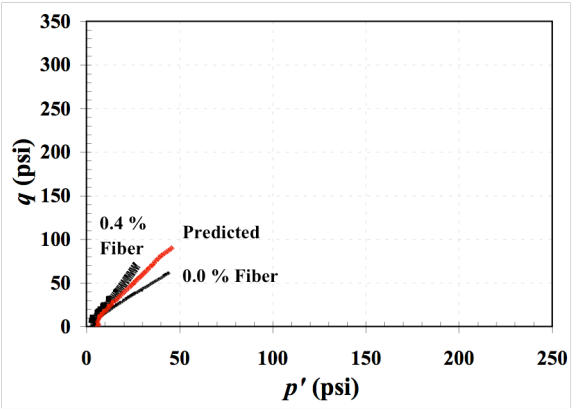

a) 5-psi effective consolidation stress

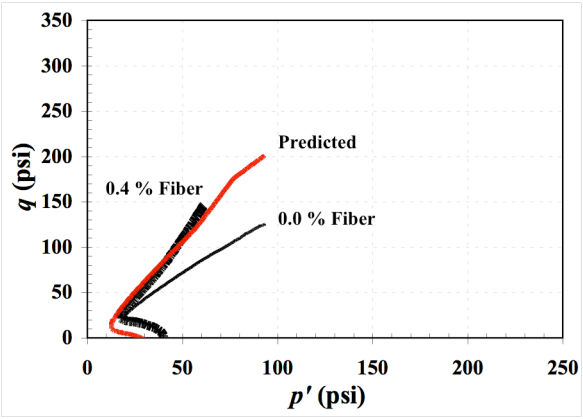

d) 40-psi effective consolidation stress

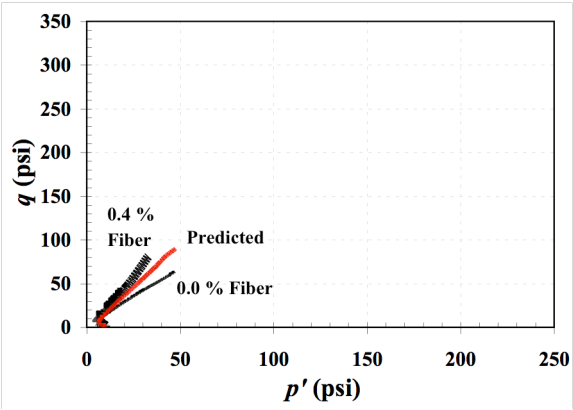

b) 10-psi effective consolidation stress

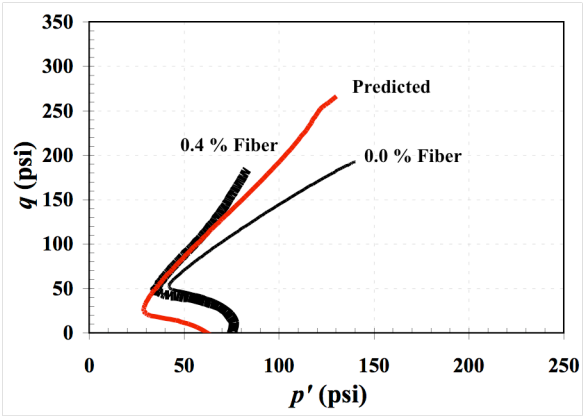

e) 80-psi effective consolidation stress

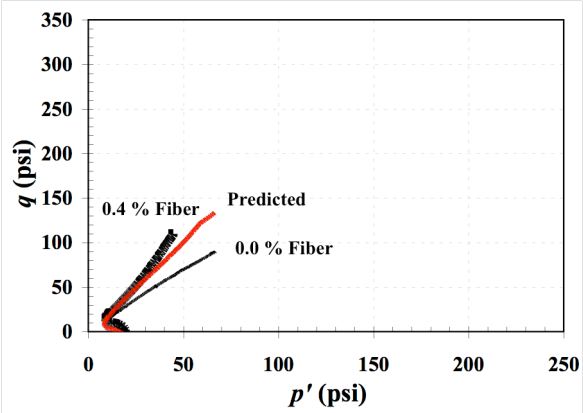

c) 20-psi effective consolidation stress

Figure 7.10 Measured and predicted stress paths from the $\overline{CU}$ tests for silty sand specimens compacted at 22 percent water content and consolidated to: a) 5-psi effective stress, b) 10-psi effective stress, c) 20-psi effective stress, d) 40-psi effective stress, and e) 80-psi effective stress.

7.4 Comparison of Measured and Predicted Response from $\overline{CU}$ Tests for Ottawa Sand Specimens

The constitutive model in this research was also used to predict the stress-strain-pore pressure change behavior of the fiber-reinforced Ottawa sand and the results were compared to the measured response for reinforced specimen from replicate undrained tests. The predicted deviatoric and hydrostatic contributions of the fibers are also presented. Finally, a comparison of the stress paths of the predicted results and the measured behavior are shown in this section.

7.4.1 Comparison of Stress-Strain Response from the $\overline{CU}$ Tests

Measured and predicted deviatoric stresses versus the triaxial shear strain for all undrained type triaxial tests for Ottawa sand samples compacted at both loose and medium-dense states are shown in Figures 7.11 and 7.12. As can be seen, the model was capable of closely reproducing the deviatoric stress for all Ottawa sand specimens compacted at loose and medium-dense states. The predictions do deviate from the measured response at large strains for the medium-dense specimens. This deviation is likely due to the model missing some failure mode (e.g. fiber pullout or fiber yield).

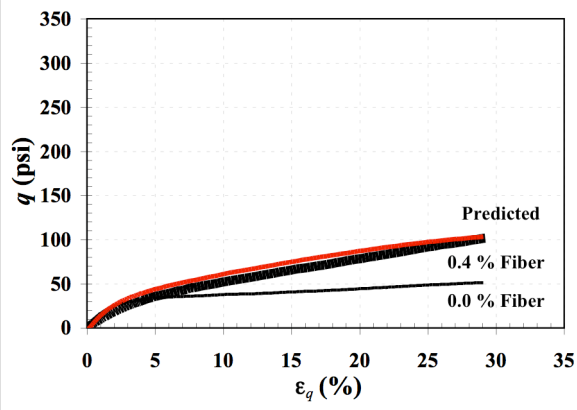

a) 5-psi effective consolidation stress

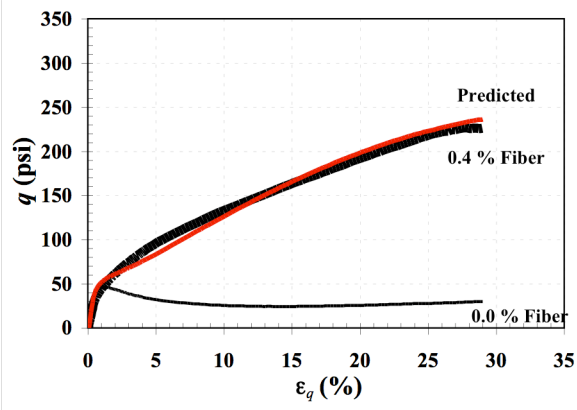

d) 40-psi effective consolidation stress

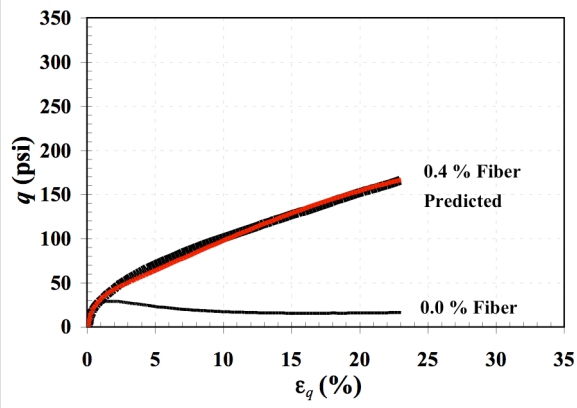

b) 20-psi effective consolidation stress

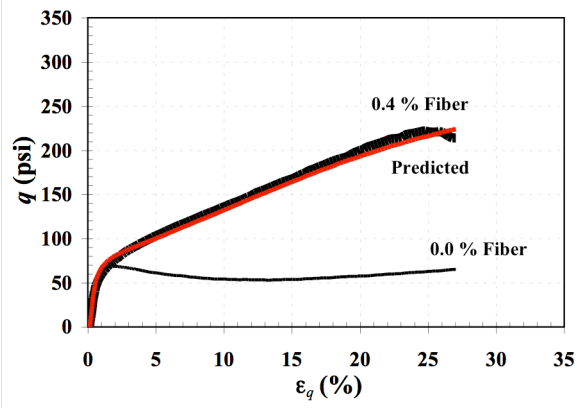

e) 60-psi effective consolidation stress

Figure 7.11 Measured and predicted q versus triaxial shear strain (ε_q) curves from the $\overline{CU}$ tests for Ottawa sand specimens compacted at a loose state and consolidated to: a) 5-psi effective stress, b) 20-psi effective stress, c) 40-psi effective stress, and d) 60-psi effective stress.

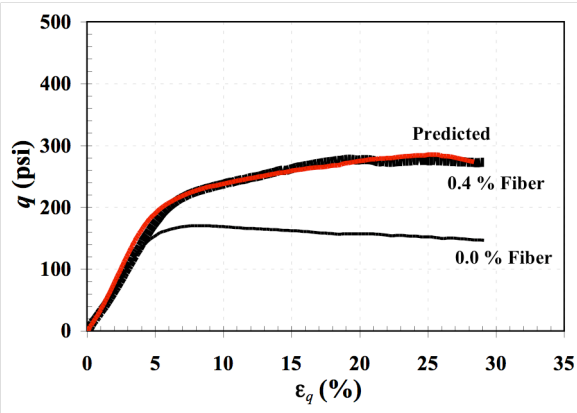

a) 5-psi effective consolidation stress

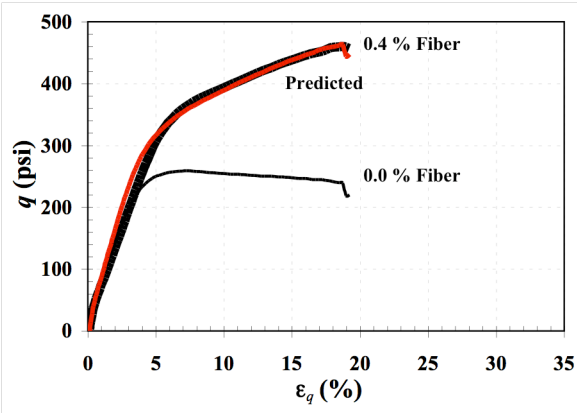

d) 40-psi effective consolidation stress

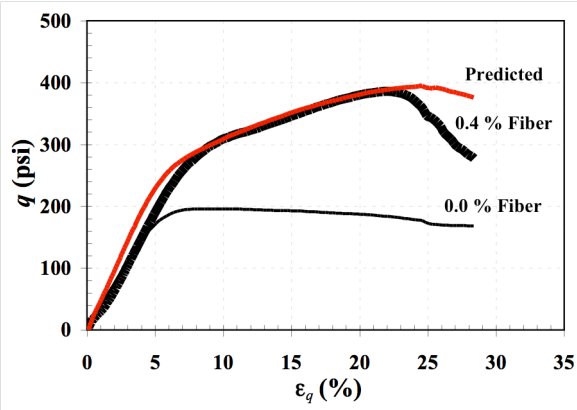

b) 20-psi effective consolidation stress

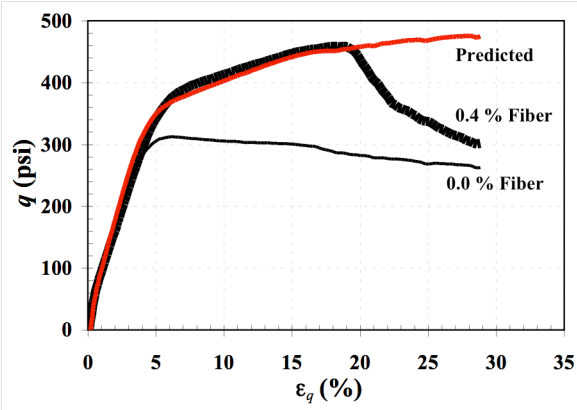

e) 60-psi effective consolidation stress

Figure 7.12 Measured and predicted q versus triaxial shear strain (ε_q) curves from the $\overline{CU}$ tests for Ottawa sand specimens compacted at a medium-dense state and consolidated to: a) 5-psi effective stress, b) 20-psi effective stress, c) 40-psi effective stress, and d) 60-psi effective stress.

7.4.2 Comparison of Pore Pressure Response from $\overline{CU}$ Tests

Figures 7.13 and 7.14 show the measured and predicted change in pore pressure (Δu) versus the triaxial shear strain for the Ottawa sand specimens. Overall, the predicted behavior agrees with the observed behavior at up to large strains except for the loose specimens consolidated to 5-psi. However, as discussed Chapter 3, the measured results of the pore pressures were suspect for the medium-dense specimens due to the absolute pore pressure becoming less than or equal to zero, but matches well.

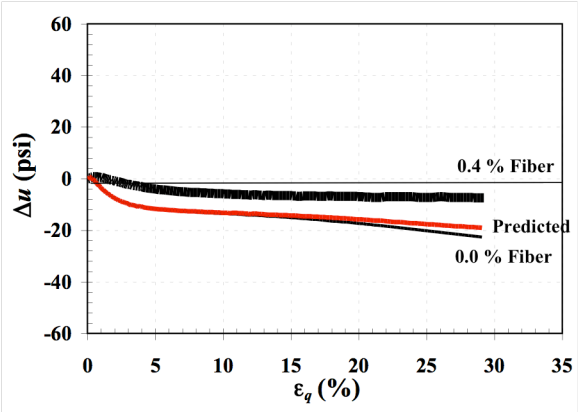

a) 5-psi effective consolidation stress

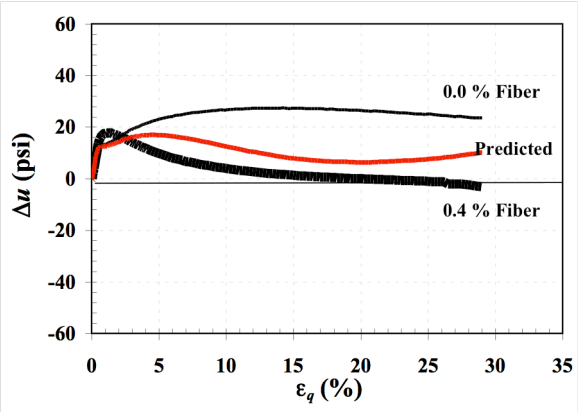

d) 40-psi effective consolidation stress

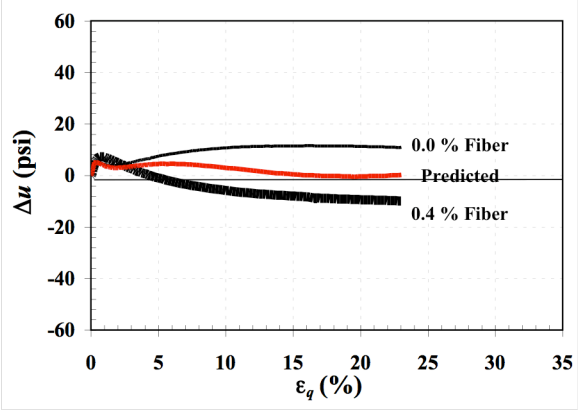

b) 20-psi effective consolidation stress

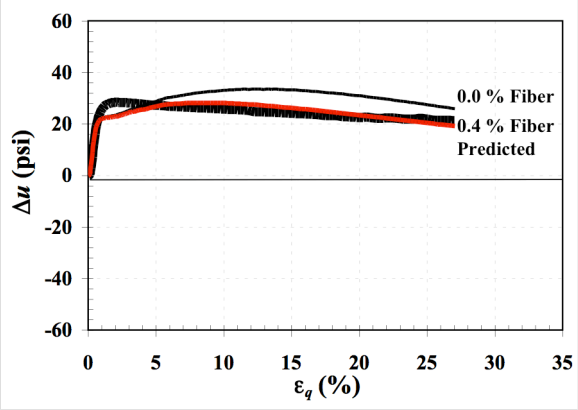

e) 60-psi effective consolidation stress

Figure 7.13 Measured and predicted Δu versus triaxial shear strain (ε_q) curves from the $\overline{CU}$ tests for Ottawa sand specimens compacted at a loose state and consolidated to: a) 5-psi effective stress, b) 20-psi effective stress, c) 40-psi effective stress, and d) 60-psi effective stress.

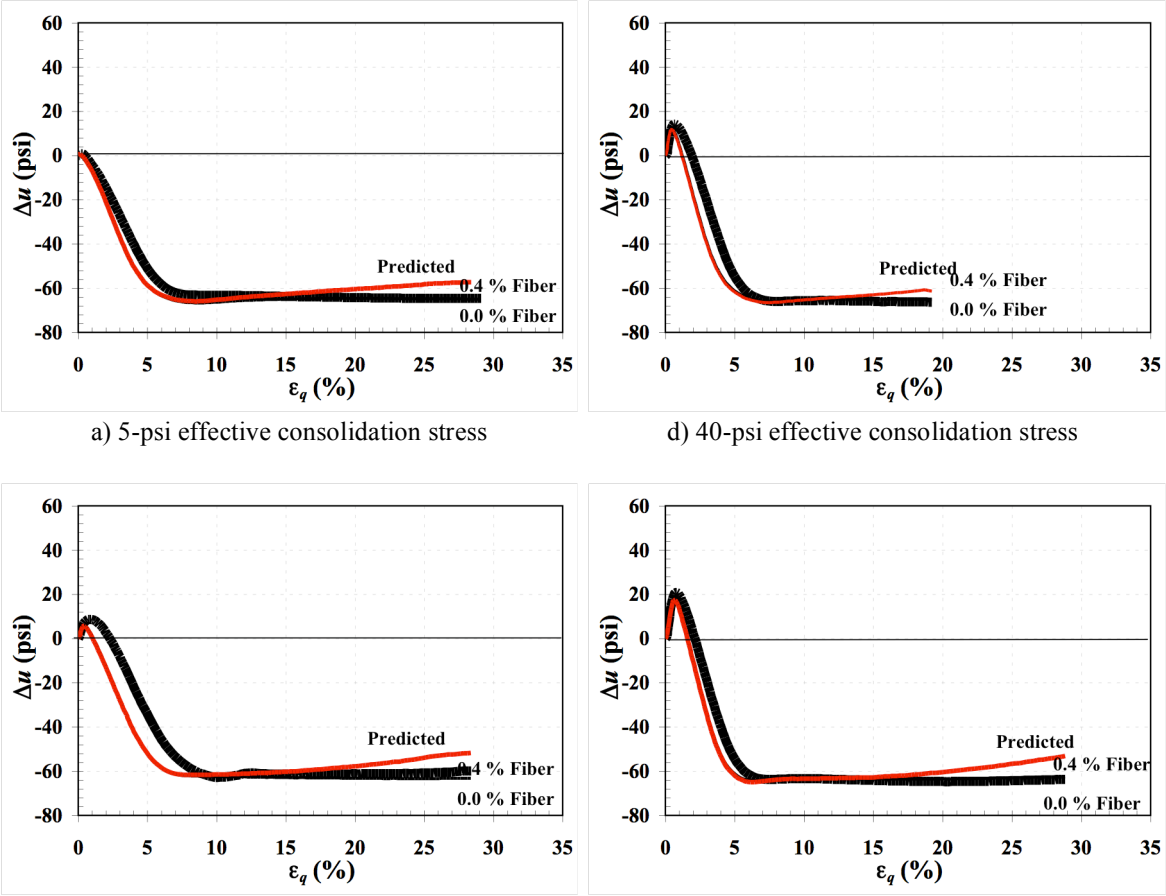

a) 5-psi effective consolidation stress

d) 40-psi effective consolidation stress

b) 20-psi effective consolidation stress

e) 60-psi effective consolidation stress

Figure 7.14 Measured and predicted q versus triaxial shear strain (ε_q) curves from the $\overline{CU}$ tests for Ottawa sand specimens compacted at a medium-dense state and consolidated to: a) 5-psi effective stress, b) 20-psi effective stress, c) 40-psi effective stress, and d) 60-psi effective stress.

7.4.3 Comparison of Fiber Contributions for the $\overline{CU}$ Tests

The measured and predicted deviatoric fiber contribution versus the triaxial shear strain from the $\overline{CU}$ tests are shown in Figures 7.15 and 7.16 for Ottawa sand specimens compacted at loose and medium-dense states, respectively. In general, the predicted response is similar to that of measured, with the exception of deviations fro the medium-dense specimens at large strains and relatively high effective confining stresses.

Figures 7.17 and 7.18 show the measured and predicted hydrostatic contribution of the fibers versus the triaxial shear strain for Ottawa sand specimens. As the changing pore pressure prediction reveals, the model is able to predict the fiber hydrostatic contributions in close agreement to the observed behavior for loose specimens. Nevertheless, the predicted behavior for the medium-dense specimens tended to be offset slightly in comparison to the measured responses.

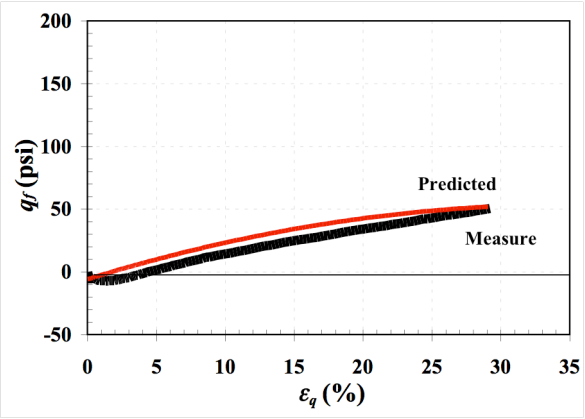

a) 5-psi effective consolidation stress

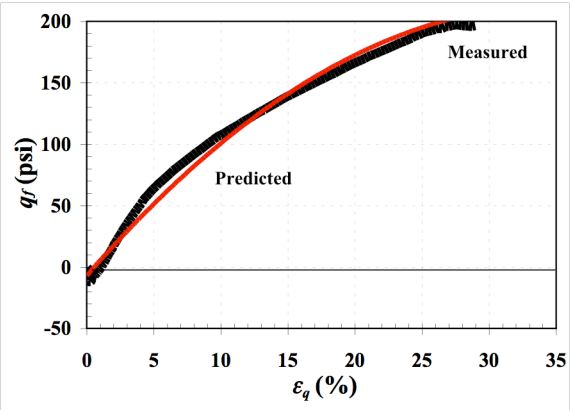

d) 40-psi effective consolidation stress

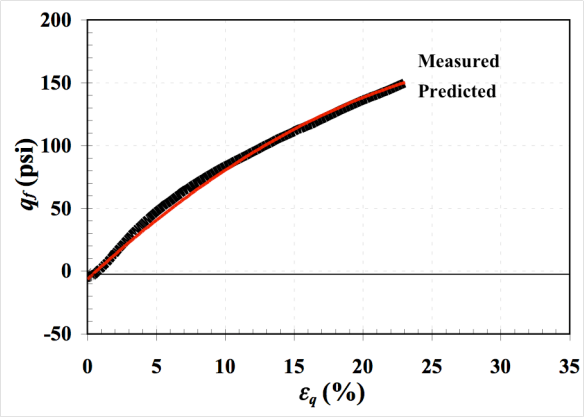

b) 20-psi effective consolidation stress

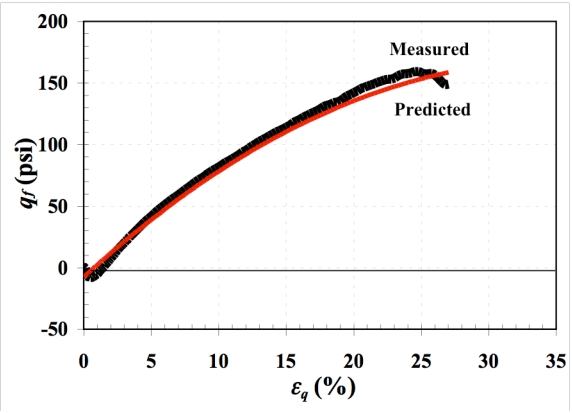

e) 60-psi effective consolidation stress

Figure 7.15 Measured and predicted deviatoric contribution of fibers (q_f) versus triaxial shear strain (ε_q) curves from the $\overline{CU}$ tests for Ottawa sand specimens compacted at a loose state and consolidated to: a) 5-psi effective stress, b) 20-psi effective stress, c) 40-psi effective stress, and d) 60-psi effective stress.

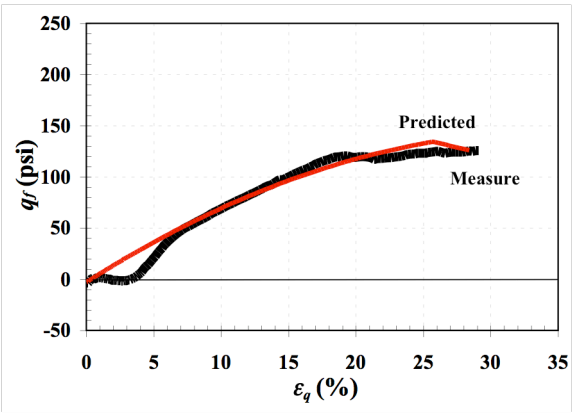

a) 5-psi effective consolidation stress

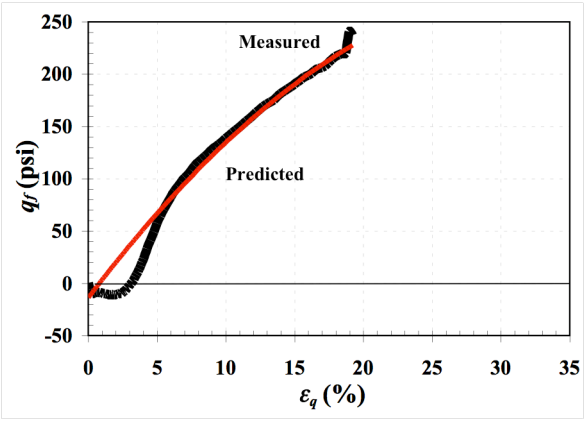

d) 40-psi effective consolidation stress

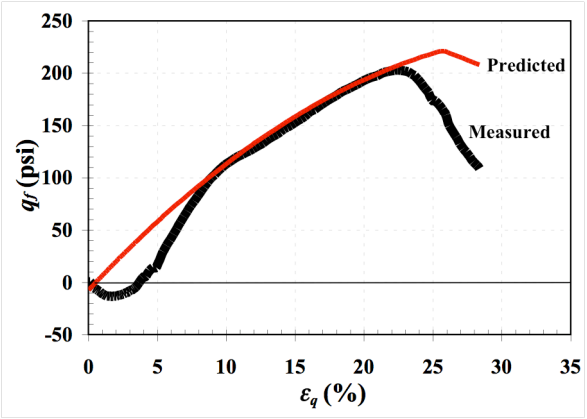

b) 20-psi effective consolidation stress

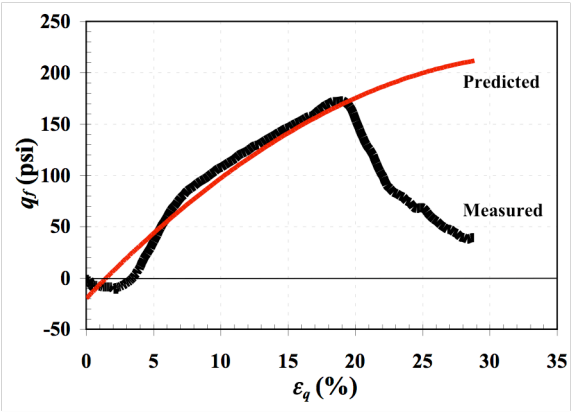

e) 60-psi effective consolidation stress

Figure 7.16 Measured and predicted deviatoric contribution of fibers (q_f) versus triaxial shear strain (ε_q) curves from the $\overline{CU}$ tests for Ottawa sand specimens compacted at medium-dense state and consolidated to: a) 5-psi effective stress, b) 20-psi effective stress, c) 40-psi effective stress, and d) 60-psi effective stress.

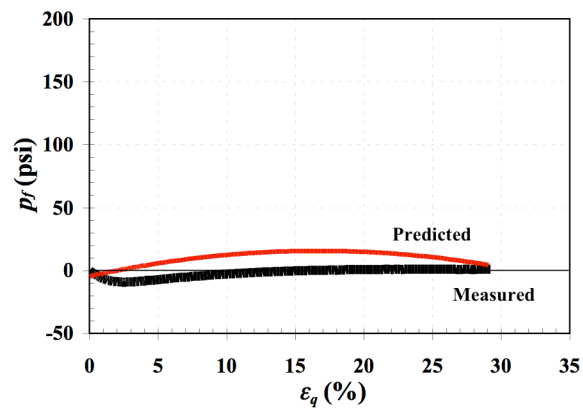

a) 5-psi effective consolidation stress

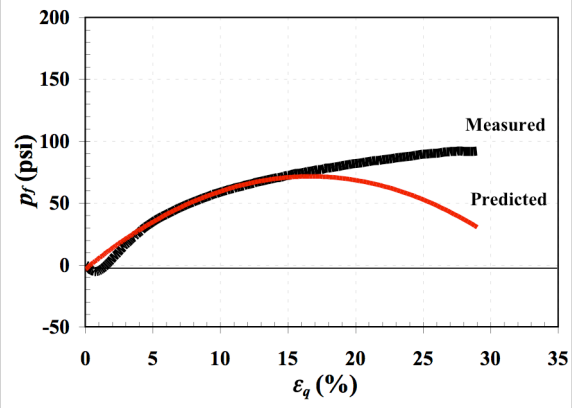

d) 40-psi effective consolidation stress

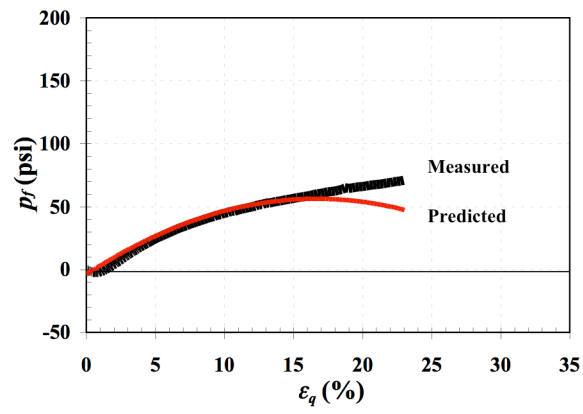

b) 20-psi effective consolidation stress

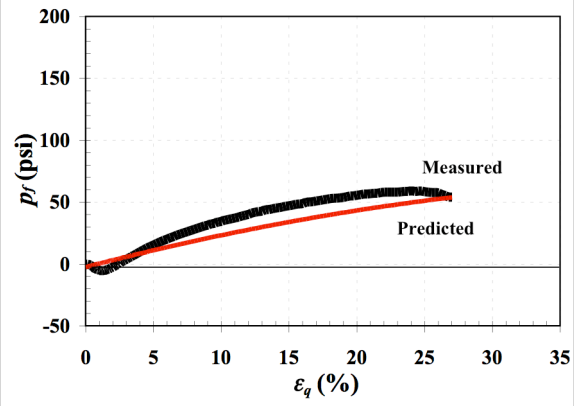

e) 60-psi effective consolidation stress

Figure 7.17 Measured and predicted hydrostatic contribution of fibers (p_f) versus triaxial shear strain (ε_q) curves from the $\overline{CU}$ tests for Ottawa sand specimens compacted at a loose state and consolidated to: a) 5-psi effective stress, b) 20-psi effective stress, c) 40-psi effective stress, and d) 60-psi effective stress.

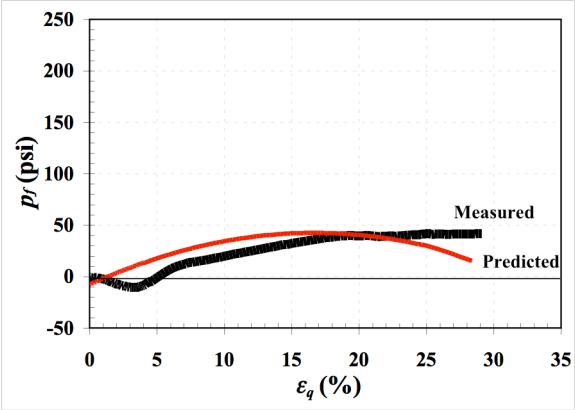

a) 5-psi effective consolidation stress

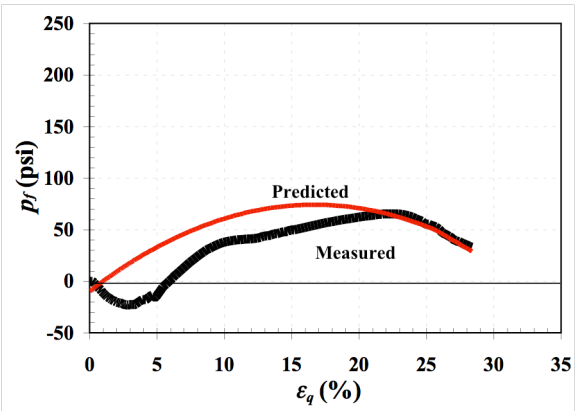

b) 20-psi effective consolidation stress

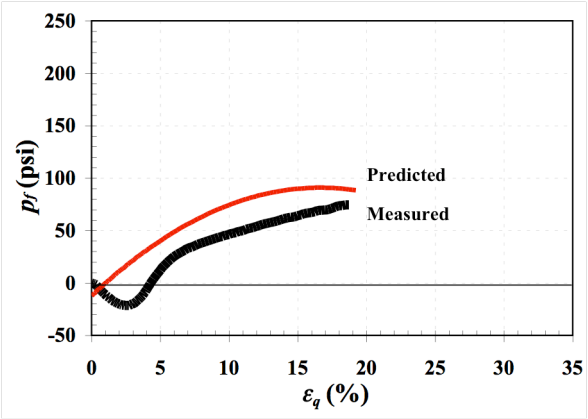

d) 40-psi effective consolidation stress

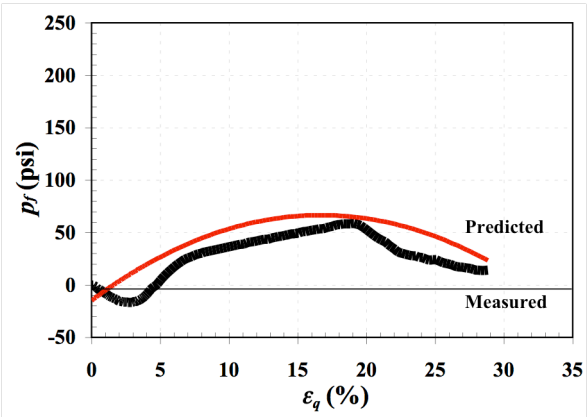

e) 60-psi effective consolidation stress

Figure 7.18 Measured and predicted hydrostatic contribution of fibers (p_f) versus triaxial shear strain (ε_q) curves from the $\overline{CU}$ tests for Ottawa sand specimens compacted at a medium-dense state and consolidated to: a) 5-psi effective stress, b) 20-psi effective stress, c) 40-psi effective stress,, and d) 60-psi effective stress.

7.4.4 Comparison of Stress Paths from $\overline{CU}$ Tests

The measured and predicted stress paths for the $\overline{CU}$ tests are shown in Figures 7.19 and 7.20 for Ottawa sand specimens compacted at loose and medium-dense states, respectively. It can be seen that predicted and measured stress paths match well along most of the early portions of the test, but then begin to deviate from the observed behavior as the peak deviatoric stress is approached. This agrees with the predicted pore pressures that were shown previously in Figures 7.13 and 7.14.

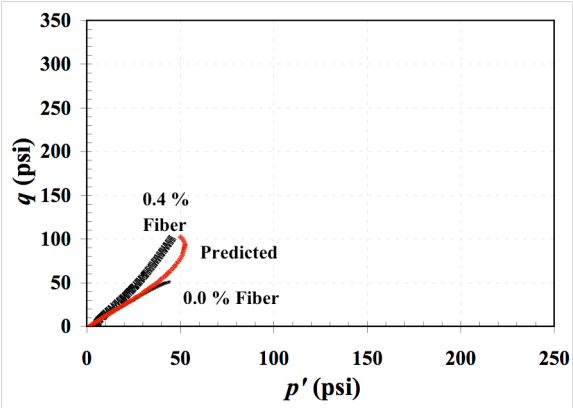

a) 5-psi effective consolidation stress

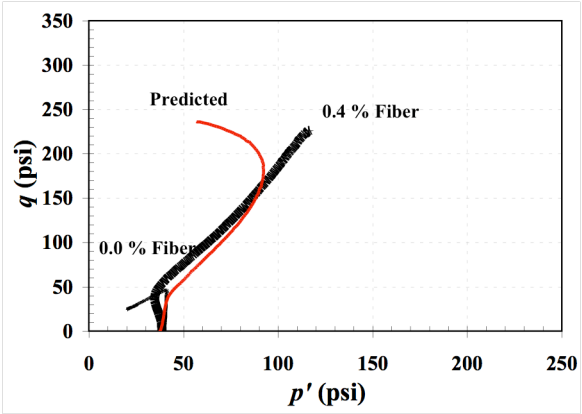

d) 40-psi effective consolidation stress

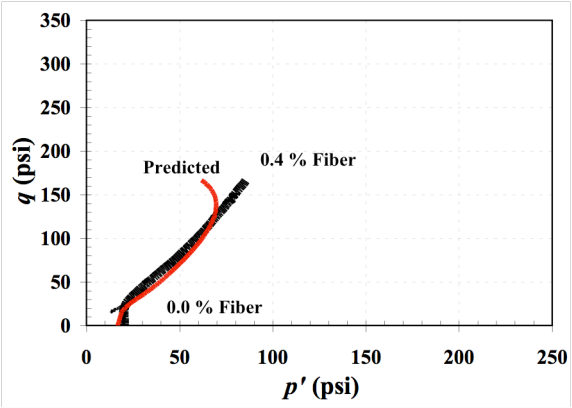

b) 20-psi effective consolidation stress

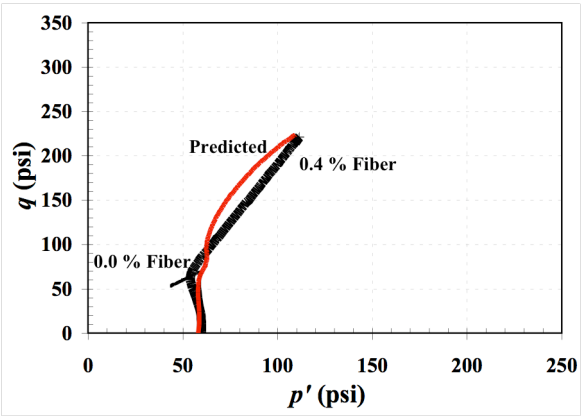

e) 60-psi effective consolidation stress

Figure 7.19 Measured and predicted stress paths from the $\overline{CU}$ tests for Ottawa sand specimens prepared at a loose state and consolidated to: a) 5-psi effective stress, b) 20-psi effective stress, c) 40-psi effective stress, and d) 60-psi effective stress.

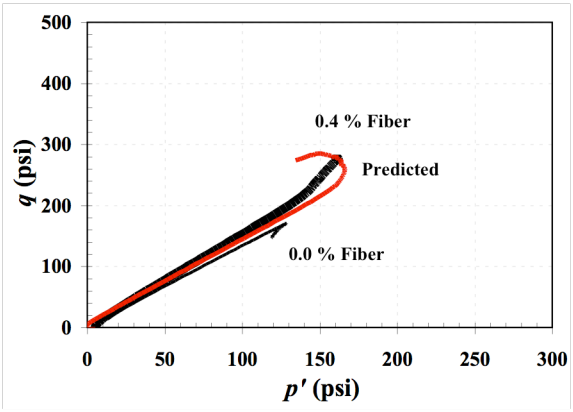

a) 5-psi effective consolidation stress

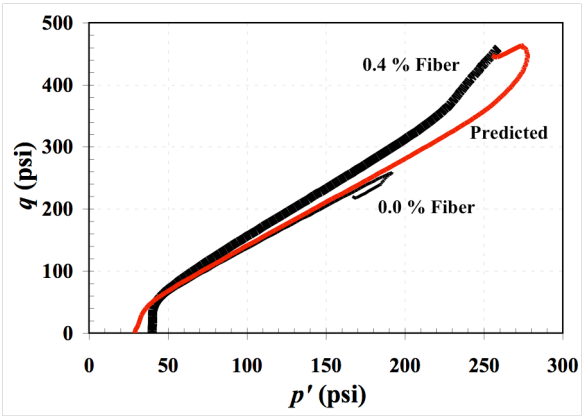

d) 40-psi effective consolidation stress

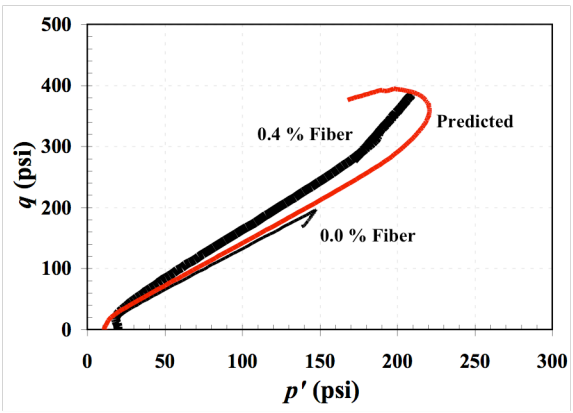

b) 20-psi effective consolidation stress

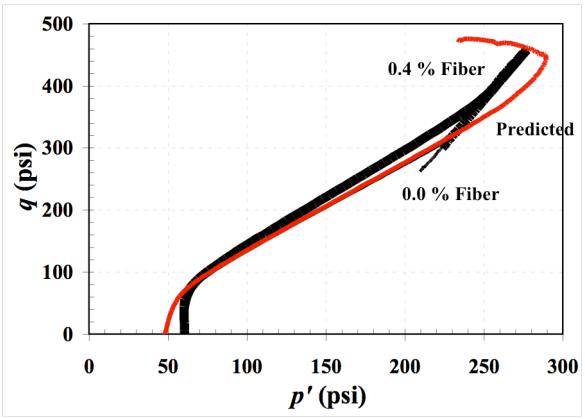

e) 60-psi effective consolidation stress

Figure 7.20 Measured and predicted stress paths from the $\overline{CU}$ tests for Ottawa sand specimens prepared at a medium-dense state and consolidated to: a) 5-psi effective stress, b) 20-psi effective stress, c) 40-psi effective stress, and d) 60-psi effective stress.

7.5 Summary

The proposed constitutive model was used to simulate response of fiber-reinforced silty sand and Ottawa sand during undrained tests. The predicted behavior and measured responses were presented, compared, and discussed in this chapter. It was found that the predicted deviatoric stresses for the silty sand specimens tended to slightly over-predict and depart from the measured behavior at large strains. The model was capable of closely reproducing the deviatoric stress for all Ottawa sand specimens compacted at loose and medium-dense states; moreover, the predicted pore pressure response was in close agreement with the observed behavior for all effective consolidation stresses tested in this study for both soils. Finally, the predictions in fiber deviatoric and fiber hydrostatic stresses matched reasonably well and followed the same trends as measured behavior, but showed a slightly tendency to over-predict the fiber contribution values.

CHAPTER 8: COMPARISON OF OBSERVED AND PREDICTED BEHAVIOR IN DRAINED (*CD*) TRIAXIAL TESTS

8.1 Introduction

In this chapter, the constitutive model to predict the stress-strain-volume change behavior of the silty sand and Ottawa sand and the results are compared to the observed responses previously described in Chapter 4.

8.2 Model Parameters

The model parameters used to predict the drained behavior for the fiber-reinforced soil include the fiber content (χ), the Young's modulus of the fibers (E_f), the initial stresses in the fibers (p_{f0} and q_{f0}), the fiber mobilization factor (f_{mob}), and the bulk modulus of fiber-reinforced soils (K_f), which was measured from isotropic consolidation tests as described in Chapter 4. The parameters χ and E_f are known and the remaining parameters were determined and interpreted from the results of tests conducted on fiber-reinforced specimens. Again, p_{pf} and q_{pf} are predicted using the measured axial and volumetric strains from tests on replicable unreinforced specimens to produce p_f and q_f as a function of shear strain. This response is then added to the response of the unreinforced specimen to produce the predicted response of a fiber-reinforced specimen prepared and tested under similar conditions. However, the disadvantage of using this approach is that scatter in the response of the unreinforced soils, which is included along with scatter in the predicted response of the reinforced soil.

8.3 Comparison of Measured and Predicted Response from *CD* Tests for Silty Sand Specimens

Predicted stress-strain-volume change behavior of the fiber-reinforced silty sand is presented here along with the observed responses for the reinforced specimens from *CD* tests. The predicted deviatoric and hydrostatic contributions of the fibers are also compared to the measured responses along with the stress paths.

8.3.1 Comparison of Stress-Strain Response from *CD* Tests

The measured and predicted deviatoric stresses versus the triaxial shear strain for all drained tests for silty sand samples compacted at 18 and 22 percent water contents are plotted in Figures 8.1 and 8.2. The figures show that the predicted and observed deviatoric stresses agree well for all effective consolidation stresses tested in this study. However, Figures 8.1d, 8.1e, 8.2d, 8.2e are good examples of differences in stress-strain behavior between the unreinforced and reinforced specimens that can result in scatters in the predicted response at moderate strains. The scatter occurs because the stress-strain behavior for unreinforced specimens reached a peak deviatoric stress at moderate strains, while the reinforced specimens showed a strain hardening type of behavior with no noticeable peak stress observed at up to 30 percent strain. This is one disadvantage of using unreinforced test data to predict the behavior of reinforced specimens, since the unreinforced silty sand specimens reveal different type of stress-strain behavior. It becomes more complicated to predict the behavior of a fiber-reinforced soil from that of the unreinforced soil plus the response of the fibers.

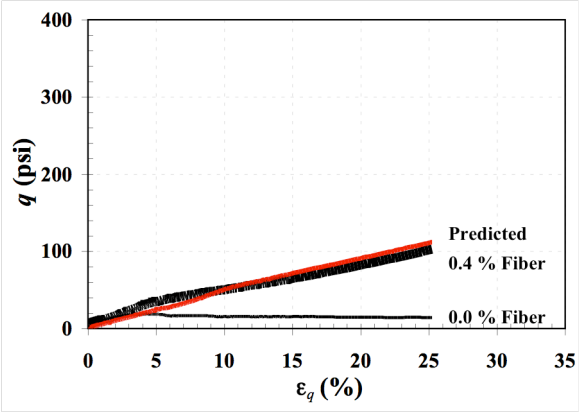

a) 5-psi effective consolidation stress

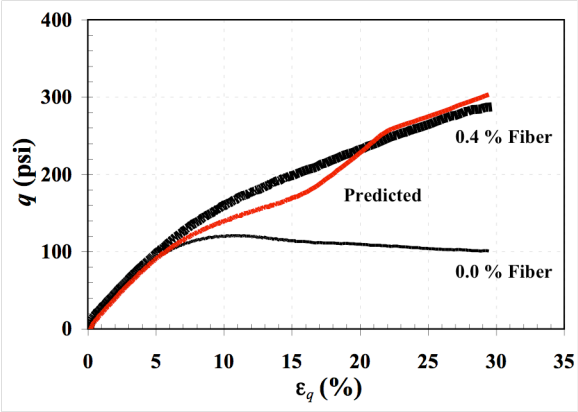

d) 40-psi effective consolidation stress

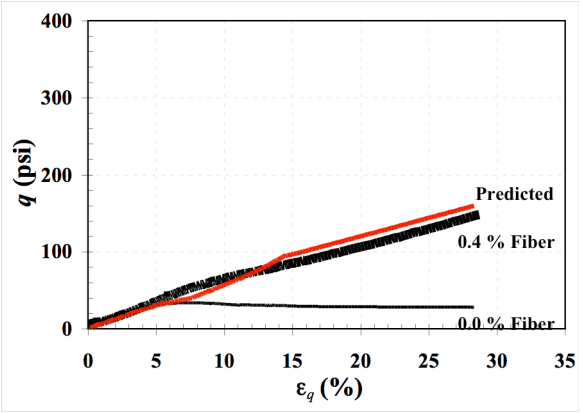

b) 10-psi effective consolidation stress

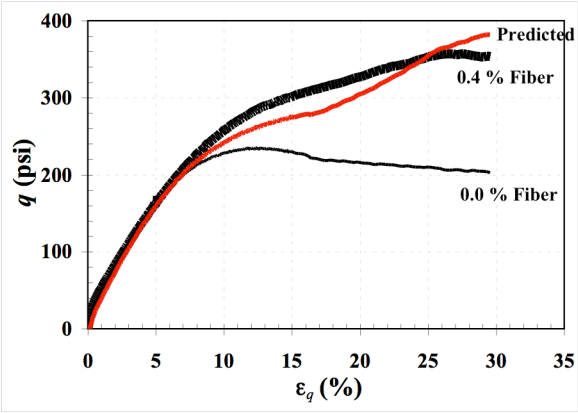

e) 80-psi effective consolidation stress

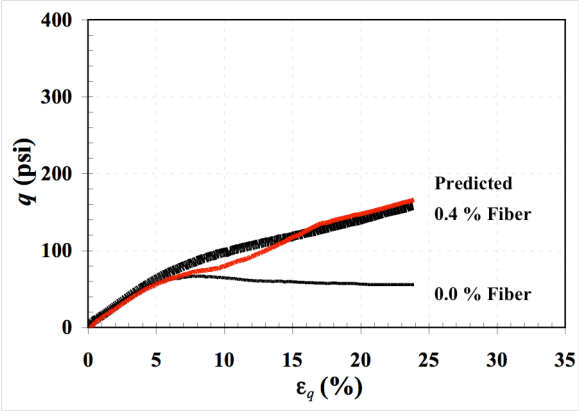

c) 20-psi effective consolidation stress

Figure 8.1 Measured and predicted q versus triaxial shear strain (ε_q) curves from the CD tests for silty sand specimens compacted at 18 percent water content and consolidated to: a) 5-psi effective stress, b) 10-psi effective stress, c) 20-psi effective stress, d) 40-psi effective stress, and e) 80-psi effective stress.

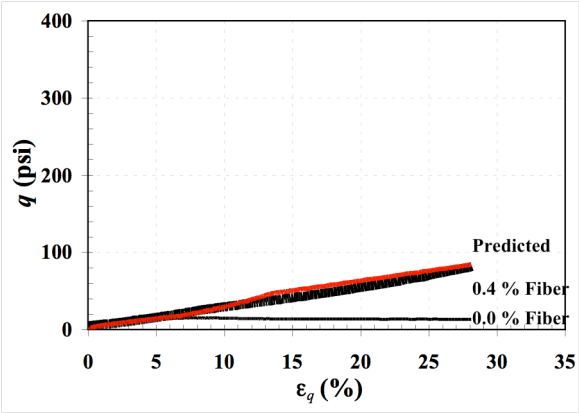

a) 5-psi effective consolidation stress

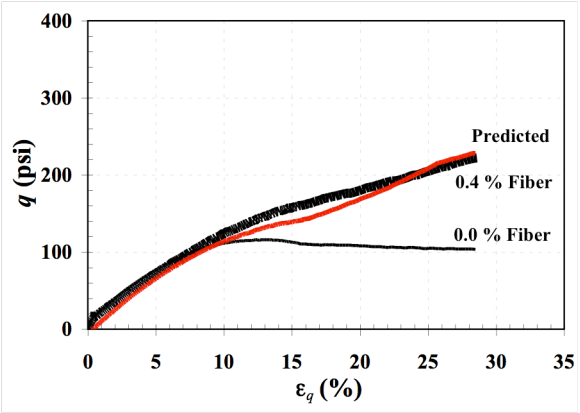

d) 40-psi effective consolidation stress

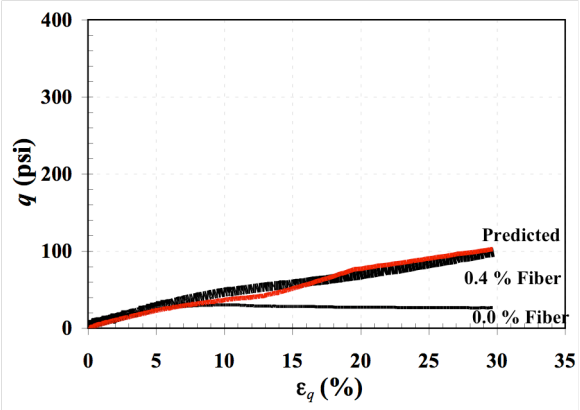

b) 10-psi effective consolidation stress

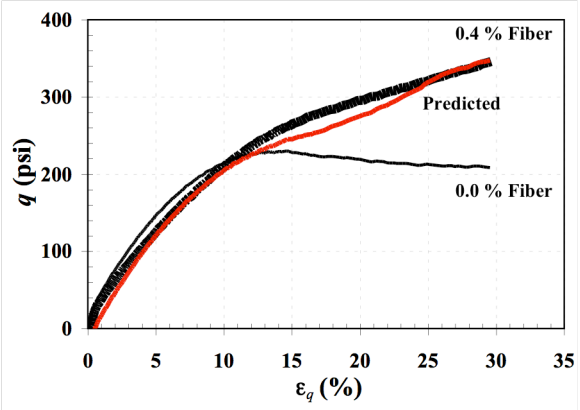

e) 80-psi effective consolidation stress

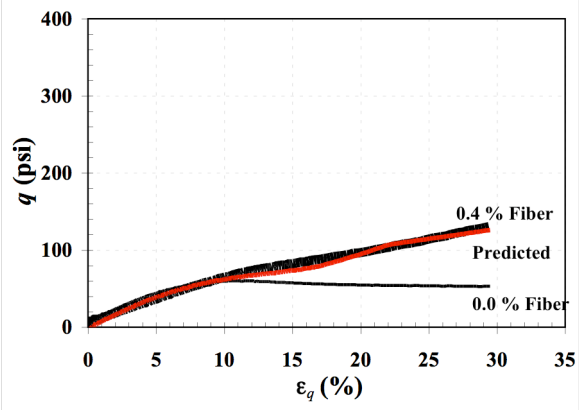

c) 20-psi effective consolidation stress

Figure 8.2 Measured and predicted q versus triaxial shear strain (ε_q) curves from the CD tests for silty sand specimens compacted at 22 percent water content and consolidated to: a) 5-psi effective stress, b) 10-psi effective stress, c) 20-psi effective stress, d) 40-psi effective stress, and e) 80-psi effective stress.

8.3.2 Comparison of Volume Change Response from *CD* Tests

Figures 8.3 and 8.4 show the measured and predicted volumetric strain (ε_v) versus the triaxial shear strain for silty sand specimens compacted at 18 and 22 percent water contents, respectively. Overall, the predicted behavior agreed well with the observed behavior. The figures show some tendency to over-predict the dilatancy when the consolidation stress is less than 20-psi (140-kPa). This may be attributed to the bulk modulus used to predict volumetric strains, which depends on the effective consolidation stress. The volumetric strain was very sensitive to the computed bulk moduli under different consolidation stress.

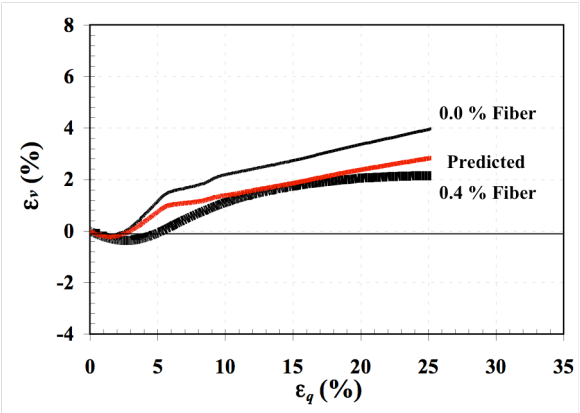

a) 5-psi effective consolidation stress

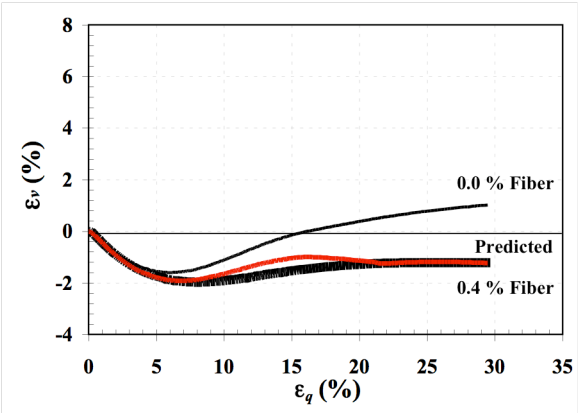

d) 40-psi effective consolidation stress

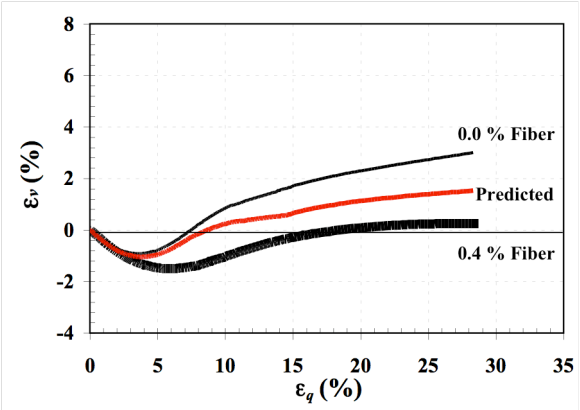

b) 10-psi effective consolidation stress

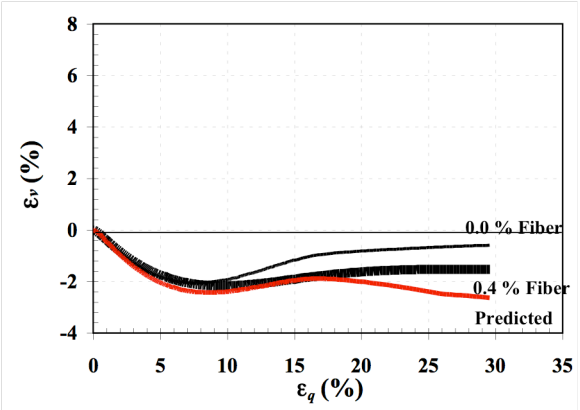

e) 80-psi effective consolidation stress

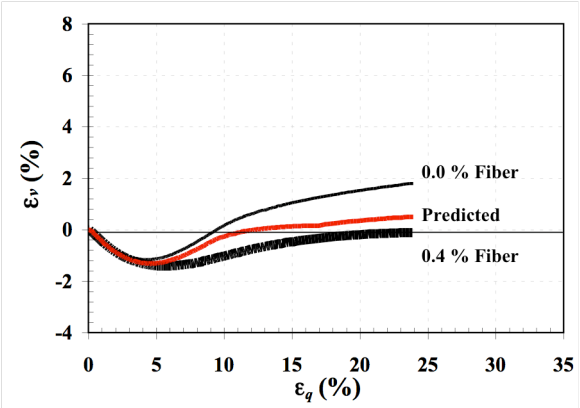

c) 20-psi effective consolidation stress

Figure 8.3 Measured and predicted (ε_v) versus triaxial shear strain (ε_q) curves from the *CD* tests for silty sand specimens compacted at 18 percent water content and consolidated to: a) 5-psi effective stress, b) 10-psi effective stress, c) 20-psi effective stress, d) 40-psi effective stress, and e) 80-psi effective stress.

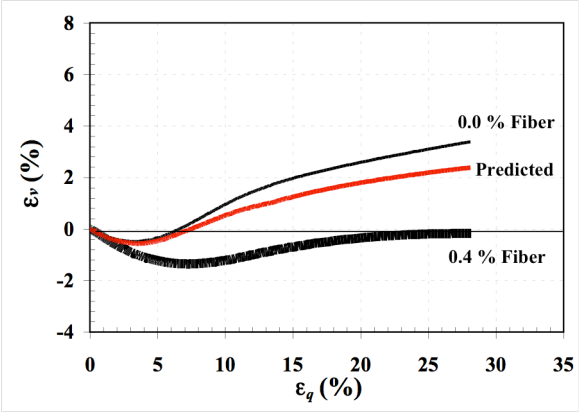

a) 5-psi effective consolidation stress

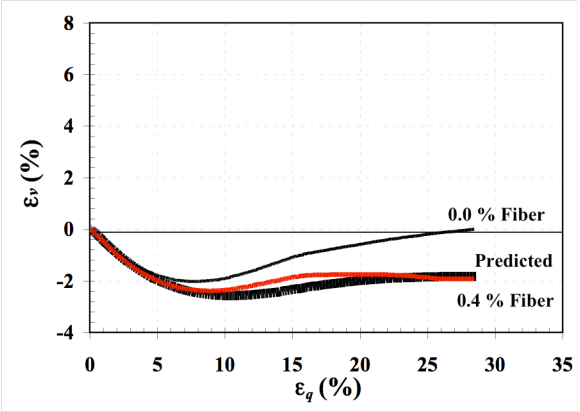

d) 40-psi effective consolidation stress

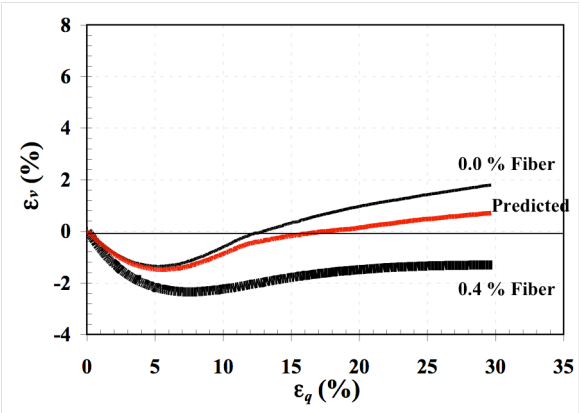

b) 10-psi effective consolidation stress

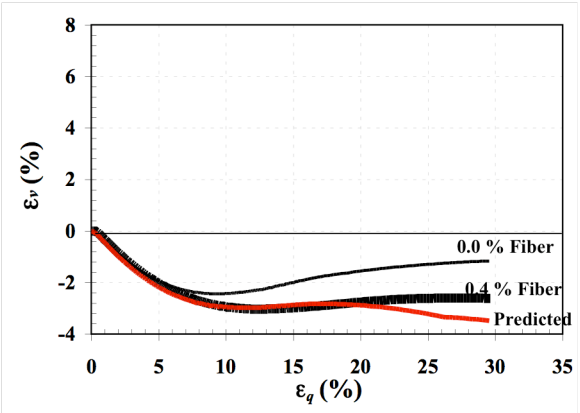

e) 80-psi effective consolidation stress

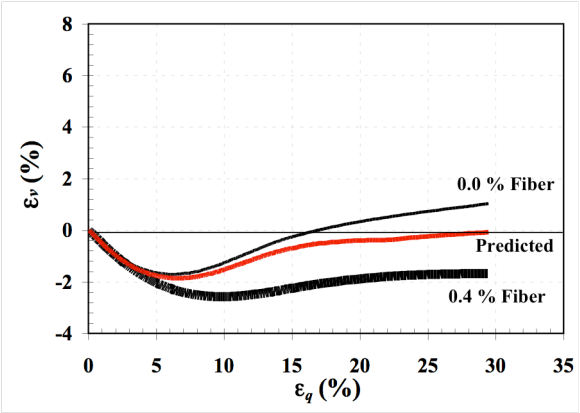

c) 20-psi effective consolidation stress

Figure 8.4 Measured and predicted ε_v versus triaxial shear strain (ε_q) curves from the CD tests for silty sand specimens compacted at 22 percent water content and consolidated to: a) 5-psi effective stress, b) 10-psi effective stress, c) 20-psi effective stress, d) 40-psi effective stress, and e) 80-psi effective stress.

8.3.3 Comparison of Fiber Contributions for *CD* Tests

The measured and predicted deviatoric contribution of fibers versus the triaxial shear strain from the *CD* tests are shown in Figures 8.5 and 8.6 for silty sand specimens compacted at 18 and 22 percent water contents, respectively. Generally, the model was capable of reproducing the deviatoric stress contributions for all tested effective consolidation stresses up to large strains.

Figures 8.7 and 8.8 show the measured and predicted hydrostatic contribution of fibers versus the triaxial shear strain for silty sand specimens. As seen in the figures, the predicted hydrostatic stress contributions match well with the observed values for all reinforced specimens tested in this study. It should be noted that the measured p' values of used to plot the "measured" stress paths are simply computed as the difference in the total (applied) mean confining stress ($p = (\sigma_1 + 2\sigma_3)/3$) minus the measured pore water pressures during the tests. Any additional stresses induced due to the fiber reinforcement cannot be measured (i.e. it is not possible to directly measure effective stresses or stress in the fibers). Since the predicted values of p' plotted in Figures 8.7 and 8.8 include a contribution to p' from the fibers, some deviation of the stress paths is expected. The same applies to stress paths shown subsequently in Figures 8.9 and 8.10.

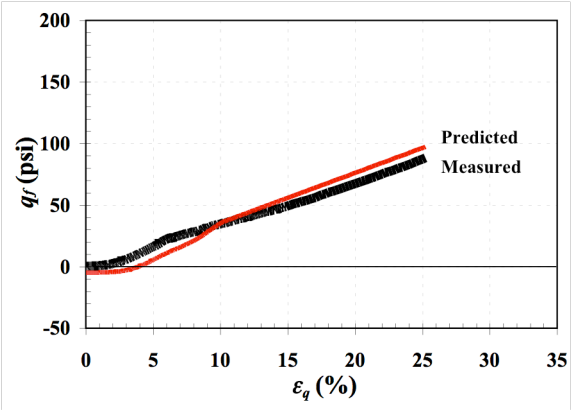

a) 5-psi effective consolidation stress

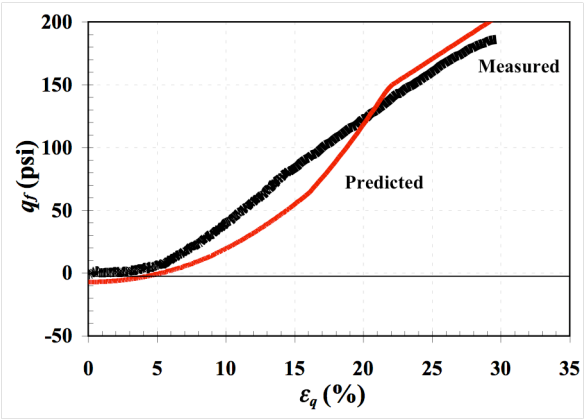

d) 40-psi effective consolidation stress

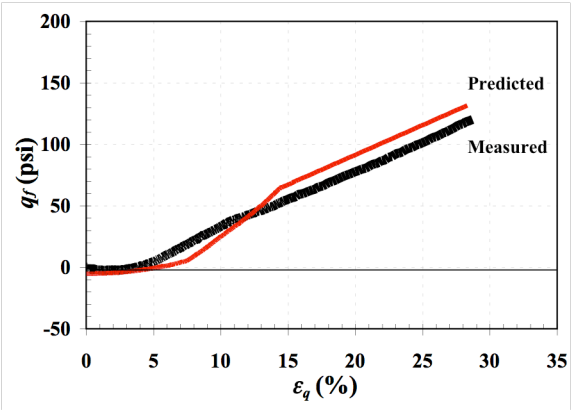

b) 10-psi effective consolidation stress

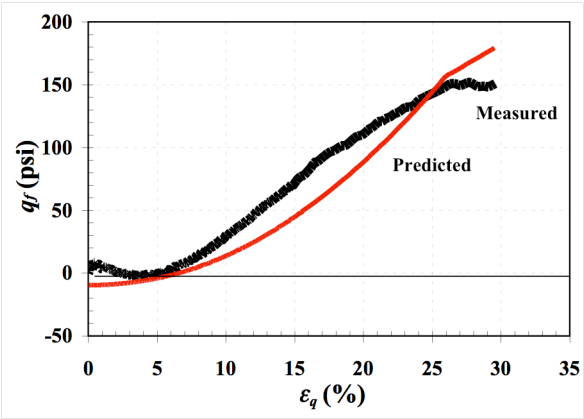

e) 80-psi effective consolidation stress

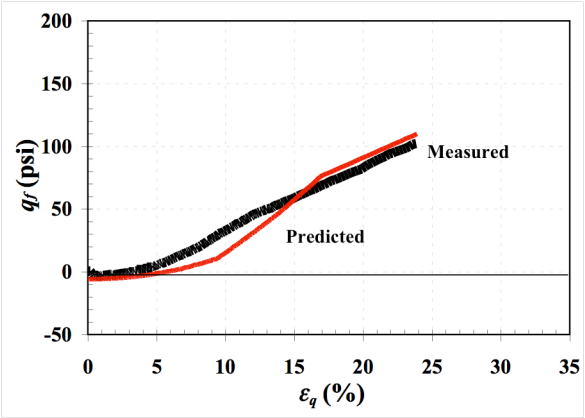

c) 20-psi effective consolidation stress

Figure 8.5 Measured and predicted deviatoric contribution of fibers (q_f) versus triaxial shear strain (ε_q) curves from the CD tests for silty sand specimens compacted at 18 percent water content and consolidated to: a) 5-psi effective stress, b) 10-psi effective stress, c) 20-psi effective stress, d) 40-psi effective stress, and e) 80-psi effective stress.

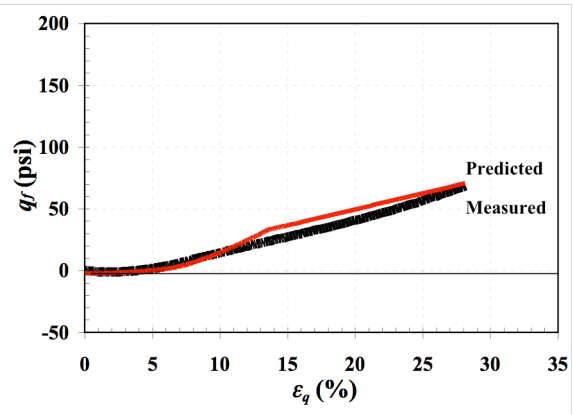

a) 5-psi effective consolidation stress

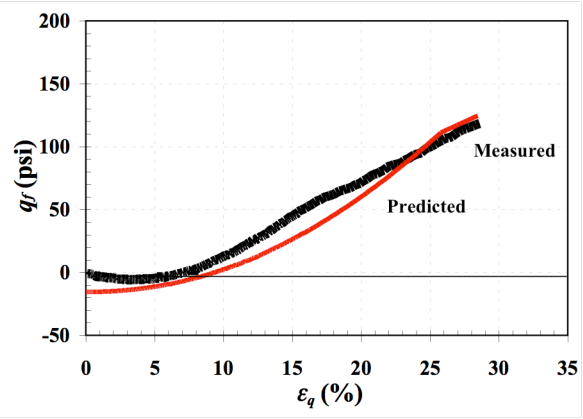

d) 40-psi effective consolidation stress

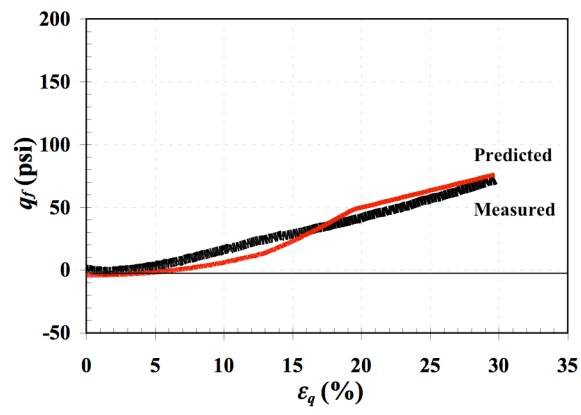

b) 10-psi effective consolidation stress

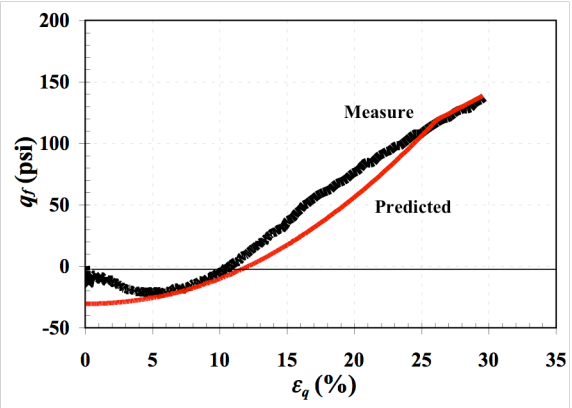

e) 80-psi effective consolidation stress

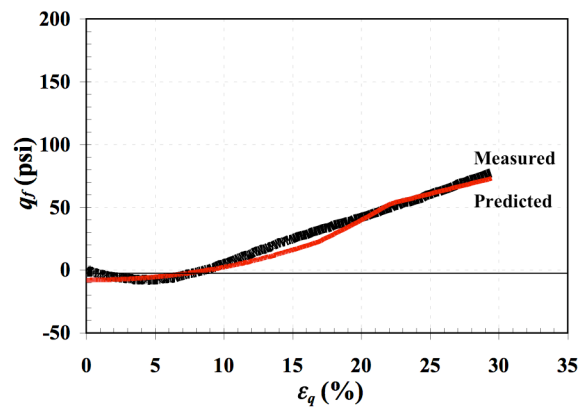

c) 20-psi effective consolidation stress

Figure 8.6 Measured and predicted deviatoric contribution of fibers (q_f) versus triaxial shear strain (ε_q) curves from the CD tests for silty sand specimens compacted at 22 percent water content and consolidated to: a) 5-psi effective stress, b) 10-psi effective stress, c) 20-psi effective stress, d) 40-psi effective stress, and e) 80-psi effective stress.

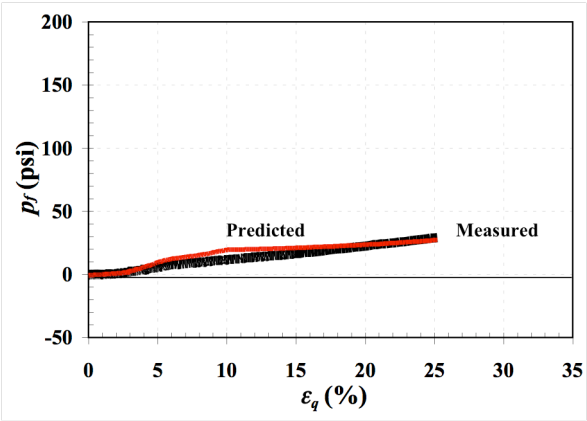

a) 5-psi effective consolidation stress

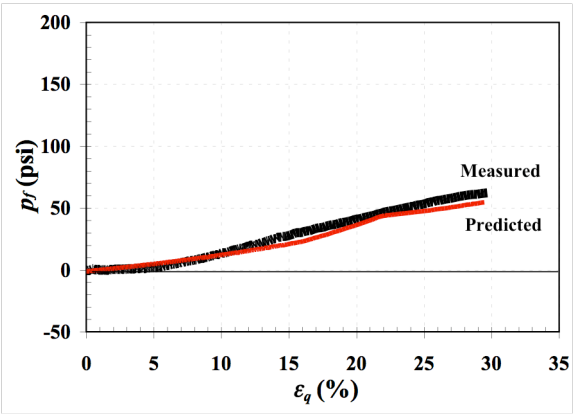

d) 40-psi effective consolidation stress

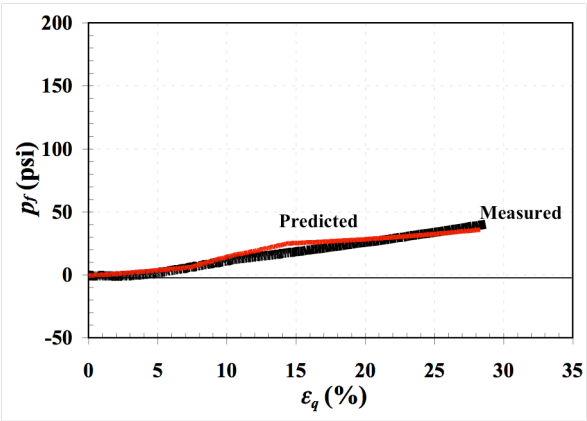

b) 10-psi effective consolidation stress

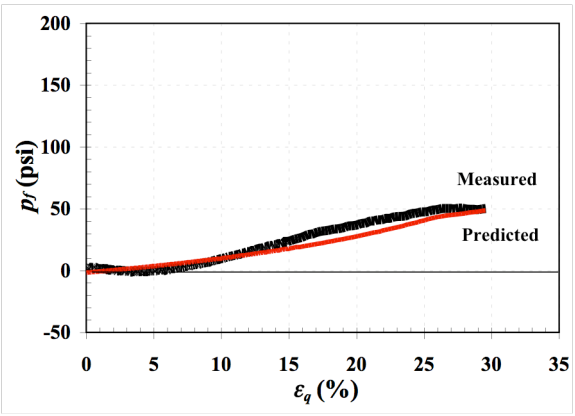

e) 80-psi effective consolidation stress

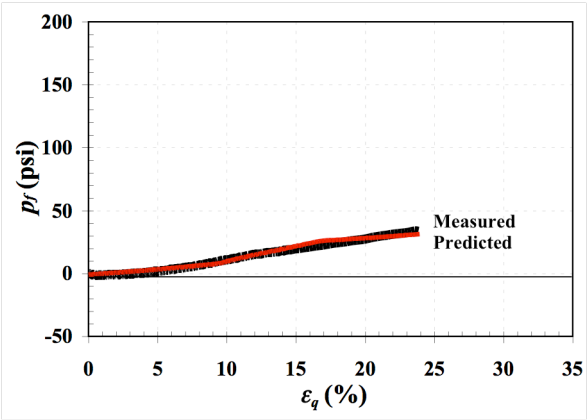

Figure 8.7 Measured and predicted hydrostatic contribution of fibers (p_f) versus triaxial shear strain (ε_q) curves from the CD tests for silty sand specimens compacted at 18 percent water content and consolidated to: a) 5-psi effective stress, b) 10-psi effective stress, c) 20-psi effective stress, d) 40-psi effective stress, and e) 80-psi effective stress.

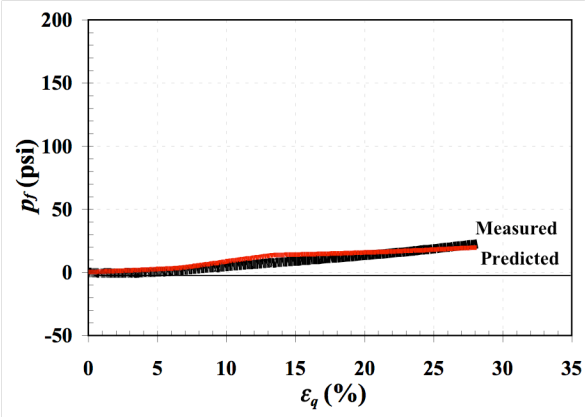

a) 5-psi effective consolidation stress

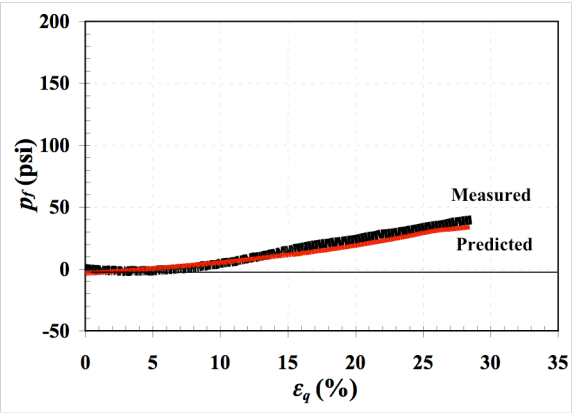

d) 40-psi effective consolidation stress

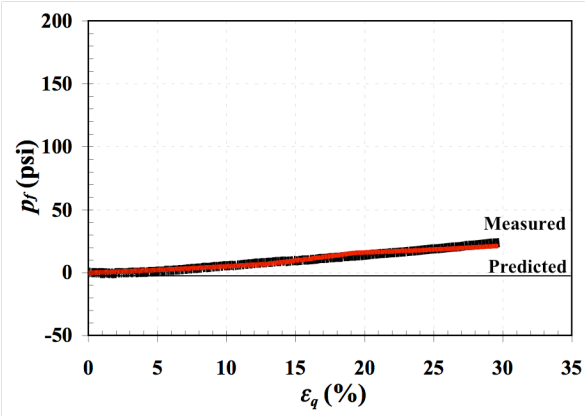

b) 10-psi effective consolidation stress

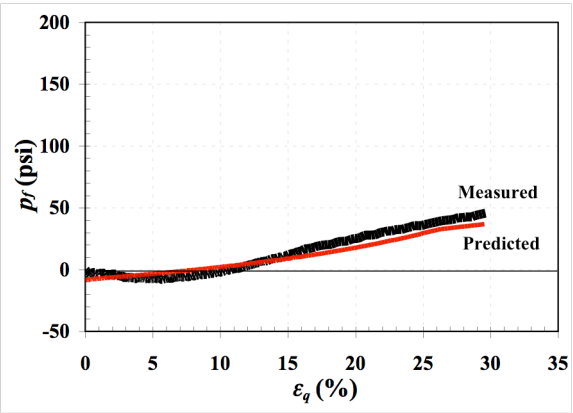

e) 80-psi effective consolidation stress

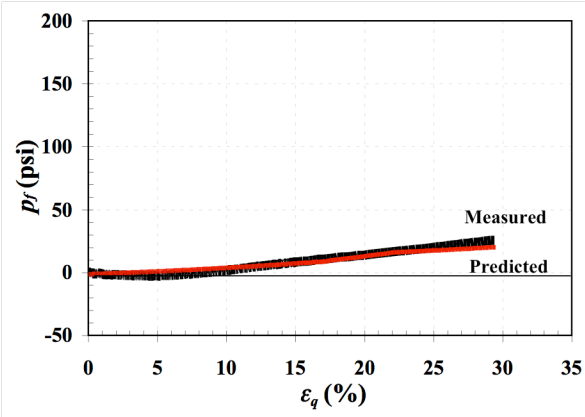

Figure 8.8 Measured and predicted hydrostatic contribution of fibers (p_f) versus triaxial shear strain (ε_q) curves from the CD tests for silty sand specimens compacted at 22 percent water content and consolidated to: a) 5-psi effective stress, b) 10-psi effective stress, c) 20-psi effective stress, d) 40-psi effective stress, and e) 80-psi effective stress.

8.3.4 Comparison of Stress Paths from *CD* Tests

The measured and predicted stress paths for the *CD* tests are shown in Figures 8.9 and 8.10 for silty sand specimens compacted at 18 and 22 percent water contents, respectively. Note that the predicted stress paths matched well to all reinforced specimens consolidated to different effective stresses due to the good agreement between the predicted and measured deviatoric stresses, which were shown in the Figures 8.1 and 8.2.

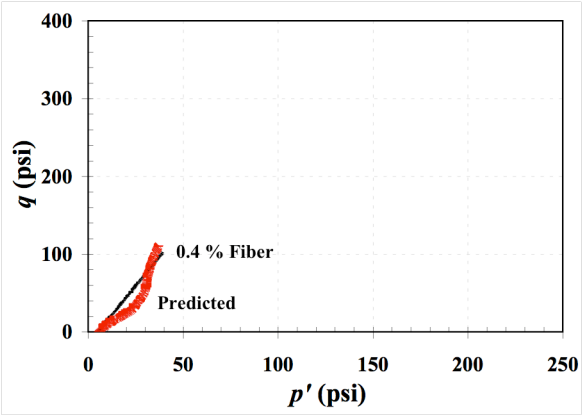

a) 5-psi effective consolidation stress

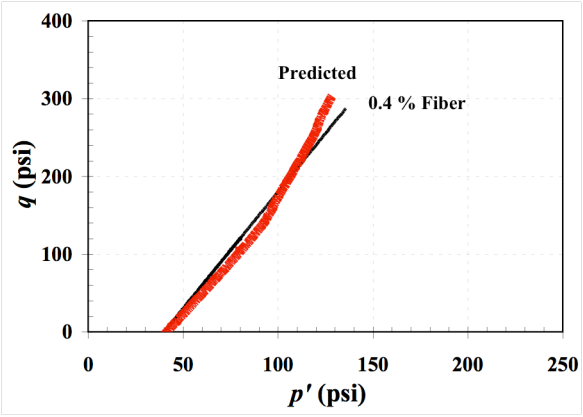

d) 40-psi effective consolidation stress

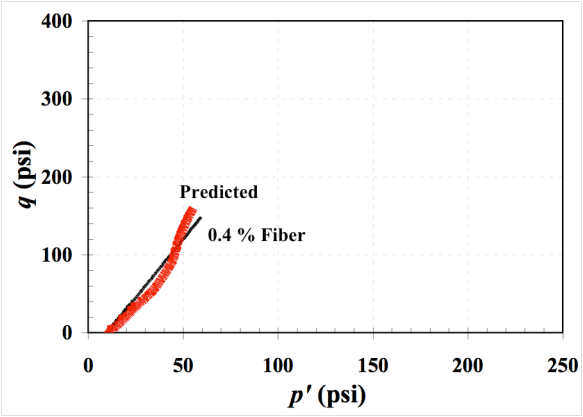

b) 10-psi effective consolidation stress

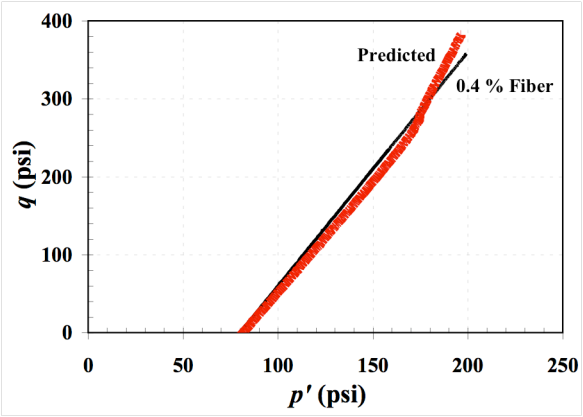

e) 80-psi effective consolidation stress

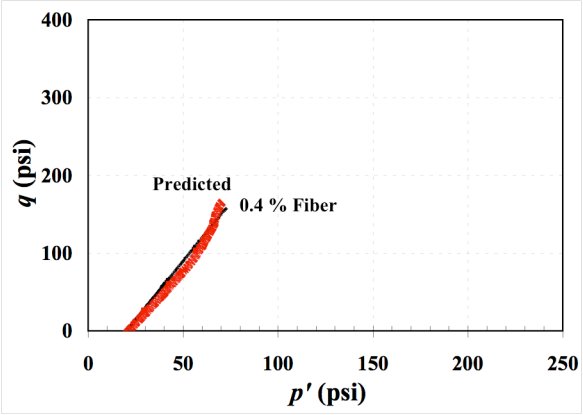

c) 20-psi effective consolidation stress

Figure 8.9 Measured and predicted stress paths from the *CD* tests for silty sand specimens compacted at 18 percent water content and consolidated to: a) 5-psi effective stress, b) 10-psi effective stress, c) 20-psi effective stress, d) 40-psi effective stress, and e) 80-psi effective stress.

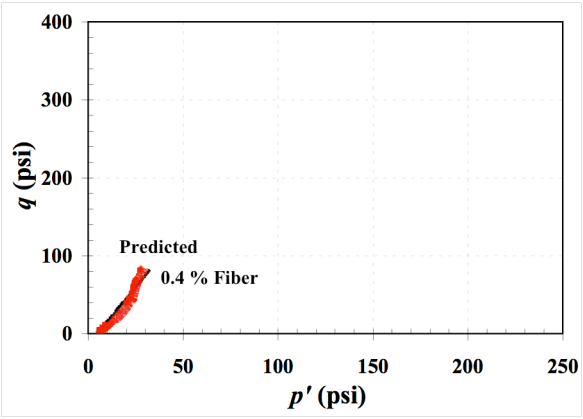

a) 5-psi effective consolidation stress

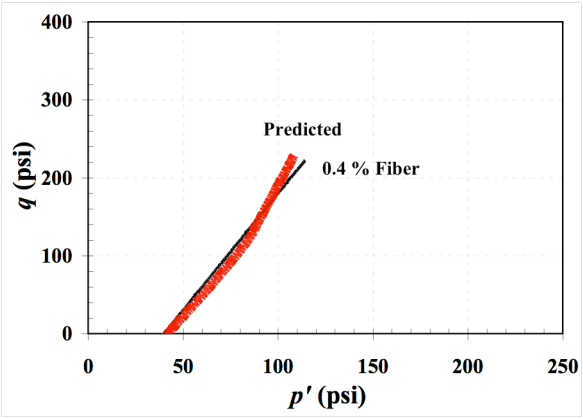

d) 40-psi effective consolidation stress

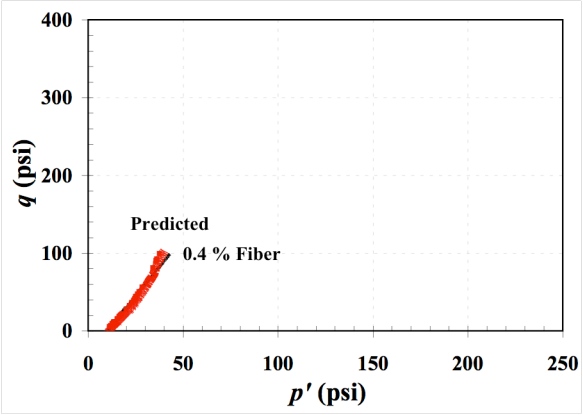

b) 10-psi effective consolidation stress

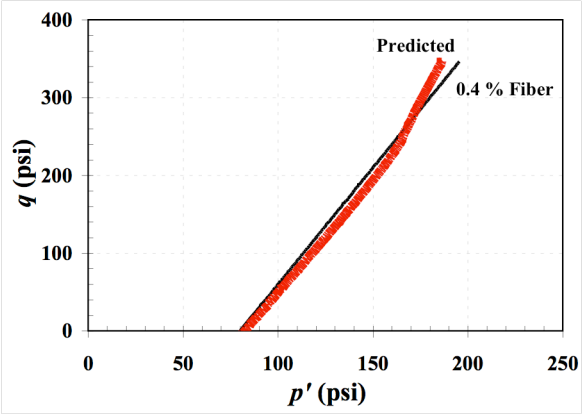

e) 80-psi effective consolidation stress

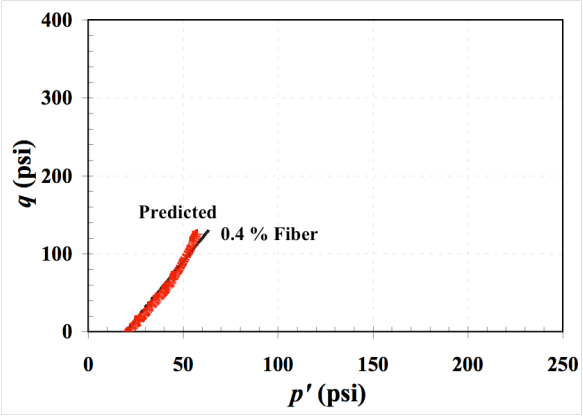

c) 20-psi effective consolidation stress

Figure 8.10 Measured and predicted stress paths from the *CD* tests for silty sand specimens compacted at 22 percent water content and consolidated to: a) 5-psi effective stress, b) 10-psi effective stress, c) 20-psi effective stress, d) 40-psi effective stress, and e) 80-psi effective stress.

8.4 Comparison of Measured and Predicted Response from *CD* Tests for Ottawa Sand Specimens

The constitutive model created in this research was used to predict the stress-strain-volume change behavior of the fiber-reinforced Ottawa sand and the results were compared to the observed response for the reinforced specimens. The predicted deviatoric and hydrostatic contributions of the fibers are also compared to the inferred values from replicate tests. Finally, the predicted stress paths are compared with measured ones in this section.

8.4.1 Comparison of Stress-Strain Response from *CD* Tests

Figures 8.11 and 8.12 show the measured and predicted deviatoric stresses versus the triaxial shear strain for all drained tests for Ottawa sand samples compacted at loose and medium-dense states, respectively. As can be seen, the model was capable of matching the deviatoric stress well for all Ottawa sand specimens compacted at loose and medium-dense states. The predictions also show a deviation from the measured response at large strain for the medium-dense specimens. The deviation is likely due to the model missing some failure mode, such as fiber pullout or fiber yield.

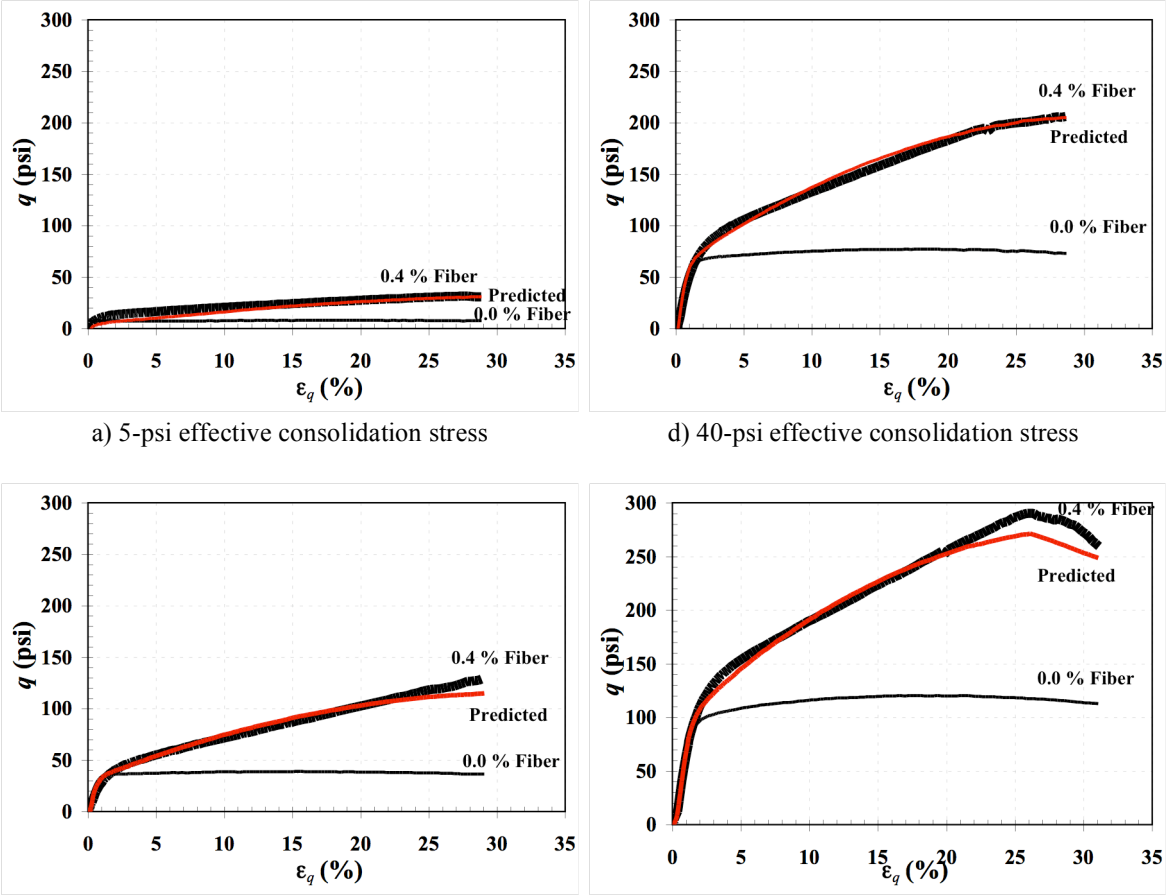

a) 5-psi effective consolidation stress

d) 40-psi effective consolidation stress

b) 20-psi effective consolidation stress

e) 60-psi effective consolidation stress

Figure 8.11 Measured and predicted q versus the triaxial shear strain (ε_q) curves from the CD tests for Ottawa sand specimens prepared at loose state and consolidated to: a) 5-psi effective stress, b) 20-psi effective stress, c) 40-psi effective stress, and d) 60-psi effective stress.

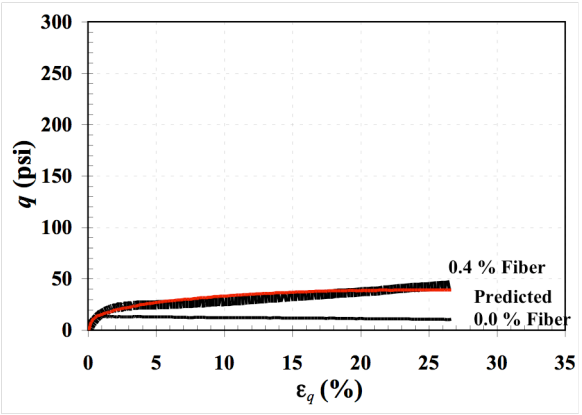

a) 5-psi effective consolidation stress

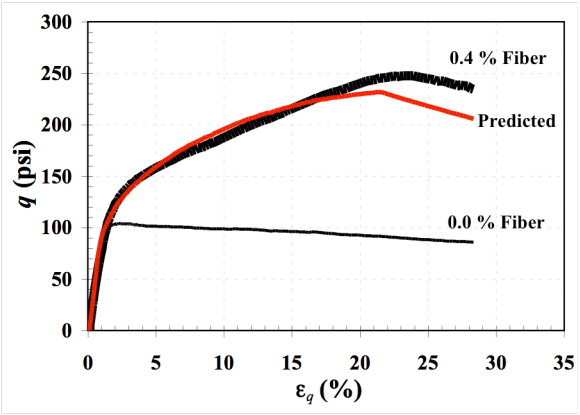

d) 40-psi effective consolidation stress

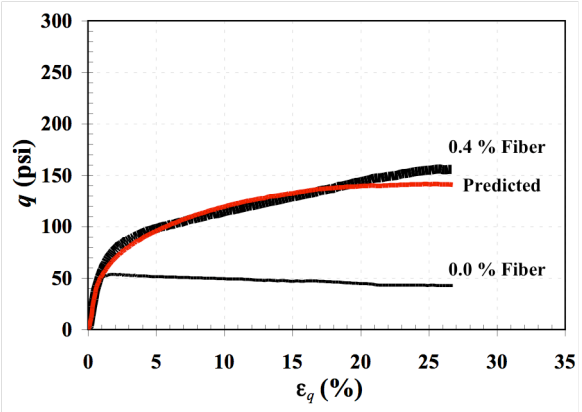

b) 20-psi effective consolidation stress

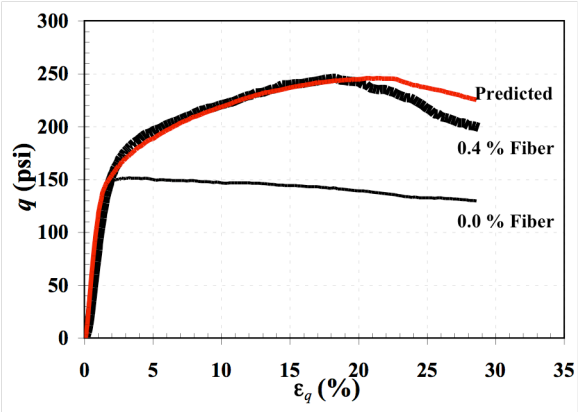

e) 60-psi effective consolidation stress

Figure 8.12 Measured and predicted q versus the triaxial shear strain (ε_q) curves from the CD tests for Ottawa sand specimens prepared at medium-dense state and consolidated to: a) 5-psi effective stress, b) 20-psi effective stress, c) 40-psi effective stress, and d) 60-psi effective stress.

8.4.2 Comparison of Volume Change Response from the *CD* Tests

The measured and predicted in volumetric strain (ε_p) versus the triaxial shear strain for Ottawa sand specimens are presented in Figures 8.13 and 8.14. Overall, the predicted behavior agrees closely with the observed behavior except for the specimens consolidated to 5-psi (35-kPa) and prepared to loose and medium-dense states.

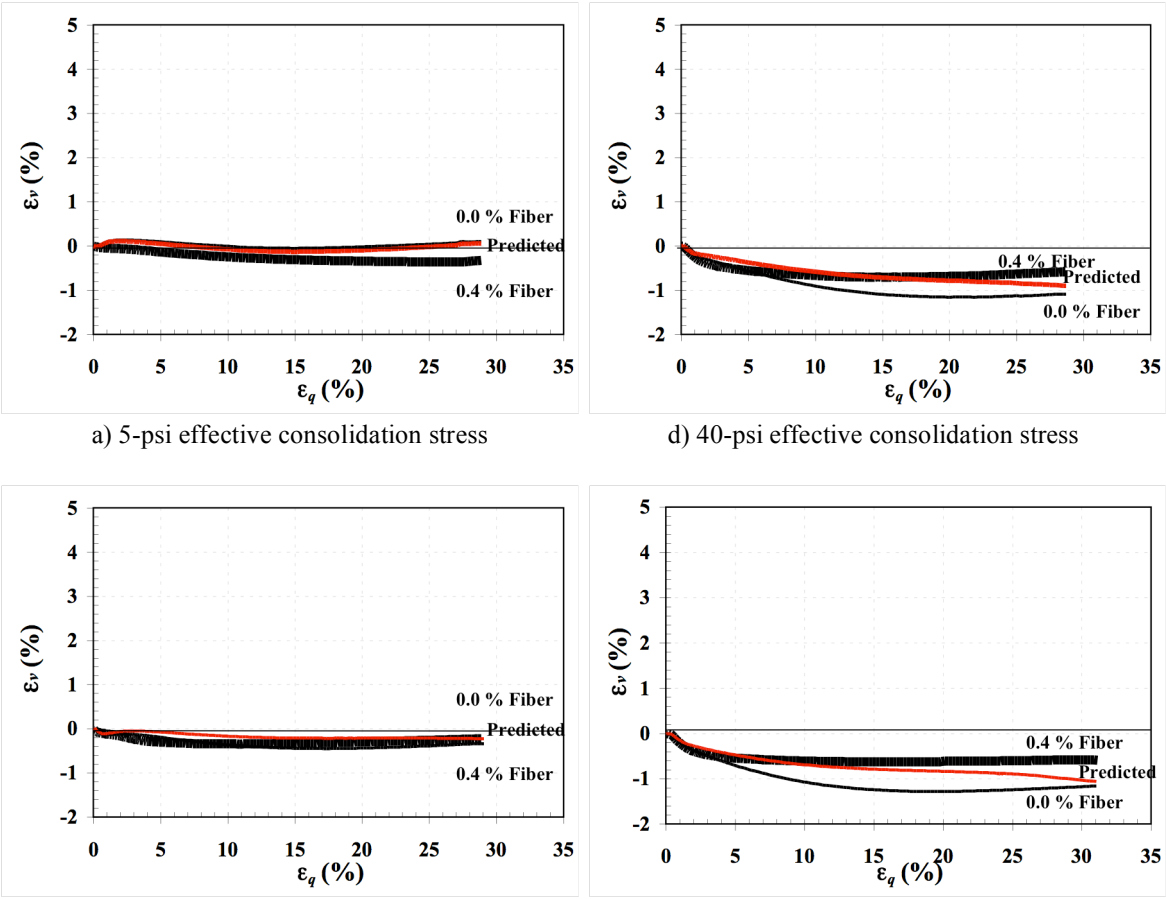

a) 5-psi effective consolidation stress

d) 40-psi effective consolidation stress

b) 20-psi effective consolidation stress

e) 60-psi effective consolidation stress

Figure 8.13 Measured and predicted ε_p versus triaxial shear strain (ε_q) curves from the CD tests for Ottawa sand specimens prepared at loose state and consolidated to: a) 5-psi effective stress, b) 20-psi effective stress, c) 40-psi effective stress, and d) 60-psi effective stress.

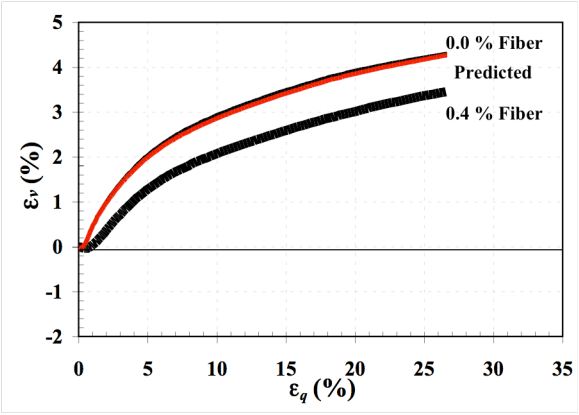

a) 5-psi effective consolidation stress

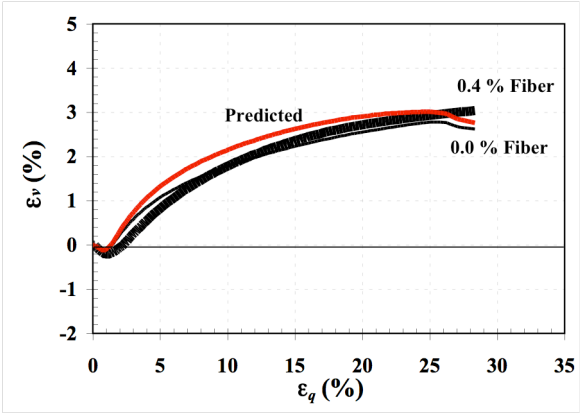

d) 40-psi effective consolidation stress

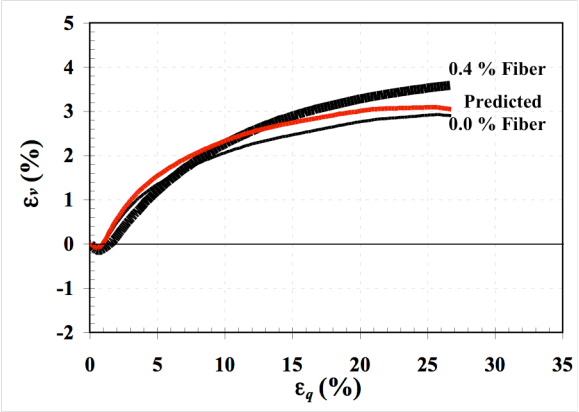

b) 20-psi effective consolidation stress

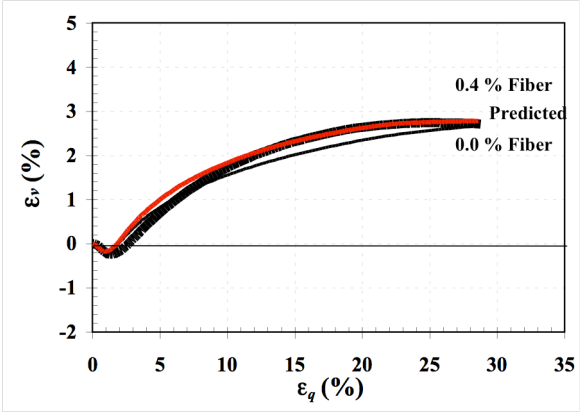

e) 60-psi effective consolidation stress

Figure 8.14 Measured and predicted ε_p versus triaxial shear strain (ε_q) curves from the *CD* tests for Ottawa sand specimens prepared at medium-dense state and consolidated to: a) 5-psi effective stress, b) 20-psi effective stress, c) 40-psi effective stress, and d) 60-psi effective stress.

8.4.3 Comparison of Fiber Contributions for *CD* Tests

The measured and predicted deviatoric contribution of fibers versus the triaxial shear strain for the *CD* tests are shown in Figures 8.15 and 8.16 for Ottawa sand specimens compacted at loose and medium-dense states, respectively. In general, the predicted behaviors agree closely with the observed behavior at most strains. However, the predicted deviatoric contributions tend to deviate slightly from the inferred values in some cases at large strains, particularly at higher confining stresses. This is attributed to slightly variations in prediction of fibers yielding at large strains, and also potentially to specimen bulging that occurs at large strains.

Figures 8.17 and 8.18 show the measured and predicted hydrostatic contribution of fibers versus the triaxial shear strain for Ottawa sand specimens. The comparisons of measured and predicted values of p_f are reasonably good at low to moderate strains, but not as good at large strains. This is primarily a result of the fact that the "measured" values of p_f do not truly account for the fiber contributions as discussed in section 8.3.3. Deviations between the measured and predicted results are therefore expected, because the measured hydrostatic stresses do not include contributions from the fibers.

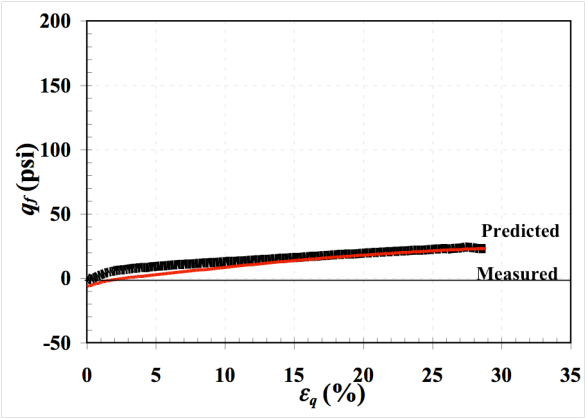

a) 5-psi effective consolidation stress

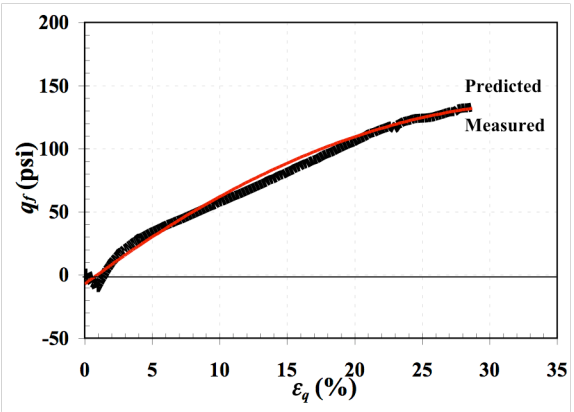

d) 40-psi effective consolidation stress

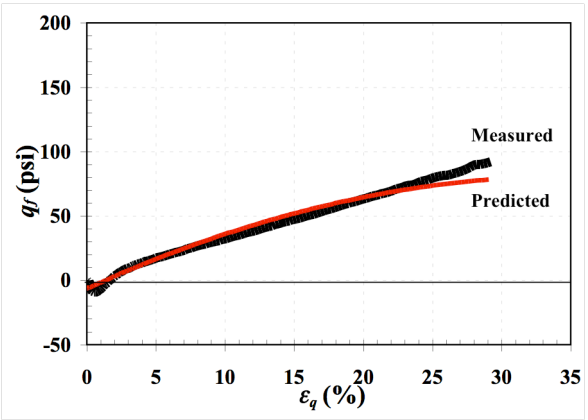

b) 20-psi effective consolidation stress

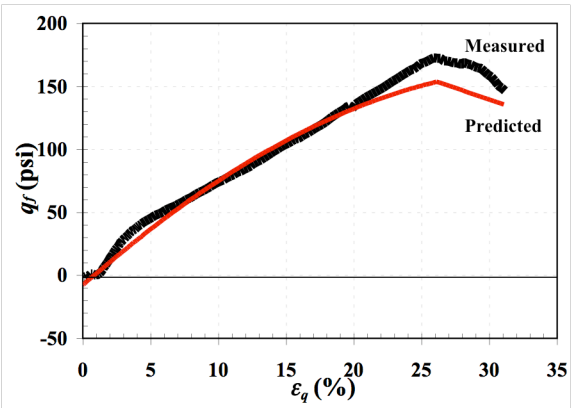

e) 60-psi effective consolidation stress

Figure 8.15 Measured and predicted deviatoric contribution of fibers (q_f) versus triaxial shear strain (ε_q) curves from the CD tests for Ottawa sand specimens prepared at loose state and consolidated to: a) 5-psi effective stress, b) 20-psi effective stress, c) 40-psi effective stress, and d) 60-psi effective stress.

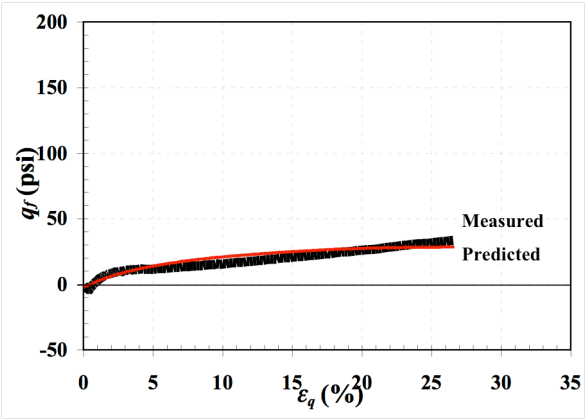

a) 5-psi effective consolidation stress

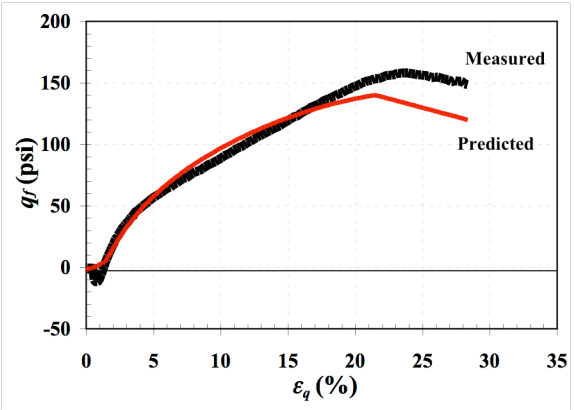

d) 40-psi effective consolidation stress

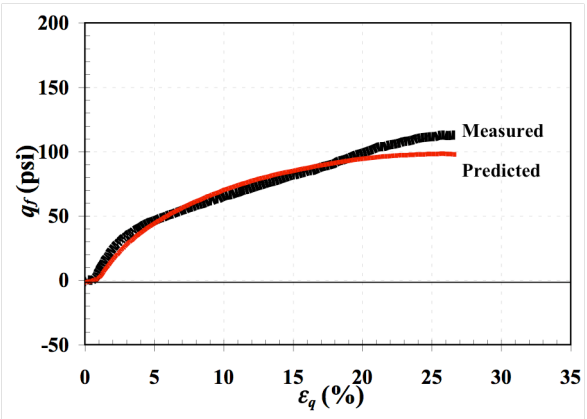

b) 20-psi effective consolidation stress

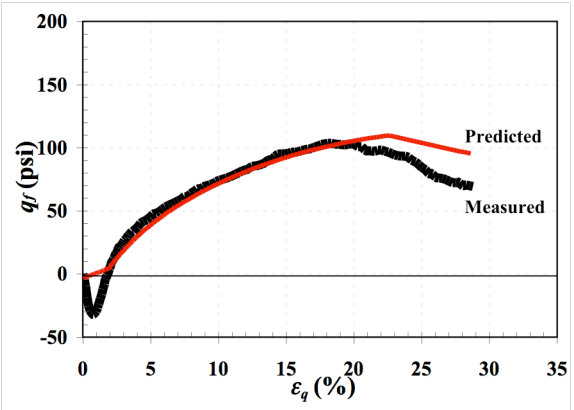

e) 60-psi effective consolidation stress

Figure 8.16 Measured and predicted deviatoric contribution of fibers (q_f) versus triaxial shear strain (ε_q) curves from the CD tests for Ottawa sand specimens prepared at medium-dense state and consolidated to: a) 5-psi effective stress, b) 20-psi effective stress, c) 40-psi effective stress, and d) 60-psi effective stress.

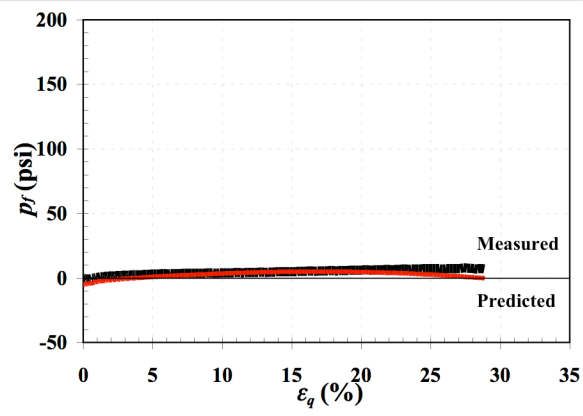

a) 5-psi effective consolidation stress

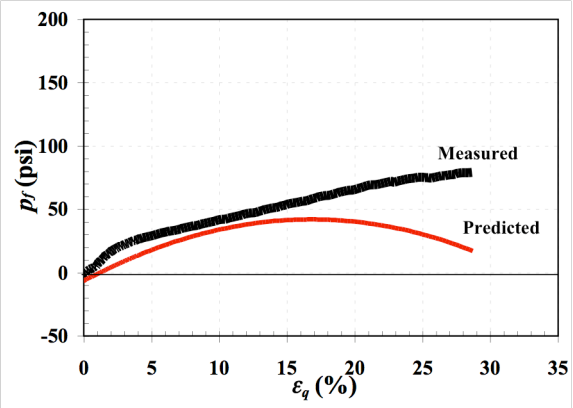

d) 40-psi effective consolidation stress

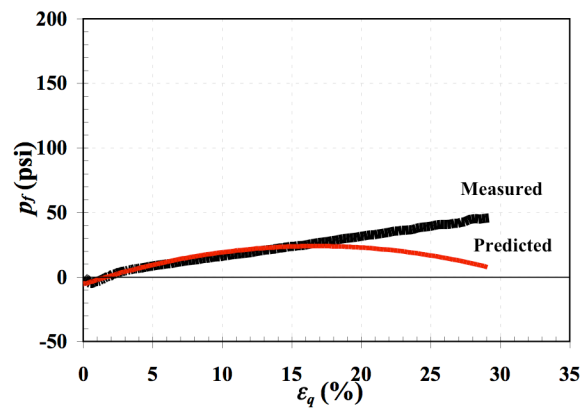

b) 20-psi effective consolidation stress

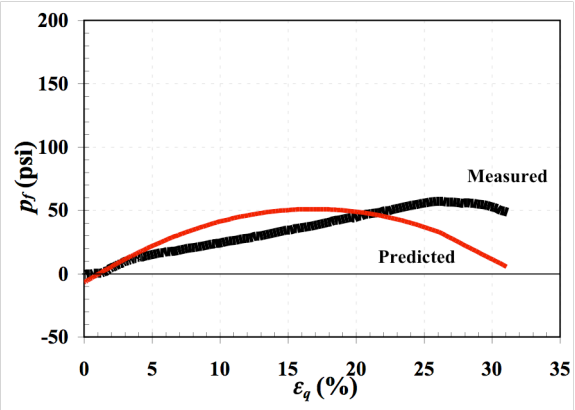

e) 60-psi effective consolidation stress

Figure 8.17 Measured and predicted hydrostatic contribution of fibers (p_f) versus triaxial shear strain (ε_q) curves from the CD tests for Ottawa sand specimens prepared at loose state and consolidated to: a) 5-psi effective stress, b) 20-psi effective stress, c) 40-psi effective stress, and d) 60-psi effective stress.

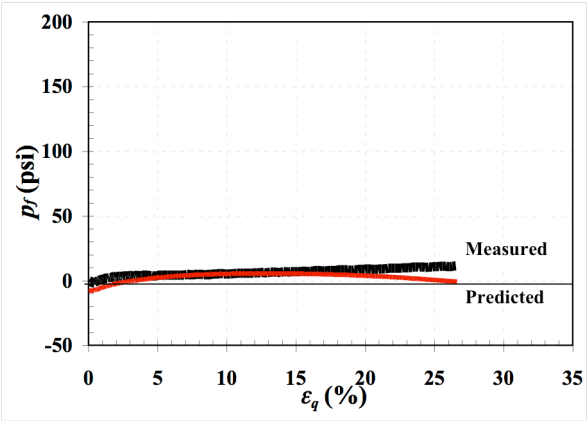

a) 5-psi effective consolidation stress

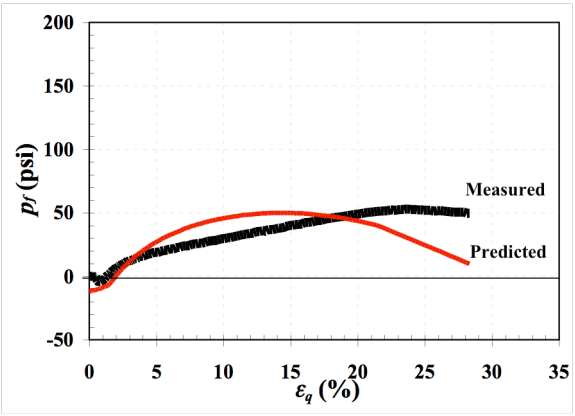

d) 40-psi effective consolidation stress

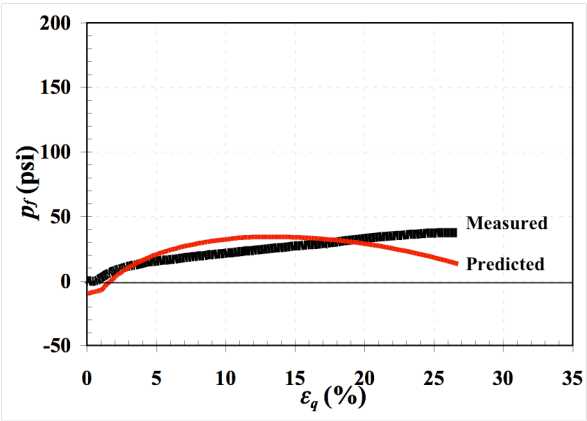

b) 20-psi effective consolidation stress

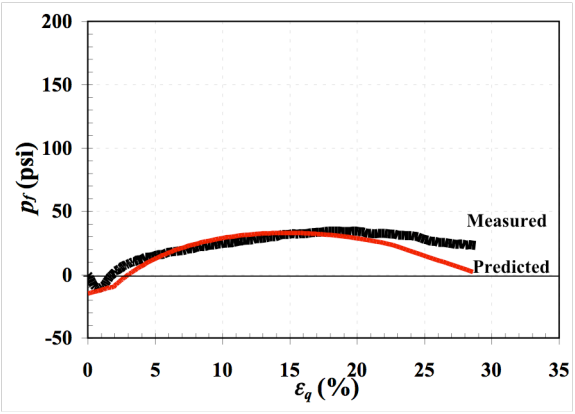

e) 60-psi effective consolidation stress

Figure 8.18 Measured and predicted hydrostatic contribution of fibers (p_f) versus triaxial shear strain (ε_q) curves from the CD tests for Ottawa sand specimens prepared at medium-dense state and consolidated to: a) 5-psi effective stress, b) 20-psi effective stress, c) 40-psi effective stress, and d) 60-psi effective stress.

8.4.4 Comparison of Stress Paths from *CD* Tests

The measured and predicted stress paths from the *CD* tests are shown in Figures 8.19 and 8.20. Note that the predicted stress paths match well at lower values for mean effective stress and depart from the observed behavior when they were close to the peak deviatoric stress. This is again a result of the measured stress paths not including contributions from the fibers. Deviations are thus expected.

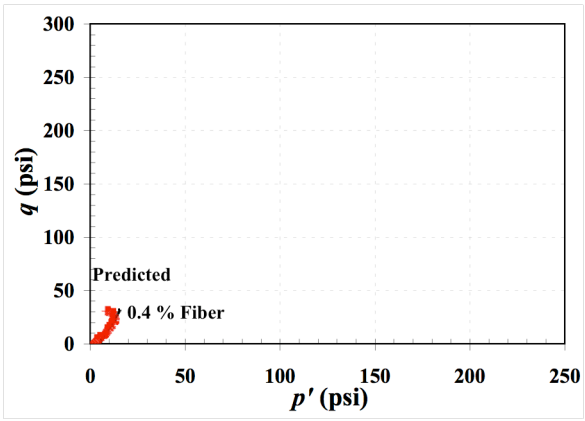

a) 5-psi effective consolidation stress

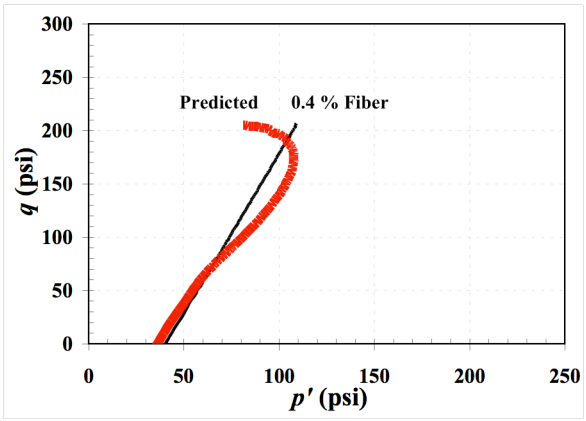

d) 40-psi effective consolidation stress

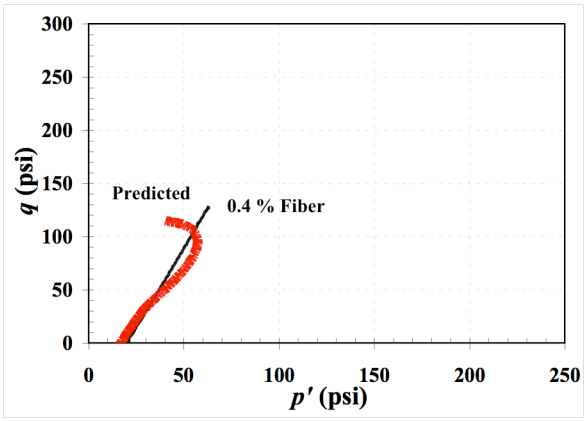

b) 20-psi effective consolidation stress

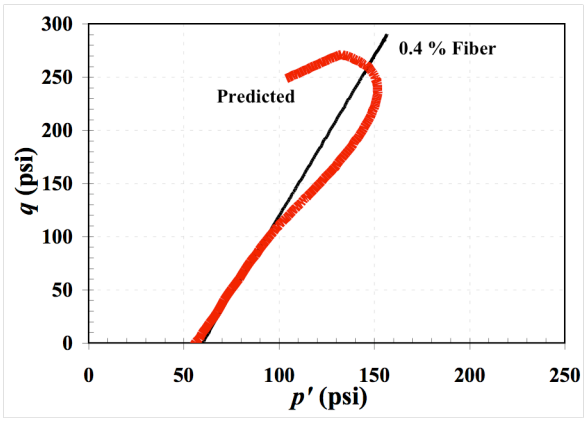

e) 60-psi effective consolidation stress

Figure 8.19 Measured and predicted stress paths from the *CD* tests for Ottawa sand specimens prepared at loose state and consolidated to: a) 5-psi effective stress, b) 20-psi effective stress, c) 40-psi effective stress, and d) 60-psi effective stress.

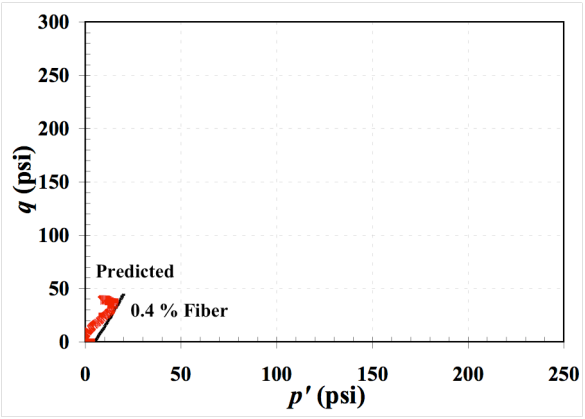

a) 5-psi effective consolidation stress

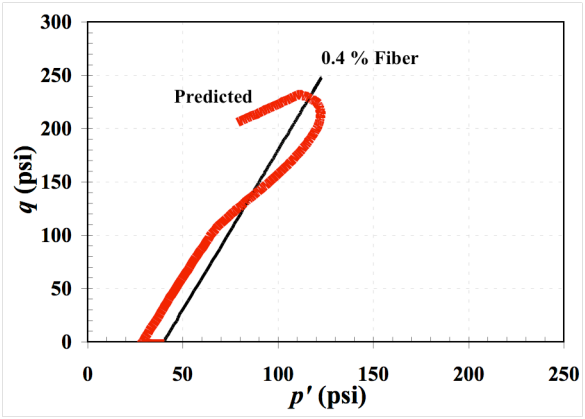

d) 40-psi effective consolidation stress

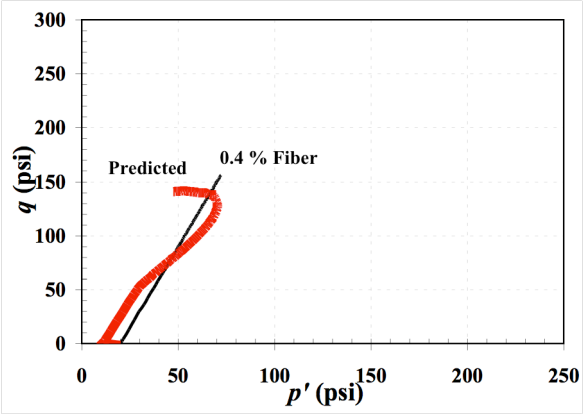

b) 20-psi effective consolidation stress

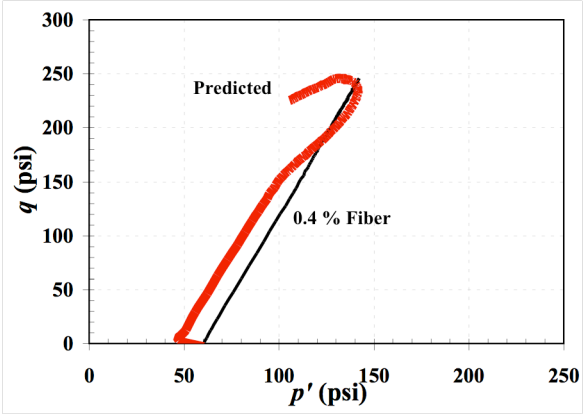

e) 60-psi effective consolidation stress

Figure 8.20 Measured and predicted stress paths from the *CD* tests for Ottawa sand specimens prepared at medium-dense state and consolidated to: a) 5-psi effective stress, b) 20-psi effective stress, c) 40-psi effective stress, and d) 60-psi effective stress.

8.5 Summary

The proposed model was used to predict the mechanical behavior for fiber-reinforced silty sand and Ottawa sand under drained loading conditions. The predicted and observed responses were presented, compared, and discussed in this chapter. It was found that the model was capable of reproducing the deviatoric stress well for all silty sand and Ottawa sand reinforced specimens at all effective consolidation stresses tested in this study. Moreover, the predicted volumetric strains agreed closely with the observed values as the effective consolidation stress increased for both soils. Comparisons of predicted and measured hydrostatic contributions of the fibers do not agree as well, but this is a result of the measured hydrostatic (mean) stresses neglecting contributions due to the fibers. This also affects comparisons between measured and observed stress paths, but such deviations are expected.

CHAPTER 9: SUMMARY, CONCLUSIONS, AND RECOMMENDATIONS FOR FUTURE WORK

9.1 Summary

The inclusion of fibers to improve the engineering properties of compacted soil is becoming an increasingly common practice in geotechnical engineering projects. However, intensive laboratory testing is needed before the fibers can be utilized for field projects. Therefore, the motivation for this work is to propose a constitutive model to predict the stress, pore pressure change, and volume change as a function of the shear strain. In doing so, this work seeks to minimize the need for laboratory tests of fiber-reinforced specimens and thereby to encourage the implementation of fiber-reinforced soils in engineering practice.

This research is based on the hypothesis that both the effective stress-strain-volume change and the effective stress-strain-pore pressure behavior of fiber-reinforced soils can be predicted from superposition of the response of the unreinforced soil and the response attributed to the fibers. The investigation described in this dissertation evaluates this hypothesis through an extensive series of laboratory tests on replicate unreinforced and reinforced soil specimens, and through the development and validation of a constitutive model to predict the stress-strain-volume-pore pressure change response of fiber-reinforced soil.

This research was divided into four tasks. The first task was to measure the strength and stress deformation response of unreinforced and fiber-reinforced silty sand and Ottawa sand in terms of effective stresses under undrained and drained loading

conditions. The second was to evaluate strength parameters based on the strain dependence of the unreinforced and fiber-reinforced silty sand and Ottawa sand. The third task was to develop and evaluate a constitutive model to predict the stress-strain-volume-pore pressure behavior of fiber-reinforced silty sand and Ottawa sand. Finally, the model was validated and calibrated to predict the mechanical behavior of fiber-reinforced silty sand and Ottawa sand tested in the $\overline{CU}$ and CD tests.

In Chapter 2, a summary of previous research on fiber-reinforced soils with emphasis on stress-strain response in terms of effective stresses, load transfer mechanics, and the development of constitutive models for predicting soil behavior are presented. The basic methodology for evaluating the stress-strain-pore pressure and stress-strain-volume change behavior of fiber-reinforced silty sand and Ottawa sand was described in Chapter 3. Results of an extensive series of undrained and drained triaxial compression tests are presented and discussed in Chapters 3 and 4, respectively.

The results presented show that silty sand reinforced with fibers requires significant shear strain (e.g. 20 percent). Reinforced Ottawa sand specimens require significantly less strain (e.g. 5 percent) to begin mobilizing resistance in undrained tests. Results of the drained tests show that some strain is also required to mobilize fiber resistance, but the amount of strain needed in drained tests is generally smaller than required in undrained tests for both reinforced silty sand and Ottawa sand. This suggests that volumetric strain plays an important role in mobilization of fiber resistance. The observed pore pressure response for fiber-reinforced specimens sheared under undrained conditions was found to be noticeably different than that of similar unreinforced samples and the pore pressure also varied with different soil types. For example, fiber-reinforced

silty sand produced higher pore pressures, whereas reinforced Ottawa sand compacted in a loose state generated very little pore pressure under undrained loading conditions. Similarly, the volumetric strain versus triaxial shear strain behavior of the reinforced silty sand differed from that of the reinforced Ottawa sand in the drained tests. The amount of dilation observed for the reinforced silty sand specimens was significantly less than for the unreinforced specimens. However, the reinforced Ottawa sand specimens tended to compress less than unreinforced specimens when specimens were consolidated to higher effective stresses (e.g. greater than or equal to 20-psi). Test results presented in Chapter 4 also demonstrated that the fibers generate an "internal confining stress" that alters the volumetric strain response in both silty sand and Ottawa sand.

In Chapter 5, the interpretation and analysis of the experimental results were presented and discussed. Results for undrained and drained tests on replicate fiber-reinforced and unreinforced soil specimens suggested that fiber-reinforcement provides both a deviatoric (q_f) and a hydrostatic (p_f) contribution to the stresses in the specimens. The deviatoric contributions of fibers can be modeled as a bi-linear function with an initial constant contribution (q_{f0}) plus a linear load transfer contribution with a slope equal to $3G_f$. The hydrostatic contribution of fiber can be modeled by the initial constant contribution (p_{f0}) plus a linear contribution of hydrostatic stresses. Soil types and loading conditions were found to play an important role in terms of the interaction of soil with the included fibers and the deviatoric and hydrostatic contributions to the response fiber-reinforced soils.

A constitutive model was proposed in Chapter 6 based on the laboratory test results to predict the stress-strain-volume-pore pressure behavior of fiber-reinforced silty

sand and Ottawa sand during any stage of undrained and drained loading. In the model, the hydrostatic and deviatoric contribution of fibers is predicted from axial (ε_a) and volumetric (ε_v) strains of an unreinforced soil, the volumetric fiber content (χ), fiber stiffness (E_f) and yield stress, and the initial hydrostatic and deviatoric stresses attributed to the fibers (p_{f0} and q_{f0}). The key assumptions in the model include: (1) fibers are uniformly distributed in the specimens. (2) f_{mob} accounts for the reductions in fiber strain due to relative slip between the fibers and the soil, and varies with effective consolidation stress, soil types, and loading conditions, (3) yielding is considered by a simple comparison of the average mobilized fiber stress, t_f, to the yield stress of the fibers (45-ksi), (4) shear distortion (θ) is equal to triaxial shear strain (ε_q), (5) the total axial strain in the fibers (ε_t) is equal to 0.25 times axial strain plus 1.68 times volumetric strain from tests on unreinforced specimens, and (6) the initial p_{f0} and q_{f0} are used to account for the compaction, extrusion, and consolidation process.

The proposed constitutive model was used to simulate response of fiber-reinforced silty sand and Ottawa sand during undrained and drained tests were presented, compared, and discussed in Chapters 7 and 8. The predicted deviatoric stresses for the silty sand specimens tended to slightly over-predict and depart from the measured behavior at large strains in undrained tests. The model was capable of closely reproducing the deviatoric stress for all Ottawa sand specimens compacted at loose and medium-dense states in undrained and drained tests; moreover, the predicted pore pressure and volumetric strains responses were in close agreement with the observed behavior for all effective consolidation stresses tested in this study for both soils.

9.2 Conclusions

Results of the laboratory tests presented indicate that the shear strength parameters of fiber-reinforced silty sand and Ottawa sand are strain dependent. Generally, the silty sand reinforced with fibers requires significant shear strain of 20 percent to mobilize fiber resistance under undrained loading condition, while the Ottawa sand specimens required only 5 percent strain before the fiber resistance under undrained conditions became noticeable. In contract, silty sand specimens required 5 percent strain or less to begin mobilizing fiber resistance, while the Ottawa sand specimens required approximately 2 percent strain to mobilize the fiber resistance under drained conditions. In both $\overline{CU}$ and CD tests, the strain required to begin mobilizing the fiber resistance for fiber-reinforced silty sand and Ottawa sand increased with the effective consolidation stress increased. This is postulated to be because the included fibers become more initially compressed as the effective confining stress increased. As a result, more shear strains are needed to mobilize fiber resistance for the specimens consolidated at higher effective stresses.

Laboratory results on replicate fiber-reinforced and unreinforced soil specimens under undrained and drained loading conditions also suggests that fiber-reinforcement provides both a deviatoric (q_f) and a hydrostatic (p_f) contribution to the stresses in the specimens. The initial deviatoric contribution of fibers (q_{f0}) and the shear modulus of the fiber contributions (G_f) tended to decrease as the effective consolidation stress increased. However, the hydrostatic contribution of fibers (p_f) also varied according to different soil types and loading conditions.

Additional conclusions reached based on the results presented:

- It was found that the model was capable of reproducing the deviatoric stress for all silty sand and Ottawa sand reinforced specimens at all effective consolidation stresses tested in this study. In the case of the silty sand specimens reinforced with fibers, however, tended to slightly over-predict and depart from the measured behavior at large strains. The predictions do deviate from the measured response at large strains for the medium-dense specimens. This deviation is likely due to the model missing some failure mode (e.g. fiber pullout or fiber yield).
- Overall, the predicted pore pressure and the predicted volumetric strain were all in a close agreement with the observed behavior up to large strains among all effective consolidation stresses tested in this study for both soils. However, the predicted volumetric strain behavior shows some tendency to over-predict the dilatancy of the reinforced silty sand specimens consolidated less than 20-psi (140-kPa).
- The predictions in fiber deviatoric and fiber hydrostatic stresses under undrained loading conditions matched reasonably well and followed the same trends as the measured behavior, but showed a slightly tendency to over-predict the fiber contribution values.
- In drained tests, predicted deviatoric contributions of fibers agree closely with the observed behavior at most strains. However, the predicted deviatoric contributions tend to deviate slightly from the inferred values in some cases at large strains, particularly at higher confining stresses. Comparisons of

predicted and measured hydrostatic contributions of the fibers do not agree as well, but this is a result of the measured hydrostatic stresses neglecting contributions due to the fibers. This also affects comparisons between measured and observed stress paths, but such deviations are expected.

9.3 Proposed Constitutive Model for Fiber-reinforced Soils

Based on the testing results and findings from this work, a proposed constitutive model for fiber-reinforced soils to be used in predicting the effective stress-strain-pore pressure and effective stress-strain-volume change behavior is the following:

Table 9.1 Proposed Constitutive Model for Fiber-Reinforced Soils

Basic Equations	A. The mobilized tensile stress of the fibers, t_f can be calculated as $t_f = \sigma_t \times \chi \times f_{mob} = E_f \times \varepsilon_t \times \chi \times f_{mob}$ Where E_f is the Young's modulus of the fibers, ε_t is the total axial strain in the fibers, χ is the volumetric fiber content, and yielding is determined as $\sigma_t = E_f \times \varepsilon_t$ being greater than ultimate tensile stress of the fibers (45-ksi), and f_{mob} is the fiber mobilization factor shown in Figure 6.13. B. The predicted deviatoric (q_{pf}) and hydrostatic (p_{pf}) contribution of fibers can be computed as $q_{pf} = t_t \times Distribution\ \ function\ \ for\ \ q_f + q_{f0}$ $p_{pf} = t_t \times Distribution\ \ function\ \ for\ \ p_f + p_{f0}$ Where the distribution functions for q_{pf} and p_{pf} are shown in Table 6.1. C. $\varepsilon_t = 0.25 \times \varepsilon_a + 1.68 \times \varepsilon_v$ Where ε_v is the volumetric strain from the unreinforced specimen. A. The predicted deviator (q_r) and hydrostatic (p'_r) stress of the fiber-reinforced soil can be estimated as $q_r = q_s + q_{pf}$ $p'_r = p'_s + p_{pf}$ Where q_s and p_s' are the deviatoric and mean effective stresses of the unreinforced specimens, and q_{pf} and p_{pf} are determined from B above

Undrained Behavior ($\overline{CU}$ test)	A. The predicted pore pressure change attributed to the fibers, Δu_{pf} can be calculated as $\Delta u_{pf} = \Delta p_{pf} + a \times \Delta q_{pf}$ Where the pore pressure parameter, $a = {-\Delta p'}/{\Delta q}$, from unreinforced specimens sheared under undrained conditions, and Δq_{pf} is the change of the predicted deviatoric contribution of fibers. B. For silty sand and silty clay, the predicted pore pressure change of the fiber-reinforced soil, Δu_p, is computed as $\Delta u_p = \Delta u_s + \Delta u_{pf}$ Where Δu_s is the change of the pore pressure from unreinforced specimen. C. For Ottawa sand, $\Delta u_p = \Delta u_s - \Delta u_{pf}$
Drained Behavior (CD test)	A. The change in volumetric strain of the fibers, $\Delta \varepsilon_{vf}$, can be estimated as $\Delta \varepsilon_{vf} = \frac{1}{K_f} \Delta p_{pf}$ Where K_f is the bulk modulus of the fiber-reinforced soils, is calculated from the results of the isotropic consolidation test, and Δp_{pf} is the change of predicted hydrostatic contribution of the fibers. B. For silty sand and silty clay, the predicted total volumetric strain (ε_p) of the fiber-reinforced specimen as $\varepsilon_p = \varepsilon_s - \Delta \varepsilon_{vf}$ Where ε_s is the volumetric strain from the unreinforced specimen. C. For Ottawa sand, $\varepsilon_p = \varepsilon_s + \Delta \varepsilon_{vf}$

9.4 Recommendations for Future Work

Additional work is needed to further refine the proposed model, to evaluate the model for various types of soil, and to establish model parameters for different soils. The largest errors in the model seem to involve the hydrostatic contribution of the fibers, particularly for the volume-change prediction. The bulk modulus utilized for the volumetric strain prediction is not a constant value for different effective consolidation stresses. Further study, therefore, should focus on isotropic consolidation tests or one-

dimensional consolidation tests for determining the properties of suitable fiber/soil composites.

Further verification and refinement of the assure fiber orientation (θ_f) in randomly distributed fiber-reinforced specimens is needed to find the appropriate angle for the calculated model. The angle of 45 degrees was assumed to be a good average value to represent the uniformly distributed fibers in the specimens. Additional work could be accomplished by evaluating inclusions of fiber at different orientations and re-evaluating the predicted values in order to improve this key assumption.

Measurements for the initial fiber contributions (i.e. q_{f0} and P_{f0}) are needed for various types of soils in order to relate the initial stresses in the fibers that the model prediction imposes. The existing data suggests that the linear fit to q_{f0} and P_{f0} may not be appropriate relationship in terms of effective confining stress, and perhaps a more refined function is needed.

Additional effort is needed to extend the model for different soil types with fiber inclusions, which would encourage the use of fiber-reinforced soil in geotechnical practice. The model parameters that should be involved in future investigations include the fiber distribution functions (f_{mob}) in the model. Additional undrained and drained triaxial tests should be conducted at a wide range of compacted densities and effective consolidation stresses to better understand the fiber mobilization factor (f_{mob}). Finally, additional triaxial extensional tests should be conducted for silty sand and Ottawa sand at different confining stresses to better understand and help to adjust the model along different loading paths.

REFERENCES

1. Al-Refeai, T.O. (1991). "Behavior of granular soils reinforced with discrete randomly oriented inclusions." *Geotexiles and Geomembranes*, 10(4), 319-333.

2. American Society for Testing and Materials ASTM. 2000. "D698-00 standard test methods for laboratory compaction characteristics of soil using standard effort (12,400 ft-lbf/ft^3(600 kN-m/m^3))." *Annual Book of ASTM Standards*, Volume 04.08, Philadelphia.

3. American Society for Testing and Materials ASTM. 2000. "D792-00 standard test methods for density and specific gravity (relative density) of plastics by displacement." *Annual Book of ASTM Standards*, Volume 08.01, Philadelphia.

4. American Society for Testing and Materials ASTM. 2002. "D854-02 standard test methods for specific gravity of soil solids by water pycnometer." *Annual Book of ASTM Standards*, Volume 04.08, Philadelphia.

5. American Society for Testing and Materials ASTM. 1994. "D2101 standard test methods for tensile properties of single man-made textile fibers taken from yarns and tows." *Annual Book of ASTM Standards*, Volume 07.01, Philadelphia.

6. American Society for Testing and Materials ASTM. 2002. "D2256-02 standard test method for tensile properties of yarns by the single-strand method." *Annual Book of ASTM Standards*, Volume 07.01, Philadelphia.

7. American Society for Testing and Materials ASTM. 2000. "D2487-00 standard practice for classification of soils for engineering purposes (Unified Soil Classification System)." *Annual Book of ASTM Standards*, Volume 04.08, Philadelphia.

8. American Society for Testing and Materials ASTM. 2004. "D4767-04 standard test method for consolidated undrained triaxial compression test for cohesive soils." *Annual Book of ASTM Standards*, Volume 04.08, Philadelphia.

9. Ang, E.C. (2001). "Engineering behavior of fiber-reinforced silty clays." Thesis, submitted in partial fulfillment for the requirements of the Master of Science Degree, University of Missouri-Columbia.

10. Atkinson, J.H., Bransby, PL. (1978). *The Mechanics of Soils – An Introduction to Critical State Soil Mechanics*, McGraw-Hill, London.

11. Bardet, J.P. (1997). *Experimental Soil Mechanics*, Prentice-Hall, Inc., Upper Saddle River, New Jersey.

12. Bauer, G., and Oancea, A. (1999). "Soils reinforced with discrete synthetic fibers." *Geosynthetics'99 – Specifying Geosynthetics and Developing Design Detail*, IFAI, Boston, MA, 465-475.

13. Chen, C.W. (2006). "Drained and undrained behavior of fiber-reinforced sand." *Midwest Transportation Consortium of Student Papers*, Transportation Scholars Conference, Iowa State University, Ames, Iowa.

14. Consoli, N.C., Prietto, P.D.M., and Ulbrich, L.A. (1998). "Influence of fiber and cement addition on behavior of sandy soil." *Journal of the Geotechnical and Geoenvironmental Engineering*, 124(12), 1211-1214.

15. Consoli, N. C., Montardo, J.P., Marques, P.D., and Pasa, G.S. (2002). "Engineering behavior of a sand reinforced with plastic waste." *Journal of the Geotechnical and Geoenvironmental Engineering*, 128(6), 462-472.

16. Consoli, N. C., Casagrande, M.D.T., Prietto, P.D.M., and Thome, A. (2003). "Plate load test on finer-reinforced soil." *Journal of the Geotechnical and Geoenvironmental Engineering*, 129(10), 951-955.

17. Ding, D., and Hargrove, S.K. (2006). "Technical note on Nonlinear stress-strain relationship of soil reinforced with flexible geofibers." *Journal of the Geotechnical and Geoenvironmental Engineering*, 132(6), 791-794.

18. Gray, D.H., and Ohashi, H. (1983). "Mechanics of fiber reinforcement in sand." *Journal of the Geotechnical Engineering*, 109(3), 335-353.

19. Gray, D.H., and Maher, M.H. (1989). "Admixture stabilization of sand with discrete, randomly distributed fibers." *Proceeding XIIth International Conference n SMFE*, Rio de Janeiro, Brazil, 1363-1366.

20. Gregory, G.H. (1996). *Design Guide for Fiber-Reinforced Soil Slopes Using Fibergrids*, Consulting Report prepared for Synthetic Industries by Fugro-McClelland (Southwest), Inc., Version 1.0.

21. Gregory, G.H., and Chill, D.S. (1998) "Stabilization of earth slopes with fiber reinforcement." *Proceedings of the Sixth International Conference on Geosynthetics*, Atlanta, Georgia, 1073-1078.

22. Harr, M.E. (1966). *Foundations of Theoretical Soil Mechanics*, McGraw-Hill, New York.

23. Heineck, K.S., Coop, M.R., and Consoli, N.C. (2005). "Effect on microreinforcement of soils from very small to large shear strains." *Journal of the Geotechnical and Geoenvironmental Engineering*, 131(8), 1024-1033.

24. Jouve, P., Bouzidi, R., and Riou, Y. (1995). "Resolution of elastoplastic constitutive relations application to the fiber reinforced sand." *Computers and Geotechnics*, 17(3), 327-347.

25. Kumar, A., Walia, B.S., and Mohan, J. (2006). "Compressive strength of fiber reinforced highly compressible clay." *Construction and Building Materials*, 20. 1063-1068.

26. Ladd, R.S. (1978). "Preparing test specimens using undercompaction." *Geotechnical Testing Journal*, 1(1), 16-23.

27. Li, C., and Zornberg, J.G. (2005). "Validation of discrete framework for the design of fiber-reinforced soil." *Geotechnical Special Publication Geo-Frontiers 2005*, Austin, Texas, 4029-4035.

28. Machado, S.L., Carvalho, M.F., and Vilar, O.M. (2002). "Constitutive model for municipal solid waste." *Journal of the Geotechnical and Geoenvironmental Engineering*, 128(11), 940-951.

29. Maher, M.H., and Gray, D.H. (1990). "Static response of sands reinforced with randomly distributed fibers." *Journal of the Geotechnical Engineering*, 116(11), 1661-1677.

30. Maher, M.H., and Ho, Y.C. (1994). "Mechanical properties of kaolinite/fiber soil composite." *Journal of the Geotechnical Engineering*, 120(8), 1381-1393.

31. Michalowski, R.L., and Zhao, A. (1996). "Failure of fiber-reinforced granular soils." *Journal of the Geotechnical Engineering*, 122(3), 226-234.

32. Michalowski, R.L., and Čermák, J. (2003). "Triaxial compression of sand reinforced with fibers." *Journal of the Geotechnical and Geoenvironmental Engineering*, 129(2), 125-136.

33. Naaman, A.E. (1972). "A statistical theory of strength for fiber reinforced concrete." Thesis, submitted in partial fulfillment for the requirements of the Master of Science Degree, Massachusetts Institute of Technology-Cambridge.

34. Nataraj, M.S., and McManis, K.L. (1997). "Strength and deformation properties of soils reinforced with fibrillated fibers." *Geosynthetics International*, 4(1), 65-79.

35. Park, T., and Tan, S.A. (2005). "Enhanced performance of reinforced soil walls by the inclusion of short fibers. " *Geotexiles and Geomembranes*, 23(4), 348-361.

36. Prisco, C.D., and Nova, R. (1993). "A constitutive model for soil reinforced by continuous threads." *Geotexiles and Geomembranes*, 12, 161-178.

37. Ranjan, G., Vasan, R.M., and Charan, H.D. (1994). "Behavior of plastic-fibre-reinforced sand." *Geotexiles and Geomembranes*, 13(8), 555-565.

38. Ranjan, G., Vasan, R.M., and Charan, H.D. (1996). "Probabilistic analysis of randomly distributed fiber-reinforced soil." *Journal of Geotechnical Engineering*, 122(6), 419-426.

39. Rifai, S.M. (2000). "Impact of polypropylene fibers on desiccation cracking and hydraulic conductivity of compacted clay liners." Dissertation submitted in partial fulfillment for the requirements of the Doctoral Degree, Wayne State University,Detroit, Michigan.

40. Romero, R.J. (2003). "Development of a constitutive model for fiber-reinforced soils." Dissertation submitted in partial fulfillment for the requirements of the Doctoral Degree, University of Missouri-Columbia.

41. Santoni, R.L., Tingle, J.S., and Webster, S.L. (2001). "Engineering properties of sand-fiber mixtures of road construction." *Journal of the Geotechnical and Geoenvironmental Engineering*, 127(3), 258-268.

42. Shewbridge, S.E., and Sitar, N. (1989). "Deformation characteristics of reinforced soil in direct shear." *Journal of the Geotechnical and Geoenvironmental Engineering*, 115(8), 1134-1147.

43. Skempton, A.W. (1954). "The pore pressure coefficient A and B." *Geotechnique*, 4, 143-47.

44. Timoshenko S.P., and Gere, J.M. (1972). *Mechanics of Materials*, VanNostrand, New York.

45. Waldron, L.J. (1977). "The shear resistance of root-permeated homogenous and stratified soil." *Soil Science Society of American Journal*, 41(3), 843-849.

46. Wood, D.M. (1990). *Soil behaviour and critical state soil mechanics*, Cambridge University Press, Cambridge, England.

47. Zornberg, J.G. (2002). "Discrete framework for limit equilibrium analysis of fibre-reinforced soil." *Georechnique*, 52(3), 593-604.

VITA

Cheng-Wei Chen, the son of Chin-Tsz Chen and Fang-Mei Cheng, was born on November 11, 1974, in Hu-Wei, Taiwan. After obtaining his diploma at Chia-Yi Senior High School in 1993, he entered Chung-Hua University at Hsin-Chu. He worked as part-time as Research Assistant for Material Laboratory in the Department of Civil Engineering for three years, and later was employed as Structure design Assistant for Lee's Consulting Engineers Office. Then, he received the degree of Bachelor of Science in Civil Engineering from Chung-Hua University in June, 1997. After that, he worked for three years, as a Structure Engineer, for Structure Design Unit of Military Property & Construction Service in Taipei and later for High Point Engineering Consultants, Inc. in Hsin-Chu., He was admitted by the Geotechnical Engineering graduate program at the University of Missouri-Columbia under the supervision of Dr. John Bowders in 2001. He received the degree of Master of Science in Civil Engineering from the University of Missouri-Columbia in August, 2003. He is married to Pei-Ling Lee and they are the parents of a son, Johnnie Kai-Shin.